The case for membrane-associated RNA-binding proteins in *Saccharomyces cerevisiae*

Dissertation

der Mathematisch-Naturwissenschaftlichen Fakultät

der Eberhard Karls Universität Tübingen

zur Erlangung des Grades eines

Doktors der Naturwissenschaften

(Dr. rer. nat.)

vorgelegt von

Muhammad Ibrahim Syed

Quetta, Pakistan

Tübingen

2019

Gedruckt mit Genehmigung der Mathematisch-Naturwissenschaftlichen Fakultät der Eberhard Karls Universität Tübingen.

Tag der mündlichen Qualifikation:	21.08.2019
Dekan:	Prof. Dr. Wolfgang Rosenstiel
1. Berichterstatter:	Prof. Dr. Ralf-Peter Jansen
2. Berichterstatter:	Prof. Dr. Gabriele Dodt

Table of contents

Table of contents

1. List of abbreviations

aa	Amino acid
ASH1	Asymmetric synthesis of HO
cDNA	Complementary DNA
cER	Cortical Endoplasmic reticulum
CFW	Calcofluor white
DAPI	4′,6-diamidino-2-phenylindole
DMS	Dimethyl sulfate
DNA	Deoxyribonucleic acid
EMSA	Electrophoretic mobility shift assay
ER	Endoplasmic reticulum
GET	Guided entry of TA proteins
GFP	Green fluorescent protein
GO	gene ontology
GPI	Glycosylphosphatidylinositol
GST	Glutathione *S*-transferase
HA	Hemagglutinin
HEK2	HEterogeneous nuclear rnp K-like gene 2
HRP	Horseradish peroxidase
IRES	Internal ribosome entry sites
KH	hnRNP K homology
LAM	La motif
LARP	La related protein
LE	Localization element
MCP	MS2 coat protein
MRN1	Multi-copy suppressor of *rsc* *nhp6ΔΔ*
mRNA	Messenger RNA
mRNP	Messenger ribonucleoprotein
MRP	Mitochondrial ribosomal protein
NAB6	Nucleic Acid Binding protein 6

NGR1	Negative growth regulatory protein 1
NPC	Nuclear pore complex
nt	nucleotides
P-body	Processing body
PBP2	Pbp1p Binding Protein 2
PCR	Polymerase chain reaction
qPCR	Quantitative PCR
qRT-PCR	Quantitative reverse transcription PCR
RBD	RNA-binding domain
RBP	RNA-binding protein
RER	Rough Endoplasmic reticulum
RNA	Ribonucleic acid
RNC	Ribosome nascent chain
RRM	RNA recognition motif
rRNA	Ribosomal RNA
SER	Smooth Endoplasmic reticulum
SG	Stress granule
SHE	Swi5p-dependent *HO* Expression
SLF	SuLFide production
SND	Srp-iNDependent
SR	Signal recognition particle Receptor
SRP	Signal recognition particle
SS	Signal sequence
TA	Tail-anchored
TCA	Trichloroacetic acid
TCL	Total cell lysate
TM	Transmembrane
TMD	Transmembrane domain
uORFs	upstream open reading frames
UTR	Untranslated region

WCE	Whole cell extract
Whi3	WHIskey
WT	Wildtype
YEPD	Yeast extract peptone dextrose
YEPG	Yeast extract peptone Glycerol

2. Summary

The endoplasmic reticulum (ER) is the site of protein synthesis for secretory and membrane proteins. Proteins are transported to the ER either co-translationally via the signal recognition particle (SRP) pathway, post-translationally via the GET pathway or via the yet poorly characterized SND pathway. Additionally, loss of ER-associated RNA-binding proteins (RBPs) in yeast and mammals can affect mRNA localization to the ER and ER-based translation. In this thesis project, I identified several RBPs that partially co-localize with ER in *Saccharomyces cerevisiae* such as Khd1p, Mrn1p, Whi3p, Pbp2p, Slf1p, Ngr1p, and Puf1p. The aim was to test if these RBPs had any role in mRNA localization and/or translation at the ER. The deletion of Khd1p resulted in the loss of *MID2* and *SLG1* mRNAs in the ER-enriched fraction and to a partial loss of *MID2* and *SLG1* localization to ER. Furthermore, the abolishment of the N-terminal signal peptide sequence did not affect *MID2* localization to ER. *MID2* localizes to ER independent of translation and only the loss of Khd1p had an effect on its ER targeting. I, therefore, suggest that Khd1p is involved in the translation- and signal sequence-independent targeting of *MID2* to ER.

The individual loss of the RBPs Mrn1p and Whi3p only mildly, but the combined deletion of Whi3p, Pbp2p, Slf1p and Ngr1p strongly affected cell wall synthesis in yeast. However, even combined with an additional knock out of the RBP gene *MRN1* (*quintuple RBP mutant*) no obvious loss of transcripts in the membrane (ER-enriched) fraction was revealed, thus excluding a role of these RBPs in mRNA localization to ER. However, I noted that transcripts encoding nuclear-related proteins are surprisingly enriched in the membrane fraction of both wildtype and *quintuple RBP mutant* strains although the SRP hypothesis suggests that only mRNAs coding for secretory/membrane proteins engage ER for translation. qPCR and microscopic analysis verified that mRNAs coding for nuclear-related proteins, such as *MOT1* and *NUP100*, indeed localize to ER. My data together with previously published studies suggest that mRNAs, irrespective of its coding nature, can localize to ER.

In the *quintuple RBP mutant* strain, I also noticed an upregulation of mRNAs coding for nuclear-encoded mitochondrial ribosomal proteins (MRPs). However, western blot analysis revealed low expression of GFP fusions of the MRPs Mrpl39p, Img2p and Mrpl44p. Since MRPs are involved in the translation of genes encoded by the mitochondrial genome, I performed western blot analysis for Cox2p (encoded by the mitochondrial genome), Cox4p and Tom70p (both encoded by the nuclear genome) and found that Cox2p, but not Cox4p and Tom70p, is not expressed in the *quintuple RBP mutant* strain. Furthermore, mitochondrial-

encoded genes such as *COX1*, *COX2* and the mitochondrial *21S* rRNA are not transcribed. Consequently, the *quintuple RBP mutant* strain cannot grow on a nonfermentable carbon source. Additionally, the mitochondrial morphology is abnormal and the mitochondrial genome is unstable. My data is consistent with previous findings that the loss of MRPs leads to the gradual loss of mitochondrial genome. In conclusion, I suggest that Mrn1p, Whi3p, Pbp2p, Slf1p and Ngr1p are involved in controlling the expression of nuclear-encoded MRPs.

In a second project I analysed the yeast bud localized *ASH1* mRNA, which contains localization elements (LEs) specifically recognized by the RBPs She2p and She3p. How these RBPs interact with the *ASH1* E3 LE at the molecular level was the subject of investigation carried out in collaboration with the group of Prof. Niessing at the Helmholtz Zentrum München. She2p works as tetramer in its functional form. In the co-structure with RNA, its two binding surfaces use two identical sets of amino acids (N36, R43, R52, K60 and R63) to contact RNA. Very few contacts between a protruding helix of She2p and RNA were observed, although this helix is important for mRNA localization *in vivo*. However, it could be shown that She3p intercalates between the protruding helix and RNA, suggesting that the helix is important for interaction with She3p. Mutations in the contact sites in She3p revealed that they were important for mRNA localization *in vivo*. In short, it was shown for the first time how a *cis*-acting LE of a localized RNA such as *ASH1* is recognized by two contacting RBPs in a symmetric way.

3. Zusammenfassung

Das endoplasmatische Retikulum (ER) ist der Ort der Proteinsynthese für sekretorische und Membranproteine. Proteine werden entweder co-translational über den Signalerkennungspartikel (SRP) -Weg, post-translational über den GET-Weg oder über den noch wenig charakterisierten SND-Mechanismus zum ER transportiert. Zusätzlich kann der Verlust von ER-assoziierten RNA-Bindungsproteinen (RBPs) in Hefe oder Säugern die Lokalisierung von mRNA in der ER- und ER-basierten Translation beeinflussen. In diesem Dissertationsprojekt identifizierte ich mehrere RBPs in Saccharomyces cerevisiae, die zumindest teilweise mit dem ER co-lokalisieren, darunter Khd1p, Mrn1p, Whi3p, Pbp2p, Slf1p, Ngr1p und Puf1p. Ziel war es zu testen, ob diese RBPs eine Rolle bei der Lokalisierung und / oder Translation von mRNA am ER spielen. Die Deletion von Khd1p führte zum Verlust von *MID2*- und *SLG1*-mRNAs in einer ER-angereicherten Fraktion und zu einem teilweisen Verlust der *MID2*- und *SLG1*-Lokalisation am ER. Darüber hinaus wirkte sich die Deletion der N-terminalen Signalpeptidsequenz nicht auf die Lokalisierung von *MID2* am ER aus. *MID2* lokalisiert daher unabhängig von der Translation zum ER, benötigt aber Khd1p. Ich postuliere daher, dass Khd1p am translatorischen und signalsequenzunabhängigen Targeting von *MID2* zu ER beteiligt ist.

Viele Proteine, die am ER translatiert werden, beeinflussen die Zellwandsynthese. Der individuelle Verlust der RBPs Mrn1p und Whi3p auf letztere war nur gering, die kombinierte Deletion von Whi3p, Pbp2p, Slf1p und Ngr1p wirkte sich jedoch stark auf die Zellwandsynthese in Hefe aus. In Kombination mit einem zusätzlichen Knock-out des RBPs MRN1 („fünffache RBP-Mutante“) wurde trotz des Zellwanddefekts jedoch keine Verschiebung von Transkripten aus der Membranfraktion (ER-angereichert) zum Cytoplasma festgestellt, so dass eine Rolle dieser RBPs bei der Lokalisierung von mRNA zum ER ausgeschlossen werden konnte. Ich stellte jedoch fest, dass Transkripte, die für Kernproteine kodieren, überraschenderweise in der Membranfraktion sowohl der Wildtyp- als auch der fünffachen RBP-Mutantenstämme angereichert sind, obwohl dies der SRP-Hypothese widerspricht. qPCR und mikroskopische Analysen bestätigten, dass mRNAs, die für Kernproteine wie Mot1 und Nup100 kodieren, tatsächlich am ER lokalisiert sind. Meine Daten zusammen mit zuvor veröffentlichten Studien legen nahe, dass mRNAs unabhängig von ihrer kodierenden Natur am ER lokalisieren können.

In dem fünffachen RBP-Mutantenstamm stellte ich auch eine Hochregulation von mRNAs fest, die für kernkodierte mitochondriale ribosomale Proteine (MRPs) kodieren. Western-Blot-

Analyse ergab jedoch eine geringe Expression von GFP-Fusionen der MRPs Mrpl39p, Img2p und Mrpl44p. MRPs sind an der Translation von Genen beteiligt sind, die vom mitochondrialen Genom kodiert werden. Die Expression von Cox2p (vom mitochondrialen Genom kodiert), Cox4p und Tom70p (beide vom Kerngenom kodiert) wurde daher untersucht und ich stellte fest, dass Cox2p nicht, allerdings Cox4p und Tom70p im fünffachen RBP-Mutantenstamm exprimiert wird. Darüber hinaus werden mitochondrial codierte Gene wie COX1, COX2 und die mitochondriale 21S-rRNA nicht transkribiert. Folglich kann der fünffache RBP-Mutantenstamm nicht auf einer nichtfermentierbaren Kohlenstoffquelle wachsen. Zusätzlich ist die mitochondriale Morphologie abnormal und das mitochondriale Genom ist instabil. Meine Daten stimmen mit früheren Beobachtungen überein, dass der Verlust von MRPs zum allmählichen Verlust des mitochondrialen Genoms führt. Zusammenfassend schlage ich vor, dass Mrn1p, Whi3p, Pbp2p, Slf1p und Ngr1p an der Kontrolle der Expression von kernkodierten MRP beteiligt sind.

In einem zweiten Projekt analysierte ich die in Hefeknospen lokalisierte *ASH1*-mRNA, die Lokalisierungselemente (LEs) enthält, die von den RBPs She2p und She3p spezifisch erkannt werden. Wie diese RBPs auf molekularer Ebene mit *ASH1* E3 LE interagieren, wurde in Zusammenarbeit mit der Arbeitsgruppe von Prof. Niessing am Helmholtz Zentrum München untersucht. She2p arbeitet als Tetramer in seiner funktionalen Form. In der Co-Struktur mit RNA konnte gezeigt werden, dass in She2p zwei Bindungsoberflächen mit zwei identischen Sätzen von Aminosäuren (N36, R43, R52, K60 und R63) verwendet werden, um RNA zu kontaktieren. Dagegen wurden nur sehr wenige Kontakte zwischen einer hervorstehenden Helix von She2p und RNA beobachtet, obwohl diese Helix für die Lokalisierung von mRNA in vivo wichtig ist. Es konnte jedoch gezeigt werden, dass She3p zwischen der hervorstehenden Helix und der RNA interkaliert, was darauf hindeutet, dass die Helix für die Interaktion mit She3p wichtig ist. Mutationen an den Kontaktstellen in She3p zeigten, dass sie für die Lokalisierung von mRNA in vivo wichtig sind. Kurz gesagt, es wurde zum ersten Mal gezeigt, wie eine cis-wirkende LE einer lokalisierten RNA wie *ASH1* von zwei kontaktierenden RBPs symmetrisch erkannt wird.

4. List of manuscripts/publications contained in this thesis

A. Syed, MI., Poths, S., Baskaran, P., Rapaport, D., and Jansen, R-P. (2019). Membrane-associated RNA-binding proteins contribute to regulation of mRNAs encoding mitochondrial ribosomal proteins. (Manuscript not yet published)

B. Syed, M.I., Moorthy, B.T., Jenner, A., Fetka, I., and Jansen, R.-P. (2018). Signal sequence-independent targeting of *MID2* mRNA to the endoplasmic reticulum by the yeast RNA-binding protein Khd1p. FEBS Lett. *592*.

C. Edelmann, F.T., Schlundt, A., Heym, R.G., Jenner, A., Niedner-Boblenz, A., Syed, M.I., Paillart, J.-C., Stehle, R., Janowski, R., Sattler, M., et al. (2017). Molecular architecture and dynamics of *ASH1* mRNA recognition by its mRNA-transport complex. Nat. Struct. Mol. Biol. *24*.

5. Personal contribution to the manuscripts/publications contained in this thesis

EBERHARD KARLS
UNIVERSITÄT
TÜBINGEN

Mathematisch-Naturwissenschaftliche Fakultät

Erklärung nach § 5 Abs. 2 Nr. 8 der Promotionsordnung der Math.-Nat. Fakultät
-Anteil an gemeinschaftlichen Veröffentlichungen-
Nur bei kumulativer Dissertation erforderlich!

Declaration according to § 5 Abs. 2 No. 8 of the PhD regulations of the Faculty of Science
-Collaborative Publications-
For Cumulative Theses Only!

Syed, Muhammad Ibrahim:

List of Manuscripts/Publications contained in this thesis:

1. Syed, MI., Poths, S., Baskaran, P., Rapaport, D., and Jansen, R-P. (2019). Membrane-associated RNA-binding proteins contribute to regulation of mRNAs encoding mitochondrial ribosomal proteins. (Manuscript not yet published)
2. Syed, M.I., Moorthy, B.T., Jenner, A., Fetka, I., and Jansen, R.-P. (2018). Signal sequence-independent targeting of *MID2* mRNA to the endoplasmic reticulum by the yeast RNA-binding protein Khd1p. FEBS Lett. *592*.
3. Edelmann, F.T., Schlundt, A., Heym, R.G., Jenner, A., Niedner-Boblenz, A., Syed, M.I., Paillart, J.-C., Stehle, R., Janowski, R., Sattler, M., et al. (2017). Molecular architecture and dynamics of *ASH1* mRNA recognition by its mRNA-transport complex. Nat. Struct. Mol. Biol. *24*.

Nr.	Accepted publication yes/no	Position of candidate in list of authors	Scientific ideas by the candidate (%)	Data generation by the candidate (%)	Analysis and Interpretation by the candidate (%)	Paper writing done by the candidate (%)
1	no	1	90%	90%	80%	90%
2	Yes	1	40%	50%	50%	40%
3	Yes	6	10%	10%	20%	10%

I confirm that the above-stated is correct.

09.07.2019
Date, Signature of the candidate

I/We certify that the above-stated is correct.

10.07.2019
Date, Signature of the doctoral committee or at least of one of the supervisors

6. Introduction

6.1 Protein delivery to ER

A cell relies on the regulated expression of its transcriptome to drive diverse cellular processes. Messenger RNA (mRNA) is synthesized in the nucleus and has to be exported out of nucleus to cytoplasm in order to be translated. mRNAs are usually translated in the cytoplasm and their protein products are post-translationally delivered to a particular destination with the exception of subcellular compartments such as endoplasmic reticulum (ER) and mitochondria where proteins can also be co-translationally delivered. In eukaryotes, the ER is a membranous compartment spread throughout cytoplasm. It can be divided into three distinct morphologies: i) perinuclear ER; ii) peripheral ER cisternae; and iii) an interconnected tubular network (English and Voeltz, 2013). In general, ER is a cellular factory for a number of processes including those involved in lipid and carbohydrate metabolism (Fagone and Jackowski, 2009; Hebert et al., 2005), calcium storage (Clapham, 2007) and protein synthesis, folding and transport (Braakman and Hebert, 2013; Rapoport, 2007; Reid and Nicchitta, 2015). The ER could be smooth ER (SER) or rough ER (RER) due to the absence or presence of membrane-bound ribosomes respectively.

RER is the major site of protein synthesis in eukaryotic cells (Mandon et al., 2013) and proteins that are to be inserted in the ER (such as secretory and endomembrane proteins) are delivered co-translationally or post-translationally. In either case, they have to go through protein-conducting channel known as translocon (Görlich and Rapoport, 1993; Stirling et al., 1992). Yeast has two kinds of translocon channels, the essential Sec61 (Ast and Schuldiner, 2013; Deshaies et al., 1991; Panzner et al., 1995) and nonessential Ssh1 (Finke et al., 1996). The Sec61 translocon channel is heterotrimer consisting of Sec61p, Sbh1p, and Sss1p (Görlich and Rapoport, 1993) that associates with signal recognition particle (SRP) receptor (SR) to participate in co-translational (SRP-dependent) protein translocation (Cheng et al., 2005; Halic and Beckmann, 2005) or forms a SEC complex with both essential (Sec63 and Sec62) (Tyedmers et al., 2000) and nonessential (Sec66 and Sec72) (Harada et al., 2011) accessory factors. The SEC complex has no ribosome binding activity and therefore serves as protein translocation channel post-translationally (SRP-independent) (Panzner et al., 1995). Ssh1 forms complex with two other subunits such as Sbh2 and Sss1 (Becker et al., 2009) and is known to participate in co-translational protein translocation (Jan et al., 2014). Up to now, multiple pathways for protein delivery to ER have been discovered and components have been

characterized that play an essential role in protein targeting to ER reviewed in (Aviram and Schuldiner, 2017; Reid and Nicchitta, 2015).

6.1.1 Signal recognition particle (SRP) pathway

The first evidence of protein translation at ER came from the discovery of membrane-bound ribosomes in the 1960s (Redman and Sabatini, 1966; Redman et al., 1966). Subsequent studies showed that a signal encoded by a secretory protein mRNA can guide the ribosome to rough ER (RER) (Blobel and Dobberstein, 1975; Milstein et al., 1972). Further studies identified that secretory proteins are synthesized as precursors having an N-terminal hydrophobic sequence and a processing site for RER-peptidase (von Heijne, 1983). Even transmembrane domains (TMDs), which are hydrophobic in nature when placed closed to the N-terminus of a protein could act as signal sequence to RER (Friedlander and Blobel, 1985; Mize et al., 1986). This mode of protein delivery to ER was named as signal recognition particle (SRP) pathway because of a ribonucleoparticle known as signal recognition particle (SRP that guides the ribosome nascent chain (RNC) complex to the ER-bound SRP receptor (SR) for its subsequent co-translational translocation into ER (Gilmore et al., 1982; Walter and Blobel, 1980, 1982).

According to the classical SRP pathway model, translation starts in cytoplasm and once the hydrophobic ER targeting sequence has emerged from the ribosome exit channel, it is bound by SRP and as a result translation is halted at this point (Walter and Blobel, 1981b, 1981a). The RNC SRP complex is then carried to ER and received at ER by the ER-bound SR. The interaction of SRP with SR brings significant structural changes in SRP and as a result the RNC complex is delivered to Sec61 ER translocon. The SRP recycles back to cytoplasm to engage another RNC, while the ER-bound ribosome resumes translation and the protein is inserted co-translationally into the ER. This co-insertional process is helped by GTP-mediated translation elongation (Connolly and Gilmore, 1989; Connolly et al., 1991). SRP is evolutionarily conserved from bacteria to humans (Bohnsack and Schleiff, 2010; Hann et al., 1989; Poritz et al., 1990) and among the different components of SRP, the SRP54 subunit is the most conserved. This subunit binds SRP RNA and has a hydrophobic signal binding cleft responsible for recognizing hydrophobic core of ER targeting sequences (High and Dobberstein, 1991; Janda et al., 2010; Zopf et al., 1990).

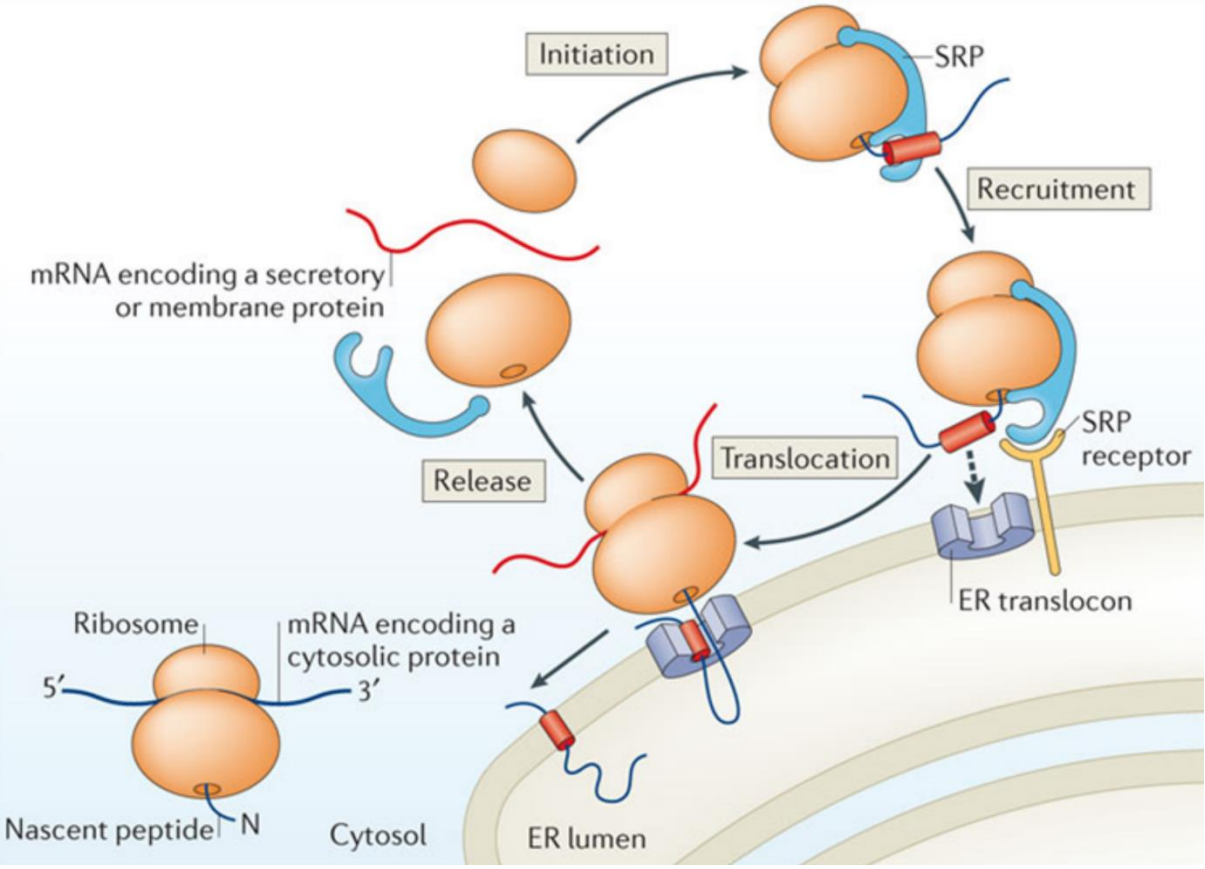

Figure 1: Protein delivery by signal recognition particle (SRP) to ER: Translation initiates in the cytoplasm and as the signal peptide or transmembrane domain (TMD) (of membrane or secretory proteins) emerges, it is bound by SRP and as a result, translation is halted. SRP targets the entire ribosome-nascent-chain complex (RNC) to ER at SRP receptor. Translation resumes and the newly synthesized protein is co-translationally inserted into ER via ER translocon. SRP recycles back into the cytoplasm for another round of co-translational substrate targeting. Figure adapted from (Reid and Nicchitta, 2015).

6.1.2 Signal recognition particle-Independent (SRP-Independent) pathways

Not all secretory and endomembrane proteins undergo SRP-dependent protein translocation to ER. This was first observed in yeast where fully translated proteins without the involvement of ribosome could translocate into ER. Additionally, yeast *(Saccharomyces cerevisiae)* cells are viable even without SRP (Hann and Walter, 1991; Waters and Blobel, 1986). One of the most prominent feature of SRP-targeted substrates is the strong hydrophobic nature of N-terminal sequences and the minimum required length of 70-80 N-terminal amino acid (aa) residues to be bound by SRP (Ast and Schuldiner, 2013; Ast et al., 2013; Hikita and Mizushimas, 1992; Yamamoto et al., 1987). In agreement with this, proteins having relatively mild hydrophobic N-terminal signal sequences (SS) and short secretory proteins (less than 70 aa in size) cannot engage SRP-dependent protein targeting (de Gier et al., 1998; Lee and Bernstein, 2001; Ng et

al., 1996; Schlenstedt and Zimmermann, 1987; Schlenstedt et al., 1992; Zimmermann et al., 1990). By looking at the hydrophobicity index, an *in silico* analysis predicted an estimated 20% of the yeast secretome to be SRP-independent (Ast et al., 2013). Similarly, tail anchored proteins, whose TMDs are at the very C-terminus (see below) and which act as ER targeting sequence, do not undergo SRP-dependent targeting because of the inaccessibility of their C-termini (Yabal et al., 2003).

The presence of mRNA on the cytoplasmic face of ER was long thought to be due to the docking of the SRP-guided RNC on the surface of ER. However, it has been shown that transcripts coding not only for secretory/endomembrane proteins but also several coding for cytoplasmic and nuclear proteins are present on the cytoplasmic face of ER (Ast and Schuldiner, 2013; Diehn et al., 2000, 2006; Reid and Nicchitta, 2012). Furthermore, knocking down SRP components, removal of signal sequence or translation inhibition could not severely diminish this mRNA patterning (Nevo-Dinur et al., 2011; Pyhtila et al., 2008; Ren et al., 2004). However, this mRNA patterning was lost when membranes were pre-treated at basic pH suggesting the involvement of membrane-bound factors in tethering mRNAs to the surface of ER (Pyhtila et al., 2008). In fact the RNA-binding protein (RBP) p180 in mammalian cells is shown to target mRNAs to ER in a ribosome free manner (Cui et al., 2012) and some RBPs in yeast influence mRNA localization to ER (Kraut-Cohen et al., 2013). Due to the above-mentioned reasons, several SRP-independent pathways have been identified and explored as discussed below.

6.1.2.1 GET pathway

The guided entry of tail-anchored proteins (GET) pathway in yeast targets tail-anchored (TA) proteins to ER (Schuldiner et al., 2008). The GET variant in mammalian cells is known as TRC40 pathway (Jonikas et al., 2009; Stefanovic and Hegde, 2007). TA proteins have a single TMD at the very C-terminus. The GET pathway can also target glycosylphosphatidylinositol (GPI)-anchored proteins whose C-terminal anchor sequence are comparatively hydrophobic to that of TA proteins (Ast et al., 2013). GET pathway components include Get1-5 and the cytosolic chaperone Sgt2p (Ast and Schuldiner, 2013; Chartron et al., 2012; Denic et al., 2013; Hegde and Keenan, 2011; Shao and Hegde, 2011). Substrates targeted to ER by the GET pathway are usually in a loosely folded state and need the chaperoning activity of Sgt2p (Ast and Schuldiner, 2013). The main component GET3 is a cytosolic ATPase, which exists as dimer and switches from “open” to “closed” state utilizing ATP hydrolysis. Get3p in open state creates a large hydrophobic groove which is thought to envelope the TMD of the TA protein

(Hu et al., 2009; Kubota et al., 2012; Mateja et al., 2009; Suloway et al., 2009). Once Get3p binds nascent TA proteins, it takes them to Get1p-Get2p receptor complex at the ER (Schuldiner et al., 2008; Vilardi et al., 2011; Yamamoto and Sakisaka, 2012). The Get3p (loaded with TA proteins) interaction with Get1p-Get2p receptor complex is very vital and believed to be initially mediated by the long flexible cytosolic arm of Get2p and subsequently by Get1p through its two rigid coiled-coils proximal to the ER membrane (Kubota et al., 2012; Mariappan et al., 2011; Stefer et al., 2011). The Get1p-Get2p receptor complex facilitates the alignment of TA proteins in close proximity to the ER membrane (Kubota et al., 2012).

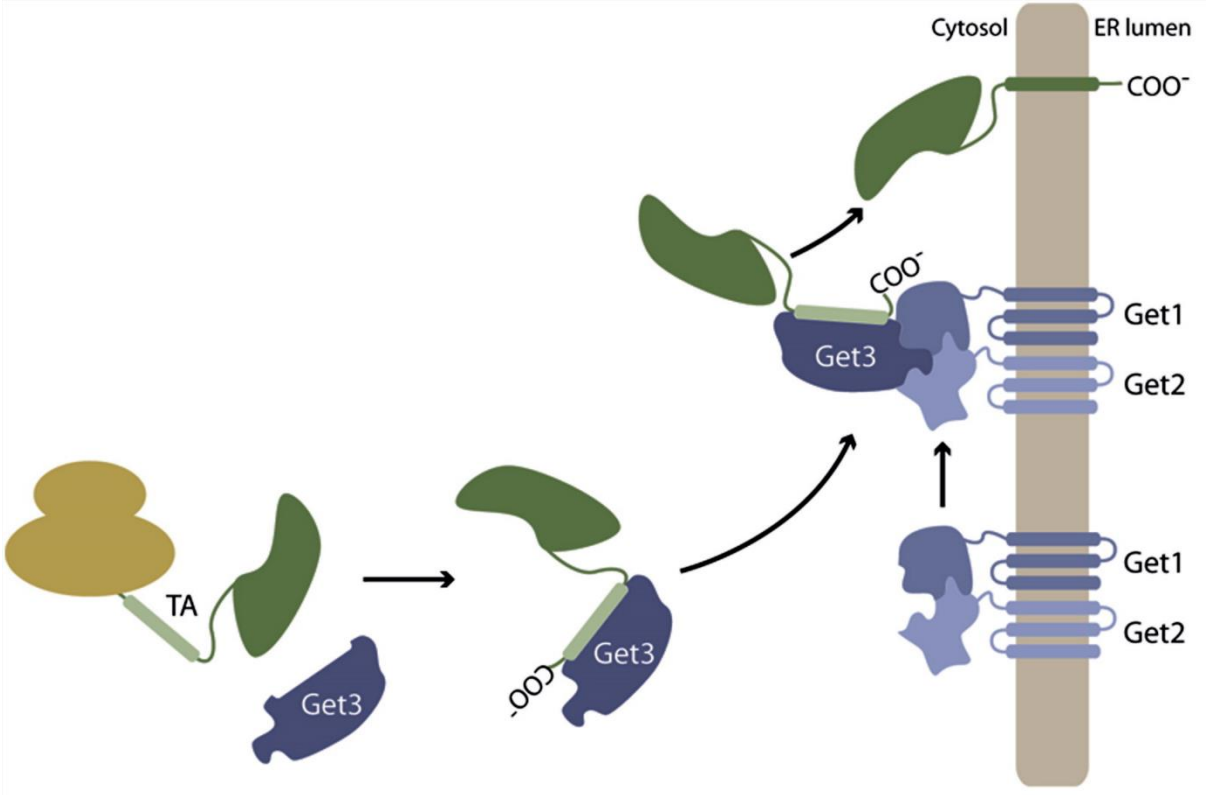

Figure 2: Schematic representation of tail-anchored (TA) proteins targeted by GET Complex: Get3p engages newly synthesized TA protein recognition in the cytoplasm and the Get3-substrate complex docks at ER via Get1p/Get2p complex and the protein is inserted in ER through yet unknown mechanism. Figure and text adapted from (Schuldiner et al., 2008).

The insertion of TA proteins in ER is not dependent on Sec61 translocon (Yabal et al., 2003) and one theory suggests that their insertion might be spontaneous as some TA proteins can insert themselves efficiently into protein-free liposomes (Ast and Schuldiner, 2013; Brambillasca et al., 2006). Another theory potentiates the involvement of TM domains of Get1p and Get2p by either forming a channel or by wedging the TM domain into the membrane through local membrane distortion (Ast and Schuldiner, 2013). How exactly GET pathway initially engages its substrates is still mystery, however, there is evidence that it might engage

them just after the translation as Get5p and Get4p are known to associate with ribosomes (Fleischer et al., 2006; Zhang et al., 2016).

6.1.2.2 SND pathway

SNDs, referring to SRP-independent targeting, are a set of three proteins namely Snd1p, Snd2p and Snd3p (Aviram et al., 2016). These SND proteins constitute the core component of a yet less characterized SRP-independent pathway of protein targeting to ER (Aviram et al., 2016). Snd1p is a cytosolic protein that is predicted to be associated with ribosomes (Fleischer et al., 2006; Huh et al., 2003), while Snd2p and Snd3p are predicted to have TMDs, with Snd2p having four and Snd3p with only one TMD (Huh et al., 2003; Ricarte et al., 2011). Both Snd2p and Snd3p are localized to ER and work in a complex (Aviram et al., 2016). It is believed that Snd1p recruits substrates and takes them to the ER membrane where it is received by Snd2p/Snd3p complex. SND engages its substrates in a co-translational manner. This is supported by proximity-based ribosome profiling, which has revealed that many transcripts are depleted at ER upon the deletion of SND components (Aviram et al., 2016). Evidence suggests that proteins in SND pathway are delivered to the SRP-independent translocon at ER (Aviram et al., 2016). A well-known substrate of the SND pathway is Gas1p, a Beta-1,3-glucanosyltransferase essential for cell wall assembly (Aviram et al., 2016; Tomishige et al., 2003). Gas1p is a glycosylphosphatidylinositol (GPI)-anchor protein that is targeted to ER for proper folding and post-translational modifications (Conzelmann et al., 1988; Nuoffer et al., 1991). Gas1p accumulates in the cytoplasm when SND components are deleted in *Saccharomyces cerevisiae* (Aviram et al., 2016). Although SND can work as a backup mechanism to both SRP and GET pathways, it preferentially engages substrates with downstream targeting sequences (TMDs) as oppose to N-terminal hydrophobic sequences (Aviram et al., 2016).

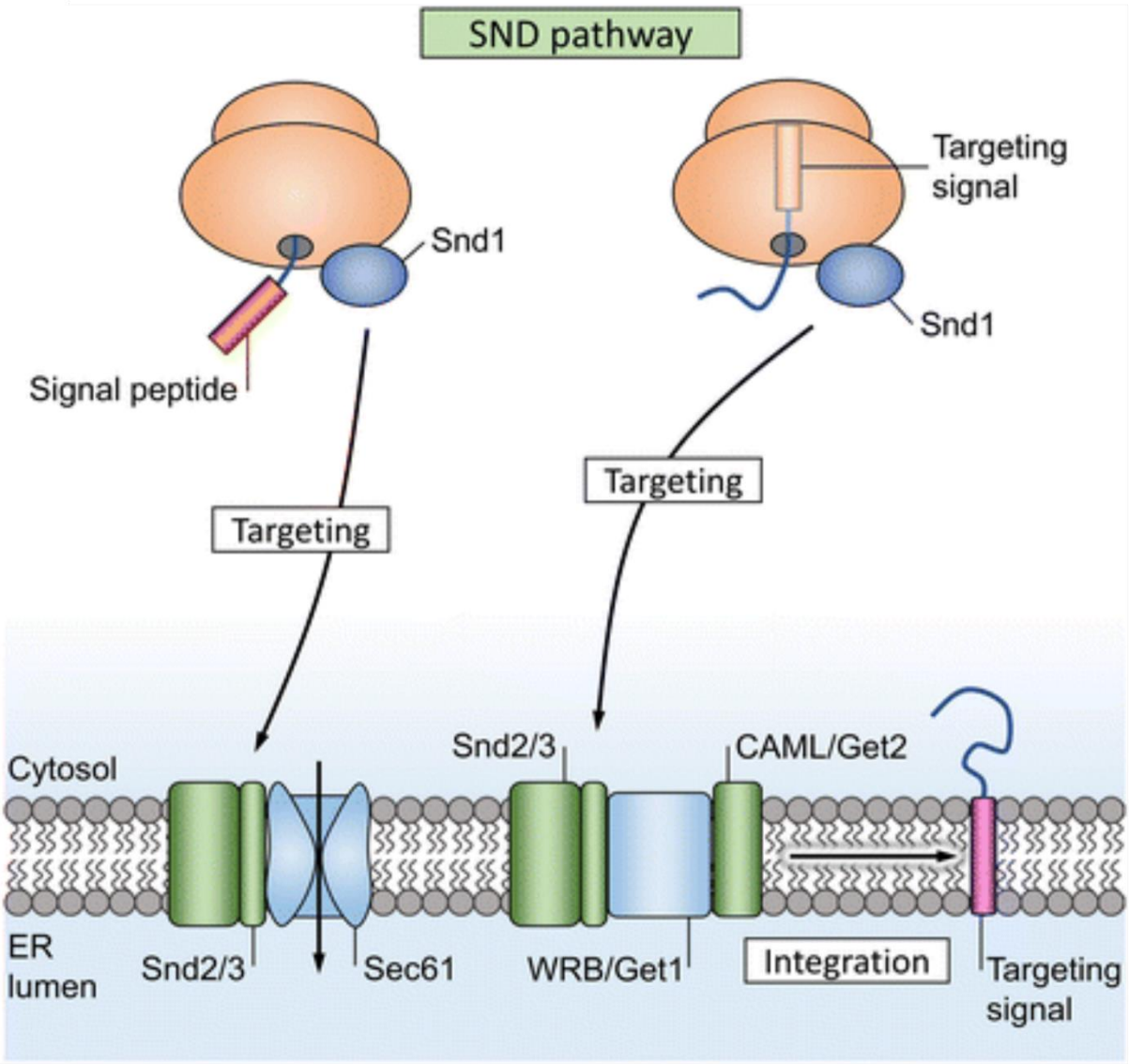

Figure 3: A schematic model of SND pathway acting as a backup to SRP and GET/TRC40 pathway for protein targeting to ER. On the right, SND is competing with GET pathway and on the left, it is competing with SRP for protein targeting to ER. Figure adapted from (Van Puyenbroeck and Vermeire, 2018).

6.1.2.3 A role of RNA-binding proteins in mRNA delivery to ER

RNA-binding proteins (RBPs) in general control key events in the life of an mRNA such as splicing, polyadenylation, export, localization, translation and mRNA turnover (reviewed in (Glisovic et al., 2008)). They generally possess structurally well-defined RNA binding domains (RBDs) such as RNA recognition motif (RRM) (Cléry et al., 2008), hnRNP K homology domain (KH) (Valverde et al., 2008)), Pumilio (Puf) (Edwards et al., 2001) or DEAD box helicase domain (Linder and Jankowsky, 2011). RBPs across different species have been identified that are involved in the asymmetric localization of mRNA (reviewed in (Herve et al., 2004; Niessing, 2013). Prominent examples include She2p in yeast, Rrm4 in *U. maydis*, ZBP1

in mammals, Staufen in *D. melanogaster*, and Vera in *Xenopus* (Herve et al., 2004; Niessing, 2013). This asymmetrical localization is mainly accomplished by the binding of RBPs to the *cis*-acting structural elements or sequences within the mRNA (Jambhekar and DeRisi, 2007) and the interaction of the RBPs with molecular motors. The unique RNA elements termed as Zipcodes or localization elements (LE) are usually present in the 3′ UTR of an mRNA but can also be found in the coding region (Jambhekar and DeRisi, 2007).

mRNAs coding for secreted or membrane proteins are usually delivered to ER as discussed above. However, it has been discovered that mRNAs coding for cytosolic and nuclear proteins having no signal sequences are also present on the surface of ER (Ast and Schuldiner, 2013; Diehn et al., 2000, 2006; Reid and Nicchitta, 2012). Interestingly, transcripts coding for membrane proteins are highly enriched in uracil in their coding regions (Prilusky and Bibi, 2009) and regions of the transcripts encoding signal sequences have less adenines (Palazzo et al., 2007). For some transcripts such as *PMP1* in *Saccharomyces cerevisiae*, the 3′ UTR sequence is sufficient to deliver mRNA to ER (Loya et al., 2008). This suggests the involvement of *cis*-acting mRNA sequences and *trans*-acting protein factors such as RBPs in mRNA delivery to ER. In fact, the mammalian RBP p180 can target mRNAs to ER in a translation-independent manner (Cui et al., 2012). Furthermore, some RBPs in yeast preferentially bind transcripts coding for secretory and membrane proteins (Hogan et al., 2008) and the deletion of some RBPs such as She2p or Puf2 even leads to partial loss of mRNA localization such as *SUC2* at ER (Kraut-Cohen et al., 2013).

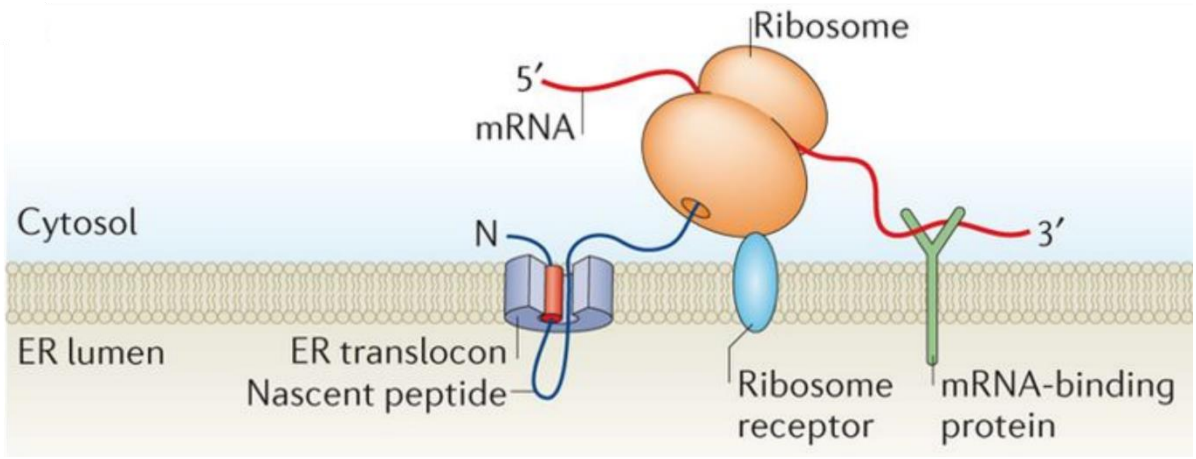

Figure 4: The well-known mode of ribosomes and mRNAs association with ER is via SRP. Several other modes of ribosomes and mRNAs associations with ER have also been described. Ribosomes may associate with the ER independently of their encoded nascent chain and with mRNAs subsequent to their association with an ER ribosome receptor. In addition, RNA-binding proteins can confer direct, ribosome-independent mRNA binding. This system requires that only one of these components bind to the ER to enable assembly of an entire polyribosome, and it is also possible that a polyribosome is

targeted to the ER via multiple mechanisms in parallel. Figure and text adapted from (Reid and Nicchitta, 2015).

6.2 RNA-binding proteins in the current study

6.2.1 She2p

She stands for Swi5p-dependent *HO* Expression (Jansen et al., 1996). She2p is an RBP that shuttles between nucleus and cytoplasm (Du et al., 2008). In functional form it exists as homotetramer (Chung and Takizawa, 2010; Muller et al., 2009). which is responsible for the transport of mRNAs to the bud in a dividing yeast cell (Aronov et al., 2007a; Hasegawa et al., 2008; Oeffinger et al., 2007; Shepard et al., 2003). She2p is known to interact with ER and is an essential part of coordinated co-migration of tubular ER structures with bud-localized mRNAs to the tip of the bud during cell division (Aronov et al., 2007b; Fundakowski et al., 2012; Schmid et al., 2006). She2p is primarily known as the RBP that is involved in the asymmetrical localization of *ASH1* (asymmetric synthesis of *HO*) in *Saccharomyces cerevisiae* (Jansen et al., 1996) that codes for a transcriptional repressor of site-specific endonuclease HO (HOmothallic switching) (Cosma, 2004). Yeast has two mating types (MATa and MATα), determined by their expression from MAT gene locus. The genomic rearrangements at MAT locus by HO leads to mating type switching (Herskowitz, 1988; Nasmyth, 1982). The mating-types can only switch in mother cells since *HO* gene is repressed in daughter cells or buds through the asymmetric or bud localization of *ASH1* (Bobola et al., 1996; Cosma, 2004; Sil and Herskowitz, 1996). The asymmetric localization of *ASH1* requires the expression of five She genes, She2p being one of them (Jansen et al., 1996). She1p or Myo4p is a type V motor protein that moves along actin cables to transport messenger ribonucleoprotein (mRNP) complexes (Bertrand et al., 1998; Haarer et al., 1994; Münchow et al., 1999; Takizawa and Vale, 2000). She3p is an RBP (Müller et al., 2011) that connects the She2p-mRNA complex to Myo4p (Münchow et al., 1999; Takizawa and Vale, 2000). She4p is a protein that binds to some motor myosins including She1p/Myo4p (Toi et al., 2003; Wesche et al., 2003) and She5p/Bni1p is a septin protein required for cytokinesis (Cosma, 2004).

The core components of She complex are She2p, the adapter protein She3p and motor protein Myo4p (Bohl et al., 2000). The entire RNA-She complex known as locasome transports more than 30 mRNAs to the bud during or before mitosis (Aronov et al., 2007a; Hasegawa et al., 2008; Oeffinger et al., 2007; Shepard et al., 2003). *ASH1* contains four localization elements, three in the coding region and one in the 3′ UTR (Chartrand et al., 1999; Gonzalez et al., 1999; Jambhekar et al., 2005; Olivier et al., 2005). She2p binds these elements of *ASH1* co-

transcriptionally (Bohl et al., 2000; Du et al., 2008; Jansen et al., 1996; Long et al., 2000; Shahbabian et al., 2014). This binding is relatively weak but is stabilized by the binding of Loc1p (Long et al., 2001; Niedner et al., 2013). Once this premature mRNP complex is exiting the nucleus, it is loaded with additional proteins including She3p/Myo4p (She3p is constitutively bound to Myo4p), translational repressors such as Dhh1p, Khd1p and Puf6 (Bohl et al., 2000; Dunn et al., 2007; Gu et al., 2004; Hasegawa et al., 2008; Heuck et al., 2007, 2010; Irie et al., 2002; Ito et al., 2011; Jansen et al., 1996; Krementsova et al., 2011; Long et al., 2000; Müller et al., 2011; Niedner et al., 2013; Shi et al., 2014; Takizawa and Vale, 2000; Zhang et al., 2017). Loc1p in the mRNP complex is replaced by She3p and returns back to nucleus (Komili et al., 2007; Long et al., 2001; Urbinati et al., 2006). Once the matured mRNP has reached its destination (the tip of the bud), Khd1p and Puf6p are phosphorylated by Yck1p or Yck2p, respectively (Deng et al., 2008; Paquin et al., 2007), thereby releasing translational repression.

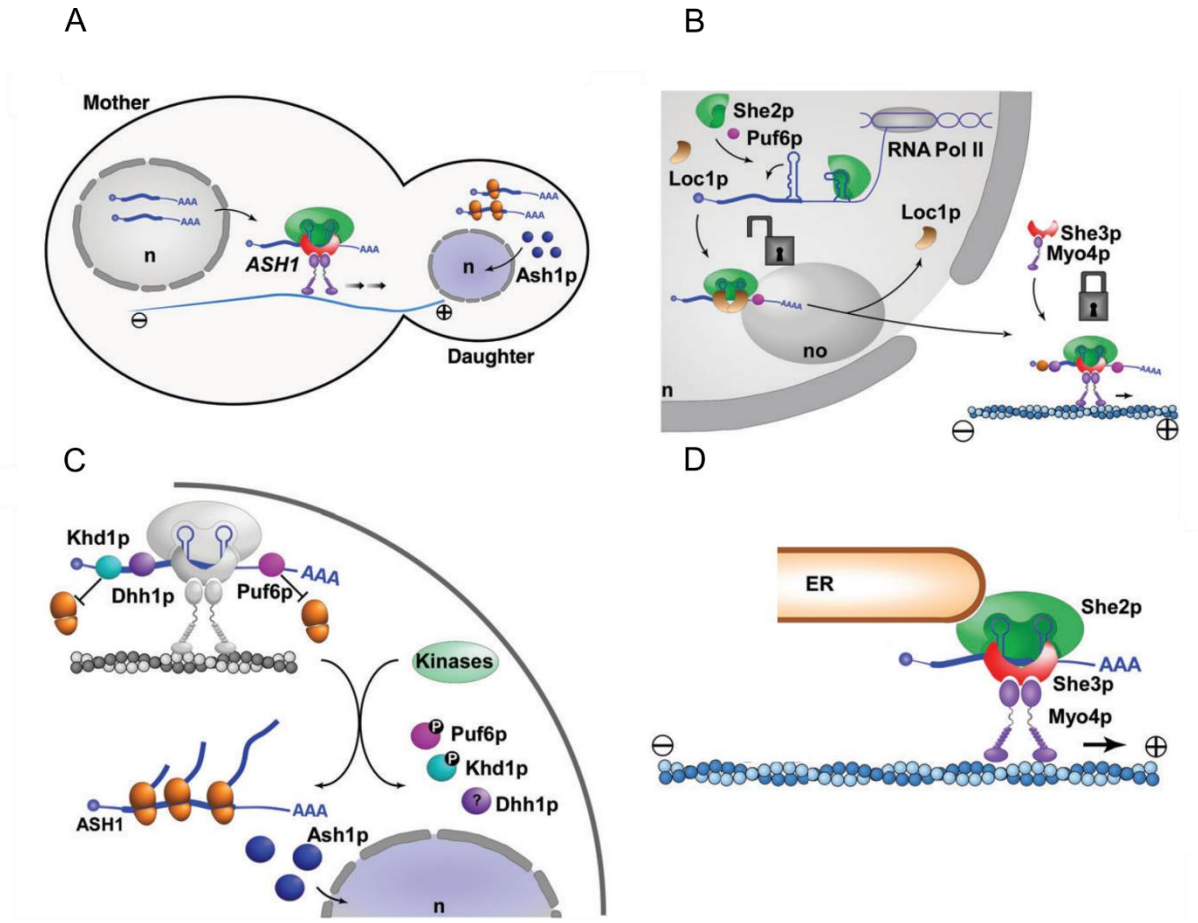

Figure 5: (A) Transport of *ASH1* along actin filaments to the daughter cell during mitosis. Upon expression, Ash1 localizes to nucleus to inhibit HO endonuclease expression. (B) mRNP assembly in the nucleus. She2p co-transcriptionally binds *ASH1* along with Loc1p and Puf6p. This complex has modest specificity (open lock). Upon transition of the nucleolus (no), export and binding by She3p the

mRNP is remodelled and locked in its transport competent form. (C) In the process of transport to the bud, *ASH1* is translationally supressed by Khd1p, Puf6p and Dhh1p. Once the entire mRNP complex has arrived at the tip of the bud, Khd1p and Puf6p are phosphorylated, thereby releasing translational repression. (D) She2p association with ER. She2p specifically binds ER tubules by recognizing their membrane curvature as well as by potentially interacting with an ER-associated orphan adaptor protein. Figure and text adapted from (Niessing et al., 2018).

6.2.2 Whi3p

Whi3 (WHIskey) was initially identified as the protein whose deletion leads to small cell size in yeast (Nash et al., 2001). It has an N-terminal region that is essential for Cdc28p recruitment and a C-terminal RNA recognition motif (RRM) that regulates *CLN3* (Garí et al., 2001; Wang et al., 2004). Cln3p is the most upstream activator of cell cycle entry in yeast (Garí et al., 2001). Whi3p negatively regulates *CLN3* in two ways. First it directly binds via its C-terminal RRM to *CLN3* and sequesters it to cytoplasmic foci, thereby locally restricting Cln3 synthesis. Secondly, it physically interacts with Cdc28p and thereby retains Cdc28p-Cln3p complexes in the cytoplasm in the early G1 phase (Garí et al., 2001; Wang et al., 2004). Whi3p has no obvious effect on mRNA and protein level of Cln3 (Garí et al., 2001). Since yeast cells deficient of Whi3p bud and enter S-phase at smaller cell volume, it is believed that Whi3p functions in controlling cell size and the G1 to S-phase transition (Garí et al., 2001). Indeed, overexpression of Whi3p leads to a lethal G1 arrest with an increase in cell volume (Nash et al., 2001). This G1 arrest is dependent on the RRM (Garí et al., 2001). Constitutive expression of *CLN2* can suppress the G1 arrest but not lethality (Garí et al., 2001). Whi3p also plays a role in mating response, filamentous growth and meiosis (Garí et al., 2001; Mösch and Fink, 1997; Nash et al., 2001). Additionally, Whi3p deletion has been implicated in cell wall phenotypes and an increase in poly-ploidy (Colomina et al., 2008; Schladebeck and Mösch, 2013). Whi3p localizes to cytoplasm and ER and several of its mRNA targets encode ER, membrane, secretory and cell cycle related proteins (Colomina et al., 2008; Vergés et al., 2007). The sequence GCAU might represent the RNA consensus motif in Whi3p target mRNAs (Colomina et al., 2008).

In *Saccharomyces cerevisiae*, processing bodies or P-bodies are factories of RNA degradation (Hilgers et al., 2006; Sheth and Parker, 2003). They exist both during steady-state and stress conditions and are associated with decapping and decay machinery (Balagopal and Parker, 2009; Sheth and Parker, 2003; Teixeira et al., 2005). The number of P-bodies increase during stress and they can nucleate the formation of related structures known as stress granules (Holmes et al., 2013). Though both P-bodies and SGs have overlapping common components

and functions, SGs only appear during stress and encompass more RNA processing proteins as compared to P-bodies including translation initiation factors, 40S ribosomal subunits, and stability-promoting RBPs (Anderson and Kedersha, 2008; Buchan et al., 2008; Erickson and Lykke-Andersen, 2011). Whi3p binds SGs during starvation and heat shock, but its deletion has no effect on SG formation (Holmes et al., 2013). Whi3 also localizes to P-bodies during mild heat shock (Holmes et al., 2013). Deletion of Whi3 leads to an increase in the level of its mRNA targets suggesting the involvement of Whi3 in the degradation of its target mRNAs (Holmes et al., 2013).

6.2.3 Mrn1p

Mrn1 was originally named as multi-copy suppressor of *rsc nhp6ΔΔ* as it's over expression repressed the synthetic sickness caused by the *rsc nhp6ΔΔ* mutation (Düring et al., 2012). Mrn1p is an RNA-binding protein with five classical RNA recognition motifs or RRMs (Düring et al., 2012). In addition, it contains repetitive single amino acid (aa) rich regions like asparagine (between aa 6 and 28), glutamine (between aa 98 and 125) and alanine (between aa 171 and 189; between aa 402 and 422). Mrn1p is predominantly cytoplasmic with a small fraction localized to the nucleus (Düring et al., 2012). *MRN1* genetically interacts with chromatin remodelling complexes (RSC or SWI/SNF), genes that encode chromatin architectural proteins (*NHP6A* and *NHP6B*) and splicing factors such as *PRP4* and *PRP3* (Costanzo et al., 2010; Düring et al., 2012; Stillman, 2010). *MRN1* is also known to genetically interact with *SNT309*, a member of the NineTeen Complex or NTC (Chen et al., 1998; Düring et al., 2012). The NTC is an integral part of active spliceosomes from yeast to humans (Hogg et al., 2010). Over expression of Mrn1p rescues the temperature sensitive phenotypes of *prp22*, *prp4-1*, *prp3-1*, *snt309Δ* and additionally the phenotypes associated with *swi/snf* and the *rsc nhp6ΔΔ* (Düring et al., 2012). Based on the these observations, Mrn1p has a proposed role in mRNA maturation in yeast (Düring et al., 2012).

Under stress conditions, Mrn1p localizes to stress granules (SG) (Jain et al., 2016), processing bodies (P-bodies) (Mitchell et al., 2013) and inclusion bodies (IBs) and once the stress is over, it can partially remove the IBs from the cell (Moldavski et al., 2015). Mrn1p binds hundreds of RNAs including those with short upstream open reading frames (uORFs) and internal ribosome entry sites (IRES) (Hogan et al., 2008). Among the most enriched gene ontology (GO) terms for Mrn1p mRNA binders are cell wall, plasma membrane and ER proteins (Hogan et al., 2008). Mrn1p physically interacts with other RBPs such as Pab1p and Nab6p (Collins et al., 2007; Hogan et al., 2008). Given the fact that Mrn1p physically interacts with Pab1p and

binds mRNAs subjected to extensive translation regulation, it is proposed that Mrn1p might be involved in translational regulation (Hogan et al., 2008).

6.2.4 Ngr1p

Ngr1, also known as negative growth regulatory protein 1 (Ngr1), is an RNA-binding protein with three RRMs, a C-terminal asparagine-methionine-proline-rich, and two glutamine-rich regions (Buu et al., 2004; Lee and Moss, 1993). Ngr1p is predominantly a cytoplasmic protein that concentrates around the perinuclear region (Buu et al., 2004). *NGR1* is a nonessential gene but its disruption leads to an increase in cell growth in early log phase and when overexpressed, it slows down cell growth (Lee and Moss, 1993). Ngr1p is known to interact *in vivo* with the cytoplasmic DEAD-box helicase Dhh1p via Dhh1p's non-conserved C-terminal region and this interaction is believed to promote the decay of the porin *POR1* mRNA in P-bodies (Chang and Lee, 2012; Jang et al., 2006). In fact, Ngr1p *in vivo* interacts with *POR1* 3′ UTR (likely via a (C/G)U-rich region) and its overexpression enhances the degradation of *POR1* mRNA (Buu et al., 2004). The *POR1* degradation by Ngr1p requires all the three RRMs of Ngr1p (Buu et al., 2004). Though Dhh1p is a component of P-bodies (Sachdev et al., 2019), Ngr1p recruitment to P-bodies does not require Dhh1p, but rather depends on the integrity of an Ngr1p complex through C-terminal self-interaction and unidentified signals at the N-terminus in the Ngr1p (Jang et al., 2006). Additionally, the overexpression of Ngr1p causes mitochondrial phenotype as cells are unable to grow on glycerol containing medium (Buu et al., 2004). Ngr1p is also known to localize to stress granules (SGs) but its deletion has no effect on SG formation (Buchan et al., 2008).

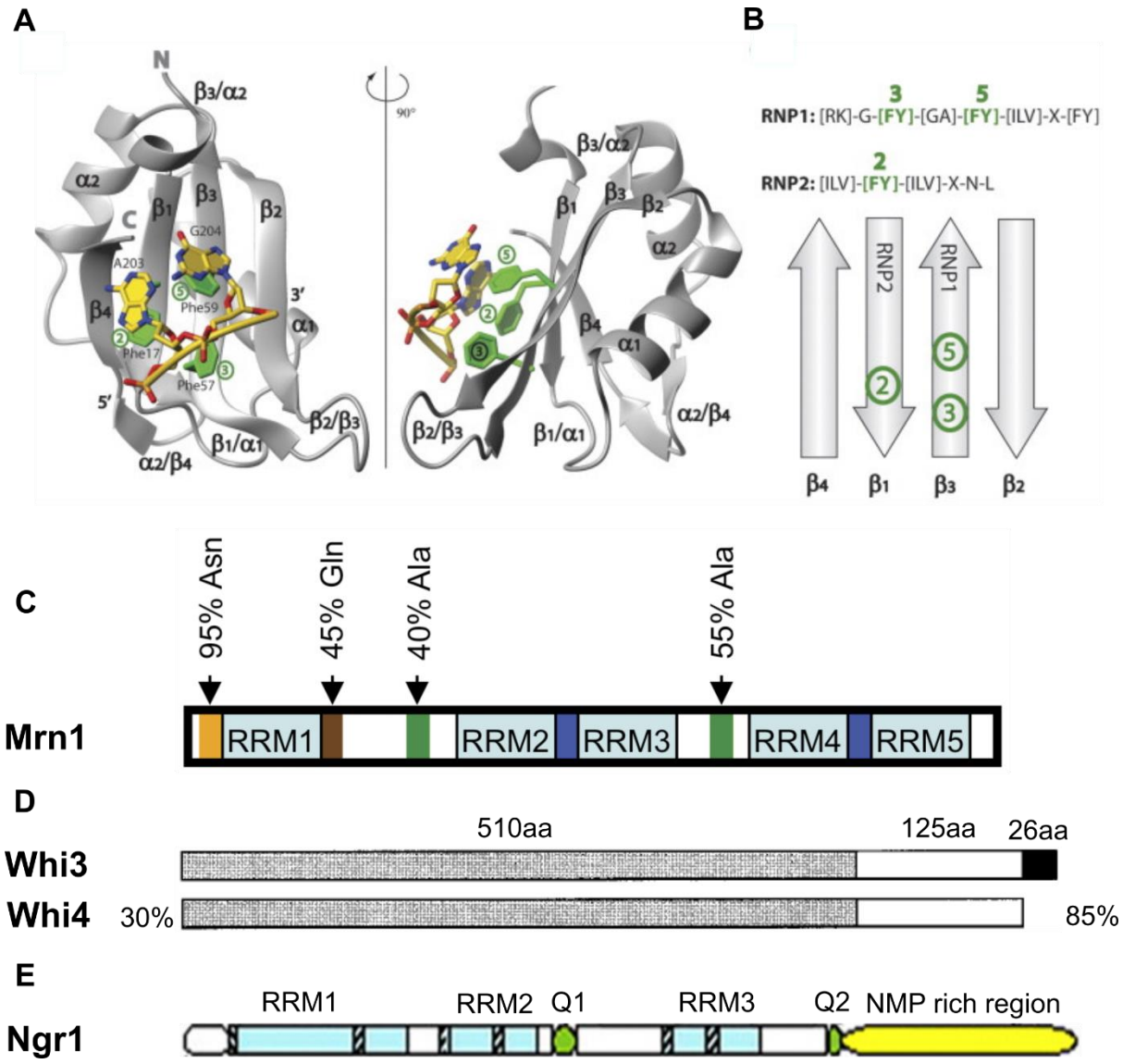

Figure 6: (A) and (B) RRM β-sheet interaction with RNA. **(A)** Structure of hnRNP A1 RRM2 in complex with single stranded telomeric DNA as a model of single stranded nucleic acid binding (Ding et al., 1999). **(B)** Scheme of the four-stranded β-sheet with the place of main conserved RNP1 and RNP2 aromatic residues indicated in green. RNP1 and RNP2 consensus sequences of RRMs are shown (X is for any amino acid). Figure and text adapted from (Cléry et al., 2008). (C) Mrn1p with 5 RRMs and multiple single amino acid rich regions. Figure adapted from (Düring et al., 2012). (D) Whi3p and its paralog Whi4p. Whi3p has three domains: a long N-terminal domain (shaded); a C-terminal RNA RRM domain (white); and a C-terminal tail (black). The percentage identity of Whi3p with Whi4p is shown, with identity to the N-terminal domain shown on the left and identity to the RNA-binding domain on the right. Figure and text taken from (Nash et al., 2001). (E) Ngr1p with three RRMs, two poly-Q rich and asparagine/methionine/proline-rich (NMP) C-terminal region. Figure adapted from (Jang et al., 2006).

6.2.5 Khd1p/*HEK2*

Khd1p, also known as *HEK2* (HEterogeneous nuclear rnp K-like gene), is an RNA-binding protein with K homology (KH) domains (Denisenko and Bomsztyk, 2002). The KH domain

was first identified in human heterogeneous nuclear ribonucleoprotein K (hnRNP K) (Siomi et al., 1993a). KH domains are found in diverse organisms and generally consist of 70 amino acids (Ashley et al., 1993; Grishin, 2001; O'Donnell and Warren, 2002; Siomi et al., 1993a, 1993b). There are two kinds of KH domains, Type I and Type II. (Grishin, 2001). Both share a minimal KH sequence motif but differ in the arrangement of secondary structural elements in the 3 dimensional (3D) structure (Grishin, 2001) as shown in figure. All typical KH domains contain the GXXG amino acid motif (Grishin, 2001). Khd1 has three KH domains and a known phosphorylation site at the C-terminus (Paquin et al., 2007) as shown in figure 7B.

Multiple functions have been reported for Khd1p. It binds hundreds of mRNAs including those coding for nuclear core complex (NPC), cell wall and membrane-associated proteins and also to the majority of the known bud localized mRNAs (Hasegawa et al., 2008; Hogan et al., 2008; Rouvière et al., 2018). Khd1p is primarily perceived as translational repressor, especially in the case of *ASH1* mRNA localization (Irie et al., 2002) and mRNAs coding for NPC components (Rouvière et al., 2018), its deletion however leads to the reduced expression of at least one gene such as *MTL1* (Hasegawa et al., 2008). This probably implies that Khd1p is differentially regulating its mRNA targets (Hasegawa et al., 2008). During the asymmetric localization of *ASH1* to the tip of the bud, Khd1p interacts with the E1 localization element of *ASH1* and with the C-terminal domain of translation initiation factor eIF4G1, perhaps constraining its translational activity (Paquin et al., 2007). Khd1 is phosphorylated by casein kinase Yck1p at the plasma membrane so that *ASH1* can be translated in the bud (Paquin et al., 2007). Additionally, Khd1p has also been linked to the structural and functional organization of telomeric chromatin (Denisenko and Bomsztyk, 2002).

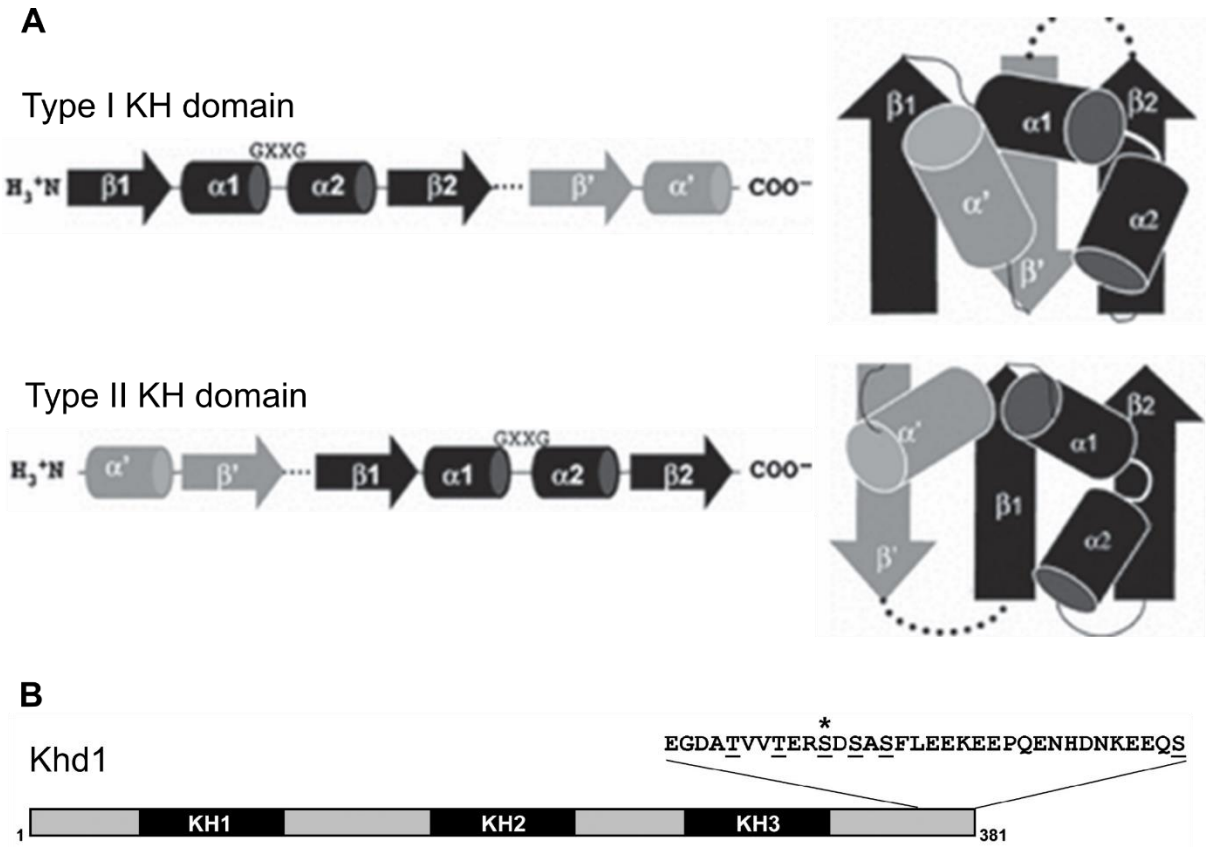

Figure 7: (A) Type I and type II KH domains fold. Secondary structures in black represents KH minimal motif, the line connecting helices α1 and α2 as the GXXG loop and the dotted line connecting the β2-strand and β′-strand represents the variable loop. Figure and text adapted from (Valverde et al., 2008). (B) Khd1p with three KH domains. The asterisk represents the phosphorylation site indetified by Chi et al., 2007. Figure adapted from (Paquin et al., 2007).

6.2.6 Pbp2p/*HEK1*

Pbp2 (Pbp1 bind protein) or Hek1, is another RNA-binding protein with three KH domains (Denisenko and Bomsztyk, 2002; Mangus et al., 1998). Pbp2p is usually found in the cytoplasm but under stress conditions is found in both cytoplasm and nucleus (Mitchell et al., 2013). It is a less well characterized RBP with fewer than ten known mRNA targets (Hogan et al., 2008), one of which is *COX1* mRNA (Klimek-Tomczak et al., 2004). It binds poly C and poly U RNA sequences (Denisenko and Bomsztyk, 2002). It is also known to interact with poly-A binding protein Pab1 via its C-terminal region (Mangus et al., 1998; Richardson et al., 2012). Its known functions include the regulation of telomeric positioning effect and telomere length (Denisenko and Bomsztyk, 2002) and to resist antimalaria drug mefloquine (Delling et al., 1998).

6.2.7 Nab6p

Nab6 (Nucleic Acid Binding protein 6; (Samanta and Liang, 2003) is an RNA-binding protein having one classical and two fungal-specific RRMs (Kramer et al., 2014). Among its mRNA

targets are those encoding cell wall proteins (Hogan et al., 2008). It physically interacts with poly (A) polymerase Pap1p (Ezeokonkwo et al., 2012) and it is believed that Nab6p recruits Pap1p to a core *cis*-sequence GUUCG/U in the 3′ UTR of some of its target mRNAs to enhance mRNA stability and protein production (Ito et al., 2016). The deletion of Rrp6, a subunit of nuclear exosome complex, leads to growth phenotype and the accumulation of processing intermediates for nuclear RNAs (Abruzzi et al., 2007). Nab6p overexpression partially rescues the *rrp6Δ* growth phenotype but cannot recover the yeast cells from the accumulation of nuclear RNA processing intermediates (Abruzzi et al., 2007). Nab6 is known to genetically interact with mRNA 3' end processing factors (Rna14 and Pcf11), co-purify with nuclear cap-binding protein Cbp20p, found in complexes containing translation factors such as EIF4G and lastly, it binds poly adenylated RNAs giving a hint of its possible role in processing, export, stability and/or in the translation of a specific set of mRNAs (Abruzzi et al., 2007; Anderson et al., 1993; Colot et al., 1996).

6.2.8 Puf1p and Puf2p

RNA-binding proteins known as PUF proteins are present across all eukaryotic domains. The name PUF is derived from *Drosophila* Pumilio and *C. elegans* fem-3 binding factor (FBF) (Zamore et al., 1997; Zhang et al., 1997). PUFs have conserved RNA-binding domain (PUM-HD) containing eight alpha helical repeats of a 36-amino acid sequence with short flanking regions. The canonical PUF binding motif is found in the 3′ UTR of an mRNA and is 8-11 nucleotide long with the core sequence UGUR (Yosefzon et al., 2011). Structural studies from different organisms show very similar interaction of PUFs with its target mRNAs. Each repeat in a PUM domain forms a three-helix structure which stacks with one another to form a crescent. The inner side of crescent contacts RNA and the outer surface is believed to interact with proteins (Edwards et al., 2001; Miller et al., 2008; Wang et al., 2001, 2002, 2009; Zhu et al., 2009).

Yeast Puf1p and Puf2p are paralogs and show 35% identical sequence along their entire length. Both RBPs have one C-terminal pumilio homology and an N-terminal classical RRM (RNA recognition Motif) domain. Both proteins are usually found in the cytoplasm. Under stress conditions, Puf1p localizes to cell wall, while Puf2p remains in the cytoplasm or is localized to processing bodies (P-bodies) or stress granules (SG) (Mitchell et al., 2013). Each can bind to over 100 mRNAs with a preference for those encoding plasma membrane proteins (Hogan et al., 2008). They bind to a consensus RNA motif ($UAAU_{0-6}UAAU$) mostly found in the 3′ UTR, which is different from the canonical PUF binding motif (Yosefzon et al., 2011). The

majority of the transcripts bound by Puf1p can also interact with Puf2p and vice versa (Gerber et al., 2004). A prime example of a Puf2p binding transcript is *PMP2* with the UAAUAAUUAAU sequence motif in its 3′ UTR. The minimal sequence motif for Puf2p binding is 11 nucleotides (Yosefzon et al., 2011). The RRM domain in Puf2p is not essential for dual motif binding (Yosefzon et al., 2011). Mutating some of the conserved amino acids (Asn 591, Thr 592, Thr 627, and Trp 628) in PUF repeats results in the loss of RNA-binding function of Puf2 (Yosefzon et al., 2011). Puf1p was first identified in a study where its overproduction caused suppression of temperature sensitive tubulin mutation phenotype (Machin et al., 1995). It has been reported that Puf1p recruits Arp2/3 complex to mitochondria and its potential role in actin-based mitochondrial movement in yeast (Fehrenbacher et al., 2005). Additionally, Puf1p together with Puf5p in yeast bind to the 3′ UTR of *TIF1* to initiate its decay (Ulbricht and Olivas, 2007).

6.2.9 Slf1p

The La motif (LAM) is a conserved RNA-binding domain, consisting of 90 amino acids, found across various eukaryotic species (Chambers et al., 1988; Van Horn et al., 1997; Lin-Marq and Clarkson, 1995; Yoo and Wolin, 1994). LAM consists of six α-helices and a three-stranded antiparallel sheet (Dong et al., 2004) as shown in figure 9A. The secondary structures are arranged in such a way that helices H1 (long), H1′ (short) and H2 (short) precede the β-strand B1 and helices H3, H4, and H5 reside between β-strands B1 and B2 (Dong et al., 2004). The conserved aromatic amino acids on the surface of LAM are critical for RNA binding (Dong et al., 2004) as shown in figure 9B. A true La protein has LAM domain and one or more RRM domains and is primarily localized to nucleus where it binds the high-affinity terminal 3′UUU-OH motif of RNA polymerase III transcripts (Stefano, 1984; Wolin and Cedervall, 2002). Beside typical or true La proteins, a large number of RNA-binding proteins (RBP) known as La related proteins or LARPs exist in different organisms (Bayfield et al., 2010; Bousquet-Antonelli and Deragon, 2009). Although most of them share a common feature of having a conserved LAM and one or more RRM domains, they instead bind poly adenylated RNAs and ribosomes (Aoki et al., 2013; Yang et al., 2011).

Yeast has three La proteins, Lhp1 being a true La ortholog, while Slf1 (SuLFide production) and Sro9 (Suppressor of rho3) are atypical-LARPs (Kagami et al., 1997; Sobel and Wolin, 1999; Yu et al., 1996). Both Slf1p and Sro9p are paralogs and are essential for survival under stress conditions (Kershaw et al., 2015; Yu et al., 1996). Both harbor a central La motif (LAM) but no RRM domain and share 37% sequence identity at amino acids level. They both interact

with poly A binding protein (Pab1) and translating ribosomes and hence it is proposed that they might have a role in the translation activation and/or stability of their mRNA targets (Aoki et al., 2013; Bayfield et al., 2010; Kershaw et al., 2015; Sobel and Wolin, 1999; Yang et al., 2011).

During normal growth conditions Slf1p binds to up to 500 transcripts. This number dramatically increases to over a thousand transcripts following stress response (Kershaw et al., 2015). The gene ontology (GO) terms for Slf1p bound transcripts post stress are enriched for oxidative stress response, mitochondrial function, electron transport and protein synthesis (Kershaw et al., 2015). Hence, Slf1p might participate in the translation of transcripts required to cope with oxidative stress. Indeed, mass spectrometry analysis of a *slf1Δ* strain during oxidative stress revealed a decrease in the expression of stress response related genes (Kershaw et al., 2015). *SLF1* mRNA has a binding site in its 3′ UTR (just after stop codon) for Puf3p and it is thought that Puf3p might repress *SLF1* translation (Chatenay-Lapointe and Shadel, 2011). Although Slf1p deletion does not interfere with mitochondrial function, it overexpression however increases mitochondrial respiration (Chatenay-Lapointe and Shadel, 2011).

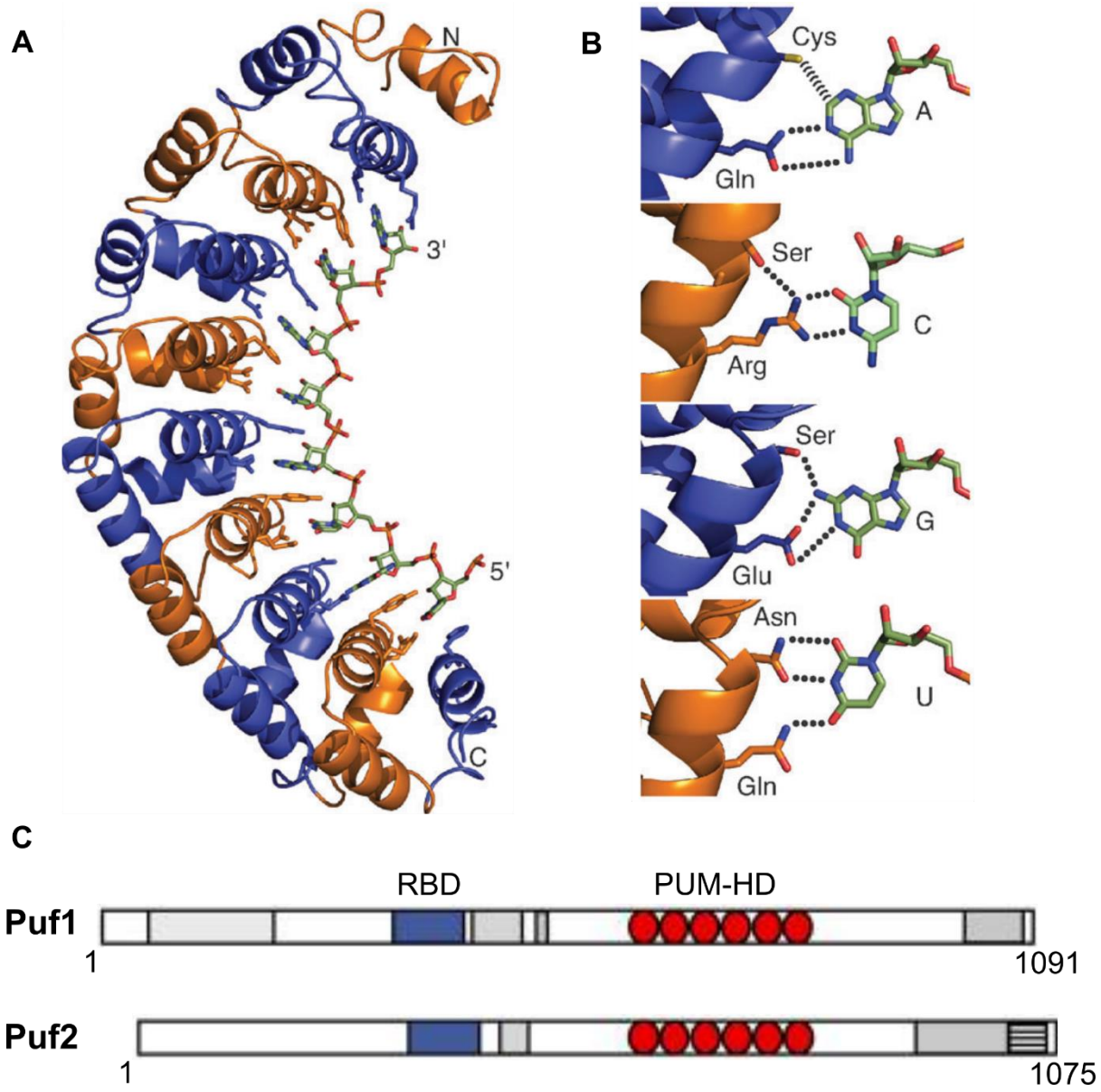

Figure 8: (A) Crystal structure of a PUF repeat of human Pumilio 1 (PDB accession code 2YJY) (Dong et al., 2011). (B) Recognition of adenine, cytosine, guanine, and uracil by PUF repeats in the crystal structure of a mutant PUM1 (Dong et al., 2011). Figure and text adapted from (Filipovska and Rackham, 2012). (C) Schematic representation of protein domains in Puf1p and Puf2p. Pum-HD repeats (Zamore et al., 1997) are shown as red ovals and classical RNA-binding domains (RBDs) are depicted as blue boxes. Regions of low complexity, such as proline-, serine-, threonine-, and/or methionine-rich domains, are shown in grey boxes; asparagine stretches are striped. The numbers correspond to the length of proteins in amino acids. Figure and text adapted from (Gerber et al., 2004).

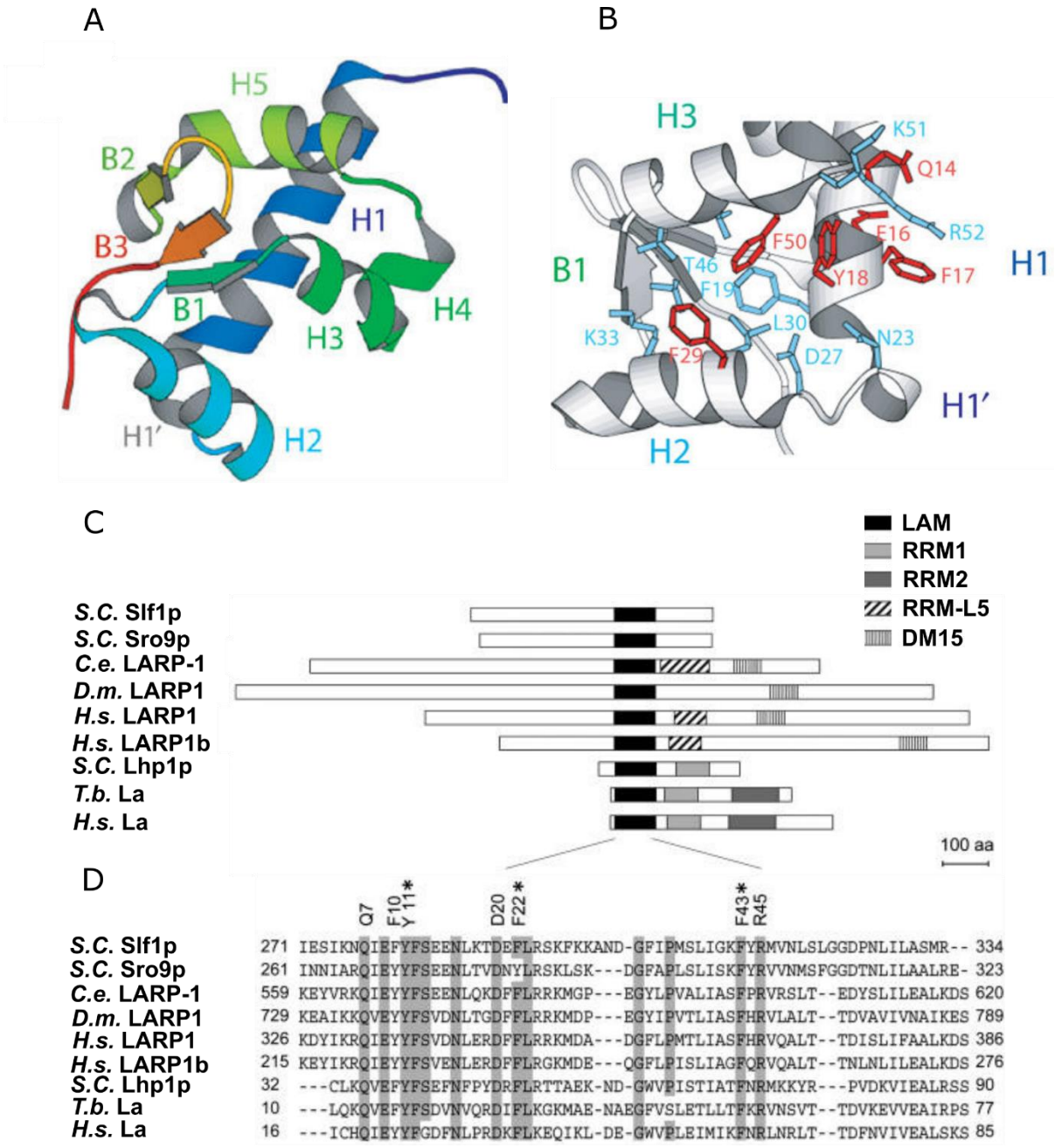

Figure 9: (A) and (B): (A) Ribbon views of the LAM of T. brucei and (B) a rendering of the aromatic patch conserved in all LAM proteins. Mutating the residues depicted in red eliminated La binding to pre-tRNA. Figures and text adapted from (Dong et al., 2004). (C) and (D): (C) Comparison of La proteins across different species and (D) multiple sequence alignment of LAMs. Residues that are >80% conserved are boxed in grey. Asterisks represent aromatic residues critical for RNA binding in Slf1p as described in (Schenk et al., 2012). Species name abbreviations are as follows: *S.c.*, *Saccharomyces cerevisiae*; *C.e.*, *Caenorhabditis elegans*; *D.m.*, *Drosophila melanogaster*; *H.s.*, *Homo sapiens*; and *T.b.*, *Trypanosoma brucei*. Figures and text adapted from (Schenk et al., 2012).

7. Aims of this work

The current thesis work is based on three separate projects:

1. **To find RNA-binding proteins (RBPs) that associate with ER and investigate if they had any role in mRNA localization and/or translation at ER in yeast:** Membrane/secretory proteins are delivered to ER either co- or post-translationally. SRP is known to target membrane/secretory proteins to ER co-translationally. Additionally, ER-associated RBPs have been identified in yeast and mammals that affect mRNA localization at ER. Here I aimed to identify additional RBPs in *Saccharomyces cerevisiae* that associate with ER. By using a combination of imaging and fractionation techniques, I identified six RBPs such as Mrn1p, Whi3p, Ngr1p, Pbp2p, Slf1p and Puf1p that associated with ER. I additionally included Puf2p and Nab6p in the project as both RBPs particularly associate with mRNAs coding for cell wall proteins and a major fraction of both proteins co-migrated with ER marker Sec61p in density gradient experiments. The aim was to investigate if these RBPs had any role in mRNA localization and/or translation at ER.
2. **The role of Khd1p in mRNA localization at ER**: This was a combined project with Balaji Thas Moorthy and Andreas Jenner. Khd1p is primarily known to participate in the localization of *ASH1* to the bud as translational repressor. It binds hundreds of mRNAs including those encoding cell wall, membrane and secretory proteins. First, we identified that Khd1p associates with ER and then we aimed to explore its role in mRNA localization and/or translation at ER.
3. **The *ASH1* E3 localization element (LE) recognition by She2p/She3p:** *ASH1* is localized to the tip of the growing bud by the SHE-complex (including She2p and She3p) in a motor-dependent way. In collaboration with Prof. Dierk Niessing's group, Institute of Structural biology, Helmholtz Zentrum München, we aimed to investigate the recognition of *ASH1* E3 localization element by the She2p/She3p complex.

8. Summary of the results

8.1 Signal sequence-independent targeting of *MID2* mRNA to the endoplasmic reticulum by the yeast RNA-binding protein Khd1p

8.1.1 Khd1p associates with membranes in an RNA-dependent manner

Khd1p is a yeast RNA-binding protein (RBP) that binds transcripts coding for secretory or membrane proteins (Hasegawa et al., 2008; Hogan et al., 2008; Kraut-Cohen and Gerst, 2010), which are translated at ER. We hypothesized that Khd1p might be involved in mRNA targeting to ER. Therefore, together with Balaji T. Moorthy, I first checked its association with ER. In density gradient experiment, a subpopulation of Myc-tagged Khd1p co-fractionated with the ER marker Sec61p (Syed et al., 2018, Figure 1A).

Secondly, GST-tagged Khd1p co-floated with protein free liposomes *in vitro* (Syed et al., 2018, Figure 1B). Imaging showed that Khd1p is predominantly cytoplasmic under steady-state conditions (Syed et al., 2018, Figure 2A). I therefore used an assay that allows the detection of temporary or weak association of a protein with ER (Genz et al., 2013; Wu et al., 2011). Indeed, TGBp3-GFP-Khd1p formed spots that colocalized with ER (Syed et al., 2018, Figure 2B), while controls such as TGBp3-GFP-Zwf1p and TGBp3-GFP-Rie1p did not form any foci at all (Syed et al., 2018, Figure 2C, D). However, Khd1p association with ER could be indirect and mediated by binding to mRNAs actively translated on ER-bound ribosomes. Consistent with this, RNase treatment significantly reduced GFP-Khd1p levels in the membrane fraction (Syed et al., 2018, Figure 3A, B). Although an RNA binding mutant Khd1p (GST-Khd1p^{GDDGmt}) still interacted with protein free liposomes *in vitro* (Syed et al., 2018, Figure 3F), GFP-Khd1p^{GDDGmt} largely cofractionated with cytosolic marker Pgk1p (Syed et al., 2018, Figure 3D, E), but it did not mimic the distribution pattern of Pgk1p. This suggests that RNA binding is involved but not essential for Khd1p association with membranes *in vivo*.

8.1.2 Association of *MID2* and *SLG1/WSC1* mRNAs with membranes depends on Khd1p

To find if Khd1p is involved in mRNA localization and/or translation at ER, we checked the distribution of its mRNA targets such as *DSE2*, *EGT2*, *KRE1*, *SCW11*, *MID2*, and *SLG1/WSC1* via qPCR. Upon the deletion of Khd1p, only *MID2* and *SLG1/WSC1* shifted from membrane to cytosol (Syed et al., 2018, Figure 4A). This suggests that only a subset of Khd1p mRNA targets require the protein for their association with membrane. Next, we tested if translation and/or the signal peptide sequences were a prerequisite for *MID2* association with membranes.

A signal sequence less *MID2* (*MID2(-AUG)*) was still enriched in the membrane fraction and only upon the deletion of Khd1p did it shift from membrane to cytosolic fraction (Syed et al., 2018, Figure 4D). Additionally, a strain harbouring *MID2(-AUG)* could not rescue the Calcofluor white sensitive phenotype of *mid2Δ* strain (Syed et al., 2018, Figure S4) indicating the protein to be non-functional. RNA distribution analysis with transmembrane less *MID2* (*MID2(-TMD)*) still showed enrichment in membrane fraction. *In vivo* imaging with MS2 tagging showed partial loss of *MID2* and *SLG1/WSC1* localization with ER when Khd1p was deleted (Syed et al., 2018, Figure 5A-C). smFISH analysis revealed that *MID2(-AUG)* still localized to ER and deletion of Khd1p resulted in partial loss of *MID2(-AUG)* mRNP particles at ER (Syed et al., 2018, Figure 5F). In conclusion, I report the signal sequence-independent targeting of *MID2* to ER and that Khd1p is partially responsible for this targeting.

8.2 Membrane-associated RNA-binding proteins contribute to regulation of mRNAs encoding mitochondrial ribosomal proteins

8.2.1 Screening for membrane-associated RNA-binding proteins (RBPs) in *Saccharomyces cerevisiae*

Membrane/secretory proteins are delivered to ER co-translationally via SRP, post-translationally through GET or through the yet uncharacterized SND pathway (reviewed in (Aviram and Schuldiner, 2017)). Additionally, loss of ER-associated RNA-binding proteins (RBPs) in yeast and mammals affect mRNA localization at ER (Cui et al., 2012; Kraut-Cohen et al., 2013) indicating that RBPs can assist in targeting these proteins by localizing their corresponding mRNAs to the ER. To find additional RBPs that associate with ER, I used a published ER association assay (Genz et al., 2013; Syed et al., 2018; Wu et al., 2011). When tagged with the C-terminal peptide of TGBp3, the GFP fusions of Whi3p, Ngr1p, Puf1p, Mrn1p, Pbp2p and Slf1p formed ER-associated foci (Figure 1 and Supporting figure S1). Sucrose density gradient experiments showed that a large fraction of these RBPs cofractionate with ER marker Sec61p (Figure 2 and Supporting figure S2).

8.2.2 Deletion of membrane-associated RBPs leads to a cell wall defect

A fraction of mRNA targets of Mrn1p, Whi3p, and Puf1p encode proteins with a cell wall related function (Colomina et al., 2008; Hogan et al., 2008), which are usually translated at ER. RBPs such as Nab6p and Puf2p also associate with transcripts coding for cell wall proteins (Hogan et al., 2008), but their GFP-TGBp3 fusions were difficult to generate. However, western blots demonstrated that both RBPs were highly enriched in the membrane fraction in

density gradient experiments (Supporting figure S1). I therefore knocked out Puf1p, Puf2p, Mrn1p, Whi3p, Slf1p, Ngr1p, Pbp2p and Nab6p individually or in different combinations for Calcofluor White (CFW) assay. The individual deletion of Mrn1p and Whi3p resulted in mild cell wall phenotype while the quadruple-gene deletion *(whi3Δ pbp2Δ slf1Δ ngr1Δ)* strain showed a strong cell wall phenotype (Figure 3 and Supporting figure S3). I then additionally knocked out Mrn1p in the fourfold deletion strain for mRNA distribution analysis.

8.2.3 RNA seq analysis upon RBPs deletion reveals no obvious shift of mRNAs from membrane to cytosolic fractions

To check if the observed cell wall phenotype is connected to loss of mRNAs at ER in the fivefold deletion (*quintuple RBP mutant*), I did RNA seq analysis with input, membrane and cytosolic fractions from both wildtype and the *quintuple RBP mutant* strain. I considered a two-fold change as the minimum threshold for RNA enrichment. RNA seq analysis showed the following: (1) Membrane vs cytosol: 1301 transcripts were two-fold more enriched in the cytosolic and 1091 in the membrane fraction in the wildtype strain (Figure 4A and Supporting table S2). (2) Membrane vs cytosol: 1085 transcripts were more abundant in the membrane and 1301 in cytosolic fraction in the *quintuple RBP mutant* strain (Figure 4B and Supporting table S3). (3) Membrane vs membrane: 108 transcripts were more enriched in the wildtype and 222 in the *quintuple RBP mutant* strain (Figure 4C and Supporting table S4). Finally, comparison of inputs from wildtype and *quintuple RBP mutant* strain (Figure 4D and Supporting table S5) showed same enrichment pattern as in the case of membrane vs membrane (Figure 4C and Supporting table S4). Therefore, there is no obvious shift of mRNAs from membrane to cytosolic fraction in *quintuple RBP mutant* strain.

8.2.4 The enrichment of transcripts coding for nuclear-related proteins in the membrane fractions

In contrast to the popular SRP model, which suggests that only mRNAs encoding membrane/secretory proteins localize to ER in translation-dependent manner (reviewed in (Reid and Nicchitta, 2015)), I observed an enrichment of transcripts encoding proteins with nuclear-related function (Figure 5A, and Supporting table S2 and S3). To further verify this observation, I randomly picked five transcripts encoding nuclear-related proteins, three enriched in the membrane (*MOT1*, *NUP100* and *IKI3*) and two in the cytosolic fraction (*HTA2* and *HHT2*) (Supporting table S2). qPCR analysis verified that *MOT1*, *NUP100* and *IKI3* are highly enriched in the membrane fraction, while *HTA2* and *HHT2* showed nearly equal distribution in both membrane and cytosolic fraction (Figure 5B and Supporting figure 5A).

As judged by RNA imaging, both MS2-tagged *MOT1* and *NUP100* colocalized with ER (Supporting figure 5B). Thus my results back up previous findings that reported the localization of mRNAs other than those coding for secretory/membrane proteins to the ER (Diehn et al., 2000; Jagannathan et al., 2014; de Jong et al., 2006; Kraut-Cohen et al., 2013).

8.2.5 Deletion of five RBPs leads to the upregulation of transcripts encoding mitochondrial ribosomal proteins

Mitochondrial ribosomes carry out the translation of genes encoded by mitochondrial genome, including the three core subunits of cytochrome c oxidase (Cooper et al., 1991). RNA seq analysis revealed an upregulation of transcripts encoding mitochondrial ribosomal proteins (MRPs) in the *quintuple RBP mutant* strain (Supporting table S5 and Figure 6A). I additionally confirmed this by qPCR against *MRPL39*, *MRPL44* and *MRP13* (Figure 6B). I further investigated if RNA upregulation is connected to changes in the protein levels. As opposed to wildtype, I see very faint bands for GFP fusions of Mrpl39p, Img2p and Mrpl44p in the membrane fraction of *quintuple RBP mutant* strain (Supporting figure S6B). Beside this, mitochondria in the *quintuple RBP mutant* strain formed aggregated structures instead of tubular network (Supporting figure S6A). The loss of MRPs in the *quintuple RBP mutant* strain could mean that they are not efficiently translated or imported and thus they might be degraded soon after their translation.

8.2.6 Deletion of five ER-associated RBPs leads to respiratory-incompetent mitochondria

The loss of MRPs (as discussed above) in *quintuple RBP mutant* strain could possibly mean the loss of mitochondrial translation. Therefore, I checked the expression of Cox2p, Cox4p and Tom70p. In contrast to Cox4p and Tom70p (both encoded by the nuclear genome), mitochondrial-encoded Cox2p was not expressed at all in *quintuple RBP mutant* strain (Figure 7A). qPCR analysis revealed that *COX1*, *COX2* and the mitochondrial *21_S*rRNA are not transcribed in the fivefold RBP deletion strain (Figure 7B). As expected, the mutant strain was unable to grow on nonfermentable carbon source (Figure 7C). Although mitochondrial genome is present, though apparently less in number in terms of nucleoids (Figure 7D), its integrity is lost as primers against *COX2* genomic locus amplified a slightly larger fragment than expected (Supporting figure 7B). Thus, the observed defect in COX expression is not due to loss of mitochondrial DNA. Further analysis is required to address this issue.

8.3 Molecular architecture and dynamics of *ASH1* mRNA recognition by its mRNA-transport complex

8.3.1 Structural analysis of the *ASH1* E3 element

To identify the minimum E3 localization element recognized by She2-She3 complex, we first chemically probed the full-length *ASH1* mRNA with dimethyl sulfate (DMS) (Tijerina et al., 2007). The validated 51 nucleotides (nt) long secondary structure of E3 LE (Edelmann et al., 2017, Figure 1a) was then set for mutations. Electrophoretic mobility shift assay (EMSA; Edelmann et al., 2017, Supplementary Figure 1a, b) helped us identify a 28-nt loop as the minimal E3 element recognized by the She2-She3 complex (Edelmann et al., 2017, Figure 1b). The crystalized RNA fragment (E3, 42-nt TL-TLR), which diffracted to 2.65-Å resolution (Edelmann et al., 2017, Table 1), revealed the final structure consisting of an elongated stem loop with both helical regions (H1 and H2) that flanked the flexible bases (Edelmann et al., 2017, Figure 1d).

8.3.2 Crystal structure of the nuclear complex consisting of She2p and the *ASH1* E3 element

For the RNA-protein co-crystal structure, the minimal E3 LE with She2p alone or with various She3 peptides was tested. In complex with RNA, two She2p dimers face each other in a head-to-head conformation with a non-crystallographic twofold point symmetry, resulting in an elongated tetramer and each of the two stem-loop-forming RNA molecules binds to the surface region between the protruding helices of She2p on one of the two sides of the tetramer (Edelmann et al., 2017, Figure 2a). Upon She2p binding, the region in the middle of the stem (positions 1,779 and 1,782/1,783; Edelmann et al., 2017, Figure 1a, d–f) underwent marked rearrangements resulting in a kinked RNA conformation (Edelmann et al., 2017, Figure 2a–c, and Supplementary Figures 3f and 4a). Four N36 and R63 residues in the tetramer specifically recognized two cytosines (C1779 and C1813) in each of the two almost identical RNAs (Edelmann et al., 2017, Supplementary Figure 3g and Figure 2b, d-e). R52 made additional RNA backbone contacts with C1779 (Edelmann et al., 2017, Figure 2b, d) and C1813 (Edelmann et al., 2017, Figure 2b, e). One set of E176 and F176 residues in the protruding helix contacted U1780, while the other set failed to do so in the corresponding position (Edelmann et al., 2017, Figure 2g), indicating that the protruding helix is probably less critical for protein-RNA interaction.

8.3.3 Structure of the mature cytoplasmic mRNA-recognition complex

The C-terminus of She3p is sufficient for synergistic RNA binding (Müller et al., 2011) and we narrowed down this region to amino acids 331–405 (Edelmann et al., 2017, Figure 3a and Supplementary Figure 5a). But this and other related fragments in complex with She2p and E3 (28-nt loop) failed to crystalize. Since She2p and She3p bind each other with a 1:1 stoichiometry (Heym et al., 2013), we used glycine-serine linkers to fuse She3p (331–405) to the C-terminus of She2p (Edelmann et al., 2017, Supplementary Figure 5b). As shown in Supplementary Figure 5c (Edelmann et al., 2017a), this fusion construct mediated synergistic RNA binding. The She2p (6-246, C-S)-$(GGSGG)_2$-She3p (331-405) along with the E3 (28-nt loop) LE yielded a crystal structure that diffracted to 2.8-Å resolution (Edelmann et al., 2017, Table 1). She2p did not undergo major changes following RNA binding (Edelmann et al., 2017, Figures 2a and 3b). For She3p, we observed electron density for two different regions that included residues 338–351 and 361–371. The first fragment (residues 338–351) known as the R site, which binds both the E3 LE and She2p, buried a surface area of 922 $Å^2$ (Edelmann et al., 2017, Supplementary Figure 5d–f). The second fragment (residues 361–371), which only contacts She2p (P site), masked a smaller region of 630 $Å^2$ (Edelmann et al., 2017, Supplementary Figure 5d). A short alpha helix formed by the R site intercalated between the protruding helix in She2p and the 3-end of the E3 RNA allowing for numerous protein-protein (Edelmann et al., 2017, Supplementary Table 1) and protein-RNA contacts (Edelmann et al., 2017, Figure 3c–e). R341 in both R sites in cooperation with K60 of She2p contacted the phosphate backbones of nucleotides U1780 and C1813 (Edelmann et al., 2017, Figure 3d, e). However, She3p binding disrupted the interaction of F176 on the protruding helix of She2p with U1780 of the RNA (Figure 2b, f). Residue Y345 in She3p then underwent aromatic stacking with She2p F176 (Edelmann et al., 2017, Figure 3f) and as a result, U1780 pointed toward the solvent (Edelmann et al., 2017, Figure 3g) and was stabilized by R341 (Edelmann et al., 2017, Figure 3f, g).

8.3.4 Three RNA bases are important for complex formation in solution

In order to find out if the nucleotides C1779, U1780 and C1813 are also crucial for LE recognition in solution we did EMSA with She2p, She3p and different versions of the E3 (51 nt) RNA. As shown in Figure 4a (Edelmann et al., 2017), uracil at position 1,780 is important for RNA binding since its exchange for adenine or cytosine impaired RNA binding. Mutating cytosines at positions 1,779 or 1,813 to guanine or uracil resulted in complete loss of RNA binding (Edelmann et al., 2017, Figure 4b, c).

8.3.5 Mutational analysis of She2p and She3p confirm binding mode in solution

Since the R site (residues 338–351) of She3p intercalates between the protruding helix of She2p and the E3 RNA (Edelmann et al., 2017, Figure 3d, e), mutating lysine, arginine and tyrosine to alanine at positions 340, 34 and 345 resulted in the loss of RNA binding (Edelmann et al., 2017, Figure 4d and Supplementary Figure 7a, b). The protruding helix of She2p is required for synergistic RNA binding and mRNA localization (Müller et al., 2011) and by mutating residues E172 and F176 in the protruding helix, that contacted U1780 in the RNA (Edelmann et al., 2017, Figure 2f), we saw the loss of binding to RNA (Edelmann et al., 2017, Figure 4e and Supplementary Figure 7c).

8.3.6 Specific contacts are essential for mRNA localization *in vivo*

We performed *in vivo ASH1* mRNA localization studies with mutant versions of *SHE2* or *SHE3*. The localization of an MS2-aptamer tagged *ASH1* to the bud was abolished when mutations were made in the R or P site of She3p (Edelmann et al., 2017, Figure 5, Table 2 and Supplementary Figure 9a). Additionally, mutating residues E172 and F176 of She2p, which contact R site in She3p, also resulted in the loss of mRNA localization to the bud (Edelmann et al., 2017, Figure 5, Table 2 and Supplementary Figure 9a).

9. Discussion

9.1 Membrane-associated RNA-binding proteins in yeast

Membrane/secretory proteins are delivered to ER for proper folding, post-translational modifications and transport to a specific destination (reviewed in (Schwarz and Blower, 2016)). Multiple pathways namely SRP, GET and SND exist in eukaryotes that target these proteins to ER co- or post-translationally (reviewed in (Aviram and Schuldiner, 2017)). Additionally, RNA-binding proteins (RBPs) in yeast and mammals that associate with ER can assist in targeting these proteins by localizing their corresponding mRNAs to the ER (Aronov et al., 2007b; Cui et al., 2012; Gelin-Licht et al., 2012; Kraut-Cohen et al., 2013; Schmid et al., 2006). In the current thesis project, together with Balaji T. Moorthy, I identified several RBPs that partially co-colocalize with ER such as Khd1p, Mrn1p, Whi3p, Pbp2, Slf1p, Ngr1p and Puf1p.

Khd1p has the capacity to interact with membranes *in vitro*. It binds numerous mRNA targets including those coding for cell wall proteins (Hogan et al., 2008). Khd1p is known to act as translational repressor, as shown for the localized *ASH1* mRNA (Paquin et al., 2007) and for mRNAs encoding NPC components (Rouvière et al., 2018). Its deletion, however, also leads to the reduced expression of genes such as *MTL1*(Hasegawa et al., 2008). In collaboration with Balaji T. Moorthy, I report yet another function of Khd1p as being involved in the translation- and signal sequence-independent targeting of *MID2* to ER. In our analysis, Khd1p is present in both cytosolic and membrane fractions. Though Khd1p-GFP is spread throughout cytoplasm, the Khd1p-GFP-TGBp3 fusion forms foci that colocalize with ER. This means that Khd1p probably only transiently interacts with ER. Mutating the RNA-binding domains in Khd1p leads to its depletion from the membrane fraction indicating its interaction with ER to be RNA dependent. Although Khd1p's association with the ER requires binding to RNA, at least two of its mRNA targets, *MID2* and *SLG1/WSC1*, depend on Khd1p for efficient ER targeting. The requirement of Khd1p for their targeting is also reflected by their genetic interaction since *KHD1* as well as *MID2* and *SLG1/WSC1* are involved in the cell wall integrity pathway (Ito et al., 2011). In short, I report the translation- and SRP-independent targeting of mRNA such as *MID2* to ER and the involvement of Khd1p in this targeting.

For RBPs such as Mrn1p, Whi3p, Pbp2, Slf1p, Nab6p, Puf2p, Ngr1p and Puf1p, I employed assay to test for cell wall defects in cells lacking these RBPs. Nab6p and Puf2 are both associated with mRNAs coding for cell wall proteins (Hogan et al., 2008) and I found them to be enriched in the membrane fractions in density gradient experiments. I observed a relatively

mild cell wall defect upon deletion of Mrn1p or Whi3p and a strong cell wall phenotype upon deletion of four RBPs (*whi3Δ pbp2Δ slf1Δ ngr1Δ*). Since Mrn1p has been shown to associate with cell wall related transcripts (Hogan et al., 2008), I additionally deleted it and created a fivefold RBP deletion (*quintuple RBP mutant*) strain to study changes in RNA expression and distribution.

I observed no obvious shift of mRNAs from membrane to cytosolic fraction in the *quintuple RBP mutant* strain. Instead, many transcripts were either up or down regulated at a global level. Although I could not find that these RBPs are involved in mRNA localization to ER, I noticed that many transcripts encoding nuclear-related proteins are enriched in the membrane fraction. The SRP model suggests that only mRNAs coding for proteins bearing an N-terminal signal peptide or transmembrane domain (TMD) are localized to ER in translation-dependent manner (reviewed in Reid and Nicchitta, 2015). But my RNA seq and qPCR data suggests that even mRNAs encoding proteins bearing no ER targeting sequence or TMD can localize to ER. Among the five mRNAs encoding nuclear-related proteins tested so far, I found *MOT1*, *NUP100* and *IKI3* to be highly enriched in the membrane fraction in a qRT-PCR analysis. I further show that MS2 loop-tagged *MOT1* and *NUP100* mRNAs can localize to ER. Several groups have also reported the localization of transcripts encoding non-secretory/non-membrane proteins to ER (Diehn et al., 2000; Jagannathan et al., 2014; de Jong et al., 2006; Kraut-Cohen et al., 2013). Our data regarding *MID2* targeting (Syed et al., 2018) and the data from Kraut-Cohen (Kraut-Cohen et al., 2013) suggest that translation is not a prerequisite for mRNA localization to ER. Kraut-Cohen (Kraut-Cohen et al., 2013) proposes that RNA itself has some inherent propensity to interact with ER. For example, *OXA1* mRNA, encoding a mitochondrial inner membrane insertase (Herrmann et al., 1997), mislocalizes to ER upon the removal of mitochondrial targeting information (Gadir et al., 2011). According to Reid and Nicchitta (Reid and Nicchitta, 2015), ER could serve as the primary site of protein synthesis, because approximately half of all ribosomes in HEK293 and HeLa are ER-bound and additionally, a similar fraction of total cellular mRNA localizes to ER (Jagannathan et al., 2014).

In *quintuple RBP mutant* strain, I also noticed an upregulation of mRNAs encoding mitochondrial ribosomal proteins (MRPs). In contrast, GFP fusions of Mrpl39p, Img2p and Mrpl44p were poorly expressed in the *quintuple RBP mutant* strain. I therefore propose the following: (1) These MRPs are not efficiently translated or (2) they are translated but failed to become imported into mitochondria and as a result might be degraded in the cytoplasm.

Nuclear-encoded MRPs are involved in the translation of mitochondrial-encoded genes and their loss results in numerous mitochondrial defects. In the current case, I find that the mitochondrially encoded Cox2p is not translated. Additionally, I noticed an absence of transcription for *COX1*, *COX2* and the mitochondrial *21S* rRNA in the *quintuple RBP mutant* strain. Concomitantly, the *quintuple RBP mutant* strain is unable to grow on nonfermentable carbon source. Furthermore, its mitochondrial genome is unstable, and I see an aberrant mitochondrial morphology. My observation is consistent with previous findings that deletion of MRPs leads to gradual loss of the mitochondrial genome (Merz and Westermann, 2009). Surprisingly, I find that only the fivefold gene deletion strain causes this mitochondrial phenotype. By checking the published mRNA targets of the deleted RBPs (Cai and Futcher, 2013; Hogan et al., 2008; Kershaw et al., 2015), I find that only Whi3p and Slf1p bind some transcripts encoding MRPs. When the top 200 mRNA targets were analysed, Whi3p associates with *MRPL49* only (sorted based on net IP ratio; see Table S1 (Cai and Futcher, 2013)), while Slf1p binds several mRNAs such as *MRPL4*, *MRPL19*, *MRPL28*, *RSM7*, *MRPL36*, *MRPL8*, *MRPL13*, *IMG1*, *MRP20*, *MRPL7*, *RSM18* and *RSM26* (sorted based on false discovery rate (FDR) taking into account the positive Log fold change (Log FC); see S3 Table (Kershaw et al., 2015)). In my case I have checked the expression levels of only five MRPs, thus it is possible that other MRPs are either absent or present in low quantity in the mitochondrial enriched fraction.

In conclusion, I report the localization of mRNAs encoding proteins with a nuclear function to ER, which further supports the model that view ER as the primary site of protein synthesis. The deletion of ER-associated RBPs in my study leads to an upregulation of mRNAs encoding MRPs and yet I see very low levels of Mrpl39p, Mrpl44p and Img2p in the organelle rich fraction. I therefore suggest that these five RBPs might play role in controlling the expression of nuclear-encoded MRPs.

9.2 The *ASH1* E3 localization element (LE) recognition by She2p/She3p

Yeast *ASH1* is one of the best-studied localized mRNAs. It is transported to the tip of the growing bud by the SHE-complex in a motor-dependent way (reviewed in (Heym and Niessing, 2012)). The *cis*-acting sequences named localization elements (LEs) within the RNA and the *trans*-acting factors such as She2p, She3p or Myo4p are vital to achieve this localization. LEs are generally unique among nucleic-acid based signals in the sense that they usually show no recognizable conservation on the sequence or secondary structure level. The knowledge at molecular level of how RBPs specifically interact with LEs is still poor. By using

the *ASH1* E3 LE together with She2p and She3p, together with the Niessing lab (Universität Ulm), I did a comprehensive structural and functional analysis of how mRNA is recognized by its transport-complex.

She2p functions as tetramer (Chung and Takizawa, 2010) that provides two binding surfaces interacting with two RNAs or two LEs. In a co-structure with RNA, this tetramer was point symmetric and not the RNA (Edelmann et al., 2017a). The two binding surfaces of the tetramer used two identical sets of amino acids (N36, R43, R52, K60 and R63) to contact RNA. The protruding helix of She2p is important for *in vivo* mRNA localization (Müller et al., 2011) and very few contacts between the protruding helix and the RNA were observed (Edelmann et al., 2017a). It is most likely that the helix is important for interacting with She3p. Indeed, the R-site of She3p intercalated between the protruding helix and RNA to stabilize their interaction. Though the P site in She3p does not provide any direct contribution to RNA recognition, both R and P sites were crucial for mRNA localization *in vivo*. Furthermore, cytosines C1779 and C1813 in *ASH1* E3 element, which are essential for mRNA localization (Olivier et al., 2005), were the only nucleotides recognized by the triad of amino acids N36, R52 and R63 in the nuclear She2p-RNA complex. The joining of She3p brought conformational change in the RNA so that the U1780 changed its orientation toward the solvent to make space for the interaction between She3p Y345 and She2p F176. In short, we were able to show for the first-time features defining a *cis*-acting LE and the recognition of asymmetric RNA in a symmetric way by both She2p and She3p.

10. References

Abruzzi, K., Denome, S., Olsen, J.R., Assenholt, J., Haaning, L.L., Jensen, T.H., and Rosbash, M. (2007). A novel plasmid-based microarray screen identifies suppressors of rrp6Delta in Saccharomyces cerevisiae. Mol. Cell. Biol. *27*, 1044–1055.

Anderson, P., and Kedersha, N. (2008). Stress granules: the Tao of RNA triage. Trends Biochem. Sci. *33*, 141–150.

Anderson, J.T., Wilson, S.M., Datar, K. V, and Swanson, M.S. (1993). NAB2: a yeast nuclear polyadenylated RNA-binding protein essential for cell viability. Mol. Cell. Biol. *13*, 2730–2741.

Aoki, K., Adachi, S., Homoto, M., Kusano, H., Koike, K., and Natsume, T. (2013). LARP1 specifically recognizes the 3′ terminus of poly(A) mRNA. FEBS Lett. *587*, 2173–2178.

Aronov, S., Gelin-Licht, R., Zipor, G., Haim, L., Safran, E., and Gerst, J.E. (2007a). mRNAs encoding polarity and exocytosis factors are cotransported with the cortical endoplasmic reticulum to the incipient bud in Saccharomyces cerevisiae. Mol. Cell. Biol. *27*, 3441–3455.

Aronov, S., Gelin-Licht, R., Zipor, G., Haim, L., Safran, E., and Gerst, J.E. (2007b). mRNAs Encoding Polarity and Exocytosis Factors Are Cotransported with the Cortical Endoplasmic Reticulum to the Incipient Bud in Saccharomyces cerevisiae. Mol. Cell. Biol. *27*, 3441–3455.

Ashley, C.T., Wilkinson, K.D., Reines, D., and Warren, S.T. (1993). FMR1 protein: conserved RNP family domains and selective RNA binding. Science *262*, 563–566.

Ast, T., and Schuldiner, M. (2013). All roads lead to Rome (but some may be harder to travel): SRP-independent translocation into the endoplasmic reticulum. Crit. Rev. Biochem. Mol. Biol. *48*, 273–288.

Ast, T., Cohen, G., and Schuldiner, M. (2013). A network of cytosolic factors targets SRP-independent proteins to the endoplasmic reticulum. Cell *152*, 1134–1145.

Aviram, N., and Schuldiner, M. (2017). Targeting and translocation of proteins to the endoplasmic reticulum at a glance. J. Cell Sci. *130*, 4079–4085.

Aviram, N., Ast, T., Costa, E.A., Arakel, E.C., Chuartzman, S.G., Jan, C.H., Haßdenteufel, S., Dudek, J., Jung, M., Schorr, S., et al. (2016). The SND proteins constitute an alternative targeting route to the endoplasmic reticulum. Nature *540*, 134–138.

Balagopal, V., and Parker, R. (2009). Polysomes, P bodies and stress granules: states and fates of eukaryotic mRNAs. Curr. Opin. Cell Biol. *21*, 403–408.

Bayfield, M.A., Yang, R., and Maraia, R.J. (2010). Conserved and divergent features of the structure and function of La and La-related proteins (LARPs). Biochim. Biophys. Acta - Gene Regul. Mech. *1799*, 365–378.

Becker, T., Bhushan, S., Jarasch, A., Armache, J.-P., Funes, S., Jossinet, F., Gumbart, J., Mielke, T., Berninghausen, O., Schulten, K., et al. (2009). Structure of monomeric yeast and mammalian Sec61 complexes interacting with the translating ribosome. Science *326*, 1369–1373.

Bertrand, E., Chartrand, P., Schaefer, M., Shenoy, S.M., Singer, R.H., and Long, R.M. (1998). Localization of ASH1 mRNA particles in living yeast. Mol. Cell *2*, 437–445.

Blobel, G., and Dobberstein, B. (1975). Transfer of proteins across membranes. I. Presence of proteolytically processed and unprocessed nascent immunoglobulin light chains on membrane-bound ribosomes of murine myeloma. J. Cell Biol. *67*, 835–851.

Bobola, N., Jansen, R.P., Shin, T.H., and Nasmyth, K. (1996). Asymmetric accumulation of Ash1p in postanaphase nuclei depends on a myosin and restricts yeast mating-type switching to mother cells. Cell *84*, 699–709.

Bohl, F., Kruse, C., Frank, A., Ferring, D., and Jansen, R.P. (2000). She2p, a novel RNA-binding protein tethers ASH1 mRNA to the Myo4p myosin motor via She3p. EMBO J. *19*, 5514–5524.

Bohnsack, M.T., and Schleiff, E. (2010). The evolution of protein targeting and translocation systems. Biochim. Biophys. Acta - Mol. Cell Res. *1803*, 1115–1130.

Bousquet-Antonelli, C., and Deragon, J.-M. (2009). A comprehensive analysis of the La-motif protein superfamily. RNA *15*, 750–764.

Braakman, I., and Hebert, D.N. (2013). Protein Folding in the Endoplasmic Reticulum. Cold Spring Harb. Perspect. Biol. *5*, a013201–a013201.

Brambillasca, S., Yabal, M., Makarow, M., and Borgese, N. (2006). Unassisted translocation of large polypeptide domains across phospholipid bilayers. J. Cell Biol. *175*, 767–777.

Buchan, J.R., Muhlrad, D., and Parker, R. (2008). P bodies promote stress granule assembly in Saccharomyces cerevisiae. J. Cell Biol. *183*, 441–455.

Buu, L.-M., Jang, L.-T., and Lee, F.-J.S. (2004). The yeast RNA-binding protein Rbp1p modifies the stability of mitochondrial porin mRNA. J. Biol. Chem. *279*, 453–462.

Cai, Y., and Futcher, B. (2013). Effects of the yeast RNA-binding protein Whi3 on the half-life and abundance of CLN3 mRNA and other targets. PLoS One *8*, e84630.

Chambers, J.C., Kenan, D., Martin, B.J., and Keene, J.D. (1988). Genomic structure and amino acid sequence domains of the human La autoantigen. J. Biol. Chem. *263*, 18043–18051.

Chang, L.-C., and Lee, F.-J.S. (2012). The RNA helicase Dhh1p cooperates with Rbp1p to promote porin mRNA decay via its non-conserved C-terminal domain. Nucleic Acids Res. *40*, 1331–1344.

Chartrand, P., Meng, X.-H., Singer, R.H., and Long, R.M. (1999). Structural elements required for the localization of ASH1 mRNA and of a green fluorescent protein reporter particle in vivo. Curr. Biol. *9*, 333–338.

Chartron, J.W., Clemons, W.M., and Suloway, C.J. (2012). The complex process of GETting tail-anchored membrane proteins to the ER. Curr. Opin. Struct. Biol. *22*, 217–224.

Chatenay-Lapointe, M., and Shadel, G.S. (2011). Repression of Mitochondrial Translation, Respiration and a Metabolic Cycle-Regulated Gene, SLF1, by the Yeast Pumilio-Family Protein Puf3p. PLoS One *6*.

Chen, H.R., Jan, S.P., Tsao, T.Y., Sheu, Y.J., Banroques, J., and Cheng, S.C. (1998). Snt309p, a component of the Prp19p-associated complex that interacts with Prp19p and associates with the spliceosome simultaneously with or immediately after dissociation of U4 in the same manner as Prp19p. Mol. Cell. Biol. *18*, 2196–2204.

Cheng, Z., Jiang, Y., Mandon, E.C., and Gilmore, R. (2005). Identification of cytoplasmic residues of Sec61p involved in ribosome binding and cotranslational translocation. J. Cell Biol. *168*, 67–77.

Chung, S., and Takizawa, P.A. (2010). Multiple Myo4 motors enhance *ASH1* mRNA transport in *Saccharomyces cerevisiae*. J. Cell Biol. *189*, 755–767.

Clapham, D.E. (2007). Calcium Signaling. Cell *131*, 1047–1058.

Cléry, A., Blatter, M., and Allain, F.H.-T. (2008). RNA recognition motifs: boring? Not quite. Curr. Opin. Struct. Biol. *18*, 290–298.

Collins, S.R., Kemmeren, P., Zhao, X.-C., Greenblatt, J.F., Spencer, F., Holstege, F.C.P., Weissman, J.S., and Krogan, N.J. (2007). Toward a Comprehensive Atlas of the Physical Interactome of Saccharomyces cerevisiae* □ S Downloaded from.

Colomina, N., Ferrezuelo, F., Wang, H., Aldea, M., and Garí, E. (2008). Whi3, a developmental regulator of budding yeast, binds a large set of mRNAs functionally related to the endoplasmic reticulum. J. Biol. Chem. *283*, 28670–28679.

Colot, H. V, Stutz, F., and Rosbash, M. (1996). The yeast splicing factor Mud13p is a commitment complex component and corresponds to CBP20, the small subunit of the nuclear cap-binding complex. Genes Dev. *10*, 1699–1708.

Connolly, T., and Gilmore, R. (1989). The signal recognition particle receptor mediates the GTP-dependent displacement of SRP from the signal sequence of the nascent polypeptide. Cell *57*, 599–610.

Connolly, T., Rapiejko, P.J., and Gilmore, R. (1991). Requirement of GTP hydrolysis for dissociation of the signal recognition particle from its receptor. Science *252*, 1171–1173.

Conzelmann, A., Riezman, H., Desponds, C., and Bron, C. (1988). A major 125-kd membrane glycoprotein of Saccharomyces cerevisiae is attached to the lipid bilayer through an inositol-containing phospholipid. EMBO J. *7*, 2233–2240.

Cooper, C.E., Nicholls, P., and Freedman, J.A. (1991). Cytochrome c oxidase: structure, function, and membrane topology of the polypeptide subunits. Biochem. Cell Biol. *69*, 586–607.

Cosma, M.P. (2004). Daughter-specific repression of Saccharomyces cerevisiae HO: Ash1 is the commander. EMBO Rep. *5*, 953–957.

Costanzo, M., Baryshnikova, A., Bellay, J., Kim, Y., Spear, E.D., Sevier, C.S., Ding, H., Koh, J.L.Y., Toufighi, K., Mostafavi, S., et al. (2010). The genetic landscape of a cell. Science *327*, 425–431.

Cui, X.A., Zhang, H., and Palazzo, A.F. (2012). p180 Promotes the Ribosome-Independent Localization of a Subset of mRNA to the Endoplasmic Reticulum. PLoS Biol. *10*, e1001336.

Delling, U., Raymond, M., and Schurr, E. (1998). Identification of Saccharomyces cerevisiae genes conferring resistance to quinoline ring-containing antimalarial drugs. Antimicrob. Agents Chemother. *42*, 1034–1041.

Deng, Y., Singer, R.H., and Gu, W. (2008). Translation of ASH1 mRNA is repressed by Puf6p-Fun12p/eIF5B interaction and released by CK2 phosphorylation. Genes Dev. *22*, 1037–1050.

Denic, V., Dötsch, V., and Sinning, I. (2013). Endoplasmic reticulum targeting and insertion of tail-anchored membrane proteins by the GET pathway. Cold Spring Harb. Perspect. Biol. *5*, a013334.

Denisenko, O., and Bomsztyk, K. (2002). Yeast hnRNP K-like genes are involved in regulation of the telomeric position effect and telomere length. Mol. Cell. Biol. *22*, 286–297.

Deshaies, R.J., Sanders, S.L., Feldheim, D.A., and Schekman, R. (1991). Assembly of yeast Sec proteins involved in translocation into the endoplasmic reticulum into a membrane-bound multisubunit complex. Nature *349*, 806–808.

Diehn, M., Eisen, M.B., Botstein, D., and Brown, P.O. (2000). Large-scale identification of secreted and membrane-associated gene products using DNA microarrays. Nat. Genet. *25*, 58–62.

Diehn, M., Bhattacharya, R., Botstein, D., and Brown, P.O. (2006). Genome-Scale Identification of Membrane-Associated Human mRNAs. PLoS Genet. *2*, e11.

Ding, J., Hayashi, M.K., Zhang, Y., Manche, L., Krainer, A.R., and Xu, R.-M. (1999). Crystal structure of the two-RRM domain of hnRNP A1 (UP1) complexed with single-stranded telomeric DNA. Genes Dev. *13*, 1102–1115.

Dong, G., Chakshusmathi, G., Wolin, S.L., and Reinisch, K.M. (2004). Structure of the La motif: a winged helix domain mediates RNA binding via a conserved aromatic patch. EMBO J. *23*, 1000–1007.

Dong, S., Wang, Y., Cassidy-Amstutz, C., Lu, G., Bigler, R., Jezyk, M.R., Li, C., Hall, T.M.T., and Wang, Z. (2011). Specific and modular binding code for cytosine recognition in Pumilio/FBF (PUF) RNA-binding domains. J. Biol. Chem. *286*, 26732–26742.

Du, T.-G., Jellbauer, S., Müller, M., Schmid, M., Niessing, D., and Jansen, R.-P. (2008). Nuclear transit of the RNA-binding protein She2 is required for translational control of localized ASH1 mRNA. EMBO Rep. *9*, 781–787.

Dunn, B.D., Sakamoto, T., Hong, M.-S.S., Sellers, J.R., and Takizawa, P.A. (2007). Myo4p is a monomeric myosin with motility uniquely adapted to transport mRNA. J. Cell Biol. *178*, 1193–1206.

Düring, L., Thorsen, M., Petersen, D.S.N., Køster, B., Jensen, T.H., and Holmberg, S. (2012). MRN1 Implicates Chromatin Remodeling Complexes and Architectural Factors in mRNA Maturation. PLoS

One *7*, e44373.

Edelmann, F.T., Schlundt, A., Heym, R.G., Jenner, A., Niedner-Boblenz, A., Syed, M.I., Paillart, J.-C., Stehle, R., Janowski, R., Sattler, M., et al. (2017a). Molecular architecture and dynamics of ASH1 mRNA recognition by its mRNA-transport complex. Nat. Struct. Mol. Biol. *24*.

Edelmann, F.T., Schlundt, A., Heym, R.G., Jenner, A., Niedner-Boblenz, A., Syed, M.I., Paillart, J.-C., Stehle, R., Janowski, R., Sattler, M., et al. (2017b). Molecular architecture and dynamics of ASH1 mRNA recognition by its mRNA-transport complex. Nat. Struct. Mol. Biol. *24*, 152–161.

Edwards, T.A., Pyle, S.E., Wharton, R.P., and Aggarwal, A.K. (2001). Structure of Pumilio Reveals Similarity between RNA and Peptide Binding Motifs. Cell *105*, 281–289.

English, A.R., and Voeltz, G.K. (2013). Endoplasmic reticulum structure and interconnections with other organelles. Cold Spring Harb. Perspect. Biol. *5*, a013227.

Erickson, S.L., and Lykke-Andersen, J. (2011). Cytoplasmic mRNP granules at a glance. J. Cell Sci. *124*, 293–297.

Ezeokonkwo, C., Ghazy, M.A., Zhelkovsky, A., Yeh, P.-C., and Moore, C. (2012). Novel interactions at the essential N-terminus of poly(A) polymerase that could regulate poly(A) addition in Saccharomyces cerevisiae. FEBS Lett. *586*, 1173–1178.

Fagone, P., and Jackowski, S. (2009). Membrane phospholipid synthesis and endoplasmic reticulum function. J. Lipid Res. *50*, S311–S316.

Fehrenbacher, K.L., Boldogh, I.R., and Pon, L.A. (2005). A Role for Jsn1p in Recruiting the Arp2/3 Complex to Mitochondria in Budding Yeast. Mol. Biol. Cell *16*, 5094–5102.

Filipovska, A., and Rackham, O. (2012). Modular recognition of nucleic acids by PUF, TALE and PPR proteins. Mol. Biosyst. *8*, 699.

Finke, K., Plath, K., Panzner, S., Prehn, S., Rapoport, T.A., Hartmann, E., and Sommer, T. (1996). A second trimeric complex containing homologs of the Sec61p complex functions in protein transport across the ER membrane of S. cerevisiae. EMBO J. *15*, 1482–1494.

Fleischer, T.C., Weaver, C.M., McAfee, K.J., Jennings, J.L., and Link, A.J. (2006). Systematic identification and functional screens of uncharacterized proteins associated with eukaryotic ribosomal complexes. Genes Dev. *20*, 1294–1307.

Friedlander, M., and Blobel, G. (1985). Bovine opsin has more than one signal sequence. Nature *318*, 338–343.

Fundakowski, J., Hermesh, O., and Jansen, R.-P. (2012). Localization of a Subset of Yeast mRNAs Depends on Inheritance of Endoplasmic Reticulum. Traffic *13*, 1642–1652.

Gadir, N., Haim-Vilmovsky, L., Kraut-Cohen, J., and Gerst, J.E. (2011). Localization of mRNAs coding for mitochondrial proteins in the yeast Saccharomyces cerevisiae. RNA *17*, 1551–1565.

Garí, E., Volpe, T., Wang, H., Gallego, C., Futcher, B., and Aldea, M. (2001). Whi3 binds the mRNA of the G1 cyclin CLN3 to modulate cell fate in budding yeast. Genes Dev. *15*, 2803–2808.

Gelin-Licht, R., Paliwal, S., Conlon, P., Levchenko, A., and Gerst, J.E. (2012). Scp160-dependent mRNA trafficking mediates pheromone gradient sensing and chemotropism in yeast. Cell Rep. *1*, 483–494.

Genz, C., Fundakowski, J., Hermesh, O., Schmid, M., and Jansen, R.-P. (2013). Association of the yeast RNA-binding protein She2p with the tubular endoplasmic reticulum depends on membrane curvature. J. Biol. Chem. *288*, 32384–32393.

Gerber, A.P., Herschlag, D., and Brown, P.O. (2004). Extensive Association of Functionally and Cytotopically Related mRNAs with Puf Family RNA-Binding Proteins in Yeast. PLoS Biol. *2*, e79.

de Gier, J.-W.L.J.-W.L., Scotti, P.A., Sääf, A., Valent, Q.A., Kuhn, A., Luirink, J., von Heijne, G., Saaf, A., Valent, Q.A., Kuhn, A., et al. (1998). Differential use of the signal recognition particle translocase

targeting pathway for inner membrane protein assembly in Escherichia coli. Proc. Natl. Acad. Sci. *95*, 14646–14651.

Gilmore, R., Blobel, G., and Walter, P. (1982). Protein translocation across the endoplasmic reticulum. I. Detection in the microsomal membrane of a receptor for the signal recognition particle. J. Cell Biol. *95*, 463–469.

Glisovic, T., Bachorik, J.L., Yong, J., and Dreyfuss, G. (2008). RNA-binding proteins and post-transcriptional gene regulation. FEBS Lett. *582*, 1977–1986.

Gonzalez, I., Buonomo, S.B., Nasmyth, K., and von Ahsen, U. (1999). ASH1 mRNA localization in yeast involves multiple secondary structural elements and Ash1 protein translation. Curr. Biol. *9*, 337–340.

Görlich, D., and Rapoport, T.A. (1993). Protein translocation into proteoliposomes reconstituted from purified components of the endoplasmic reticulum membrane. Cell *75*, 615–630.

Grishin, N. V (2001). KH domain: one motif, two folds. Nucleic Acids Res. *29*, 638–643.

Gu, W., Deng, Y., Zenklusen, D., and Singer, R.H. (2004). A new yeast PUF family protein, Puf6p, represses ASH1 mRNA translation and is required for its localization. Genes Dev. *18*, 1452–1465.

Haarer, B.K., Petzold, A., Lillie, S.H., and Brown, S.S. (1994). Identification of MYO4, a second class V myosin gene in yeast. J. Cell Sci. *107 (Pt 4)*, 1055–1064.

Halic, M., and Beckmann, R. (2005). The signal recognition particle and its interactions during protein targeting. Curr. Opin. Struct. Biol. *15*, 116–125.

Hann, B.C., and Walter, P. (1991). The signal recognition particle in S. cerevisiae. Cell *67*, 131–144.

Hann, B.C., Poritz, M.A., and Walter, P. (1989). Saccharomyces cerevisiae and Schizosaccharomyces pombe contain a homologue to the 54-kD subunit of the signal recognition particle that in S. cerevisiae is essential for growth. J. Cell Biol. *109*, 3223–3230.

Harada, Y., Li, H.H., Wall, J.S., Li, H.H., and Lennarz, W.J. (2011). Structural studies and the assembly of the heptameric post-translational translocon complex. J. Biol. Chem. *286*, 2956–2965.

Hasegawa, Y., Irie, K., and Gerber, A.P. (2008). Distinct roles for Khd1p in the localization and expression of bud-localized mRNAs in yeast. RNA *14*, 2333–2347.

Hebert, D.N., Garman, S.C., and Molinari, M. (2005). The glycan code of the endoplasmic reticulum: asparagine-linked carbohydrates as protein maturation and quality-control tags. Trends Cell Biol. *15*, 364–370.

Hegde, R.S., and Keenan, R.J. (2011). Tail-anchored membrane protein insertion into the endoplasmic reticulum. Nat. Rev. Mol. Cell Biol. *12*, 787–798.

von Heijne, G. (1983). Patterns of amino acids near signal-sequence cleavage sites. Eur. J. Biochem. *133*, 17–21.

Herrmann, J.M., Neupert, W., and Stuart, R.A. (1997). Insertion into the mitochondrial inner membrane of a polytopic protein, the nuclear-encoded Oxa1p. EMBO J. *16*, 2217–2226.

Herskowitz, I. (1988). Life cycle of the budding yeast Saccharomyces cerevisiae. Microbiol. Rev. *52*, 536–553.

Herve, C., Mickleburgh, I., and Hesketh, J. (2004). Zipcodes and postage stamps: mRNA localisation signals and their trans-acting binding proteins. Briefings Funct. Genomics Proteomics *3*, 240–256.

Heuck, A., Du, T.-G., Jellbauer, S., Richter, K., Kruse, C., Jaklin, S., Muller, M., Buchner, J., Jansen, R.-P., and Niessing, D. (2007). Monomeric myosin V uses two binding regions for the assembly of stable translocation complexes. Proc. Natl. Acad. Sci. *104*, 19778–19783.

Heuck, A., Fetka, I., Brewer, D.N., Hüls, D., Munson, M., Jansen, R.-P., and Niessing, D. (2010). The structure of the Myo4p globular tail and its function in ASH1 mRNA localization. J. Cell Biol. *189*,

497–510.

Heym, R.G., and Niessing, D. (2012). Principles of mRNA transport in yeast. Cell. Mol. Life Sci. *69*, 1843–1853.

Heym, R.G., Zimmermann, D., Edelmann, F.T., Israel, L., Ökten, Z., Kovar, D.R., and Niessing, D. (2013). In vitro reconstitution of an mRNA-transport complex reveals mechanisms of assembly and motor activation. J. Cell Biol. *203*, 971–984.

High, S., and Dobberstein, B. (1991). The signal sequence interacts with the methionine-rich domain of the 54-kD protein of signal recognition particle. J. Cell Biol. *113*, 229–233.

Hikita, C., and Mizushimas, S. (1992). THE JOURNAL OF BIOLOGICAL CHEMISTRY Effects of Total Hydrophobicity and Length of the Hydrophobic Domain of a Signal Peptide on in Vitro Translocation Efficiency*.

Hilgers, V., Teixeira, D., and Parker, R. (2006). Translation-independent inhibition of mRNA deadenylation during stress in Saccharomyces cerevisiae. RNA *12*, 1835–1845.

Hogan, D.J., Riordan, D.P., Gerber, A.P., Herschlag, D., and Brown, P.O. (2008). Diverse RNA-Binding Proteins Interact with Functionally Related Sets of RNAs, Suggesting an Extensive Regulatory System. PLoS Biol. *6*, e255.

Hogg, R., McGrail, J.C., and O'Keefe, R.T. (2010). The function of the NineTeen Complex (NTC) in regulating spliceosome conformations and fidelity during pre-mRNA splicing. Biochem. Soc. Trans. *38*, 1110–1115.

Holmes, K.J., Klass, D.M., Guiney, E.L., and Cyert, M.S. (2013). Whi3, an S. cerevisiae RNA-Binding Protein, Is a Component of Stress Granules That Regulates Levels of Its Target mRNAs. PLoS One *8*, e84060.

Van Horn, D.J., Yoo, C.J., Xue, D., Shi, H., and Wolin, S.L. (1997). The La protein in Schizosaccharomyces pombe: a conserved yet dispensable phosphoprotein that functions in tRNA maturation. RNA *3*, 1434–1443.

Hu, J., Li, J., Qian, X., Denic, V., and Sha, B. (2009). The Crystal Structures of Yeast Get3 Suggest a Mechanism for Tail-Anchored Protein Membrane Insertion. PLoS One *4*, e8061.

Huh, W.-K., Falvo, J. V., Gerke, L.C., Carroll, A.S., Howson, R.W., Weissman, J.S., and O'Shea, E.K. (2003). Global analysis of protein localization in budding yeast. Nature *425*, 686–691.

Irie, K., Tadauchi, T., Takizawa, P.A., Vale, R.D., Matsumoto, K., and Herskowitz, I. (2002). The Khd1 protein, which has three KH RNA-binding motifs, is required for proper localization of ASH1 mRNA in yeast. EMBO J. *21*, 1158–1167.

Ito, W., Li, X., Irie, K., Mizuno, T., and Irie, K. (2011). RNA-Binding Protein Khd1 and Ccr4 Deadenylase Play Overlapping Roles in the Cell Wall Integrity Pathway in Saccharomyces cerevisiae. Eukaryot. Cell *10*, 1340–1347.

Ito, Y., Kitagawa, T., Yamanishi, M., Katahira, S., Izawa, S., Irie, K., Furutani-Seiki, M., and Matsuyama, T. (2016). Enhancement of protein production via the strong DIT1 terminator and two RNA-binding proteins in Saccharomyces cerevisiae. Sci. Rep. *6*, 36997.

Jagannathan, S., Reid, D.W., Cox, A.H., and Nicchitta, C. V. (2014). De novo translation initiation on membrane-bound ribosomes as a mechanism for localization of cytosolic protein mRNAs to the endoplasmic reticulum. RNA *20*, 1489–1498.

Jain, S., Wheeler, J.R., Walters, R.W., Agrawal, A., Barsic, A., and Parker, R. (2016). ATPase-Modulated Stress Granules Contain a Diverse Proteome and Substructure. Cell *164*, 487–498.

Jambhekar, A., and DeRisi, J.L. (2007). Cis-acting determinants of asymmetric, cytoplasmic RNA transport. RNA *13*, 625–642.

Jambhekar, A., McDermott, K., Sorber, K., Shepard, K.A., Vale, R.D., Takizawa, P.A., and DeRisi,

J.L. (2005). Unbiased selection of localization elements reveals cis-acting determinants of mRNA bud localization in Saccharomyces cerevisiae. Proc. Natl. Acad. Sci. *102*, 18005–18010.

Jan, C.H., Williams, C.C., and Weissman, J.S. (2014). Principles of ER cotranslational translocation revealed by proximity-specific ribosome profiling. Science (80-.). *346*, 1257521–1257521.

Janda, C.Y., Li, J., Oubridge, C., Hernández, H., Robinson, C. V, and Nagai, K. (2010). Recognition of a signal peptide by the signal recognition particle. Nature *465*, 507–510.

Jang, L.-T., Buu, L.-M., and Lee, F.-J.S. (2006). Determinants of Rbp1p localization in specific cytoplasmic mRNA-processing foci, P-bodies. J. Biol. Chem. *281*, 29379–29390.

Jansen, R.P., Dowzer, C., Michaelis, C., Galova, M., and Nasmyth, K. (1996). Mother cell-specific HO expression in budding yeast depends on the unconventional myosin myo4p and other cytoplasmic proteins. Cell *84*, 687–697.

de Jong, M., van Breukelen, B., Wittink, F.R., Menke, F.L.H., Weisbeek, P.J., and Ackerveken, G. Van den (2006). Membrane-associated transcripts in Arabidopsis; their isolation and characterization by DNA microarray analysis and bioinformatics. Plant J. *46*, 708–721.

Jonikas, M.C., Collins, S.R., Denic, V., Oh, E., Quan, E.M., Schmid, V., Weibezahn, J., Schwappach, B., Walter, P., Weissman, J.S., et al. (2009). Comprehensive characterization of genes required for protein folding in the endoplasmic reticulum. Science *323*, 1693–1697.

Kagami, M., Toh-e, A., and Matsui, Y. (1997). SRO9, a multicopy suppressor of the bud growth defect in the Saccharomyces cerevisiae rho3-deficient cells, shows strong genetic interactions with tropomyosin genes, suggesting its role in organization of the actin cytoskeleton. Genetics *147*, 1003–1016.

Kershaw, C.J., Costello, J.L., Castelli, L.M., Talavera, D., Rowe, W., Sims, P.F.G., Ashe, M.P., Hubbard, S.J., Pavitt, G.D., and Grant, C.M. (2015). The Yeast La Related Protein Slf1p Is a Key Activator of Translation during the Oxidative Stress Response. PLoS Genet. *11*, e1004903.

Klimek-Tomczak, K., Wyrwicz, L.S., Jain, S., Bomsztyk, K., and Ostrowski, J. (2004). Characterization of hnRNP K Protein–RNA Interactions. J. Mol. Biol. *342*, 1131–1141.

Komili, S., Farny, N.G., Roth, F.P., and Silver, P.A. (2007). Functional Specificity among Ribosomal Proteins Regulates Gene Expression. Cell *131*, 557–571.

Kramer, K., Sachsenberg, T., Beckmann, B.M., Qamar, S., Boon, K.-L., Hentze, M.W., Kohlbacher, O., and Urlaub, H. (2014). Photo-cross-linking and high-resolution mass spectrometry for assignment of RNA-binding sites in RNA-binding proteins. Nat. Methods *11*, 1064–1070.

Kraut-Cohen, J., and Gerst, J.E. (2010). Addressing mRNAs to the ER: cis sequences act up! Trends Biochem. Sci. *35*, 459–469.

Kraut-Cohen, J., Afanasieva, E., Haim-Vilmovsky, L., Slobodin, B., Yosef, I., Bibi, E., and Gerst, J.E. (2013). Translation- and SRP-independent mRNA targeting to the endoplasmic reticulum in the yeast Saccharomyces cerevisiae. Mol. Biol. Cell *24*, 3069–3084.

Krementsova, E.B., Hodges, A.R., Bookwalter, C.S., Sladewski, T.E., Travaglia, M., Sweeney, H.L., and Trybus, K.M. (2011). Two single-headed myosin V motors bound to a tetrameric adapter protein form a processive complex. J. Cell Biol. *195*, 631–641.

Kubota, K., Yamagata, A., Sato, Y., Goto-Ito, S., and Fukai, S. (2012). Get1 Stabilizes an Open Dimer Conformation of Get3 ATPase by Binding Two Distinct Interfaces. J. Mol. Biol. *422*, 366–375.

Lee, F.J., and Moss, J. (1993). An RNA-binding protein gene (RBP1) of Saccharomyces cerevisiae encodes a putative glucose-repressible protein containing two RNA recognition motifs. J. Biol. Chem. *268*, 15080–15087.

Lee, H.C., and Bernstein, H.D. (2001). The targeting pathway of Escherichia coli presecretory and integral membrane proteins is specified by the hydrophobicity of the targeting signal. Proc. Natl. Acad. Sci. U. S. A. *98*, 3471–3476.

Lee, H.C., Bernstein, H.D., and Beckwith, J. The targeting pathway of Escherichia coli presecretory and integral membrane proteins is specified by the hydrophobicity of the targeting signal.

Lin-Marq, N., and Clarkson, S.G. (1995). A Yeast RNA Binding Protein that Resembles the Human Autoantigen La. J. Mol. Biol. *245*, 81–85.

Linder, P., and Jankowsky, E. (2011). From unwinding to clamping — the DEAD box RNA helicase family. Nat. Rev. Mol. Cell Biol. *12*, 505–516.

Long, R.M., Gu, W., Lorimer, E., Singer, R.H., and Chartrand, P. (2000). She2p is a novel RNA-binding protein that recruits the Myo4p-She3p complex to ASH1 mRNA. EMBO J. *19*, 6592–6601.

Long, R.M., Gu, W., Meng, X., Gonsalvez, G., Singer, R.H., and Chartrand, P. (2001). An exclusively nuclear RNA-binding protein affects asymmetric localization of ASH1 mRNA and Ash1p in yeast. J. Cell Biol. *153*, 307–318.

Loya, A., Pnueli, L., Yosefzon, Y., Wexler, Y., Ziv-Ukelson, M., and Arava, Y. (2008). The 3'-UTR mediates the cellular localization of an mRNA encoding a short plasma membrane protein. RNA *14*, 1352–1365.

Machin, N.A., Lee, J.M., and Barnes, G. (1995). Microtubule stability in budding yeast: characterization and dosage suppression of a benomyl-dependent tubulin mutant. Mol. Biol. Cell *6*, 1241–1259.

Mandon, E.C., Trueman, S.F., and Gilmore, R. (2013). Protein translocation across the rough endoplasmic reticulum. Cold Spring Harb. Perspect. Biol. *5*, a013342.

Mangus, D.A., Amrani, N., and Jacobson, A. (1998). Pbp1p, a factor interacting with Saccharomyces cerevisiae poly(A)-binding protein, regulates polyadenylation. Mol. Cell. Biol. *18*, 7383–7396.

Mariappan, M., Mateja, A., Dobosz, M., Bove, E., Hegde, R.S., and Keenan, R.J. (2011). The mechanism of membrane-associated steps in tail-anchored protein insertion. Nature *477*, 61–66.

Mateja, A., Szlachcic, A., Downing, M.E., Dobosz, M., Mariappan, M., Hegde, R.S., and Keenan, R.J. (2009). The structural basis of tail-anchored membrane protein recognition by Get3. Nature *461*, 361–366.

Merz, S., and Westermann, B. (2009). Genome-wide deletion mutant analysis reveals genes required for respiratory growth, mitochondrial genome maintenance and mitochondrial protein synthesis in Saccharomyces cerevisiae. Genome Biol. *10*, R95.

Miller, M.T., Higgin, J.J., and Tanaka Hall, T.M. (2008). Basis of altered RNA-binding specificity by PUF proteins revealed by crystal structures of yeast Puf4p. Nat. Struct. Mol. Biol. *15*, 397–402.

Milstein, C., Brownlee, G.G., Harrison, T.M., and Mathews, M.B. (1972). A possible precursor of immunoglobulin light chains. Nat. New Biol. *239*, 117–120.

Mitchell, S.F., Jain, S., She, M., and Parker, R. (2013). Global analysis of yeast mRNPs. Nat. Struct. Mol. Biol. *20*, 127–133.

Mize, N.K., Andrews, D.W., and Lingappa, V.R. (1986). A stop transfer sequence recognizes receptors for nascent chain translocation across the endoplasmic reticulum membrane. Cell *47*, 711–719.

Moldavski, O., Amen, T., Levin-Zaidman, S., Eisenstein, M., Rogachev, I., Brandis, A., Kaganovich, D., and Schuldiner, M. (2015). Lipid Droplets Are Essential for Efficient Clearance of Cytosolic Inclusion Bodies. Dev. Cell *33*, 603–610.

Mösch, H.U., and Fink, G.R. (1997). Dissection of filamentous growth by transposon mutagenesis in Saccharomyces cerevisiae. Genetics *145*, 671–684.

Muller, M., Richter, K., Heuck, A., Kremmer, E., Buchner, J., Jansen, R.-P., and Niessing, D. (2009). Formation of She2p tetramers is required for mRNA binding, mRNP assembly, and localization. RNA *15*, 2002–2012.

Müller, M., Heym, R.G., Mayer, A., Kramer, K., Schmid, M., Cramer, P., Urlaub, H., Jansen, R.-P., and Niessing, D. (2011). A Cytoplasmic Complex Mediates Specific mRNA Recognition and

Localization in Yeast. PLoS Biol. *9*, e1000611.

Münchow, S., Sauter, C., and Jansen, R.P. (1999). Association of the class V myosin Myo4p with a localised messenger RNA in budding yeast depends on She proteins. J. Cell Sci. *112 (Pt 10)*, 1511–1518.

Nash, R.S., Volpe, T., and Futcher, B. (2001). Isolation and characterization of WHI3, a size-control gene of Saccharomyces cerevisiae. Genetics *157*, 1469–1480.

Nasmyth, K.A. (1982). Molecular Genetics of Yeast Mating Type. Annu. Rev. Genet. *16*, 439–500.

Nevo-Dinur, K., Nussbaum-Shochat, A., Ben-Yehuda, S., and Amster-Choder, O. (2011). Translation-Independent Localization of mRNA in E. coli. Science (80-.). *331*, 1081–1084.

Ng, D.T., Brown, J.D., and Walter, P. (1996). Signal sequences specify the targeting route to the endoplasmic reticulum membrane. J. Cell Biol. *134*, 269–278.

Niedner, A., Muller, M., Moorthy, B.T., Jansen, R.-P., and Niessing, D. (2013). Role of Loc1p in assembly and reorganization of nuclear ASH1 messenger ribonucleoprotein particles in yeast. Proc. Natl. Acad. Sci. *110*, E5049–E5058.

Niessing, D. (2013). RNA-BINDING PROTEINS IN FUNGI AND THEIR ROLE IN mRNA LOCALIZATION.

Niessing, D., Jansen, R.-P., Pohlmann, T., and Feldbrügge, M. (2018). mRNA transport in fungal top models. Wiley Interdiscip. Rev. RNA *9*, e1453.

Nuoffer, C., Jenö, P., Conzelmann, A., and Riezman, H. (1991). Determinants for glycophospholipid anchoring of the Saccharomyces cerevisiae GAS1 protein to the plasma membrane. Mol. Cell. Biol. *11*, 27–37.

O'Donnell, W.T., and Warren, S.T. (2002). A Decade of Molecular Studies of Fragile X Syndrome. Annu. Rev. Neurosci. *25*, 315–338.

Oeffinger, M., Wei, K.E., Rogers, R., DeGrasse, J.A., Chait, B.T., Aitchison, J.D., and Rout, M.P. (2007). Comprehensive analysis of diverse ribonucleoprotein complexes. Nat. Methods *4*, 951–956.

Olivier, C., Poirier, G., Gendron, P., Boisgontier, A., Major, F., and Chartrand, P. (2005). Identification of a Conserved RNA Motif Essential for She2p Recognition and mRNA Localization to the Yeast Bud. Mol. Cell. Biol. *25*, 4752–4766.

Palazzo, A.F., Springer, M., Shibata, Y., Lee, C.-S., Dias, A.P., and Rapoport, T.A. (2007). The signal sequence coding region promotes nuclear export of mRNA. PLoS Biol. *5*, e322.

Panzner, S., Dreier, L., Hartmann, E., Kostka, S., and Rapoport', T.A. (1995). Posttranslational Protein Transport in Yeast Reconstituted with a Purified Complex of Set Proteins and Kar2p.

Paquin, N., Ménade, M., Poirier, G., Donato, D., Drouet, E., and Chartrand, P. (2007). Local Activation of Yeast ASH1 mRNA Translation through Phosphorylation of Khd1p by the Casein Kinase Yck1p. Mol. Cell *26*, 795–809.

Poritz, M.A., Bernstein, H.D., Strub, K., Zopf, D., Wilhelm, H., and Walter, P. (1990). An E. coli ribonucleoprotein containing 4.5S RNA resembles mammalian signal recognition particle. Science *250*, 1111–1117.

Prilusky, J., and Bibi, E. (2009). Studying membrane proteins through the eyes of the genetic code revealed a strong uracil bias in their coding mRNAs. Proc. Natl. Acad. Sci. U. S. A. *106*, 6662–6666.

Van Puyenbroeck, V., and Vermeire, K. (2018). Inhibitors of protein translocation across membranes of the secretory pathway: novel antimicrobial and anticancer agents. Cell. Mol. Life Sci. *75*, 1541–1558.

Pyhtila, B., Zheng, T., Lager, P.J., Keene, J.D., Reedy, M.C., and Nicchitta, C. V (2008). Signal sequence- and translation-independent mRNA localization to the endoplasmic reticulum. RNA *14*, 445–453.

Rapoport, T.A. (2007). Protein translocation across the eukaryotic endoplasmic reticulum and bacterial plasma membranes. Nature *450*, 663–669.

Redman, C.M., and Sabatini, D.D. (1966). Vectorial discharge of peptides released by puromycin from attached ribosomes. Proc. Natl. Acad. Sci. U. S. A. *56*, 608–615.

Redman, C.M., Siekevitz, P., and Palade, G.E. (1966). Synthesis and transfer of amylase in pigeon pancreatic micromosomes. J. Biol. Chem. *241*, 1150–1158.

Reid, D.W., and Nicchitta, C. V. (2012). Primary Role for Endoplasmic Reticulum-bound Ribosomes in Cellular Translation Identified by Ribosome Profiling. J. Biol. Chem. *287*, 5518–5527.

Reid, D.W., and Nicchitta, C. V. (2015). Diversity and selectivity in mRNA translation on the endoplasmic reticulum. Nat. Rev. Mol. Cell Biol. *16*, 221–231.

Ren, Y.-G., Wagner, K.W., Knee, D.A., Aza-Blanc, P., Nasoff, M., and Deveraux, Q.L. (2004). Differential Regulation of the TRAIL Death Receptors DR4 and DR5 by the Signal Recognition Particle. Mol. Biol. Cell *15*, 5064–5074.

Ricarte, F., Menjivar, R., Chhun, S., Soreta, T., Oliveira, L., Hsueh, T., Serranilla, M., and Gharakhanian, E. (2011). A Genome-Wide Immunodetection Screen in S. cerevisiae Uncovers Novel Genes Involved in Lysosomal Vacuole Function and Morphology. PLoS One *6*, e23696.

Richardson, R., Denis, C.L., Zhang, C., Nielsen, M.E.O., Chiang, Y.-C., Kierkegaard, M., Wang, X., Lee, D.J., Andersen, J.S., and Yao, G. (2012). Mass spectrometric identification of proteins that interact through specific domains of the poly(A) binding protein. Mol. Genet. Genomics *287*, 711–730.

Rouvière, J.O., Bulfoni, M., Tuck, A., Cosson, B., Devaux, F., and Palancade, B. (2018). A SUMO-dependent feedback loop senses and controls the biogenesis of nuclear pore subunits. Nat. Commun. *9*, 1665.

Sachdev, R., Hondele, M., Linsenmeier, M., Vallotton, P., Mugler, C.F., Arosio, P., and Weis, K. (2019). Pat1 promotes processing body assembly by enhancing the phase separation of the DEAD-box ATPase Dhh1 and RNA. Elife *8*.

Samanta, M.P., and Liang, S. (2003). Predicting protein functions from redundancies in large-scale protein interaction networks. Proc. Natl. Acad. Sci. U. S. A. *100*, 12579–12583.

Schenk, L., Meinel, D.M., Strässer, K., and Gerber, A.P. (2012). La-motif–dependent mRNA association with Slf1 promotes copper detoxification in yeast. RNA *18*, 449–461.

Schladebeck, S., and Mösch, H.-U. (2013). The RNA-binding protein Whi3 is a key regulator of developmental signaling and ploidy in Saccharomyces cerevisiae. Genetics *195*, 73–86.

Schlenstedt, G., and Zimmermann, R. (1987). Import of frog prepropeptide GLa into microsomes requires ATP but does not involve docking protein or ribosomes. EMBO J. *6*, 699–703.

Schlenstedt, G., Gudmundsson, G.H., Boman, H.G., and Zimmermann, R. (1992). Structural requirements for transport of preprocecropinA and related presecretory proteins into mammalian microsomes. J. Biol. Chem. *267*, 24328–24332.

Schmid, M., Jaedicke, A., Du, T.-G., and Jansen, R.-P. (2006). Coordination of Endoplasmic Reticulum and mRNA Localization to the Yeast Bud. Curr. Biol. *16*, 1538–1543.

Schuldiner, M., Metz, J., Schmid, V., Denic, V., Rakwalska, M., Schmitt, H.D., Schwappach, B., and Weissman, J.S. (2008). The GET complex mediates insertion of tail-anchored proteins into the ER membrane. Cell *134*, 634–645.

Schwarz, D.S., and Blower, M.D. (2016). The endoplasmic reticulum: structure, function and response to cellular signaling. Cell. Mol. Life Sci. *73*, 79–94.

Shahbabian, K., Jeronimo, C., Forget, A., Robert, F., and Chartrand, P. (2014). Co-transcriptional recruitment of Puf6 by She2 couples translational repression to mRNA localization. Nucleic Acids Res. *42*, 8692–8704.

Shao, S., and Hegde, R.S. (2011). Membrane Protein Insertion at the Endoplasmic Reticulum. Annu. Rev. Cell Dev. Biol. *27*, 25–56.

Shepard, K.A., Gerber, A.P., Jambhekar, A., Takizawa, P.A., Brown, P.O., Herschlag, D., DeRisi, J.L., and Vale, R.D. (2003). Widespread cytoplasmic mRNA transport in yeast: Identification of 22 bud-localized transcripts using DNA microarray analysis. Proc. Natl. Acad. Sci. *100*, 11429–11434.

Sheth, U., and Parker, R. (2003). Decapping and decay of messenger RNA occur in cytoplasmic processing bodies. Science *300*, 805–808.

Shi, H., Singh, N., Esselborn, F., and Blobel, G. (2014). Structure of a myosin•adaptor complex and pairing by cargo. Proc. Natl. Acad. Sci. U. S. A. *111*, E1082-90.

Sil, A., and Herskowitz, I. (1996). Identification of asymmetrically localized determinant, Ash1p, required for lineage-specific transcription of the yeast HO gene. Cell *84*, 711–722.

Siomi, H., Matunis, M.J., Michael, W.M., and Dreyfuss, G. (1993a). The pre-mRNA binding K protein contains a novel evolutionarily conserved motif. Nucleic Acids Res. *21*, 1193–1198.

Siomi, H., Siomi, M.C., Nussbaum, R.L., and Dreyfuss, G. (1993b). The protein product of the fragile X gene, FMR1, has characteristics of an RNA-binding protein. Cell *74*, 291–298.

Sobel, S.G., and Wolin, S.L. (1999). Two yeast La motif-containing proteins are RNA-binding proteins that associate with polyribosomes. Mol. Biol. Cell *10*, 3849–3862.

Stefano, J.E. (1984). Purified lupus antigen La recognizes an oligouridylate stretch common to the 3' termini of RNA polymerase III transcripts. Cell *36*, 145–154.

Stefanovic, S., and Hegde, R.S. (2007). Identification of a targeting factor for posttranslational membrane protein insertion into the ER. Cell *128*, 1147–1159.

Stefer, S., Reitz, S., Wang, F., Wild, K., Pang, Y.-Y., Schwarz, D., Bomke, J., Hein, C., Löhr, F., Bernhard, F., et al. (2011). Structural basis for tail-anchored membrane protein biogenesis by the Get3-receptor complex. Science *333*, 758–762.

Stillman, D.J. (2010). Nhp6: a small but powerful effector of chromatin structure in Saccharomyces cerevisiae. Biochim. Biophys. Acta *1799*, 175–180.

Stirling, C.J., Rothblatt, J., Hosobuchi, M., Deshaies, R., and Schekman, R. (1992). Protein Translocation Mutants Defective in the Insertion of Integral Membrane Proteins into the Endoplasmic Reticulum.

Suloway, C.J.M., Chartron, J.W., Zaslaver, M., and Clemons, W.M. (2009). Model for eukaryotic tail-anchored protein binding based on the structure of Get3. Proc. Natl. Acad. Sci. U. S. A. *106*, 14849–14854.

Syed, M.I., Moorthy, B.T., Jenner, A., Fetka, I., and Jansen, R.-P. (2018). Signal sequence-independent targeting of MID2 mRNA to the endoplasmic reticulum by the yeast RNA-binding protein Khd1p. FEBS Lett. *592*.

Takizawa, P.A., and Vale, R.D. (2000). The myosin motor, Myo4p, binds Ash1 mRNA via the adapter protein, She3p. Proc. Natl. Acad. Sci. U. S. A. *97*, 5273–5278.

Teixeira, D., Sheth, U., Valencia-Sanchez, M.A., Brengues, M., and Parker, R. (2005). Processing bodies require RNA for assembly and contain nontranslating mRNAs. RNA *11*, 371–382.

Tijerina, P., Mohr, S., and Russell, R. (2007). DMS footprinting of structured RNAs and RNA–protein complexes. Nat. Protoc. *2*, 2608–2623.

Toi, H., Fujimura-Kamada, K., Irie, K., Takai, Y., Todo, S., and Tanaka, K. (2003). She4p/Dim1p Interacts with the Motor Domain of Unconventional Myosins in the Budding Yeast, *Saccharomyces cerevisiae*. Mol. Biol. Cell *14*, 2237–2249.

Tomishige, N., Noda, Y., Adachi, H., Shimoi, H., Takatsuki, A., and Yoda, K. (2003). Mutations that are synthetically lethal with a gas1? allele cause defects in the cell wall of Saccharomyces cerevisiae.

Mol. Genet. Genomics *269*, 562–573.

Tyedmers, J., Lerner, M., Bies, C., Dudek, J., Skowronek, M.H., Haas, I.G., Heim, N., Nastainczyk, W., Volkmer, J., and Zimmermann, R. (2000). Homologs of the yeast Sec complex subunits Sec62p and Sec63p are abundant proteins in dog pancreas microsomes. Proc. Natl. Acad. Sci. U. S. A. *97*, 7214–7219.

Ulbricht, R.J., and Olivas, W.M. (2007). Puf1p acts in combination with other yeast Puf proteins to control mRNA stability. RNA *14*, 246–262.

Urbinati, C.R., Gonsalvez, G.B., Aris, J.P., and Long, R.M. (2006). Loc1p is required for efficient assembly and nuclear export of the 60S ribosomal subunit. Mol. Genet. Genomics *276*, 369–377.

Valverde, R., Edwards, L., and Regan, L. (2008). Structure and function of KH domains. FEBS J. *275*, 2712–2726.

Vergés, E., Colomina, N., Garí, E., Gallego, C., and Aldea, M. (2007). Cyclin Cln3 Is Retained at the ER and Released by the J Chaperone Ydj1 in Late G1 to Trigger Cell Cycle Entry. Mol. Cell *26*, 649–662.

Vilardi, F., Lorenz, H., and Dobberstein, B. (2011). WRB is the receptor for TRC40/Asna1-mediated insertion of tail-anchored proteins into the ER membrane. J. Cell Sci. *124*, 1301–1307.

Walter, P., and Blobel, G. (1980). Purification of a membrane-associated protein complex required for protein translocation across the endoplasmic reticulum. Proc. Natl. Acad. Sci. U. S. A. *77*, 7112–7116.

Walter, P., and Blobel, G. (1981a). Translocation of proteins across the endoplasmic reticulum III. Signal recognition protein (SRP) causes signal sequence-dependent and site-specific arrest of chain elongation that is released by microsomal membranes. J. Cell Biol. *91*, 557–561.

Walter, P., and Blobel, G. (1981b). Translocation of proteins across the endoplasmic reticulum. II. Signal recognition protein (SRP) mediates the selective binding to microsomal membranes of in-vitro-assembled polysomes synthesizing secretory protein. J. Cell Biol. *91*, 551–556.

Walter, P., and Blobel, G. (1982). Signal recognition particle contains a 7S RNA essential for protein translocation across the endoplasmic reticulum. Nature *299*, 691–698.

Wang, H., Garí, E., Vergés, E., Gallego, C., and Aldea, M. (2004). Recruitment of Cdc28 by Whi3 restricts nuclear accumulation of the G1 cyclin-Cdk complex to late G1. EMBO J. *23*, 180–190.

Wang, X., Zamore, P.D., and Hall, T.M.T. (2001). Crystal Structure of a Pumilio Homology Domain. Mol. Cell *7*, 855–865.

Wang, X., McLachlan, J., Zamore, P.D., and Hall, T.M.T. (2002). Modular recognition of RNA by a human pumilio-homology domain. Cell *110*, 501–512.

Wang, Y., Opperman, L., Wickens, M., and Hall, T.M.T. (2009). Structural basis for specific recognition of multiple mRNA targets by a PUF regulatory protein. Proc. Natl. Acad. Sci. *106*, 20186–20191.

Waters, M.G., and Blobel, G. (1986). Secretory protein translocation in a yeast cell-free system can occur posttranslationally and requires ATP hydrolysis. J. Cell Biol. *102*, 1543–1550.

Wesche, S., Arnold, M., and Jansen, R.-P. (2003). The UCS domain protein She4p binds to myosin motor domains and is essential for class I and class V myosin function. Curr. Biol. *13*, 715–724.

Wolin, S.L., and Cedervall, T. (2002). The La Protein. Annu. Rev. Biochem. *71*, 375–403.

Wu, C.-H., Lee, S.-C., and Wang, C.-W. (2011). Viral protein targeting to the cortical endoplasmic reticulum is required for cell–cell spreading in plants. J. Cell Biol. *193*, 521–535.

Yabal, M., Brambillasca, S., Soffientini, P., Pedrazzini, E., Borgese, N., and Makarow, M. (2003). Translocation of the C terminus of a tail-anchored protein across the endoplasmic reticulum membrane in yeast mutants defective in signal peptide-driven translocation. J. Biol. Chem. *278*, 3489–3496.

Yamamoto, Y., and Sakisaka, T. (2012). Molecular Machinery for Insertion of Tail-Anchored Membrane Proteins into the Endoplasmic Reticulum Membrane in Mammalian Cells. Mol. Cell *48*, 387–397.

Yamamoto, Y., Taniyama, Y., Kukuchi, M., and Ikehara, M. (1987). Engineering of the hydrophobic segment of the signal sequence for efficient secretion of human lysozyme by Saccharomycescerevisiae. Biochem. Biophys. Res. Commun. *149*, 431–436.

Yang, R., Gaidamakov, S.A., Xie, J., Lee, J., Martino, L., Kozlov, G., Crawford, A.K., Russo, A.N., Conte, M.R., Gehring, K., et al. (2011). La-related protein 4 binds poly(A), interacts with the poly(A)-binding protein MLLE domain via a variant PAM2w motif, and can promote mRNA stability. Mol. Cell. Biol. *31*, 542–556.

Yoo, C.J., and Wolin, S.L. (1994). La proteins from Drosophila melanogaster and Saccharomyces cerevisiae: a yeast homolog of the La autoantigen is dispensable for growth. Mol. Cell. Biol. *14*, 5412–5424.

Yosefzon, Y., Koh, Y.Y., Chritton, J.J., Lande, A., Leibovich, L., Barziv, L., Petzold, C., Yakhini, Z., Mandel-Gutfreund, Y., Wickens, M., et al. (2011). Divergent RNA binding specificity of yeast Puf2p. Rna *17*, 1479–1488.

Yu, W., Farrell, R.A., Stillman, D.J., and Winge, D.R. (1996). Identification of SLF1 as a new copper homeostasis gene involved in copper sulfide mineralization in Saccharomyces cerevisiae. Mol. Cell. Biol. *16*, 2464–2472.

Zamore, P.D., Williamson, J.R., and Lehmann, R. (1997). The Pumilio protein binds RNA through a conserved domain that defines a new class of RNA-binding proteins. RNA *3*, 1421–1433.

Zhang, B., Gallegos, M., Puoti, A., Durkin, E., Fields, S., Kimble, J., and Wickens, M.P. (1997). A conserved RNA-binding protein that regulates sexual fates in the C. elegans hermaphrodite germ line. Nature *390*, 477–484.

Zhang, Q., Meng, X., Li, D., Chen, S., Luo, J., Zhu, L., Singer, R.H., and Gu, W. (2017). Binding of DEAD-box helicase Dhh1 to the 5'-untranslated region of ASH1 mRNA represses localized translation of ASH1 in yeast cells. J. Biol. Chem. *292*, 9787–9800.

Zhang, Y., Schäffer, T., Wölfle, T., Fitzke, E., Thiel, G., and Rospert, S. (2016). Cotranslational Intersection between the SRP and GET Targeting Pathways to the Endoplasmic Reticulum of Saccharomyces cerevisiae. Mol. Cell. Biol. *36*, 2374–2383.

Zhu, D., Stumpf, C.R., Krahn, J.M., Wickens, M., and Hall, T.M.T. (2009). A 5' cytosine binding pocket in Puf3p specifies regulation of mitochondrial mRNAs. Proc. Natl. Acad. Sci. *106*, 20192–20197.

Zimmermann, R., Zimmermann, M., Wiech, H., Schlenstedt, G., Müller, G., Morel, F., Klappa, P., Jung, C., and Cobet, W.W. (1990). Ribonucleoparticle-independent transport of proteins into mammalian microsomes. J. Bioenerg. Biomembr. *22*, 711–723.

Zopf, D., Bernstein, H.D., Johnson, A.E., and Walter, P. (1990). The methionine-rich domain of the 54 kd protein subunit of the signal recognition particle contains an RNA binding site and can be crosslinked to a signal sequence. EMBO J. *9*, 4511–4517.

11. Acknowledgements

First of all, I sincerely thank Prof. Dr. Ralf-Peter Jansen for providing me the opportunity to do Ph.D. in his laboratory. I am extremely grateful for his extensive supervision and the constructive feedback that I got from him during that time. I am also thankful to my lab colleagues (especially Joyita Mukherji, Manchalu Srinivas, Nidhi Kanwal and Matthew Cheng) for their help, guidance and for maintaining a socially-friendly environment during my entire Ph.D. period.

Additionally, I want to thank Prof. Dr. Doron Rapaport, Prof. Dr. Gabriele Dodt and Prof. Dr. Thorsten Stafforst for their time and effort as members of my doctoral examination committee.

I want to acknowledge everyone working in AG Rapaport for the successful collaboration and for sharing materials and methods. I also want to express my gratitude for the time and effort of all the people working in the institute, especially Dr. Klaus Möschel, Alexandra Maurer, Birgit Kiesel, Mine Cosgun, Ursula Schaal, Luis Hartmann, Hermann Liggesmeyer, Dietmar Wieland and Egon Theurer.

Lastly, I am especially grateful to my family members for their continuous support and sympathy during all those years.

12. Appendix

A. Syed, MI., Poths, S., Baskaran, P., Rapaport, D., and Jansen, R-P. (2019). Membrane-associated RNA-binding proteins contribute to regulation of mRNAs encoding mitochondrial ribosomal proteins. (not yet published)

B. Syed, M.I., Moorthy, B.T., Jenner, A., Fetka, I., and Jansen, R.-P. (2018). Signal sequence-independent targeting of MID2 mRNA to the endoplasmic reticulum by the yeast RNA-binding protein Khd1p. FEBS Lett. *592*.

C. Edelmann, F.T., Schlundt, A., Heym, R.G., Jenner, A., Niedner-Boblenz, A., Syed, M.I., Paillart, J.-C., Stehle, R., Janowski, R., Sattler, M., et al. (2017). Molecular architecture and dynamics of ASH1 mRNA recognition by its mRNA-transport complex. Nat. Struct. Mol. Biol. *24*.

Membrane-associated RNA-binding proteins contribute to regulation of mRNAs encoding mitochondrial ribosomal proteins

Muhammad Ibrahim Syed[1], Sven Poths[2], Praveen Baskaran[3], Doron Rapaport[1] and Ralf-Peter Jansen[1]

1 Interfaculty Institute of Biochemistry, University of Tübingen, Tübingen, Germany

2 Institute for Medical Genetics and Applied Genomics, c.ATG, University of Tübingen, Tübingen, Germany

3 Quantitative Biology Center (QBiC), University of Tübingen, Tübingen, Germany

Abstract

RNA-binding proteins (RBPs) determine the fate of mRNA from its synthesis to decay. This includes localization of mRNAs and local protein synthesis. Although the classical model of protein targeting indicates that protein targeting to the ER generally occurs co- or post-translationally, RBPs in yeast and mammals have been identified that associate with the ER and influence mRNA localization at the ER. We have identified several yeast RBPs that associate with the ER. A combined deletion of their corresponding genes results in defects of cell wall biogenesis. However, loss of these RBPs did not result in changes of mRNA distribution between ER and cytosol. Further analysis of mRNA distribution surprisingly showed that mRNAs encoding proteins with nuclear function are enriched in the ER fractions in both wildtype and RBP deletion strains. Furthermore, loss of these RBPs results in respiratory-incompetent mitochondria since transcripts encoding mitochondrial ribosomal proteins are upregulated while their translation is decreased. We therefore suggest a potential role of these RBPs in controlling expression of nuclear-encoded MRPs.

Key words: RNA-binding protein; mRNA localization; endoplasmic reticulum; SRP-independent targeting; mitochondrial ribosomal protein; *Saccharomyces cerevisiae*

Introduction

RNA-binding proteins (RBPs) in general possess structurally well-defined RNA-binding domains including the RNA recognition motif (RRM) (Cléry et al., 2008), hnRNP K homology domain (KH) (Valverde et al., 2008)), Pumilio (Puf) (Edwards et al., 2001) or DEAD box helicase domain (Linder and Jankowsky, 2011). They control different aspects of an mRNA's life, such as splicing, polyadenylation, export, storage, turnover, and localization, (reviewed in (Glisovic et al., 2008)). mRNA localization to a specific site in a cell and subsequent local protein synthesis is implicated in various cellular phenomena. The asymmetric localization of *ASH1* to the daughter cell during cell division controls differential mating type switching in budding yeast (Paquin and Chartrand, 2008). The localization of *bicoid*, *oskar*, and *nanos*, mRNAs to the anterior or posterior poles of the *Drosophila* oocyte establishes axis determination during embryonic development and germ cell development (Johnstone and Lasko, 2001). Localization of VegT mRNA that encodes a T-box transcription factor, to the vegetal pole in *Xenopus* embryo induces endodermal and mesodermal cell fates (King et al., 2005). The asymmetrical distribution of *β-actin* mRNA to the lamellipodia in fibroblasts drives cytoskeletal-mediated motility (Condeelis and Singer, 2005). These localization processes are mediated by RBPs via binding to specific *cis*-acting structural RNA elements known as zipcodes or localization elements (LE), which are frequently positioned in the *3'UTR* of an mRNA (Jambhekar and DeRisi, 2007).

The endoplasmic reticulum (ER) in eukaryotes is a major site of protein synthesis for membrane/secretory proteins. The localization of mRNAs encoding membrane/secretory proteins to ER has been primarily viewed as co-translational docking of the ribosome-nascent chain complex (RNC) at the ER, which is directed by the signal recognition particle (SRP) (Friedlander and Blobel, 1985; von Heijne, 1983; Mize et al., 1986). SRP, a ribonucleoparticle (reviewed in (Pool, 2005)), engages a translating mRNA-ribosome complex in the cytoplasm after an N-terminal hydrophobic peptide signal or transmembrane domain (TMD) has emerged from the ribosome exit channel (Walter and Blobel, 1981b, 1981a). Translation at this point is paused and the SRP carries the RNC to the ER-bound SRP receptor (SR), where translation resumes and the protein is either integrated into the ER membrane or inserted through a protein conducting channel into ER (Gilmore et al., 1982; Görlich and Rapoport, 1993; Stirling et al., 1992; Walter and Blobel, 1980, 1982).

Though SRP guides mRNAs encoding membrane/secretory proteins in a translation-dependent manner, several studies have reported the partitioning of mRNAs to ER in a translation-

independent manner in yeast and mammals (Adesnik et al., 1976; Cardelli et al., 1976; Kraut-Cohen et al., 2013; Lande et al., 1975; Mechler and Vassalli, 1975; Milcarek and Penman, 1974; Syed et al., 2018). Moreover, sequence analysis of transcripts encoding membrane proteins shows a high enrichment of uracil in their coding region and regions of the transcripts encoding signal sequences as being less-enriched with adenine (Palazzo et al., 2007; Prilusky and Bibi, 2009). In some cases, the sequence in the *3' UTR* is sufficient to deliver mRNA to ER (Loya et al., 2008). It has been therefore proposed that *cis*-acting signals within an mRNA and *trans*-acting factors such as RNA-binding proteins (RBPs) that bind to these signals might constitute an alternative route of mRNA deliver to ER (Cui and Palazzo, 2014). In fact, ER-associated RBPs have been identified in yeast and mammals (Aronov et al., 2007; Cui et al., 2012; Gelin-Licht et al., 2012; Schmid et al., 2006), including the protein p180 in mammals that can deliver mRNAs to ER in a translation-independent manner (Cui et al., 2012). Furthermore, a high-throughput protein-RNA interactome analysis in *Saccharomyces cerevisiae* revealed that some RBPs preferentially associate with transcripts encoding membrane and secretory proteins (Hogan et al., 2008) and the deletion of ER associated RBPs such as She2p or Puf2p even leads to partial loss of mRNA localization such as *SUC2* at ER (Kraut-Cohen et al., 2013).

In the current study, we attempt to investigate the effect of the loss of ER-associated RBPs on the mRNA localization to the ER using *Saccharomyces cerevisiae* as a model. We demonstrate for several RBPs that they associate with ER, including Whi3p, Mrn1p, Pbp2p, Slf1p, and Ngr1p. Whi3p negatively regulates *CLN3* mRNA by sequestering it to cytoplasmic foci (Garí et al., 2001). It also physically interacts with Cdc28p and as a result keeps the Cdc28p-Cln3p complex in the cytoplasm in the early G1 phase (Garí et al., 2001; Wang et al., 2004). Furthermore, cells without Whi3p enter S-phase at smaller cell volume and hence it is believed that Whi3p plays a role in controlling cell size and the G1 to S-phase transition (Garí et al., 2001). *MRN1* genetically interacts with chromatin remodelling complexes (RSC or SWI/SNF), genes that encode chromatin architectural proteins (*NHP6A* and *NHP6B*) and splicing factors such as *PRP4* and *PRP3* (Costanzo et al., 2010; Düring et al., 2012; Stillman, 2010). Mrn1p is believed to function in mRNA maturation, since its overexpression rescues the temperature sensitive phenotypes of prp22, prp4-1, prp3-1, snt309Δ and additionally the phenotypes associated with *swi/snf* and the *rsc nhp6ΔΔ* (Düring et al., 2012). Ngr1p is implicated in porin (*POR1)* mRNA degradation, since its overexpression enhances *POR1* degradation leading to low porin levels (Buu et al., 2004). It interacts with cytoplasmic DEAD-box helicase Dhh1p

and this interaction might enhance *POR1* decay in P-bodies in Xrn1p-dependent manner (Chang and Lee, 2012; Jang et al., 2006). Pbp2p functions in the regulation of telomeric positioning effect and telomere length (Denisenko and Bomsztyk, 2002). It specifically binds poly C and poly U RNA sequences (Denisenko and Bomsztyk, 2002). Slf1p is a La-motif protein required for survival under stress conditions (Kershaw et al., 2015; Yu et al., 1996). It interacts with poly A binding protein (Pab1) and translating ribosomes. Therefore, it is thought that Slf1p might play a role in the translation activation and/or stability of their mRNA targets (Aoki et al., 2013; Bayfield et al., 2010; Kershaw et al., 2015; Sobel and Wolin, 1999; Yang et al., 2011).

We show that deletion of some these non-essential RBPs, such as Mrn1p and Whi3p, results in defects in cell wall biogenesis, and that this is enhanced upon their deletion as a group (such as Whi3p, Slf1p, Pbp2p and Ngr1p). We additionally knocked out Mrn1p and then the quintuple-gene deletion (*quintuple RBP mutant*) and wildtype yeast strains were subjected to subcellular fractionation. However, RNA seq analysis from membrane (organelle-rich) and cytosolic fractions reveals no significant transcript loss in the membrane fraction of *quintuple RBP mutant* versus wildtype yeast strain although many transcripts change their abundance at the cell level. Additionally, we see an enrichment of mRNAs encoding proteins with nuclear function in the membrane fraction in both wildtype and *quintuple RBP mutant* strain. We particularly noticed that nuclear transcripts encoding mitochondrial ribosomal proteins (MRPs) are at least two-fold up-regulated in quintuple-gene deletion strain, which is accompanied by inability of the *quintuple RBP mutant* strain to grow on non-fermentable carbon sources. Furthermore, we see very low levels of Mrpl39p, Mrpl44p and Img2p in the organelle rich fraction of *quintuple RBP mutant* strain. We suggest that RBPs such as Whi3p, Mrn1p, Pbp2p, Slf1p, and Ngr1p play role in controlling expression of nuclear-encoded MRPs.

Materials and methods

Yeast strains and plasmids

Yeast strains used in this study are listed in Supporting tables 6-8S. Gene deletions and taggings were accomplished via homologous recombination using High-efficiency yeast transformation (Gietz and Schiestl, 2007). Details are listed in Supporting table S6 and S7. To delete *NAB6*, *his5* (*Schizosaccharomyces pombe*) with *LoxP* sequence at both 5′ and 3′ ends was amplified with oligos RJO5509 and RJO5510 from pRJ1485. Next the 5′*UTR* (500 bp) and 3′*UTR* (817 bp) regions of *NAB6* were amplified with oligos pair RJO5511/RJO5512 and RJO5513/RJO5514 respectively. The three fragments were combined together in a single PCR reaction using oligos RJO5512 and RJO5514. This final PCR product was then transformed in RJY358 and colonies were selected on synthetic complete (SC) medium lacking histidine. For further deletions in the same strain, *his5* was first kicked out with Cre recombinase. For plasmids transformation, a rapid one-step yeast transformation protocol was followed (Chen et al., 1992). Standard yeast growth conditions were followed using either YEPD (2% glucose) or SC medium lacking appropriate amino acid or nucleobase.

All plasmids used in this study are listed in Supporting table S9 and S10. To create TGBp3 fusions, the coding regions of *MRN1*, *WHI3*, *PBP2*, *SLF1*, *NGR1*, and *PUF1* were amplified with oligos (listed in Supporting table S11) and cloned between GFP and the C-terminal peptide of TGBp3 (amino acids 25-52) in pRJ1846 using restriction enzymes as listed in Supporting table S9. *WHI3* and *NGR1* both have an additional HindIII restriction site in their coding region. To construct pRJ2196, the *LEU2* in pRJ2121 was replaced with *TRP1* (from pRJ138) using HindIII and SpeI.

Subcellular fractionation methods

Density gradient: Yeast strains tagged with three or six hemagglutinin (HA) tags were set to sucrose density gradient centrifugation as described in (Schmid et al., 2006; Syed et al., 2018). With the exception of Whi3p-HA_6, information for all other HA tagged yeast strains such as RJY5048, RJY4290, RJY5049, RJY4377, RJY4378, RJY2949 and RJY5411 is available in Supporting table S7.

Quick subcellular fraction for western blot analysis: A similar method as described in (Syed et al., 2018) was used with yeast strains RJY5281, RJY5290, RJY5286, RJY5295, RJY5287, RJY5296, RJY5405, RJY5406, RJY5407 and RJY5408.

Quick subcellular fraction for RNA seq and qRT-PCR experiments: First, a single colony from WT strain (RJY358) was grown to mid log phase in 100 mL YEPD medium. Cells were then harvested and washed twice, first with ice-cold water and then with potassium phosphate buffer (1.2 M sucrose and 100 mM potassium phosphate, pH 7.5). The pellet was resuspended in HEPES lysis buffer [20 mM HEPES/KOH pH 7.5, 140 mM potassium acetate, 1 mM magnesium acetate, 1 mM DTT, 250 mM sucrose, 1x EDTA-free Protease Inhibitor Cocktail (Roche, Basel, Switzerland)]. Cells were lysed with the help of glass beads with four pulses of 90 s with a break of 1 minute on ice at the end of each pulse. Glass beads and cell debris were removed at 800 g for 5 minutes. The total cell lysate (TCL) or whole cell extract (WCE) (amounting to 20 μg in 200 uL) were set to successive centrifugation steps at 2000 g, 3000 g, 4000 g, 5000 g, 6000 g and 18000 g. The pellets were resuspended in 200 uL HEPES lysis buffer and along with WCE and supernatant (S18000) were set to SDS/PAGE followed by western blotting. As shown in Supplementary figure 4A, the nuclear marker Hht1p can almost be depleted at 3000 g.

For RNA seq and qRT-PCR experiments using WT (RJY358) and *mutant* strain (RJY5278), a modified version of the above-mentioned fractionation method was used. Prior to harvesting, cells were incubated with cycloheximide (100 μg- mL^{-1}) at $30C^{0}$ for 15 minutes. The lysis buffer also contained 100 μg- mL^{-1} cycloheximide plus 100 U- mL^{-1} Ribolock RNase inhibitor (ThermoFisher Scientific). Cell debris were removed at 800 g and then the lysates were further spinned at 3000 g to deplete nuclear fraction. The resulting lysates were considered as whole cell extracts (WCEs) or total cell lysates (TCLs). The WCEs were further centrifuged at 18000 g to separate the membrane rich fraction (P18000) from cytosolic fraction (S18000). The RNA from input (WCE), P18000 and S18000 was precipitated with Phenol/Chloroform/Isoamyl alcohol (Carl Roth, Germany).

Other yeast lysate preparation methods

For the qRT-PCR analysis of *MRPs*, *COX1*, *COX2* and *21s_rRNA*, cells (50 OD_{600} units) from RJY358 and RJY5278 were lysed in 500 μL breakage buffer (10 mM Tris-HCl pH 7.5, 150 mM NaCl, 2 mM EDTA pH 8, 0.1% Triton X-100, 1x protease inhibitor cocktail (Roche) and and Ribolock RNase inhibitor 0.5 U- μL^{-1}) using glass beads. The broken cells were spinned at 3000 g for 5 minutes to clear cell debris. RNA was then precipitated with Phenol/Chloroform/Isoamyl alcohol (Carl Roth, Germany).

Yeast mitochondrial DNA was isolated by lysing 50 OD_{600} units of yeast in 500 µL HEPES lysis buffer using glass beads. Cell debris was cleared at 3000 g for 5 minutes and the lysate was further centrifuged at 18000 g for 30 minutes. The pellet was resuspended in HEPES lysis buffer supplemented with 1% SDS followed by nucleic acid precipitation with Phenol/Chloroform/Isoamyl alcohol (Carl Roth, Germany).

RNA seq analysis

For whole transcriptome analysis, RNA samples from input, P18000 and S18000 in duplicates were sent to Core Facility for Applied Transcriptomics and Genomics (c.ATG) at the university clinic in Tuebingen. The sequence reads obtained were analysed at The Quantitative Biology Center (QBiC) at the university of Tuebingen. No RNA spike-in controls were used, instead reads for each transcript were normalised against the total number of reads. FastQC ((http://www.bioinformatics.babraham.ac.uk/projects/fastqc/), version v0.11.4) was used to determine quality of sequencing reads. Subsequently, adapter trimming/removal process was conducted with Cutadapt (version 1.8.3) (Martin, 2011). This step used FastQC output to identify reads that showed a match to some typical overrepresented (Illumina) sequences/adapters. STAR Rna-seq aligner (version v2.0.12) (Dobin et al., 2013) was used to map the remaining quality controlled reads to the Saccharomyces cerevisiae genome (S288C). Read counting to features (e.g. genes or exons) in the genome was performed with featureCounts (version 1.5) (Liao et al., 2014) using default parameters. For differential expression analysis the raw read count table resulting from featureCounts is used and fed into the R package DESeq2 (version 1.10.1) (Love et al., 2014). Graphs were also produced in the R language (R version 3.2.1) mainly using the R package ggplot2 (version 2.2.0) (Wickham 2009). pheatmap (Kolde 2015) was used to create the sample distances heatmap. When needed, the figures for RNA seq analysis were manually edited in INKSCAPE (inkscape.org).

Western blotting

For the western blot analysis of Cox2p, Cox4p and Tom70p, cells (2.5 OD_{600} units) from RJY358 and RJY5278 were first treated with 0.1 M NaOH and then boiled for 3 minutes in Laemmli buffer followed by SDS/PAGE and western blotting. Western blots for MRPs, Cox2p, Cox4p and Tom70p were developed through chemiluminescence using ECL (GE Healthcare). All other western blots were visualized by LICOR Odyssey system, which requires the use of fluorescently labelled secondary antibodies. All antibodies used in this study are listed in Supporting table S12.

PCR and qRT-PCR

100 ng yeast mitochondrial DNA was used for *COX2* detection. The PCR was set up with Herculase II Fusion DNA Polymerase (Agilent) using oligos RJO6437 and RJO6438 in 20 µL reaction supplemented with 2.5 mM $MgCl_2$. For quantitative RT-PCR (qRT-PCR) analysis, 2 µg RNA was treated with RQ1 DNase (Promega, Mannheim, Germany) in 20 µL reaction volume. 13.2 µL was then set to cDNA synthesis using a High-Capacity cDNA Reverse Transcription Kit (Applied Biosystems). Just prior to DNase treatment, 10 ng spike RNA (*in vitro* transcribed *Arabidopsis* phosphoribulokinase RNA) was added to each RNA sample. qRT-PCR reactions were carried out in 10 µL containing 2.5 µL of 1:20 or 1:100 dilutions of the individual cDNA samples. Primers were designed at http://primer3.ut.ee/. Any mispriming or primer dimer formation were checked through melting curve analysis or through visual inspection on agarose gel of the individual amplified products. Three biological and two technical replicates were used for the qRT-PCR analysis of all genes except *PGK1* and *PMA1*, which were quantified only once (one biological replicate and two technical replicates). *PGK1* and *PMA1* both were used as cytosolic and membrane markers respectively to ensure the separation of membrane rich fraction from cytosolic fraction prior to RNA seq experiments. Comparative C_t method as described in (Livak and Schmittgen, 2001) was used for the quantification of individual transcripts. For *MOT1*, *NUP100*, *IKI3*, *HHT2* and *HTA2* quantification in the membrane and cytosolic fractions, the C_t values were first normalized against the spike and then against the input. For *PGK1* and *PMA1*, the Ct values were only normalized against the input. The C_t values of all other transcripts were normalized only against the spike.

***In vivo* imaging**

All imagings were performed with AxioExaminer equipped with a CSU unit (Visitron Systems, Puchheim, Germany) followed by image processing with FIJI.

Imaging of TGBp3 fusions and *MS2L*-tagged mRNAs: A single yeast colony was grown in SC complete medium lacking appropriate amino acid or nucleobase with 2% glucose to mid log phase. Prior to microscopy, the cells were spread on freshly prepared thin agarose pads containing dropped-out SC medium plus 2% glucose.

DAPI staining: Yeast cells were grown in SC complete medium with 2% glucose to mid log phase. The cells were then treated with DAPI (2 µg- mL^{-1}) for 30 minutes at 30°C, washed with PBS and then imaged.

Mitochondrial staining: MitoTracker Green FM (Invitrogen) with the wavelength range of 490/516 was used to stain yeast mitochondria following a protocol recommended by the manufacturer.

Phenotype analysis

Calcofluor white assay was performed as described in (Ketela et al., 1999; Syed et al., 2018). To check the growth on glycerol containing medium, yeast strains were grown to mid log phase in YPD medium and then washed 2 times with water. Cells were then diluted to OD_{600} = 0.3 followed by subsequent three to four 10-fold dilutions. 5 µL of each dilution was spotted on YEPD, YEPG or SC complete plates and the plates were incubated for 3-5 days at 30°C.

Results

Screening for membrane-associated RNA-binding proteins (RBPs) in *Saccharomyces cerevisiae*

In order to screen for RBPs that associate with the ER membrane, we employed an assay that takes advantage of the C-terminal peptide from the small protein TGBp3 of Bamboo mosaic potexovirus (Genz et al., 2013; Syed et al., 2018; Wu et al., 2011). If attached to a peripheral or integral membrane protein, this peptide becomes targeted to and stably integrated into ER (Wu et al., 2011). The assay has successfully demonstrated the *in vivo* association of RBPs such as She2p and Khd1p with ER (Genz et al., 2013; Syed et al., 2018). Both proteins are present in the nucleus and cytoplasm (Tkach et al., 2012) and a fraction of these proteins is found to be present in the ER-enriched fraction in density gradient experiments (Genz et al., 2013; Syed et al., 2018). We choose 19 RBPs for our screening, namely Mrn1p, Slf1p, Sro9p, Tma20p, Tma22p, Sgn1p, Rnp1p, Whi4p, Puf4p, Lsm12p, Rie1p, Pub1p, Pbp2p, Ngr1p, Nab6p, Puf1, Puf2, Whi3 and Vts1p. Since most of these RBPs are predominately cytoplasmic under normal growth conditions (Tkach et al., 2012; Weill et al., 2018; Yofe et al., 2016), we wanted to check if they temporarily or weakly associate with ER membrane by tagging them at the N-terminus with GFP and at the C-terminus with the C-terminal peptide of TGBp3. Several RBPs such as Whi3p, Ngr1p, Puf1p, Mrn1p, Pbp2p and Slf1p formed ER-associated foci when fused with the C-terminal peptide of TGBp3 (representative images are shown in Figure 1 and Supporting figure S1). This formation of foci that colocalize with ER has also been reported for other TGBp3 fusions (Genz et al., 2013; Syed et al., 2018; Wu et al., 2011). In the case of Slf1p (Figure 1C and supporting figure S1A), only a fraction of cells showed ER-colocalizing foci. In addition, the Slf1p-TGBp3 fusion also formed foci that did not colocalize with ER (Supporting figure S1B). As controls, we used the cytoplasmic glucose-6-phosphate dehydrogenase Zwf1p (Nogae and Johnston, 1990) and Rie1p, a putative RBP that localizes to stress granules (SGs) upon glucose deprivation (Buchan et al., 2008). Neither formed foci when fused to the TGBp3 peptide (Figure 1G and 1H). A Puf1p-TGBp3 fusion did not form foci but instead partly colocalized with the cortical ER (cER) (Figure 1F).

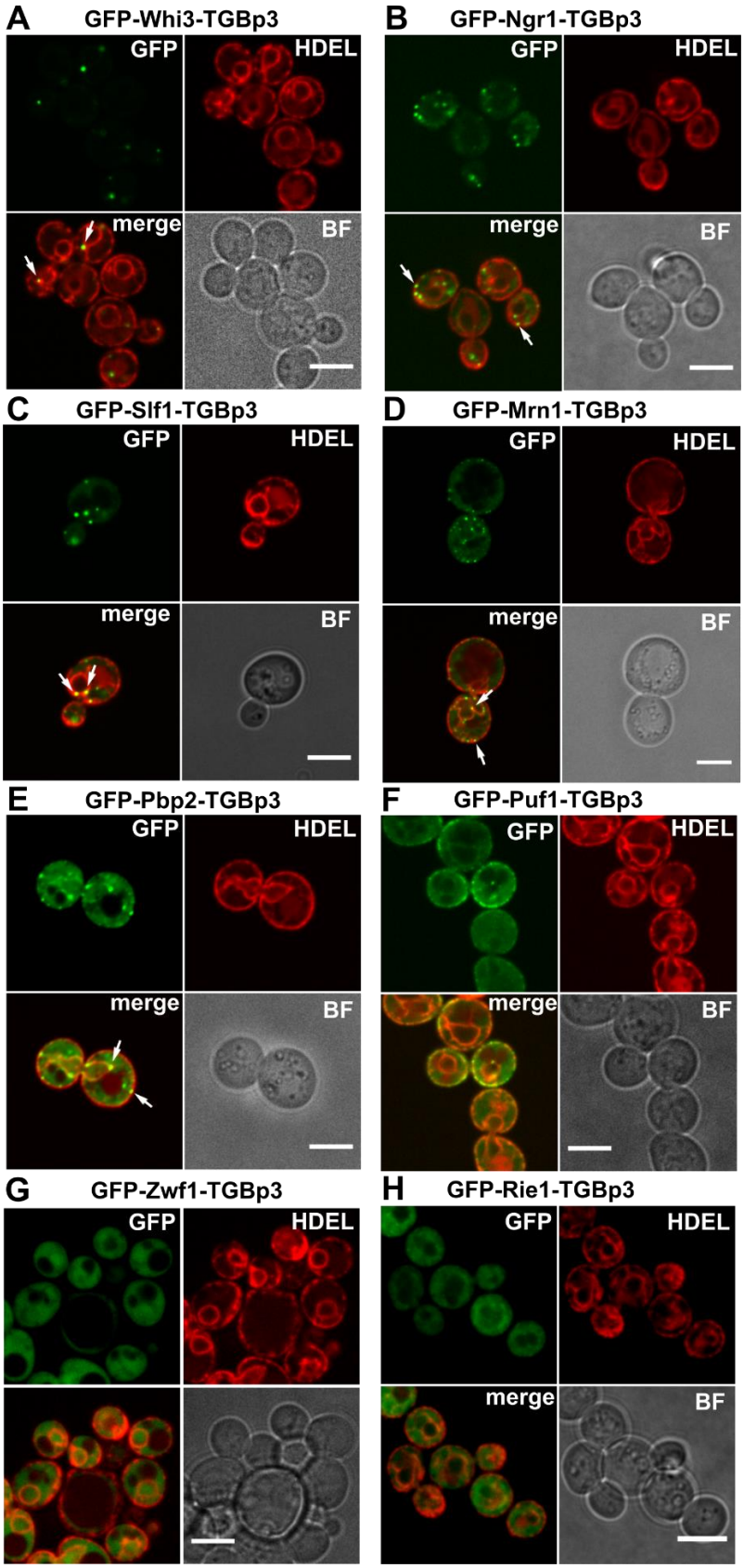

Figure 1. (A-H) Representative images of GFP-TGBP3 fusion proteins. To label ER, HDEL-DsRed (a luminal ER marker) or Rtn1p-mCherry (labels the cER) was used. All GFP-TGBP3 fusion proteins, except Puf1p, Zwf1p and Rie1p, form foci that colocalize with ER (white arrows). Puf1p-TGBp3 fusion does not form foci but partly colocalize with cER (F). BF: Bright Field. Scale bar: 5 μm.

To support our findings, we performed cell fractionations. Yeast lysates were generated in low salt lysis buffer (see material and methods) and then separated on linear sucrose gradient. A large fraction of all RBPs that showed co-localization with ER (Figure 1 and Supporting figure S1) also co-migrated with the ER marker Sec61p (Figure 2 and Supporting figure S2).

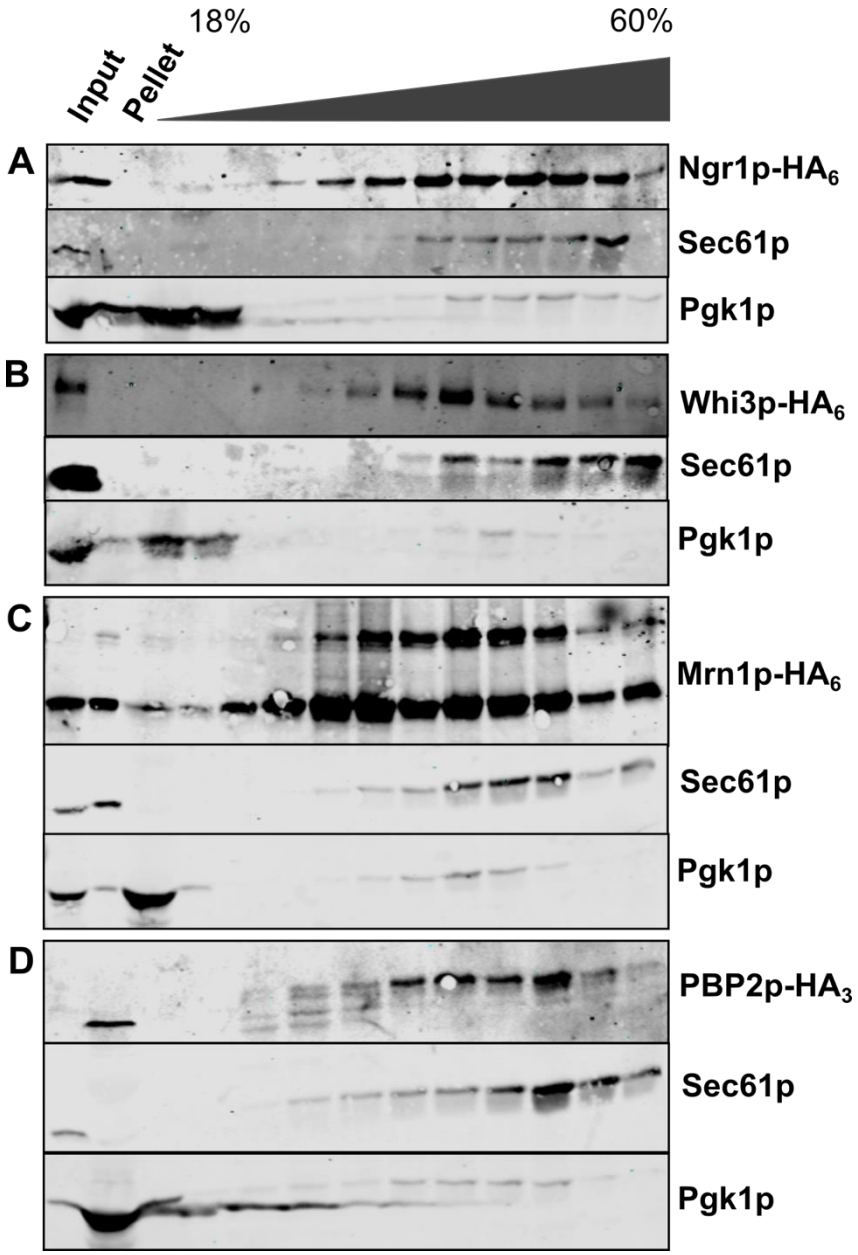

Figure 2. RBPs were tagged at the C-terminus with hemagglutinin (HA) tags (see materials and methods). Yeast whole cell lysates (WCLs) were generated in low salt lysis buffer and then fractionated on linear sucrose gradient (18-60%). 11 or 12 fractions were collected and then subjected to protein precipitation with trichloroacetic acid (TCA). These fractions along with WCLs (as inputs) and membrane pellets were analysed by western blotting against HA, Sec61p (microsomal marker), and Pgk1p (cytosolic marker). A large fraction of the tested RBPs co-migrate with Sec61p.

Deletion of membrane-associated RBPs leads to a cell wall defect

All RBPs in the current study except Pbp2p bind to 100 or more mRNAs. A significant subset of Mrn1p, Whi3p, and Puf1p target RNAs code for proteins with a cell wall-related function (Colomina et al., 2008; Hogan et al., 2008). One example is Puf2p and its paralog of Puf1p. Both bind to over 100 mRNAs including cell wall-related transcripts (Hogan et al., 2008). Most transcripts bound by Puf1p can also interact with Puf2p vice versa (Gerber et al., 2004). We failed to test the *in vivo* association of Puf2p with ER since no expression construct resulting in a Puf2p-TGBp3 fusion protein could be generated. However, in sucrose density gradient experiment, a large fraction of Puf2p co-fractionated with ER (Supporting figure S2). A similar observation was made for Nab6p, an RBP that particularly associates with transcripts encoding proteins of the cell wall (Hogan et al., 2008). In this case, our density gradient assay supports the idea that that the protein is enriched in the membrane fraction (Supporting figure

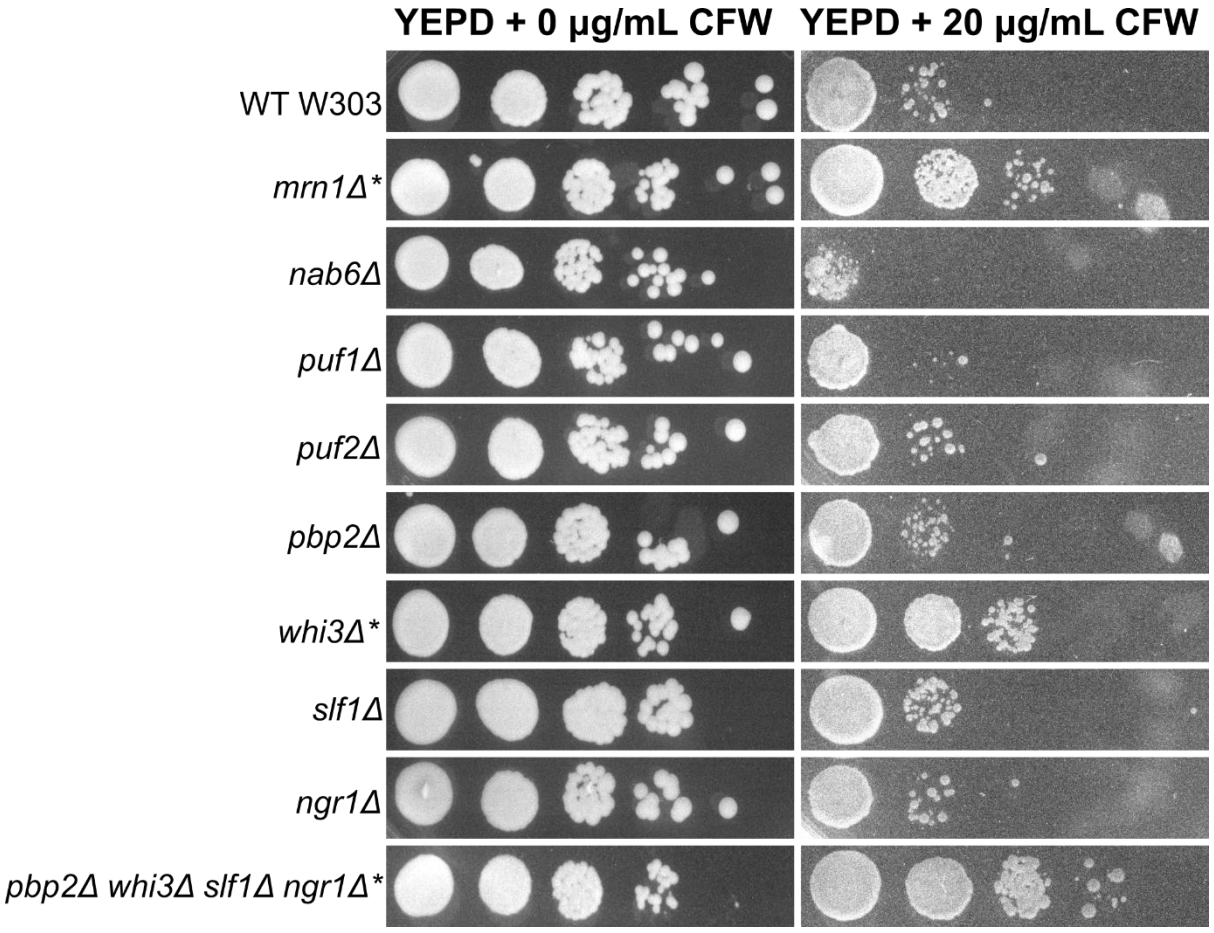

Figure 3. Calcofluor White (CFW) assay for Wild type and different gene deletion strains. Yeast cells were grown to mid-log phase and the final OD_{600} was set to 0.3. Cells were then serially diluted and spotted on YEPD plates with or without CFW. The asterisk (*) represents yeast strain with cell wall phenotype.

S2). To investigate if these RBPs have a function in ER-related mRNA translation, we knocked out Puf1p, Puf2p, Mrn1p, Whi3p, Slf1p, Ngr1p, Pbp2p and Nab6p individually or in different combinations using deletion cassettes (see material and methods). We subjected these deletion strains to a Calcofluor White (CFW) assay. CFW is a fluorochrome that interacts with beta 1-3 and beta 1-4 polysaccharides in cellulose and chitin and as a result disrupts the microfibril assembly of cellulose and chitin (Harrington and Hageage, 1991; Roncero and Duran, 1985). CFW is lethal at high concentrations for yeast (Roncero and Duran, 1985) and sensitivity to CFW is used as proxy for defects in cell wall synthesis and/or maintenance. Observation of a cell wall phenotype in cells with deleted RBPs might result from failure of delivery or translation of mRNAs coding for cell wall-related proteins. We found that the individual deletion of Mrn1p and Whi3p caused a mild cell wall phenotype while the quadruple-gene deletion *(whi3Δ pbp2Δ slf1Δ ngr1Δ)* strain showed a strong cell wall phenotype (Figure 3 and Supporting figure S3). We then additionally deleted Mrn1p in the quadruple-gene deletion strain for further studies. We refer to this mutant strain as „*quintuple RBP mutant* ".

RNA seq analysis upon RBPs deletion reveals no obvious shift of mRNAs from membrane to cytosolic fractions

To evaluate if the observed cell wall phenotype is connected to mistargeting of mRNAs in the quintuple mutant, we established a rapid cell fractionation method to separate organelle (membrane) rich fraction from cytosolic fraction (see material and methods) with minimal RNA degradation. With successive centrifugation steps, we found that the major fraction of nuclear marker Hht1p is removed at 3000 g indicating the depletion of nuclear fraction (Supporting figure S4A). As expected, we also lost part of the ER at this step since a fraction of the perinuclear ER should be removed as well (Sec61p in Supporting figure S4A). However, we found the removal of nuclear material more important in order to avoid contamination with transcripts that were transcribed but not yet exported. The supernatant lysates after the 3000 g pelleting step were considered as whole cell lysates (WCLs). These WCLs were further fractionated at 18000 g to separate the membrane rich fraction (pellet) from the cytosolic fraction (supernatant). For quality control, WCLs (as inputs), membrane, and cytosolic fractions were analyzed by RT-qPCR for presence of *PMA1* mRNA (encoding a plasma membrane ATPase (Serrano et al., 1986)) and *PGK1* mRNA (coding for a cytosolic enzyme (Blake and Rice, 1981; Hitzeman et al., 1980)). As expected (Huch et al., 2016), *PMA1* was highly enriched in the membrane fraction whereas *PGK1* was slightly enriched in the cytosolic fractions, although not totally absent from the membrane fraction in wildtype and *quintuple*

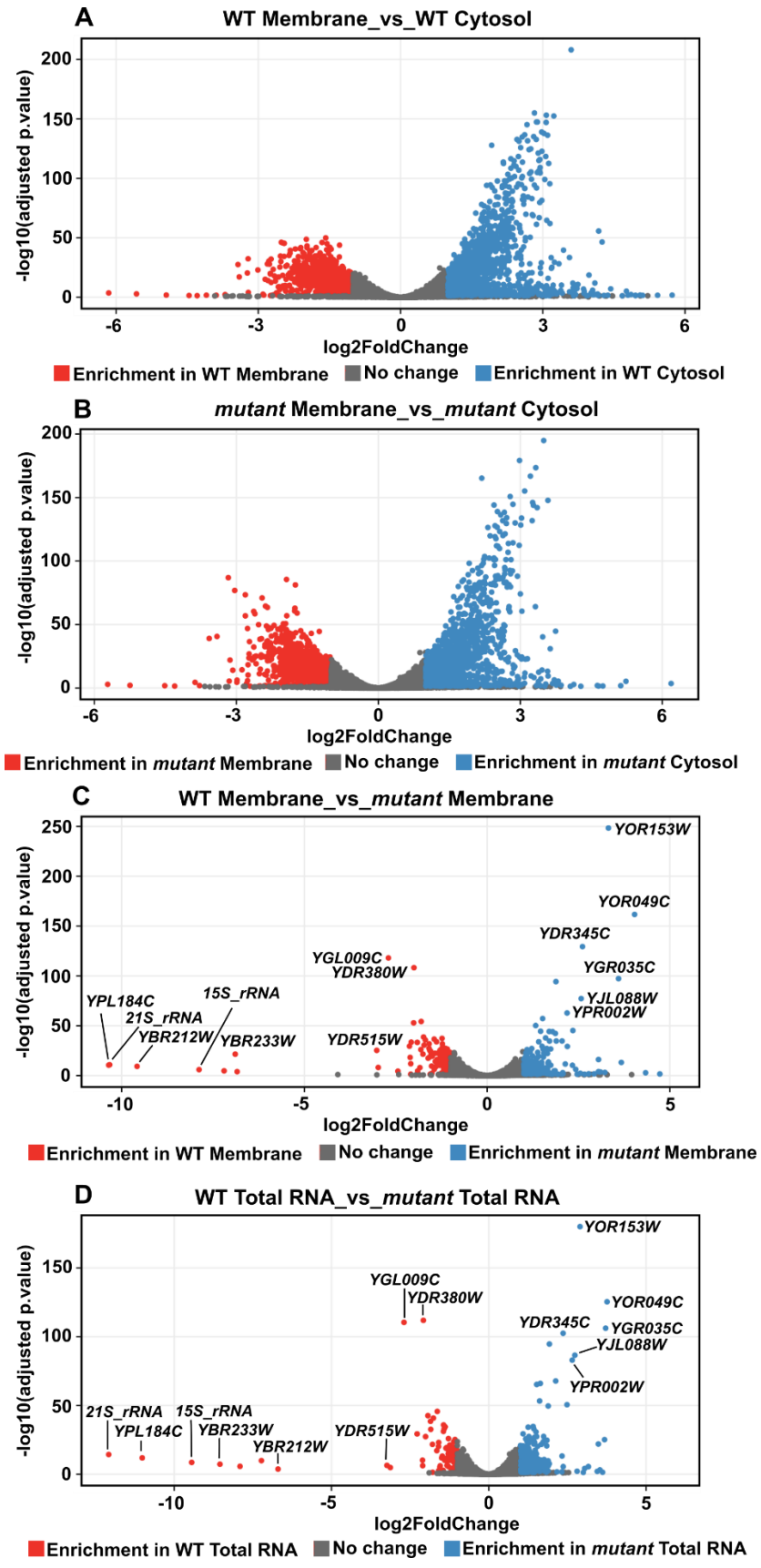

Figure 4. Volcano plots showing the log2 fold enrichments of transcripts in different fractions. (A) A comparison of membrane vs cytosolic fractions in wildtype (WT) strain and (B) a similar comparison in *quintuple RBP mutant* (here mentioned as *mutant*) strain. (C) Showing a comparison of transcripts

distribution in wildtype membrane vs *quintuple RBP mutant* membrane. (D) The comparison of transcripts enrichment at Total RNA (input) level in wildtype vs *quintuple RBP mutant* strain.

RBP mutant strains (Supporting figure S4B and S4C). The RNA samples were therefore further processed for RNA-seq analysis.

We considered a two-fold change as threshold for an enrichment in our RNA-seq analysis. Most of the transcriptome was below this threshold and considered to be equally enriched in both membrane and cytosolic fraction of both strains (Supporting table S1). 1301 transcripts were at least two-fold more enriched in the cytosolic fraction and 1091 transcripts more abundant in the membrane fraction in the wildtype strain (Figure 4A and Supporting table S2). Similarly, 1085 transcripts were more abundant in the membrane fraction and 1301 transcripts in the cytosolic fraction in the *quintuple RBP mutant* strain (Figure 4B and Supporting table S3). Contradictory to our expectation, we observed no shift of mRNAs from the membrane fraction to the cytosol in *quintuple RBP mutant* strain when compared to wildtype strain (Figure 4). Direct comparison of transcripts from the membrane fractions of both wildtype and *quintuple RBP mutant* showed 108 transcripts that were at least two-fold more enriched in the wildtype or 222 transcripts more enriched in the *quintuple RBP mutant* strain (Figure 4C and Supporting table S4). However, normalization to the corresponding input from both strains revealed that these differences are due to corresponding abundance changes in the overall transcriptome (Figure 4D and Supporting table S5).

The enrichment of transcripts coding for nuclear-related proteins in the membrane fractions

It has been reported that transcripts other than those encoding membrane/secretory proteins are also present on the cytoplasmic face of ER (Ast and Schuldiner, 2013; Diehn et al., 2000, 2006; Reid and Nicchitta, 2012). Our analysis also confirmed the presence of non-membrane/non-secretory-related transcripts in the membrane fractions (Figure 5, Supporting figure S5 and Supporting table S2 and S3). In particular, transcripts encoding proteins with a nuclear function (15 out of top 44 highly abundant transcripts in our membrane fractions) were enriched in the membrane fractions (Figure 5, Supporting figure S5 and Supporting table S2 and S3). We randomly picked five transcripts encoding nuclear-related proteins, three were enriched in the membrane fraction (such as *MOT1*, *NUP100* and *IKI3*) and two in the cytosolic fraction (such as *HTA2* and *HHT2*) (Supporting table S2). The log2 fold enrichments for *MOT1*, *NUP100*,

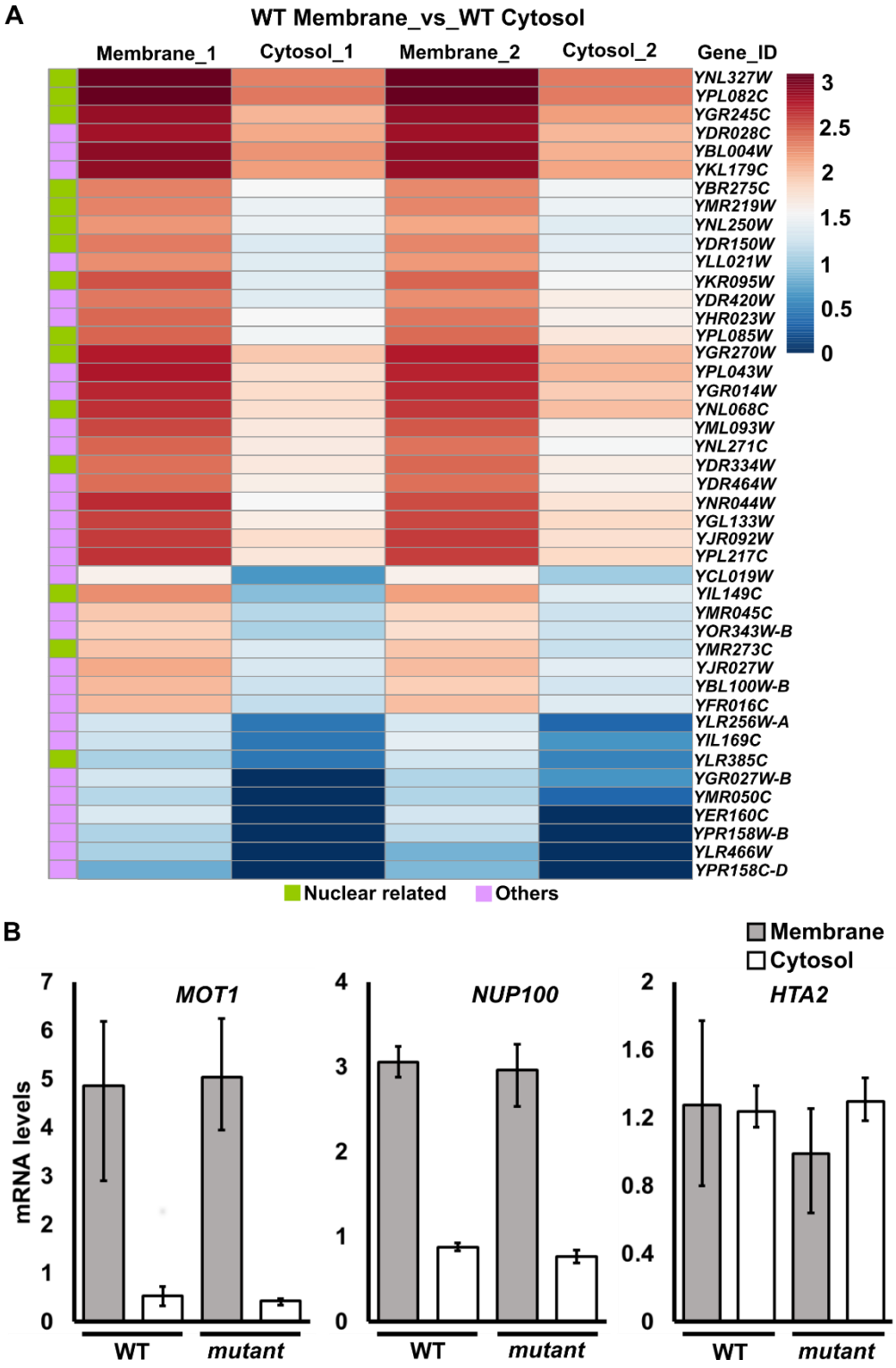

Figure 5. (A) Heat map of the top 44 transcripts enriched in the membrane fraction vs the cytosolic fraction in the wildtype (WT) strain. (B) qPCR analysis for *MOT1*, *NUP100* and *HTA2* in the membrane as well as cytosolic fraction. First, lysates from wildtype (WT) and *quintuple RBP mutant* (*mutant*) strain were set to fractionation to separate the membrane fraction from the cytosolic fraction. RNA was then extracted and prior to DNAse treatment followed by cDNA synthesis, 10 ng of spike RNA was added to each sample. C_t values obtained were normalized against the spike. Relative quantifications were obtained by the formula $2^{-\Delta CT}$.

IKI3, *HTA2* and *HHT2* in the membrane or cytosolic fraction were 2.45, 2.21, 1.97, 2.67 and 2.40, respectively (Supporting table S2). To validate our RNA-seq data, we performed qPCR analysis with these five genes. In contrast to RNA-seq data (Supporting table S2), *HTA2* and *HHT2* nearly equally distributed to membrane and cytosolic fractions (Figure 5B and Supporting figure S5A). *MOT1*, *NUP100* and *IKI3* were at least two-fold more abundant in the membrane fraction as compared to the cytosolic fraction in both strains (Figure 5B and Supporting figure S5A). Therefore, at least for these three transcripts, we can support the claim that mRNAs other than those encoding membrane/secretory proteins can also localize to ER (Ast and Schuldiner, 2013; Diehn et al., 2000, 2006; Reid and Nicchitta, 2012).

As an orthogonal approach, we applied *in vivo* RNA imaging to *MOT1* and *NUP100*, using a recently optimised MS2 system (Tutucci et al., 2017). We tagged *MOT1* and *NUP100* with 24 MS2 loops and found that the mRNA particles are localized at or very close to cortical ER (cER) (representative images are shown in Supporting figure S5B).

Deletion of five RBPs leads to the upregulation of transcripts encoding mitochondrial ribosomal proteins

In yeast, nearly 600 nuclear genes code for mitochondrial proteins (Elstner et al., 2009), of which 78 genes encode mitochondrial ribosomal proteins (MRPs). 44 of these are proteins of the large ribosomal subunit and 34 of the small ribosomal subunit (Claros, 1995; Emanuelsson et al., 2007; Vögtle et al., 2009). Mitochondrial ribosomes are involved in the translation of only eight genes encoded by the mitochondrial genome, including the three core subunits of cytochrome c oxidase (Cooper et al., 1991). In our RNA-seq data, we observed an upregulation of 30 transcripts encoding MRPs in the *quintuple RBP mutant* strain (Supporting table S5 and Figure 6A). We confirmed this upregulation for three of these genes, *MRPL39*, *MRPL44* and *MRP13* by qPCR (Figure 6B). In addition, the *quintuple RBP mutant* strain had a slight growth defect. As opposed to wildtype, mitochondria in the *quintuple RBP mutant* strain formed aggregated structures instead of tubular network (Supporting figure S6A) when stained with mito tracker. To investigate if RNA upregulation is connected to changes in the protein levels, we tagged five MRPs (Mrpl39p, Mrpl15p, Mrpl49p, Mrpl44p, and Img2p) genomically at the C-terminus with GFP. As shown in Supporting figure S6B, we see very faint bands for Mrpl39p, Img2p and Mrpl44p in the membrane fraction of *quintuple RBP mutant* strain as

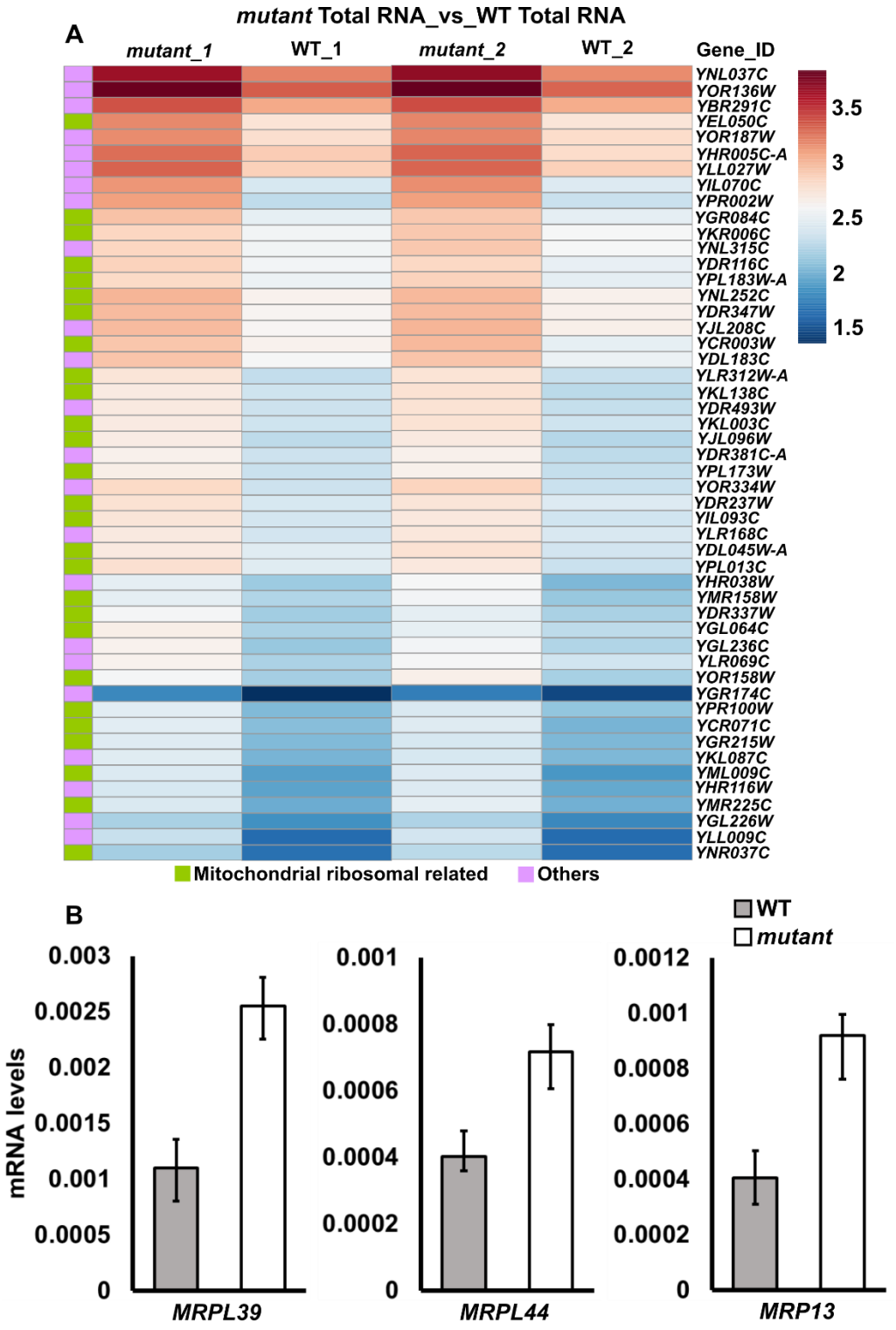

Figure 6. (A) Heat map of the mitochondria-related transcripts (Top 50). These transcripts (including those encoding MRPs, shown in green) are up regulated in the *quintuple RBP mutant* (*mutant*) strain as compared to the wildtype (WT) strain. (B) qPCR analysis for *MRPL39*, *MRPL44* and *MRP13* in the wildtype (WT) and *quintuple RBP mutant* (*mutant*) strain. WCLs from wildtype and *quintuple RBP mutant* strain were set to RNA extractions, DNAse treatment and then cDNA synthesis. 10 ng of spike RNA was added to each sample prior to DNAse treatment. C_t values obtained were normalized against the spike. Relative quantifications were obtained by the formula $2^{-\Delta CT}$. *MRPs* are clearly up regulated in the *quintuple RBP mutant* strain.

compared to the wildtype strain. This could mean that these MRPs are not efficiently translated or imported and thus they might be degraded soon after their translation.

Deletion of five ER-associated RBPs leads to respiratory-incompetent mitochondria

Having noticed abnormalities with MRPs and the mitochondrial morphology (as discussed above), we set out to analyse the mitochondrial function in the *quintuple RBP mutant* strain. The complex IV or cytochrome *c* oxidase in yeast contains three core subunits (Cox1, Cox2 and Cox3) encoded by the mitochondrial genome and translated by mitochondrial ribosomes. We wondered if the core subunits are expressed in the *quintuple RBP mutant* strain and chose Cox2p, whose expression was tested together with Cox4p (a cytochrome *c* oxidase additional subunit encoded by the nuclear genome) and Tom70p (a component of the TOM complex). As shown in figure 7A, Cox4p and Tom70p are expressed in both wildtype and *quintuple RBP mutant* strain, while the signal for Cox2p is only seen in the wildtype strain. We next checked the mRNA levels of *COX1*, *COX2* and the mitochondrial *21_S*rRNA via qRT-PCR. None of the three mRNAs were detected in the *quintuple RBP mutant* strain (Figure 7B). Now it is clear that the *quintuple RBP mutant* strain cannot utilize the nonfermentable carbon source such as glycerol as at least the key components of the cytochrome *c* oxidase are missing. We anyway confirmed this by doing spot assay on agar plates containing yeast extract peptone supplemented with either dextrose or glycerol as carbon source for *quintuple RBP mutant* as well as wildtype strain (Figure 7C). In order to investigate which of the studied RBPs is responsible for the defect, we made a series of multiple deletions in all possible combinations of two, three and four RBP genes and found that only the deletion of all five (*mrn1Δ whi3Δ pbp2Δ slf1Δ ngr1Δ*) caused the respiratory defective mitochondrial phenotype (Supporting figure S7A). Since the observed defect is like that of rho0 cells that have lost their mitochondrial genome, we next checked mitochondrial genome integrity with a PCR of the *COX2* locus. The PCR primers used bind within the coding region of *COX2* and should amplify a 610 base pair (bp) fragment if the mitochondrial genome in that region is intact. As shown in Supporting figure S7B, the amplified band in wildtype cells is of the expected size (610 bp), but although a fragment could be amplified from the *quintuple RBP mutant* cells, it was slightly larger (between 700 bp and 750 bp) indicating an insertion in the coding region of *COX2*. Nevertheless, we confirmed the presence of mitochondrial DNA in the *quintuple RBP mutant*

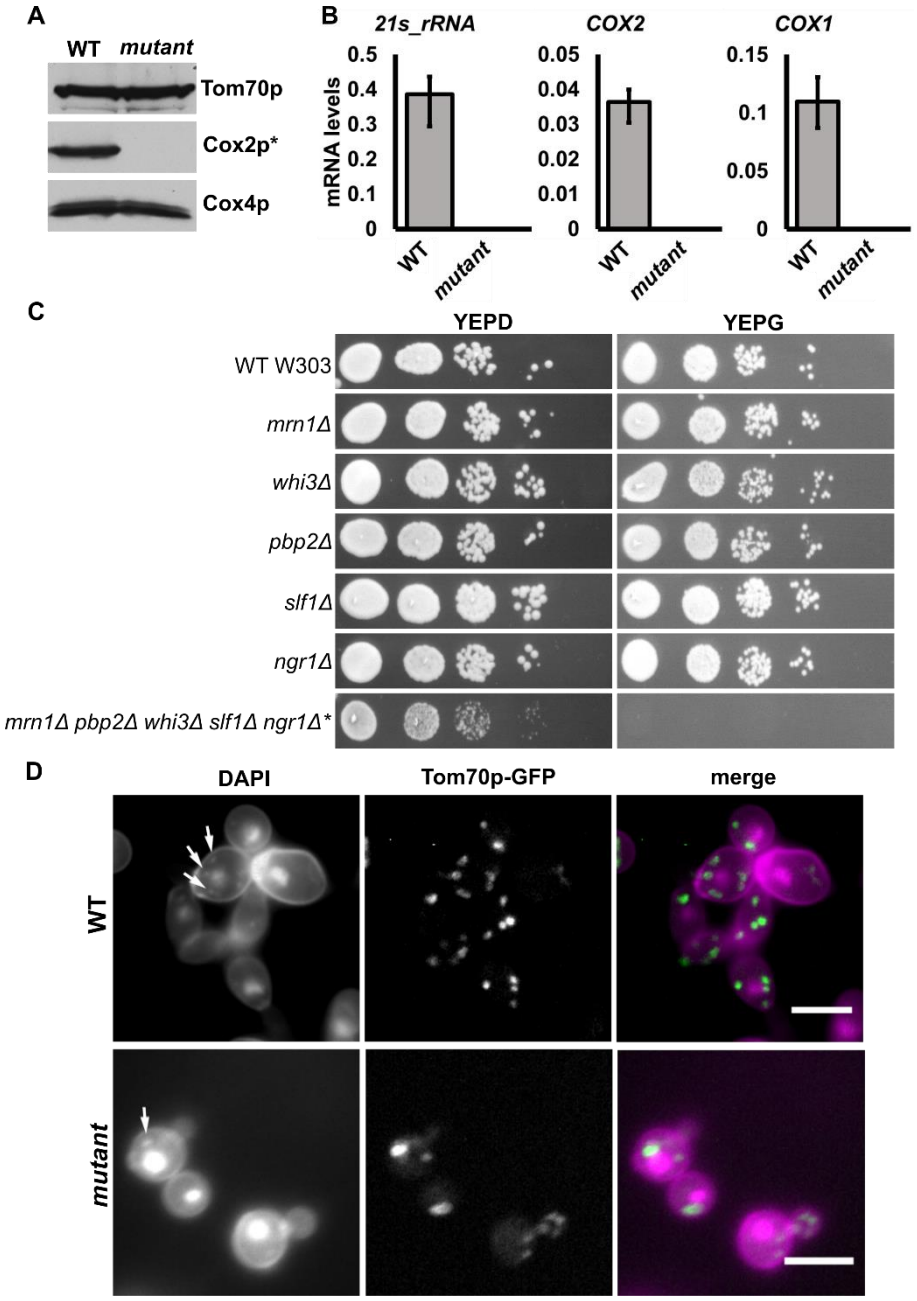

Figure 7. (A) Lysate from wildtype (WT) and *quintuple RBP mutant* (*mutant*) strain was set to western blot analysis against Cox2p, Cox4p and Tom70p. Cox2p is not expressed in the *quintuple RBP mutant* strain. (B) qPCR analysis for *COX1, COX2* and *21s_rRNA*. Whole cell lysates from wildtype (WT) and *quintuple RBP mutant* (*mutant*) strain were subjected to RNA extraction followed by qPCR. The relative RNA quantification (see material and methods) yielded zero values for *COX1, COX2* and *21_srRNA* in the *quintuple RBP mutant* strain. (C) Spot assay for different deletion strains on agar plates containing yeast extract peptone plus dextrose (YEPD) or yeast extract peptone plus glycerol (YEPG). The asterisk (*) represents yeast strain with respiratory defective mitochondria as it cannot grow on medium supplemented with glycerol as the carbon source. (D) DAPI staining for wildtype (WT) and *quintuple RBP mutant* (*mutant*) strain for the analysis of mitochondrial nucleoids. Tom70 in both strains was genomically tagged at the C-terminus with GFP. White arrows mark the staining of mitochondrial nucleoids. Scale bar: 5 μm.

strain. In addition, DAPI (4′,6-diamidino-2-phenylindole) staining revealed the presence of nucleoids in the *quintuple RBP mutant* strain although in contrast to the several mitochondrial nucleoids that can be seen in wildtype cells (representative image shown in Figure 7D), very frequently only a single but relatively large nucleoid is detected in the *quintuple RBP mutant* cells (Figure 7D). Thus, although mitochondria are also less in number and are apparently aberrant in structure and composition, the observed defect in COX expression is not due to loss of mitochondrial DNA. Further analysis is required to address this issue.

Discussion

Membrane and secretory proteins are delivered to the ER for proper folding, post-translational modifications and transport to a specific destination (reviewed in (Schwarz and Blower, 2016)). RNA-binding proteins (RBPs) in yeast and mammals that associate with the ER can assist in targeting these proteins by localizing their corresponding mRNAs to the ER (Aronov et al., 2007; Cui et al., 2012; Gelin-Licht et al., 2012; Kraut-Cohen et al., 2013; Schmid et al., 2006). In the current study, we identified several yeast RBPs (Mrn1p, Whi3p, Pbp2p, Slf1p, Ngr1p, and Puf1p) that partially colocalize with the ER. In addition, we show that RBPs Nab6p and Puf2p are enriched during subcellular fractionation in a membrane-containing fraction. Since these two RBPs have been especially associated with mRNAs encoding proteins with cell wall-related function (Hogan et al., 2008), we employed an assay to test for cell wall defects in cells lacking ER-associated RBPs. We observed a relatively mild cell wall defect upon deletion of *MRN1* or *WHI3* and a strong cell wall phenotype upon deletion of four RBPs (*whi3Δ pbp2Δ slf1Δ ngr1Δ*). Since Mrn1p has also been shown to associate with transcripts encoding cell wall-related transcripts (Hogan et al., 2008), we additionally deleted it and created fivefold RBP deletion strain to study changes in RNA expression and distribution.

Our analysis revealed no obvious shift of transcripts from a membrane (organelle rich) fraction to the cytosol upon the deletion of these five RBPs. However, as expected, their loss results in changes in the abundance of many transcripts. In addition, we noted that specific classes of mRNAs are enriched in the membrane fraction. In particular, we noticed an enrichment of mRNAs encoding nuclear-related proteins. We therefore did a qPCR analysis of five mRNAs encoding nuclear-related proteins and found that three of them such as *MOT1*, *NUP100* and *IKI3* are highly enriched in the organelle rich fraction. We further show that *MOT1* and *NUP100* colocalize with ER when checked by microscopy. According to the established SRP model, only mRNAs encoding secretory/membrane proteins localize to ER in translation-dependent manner (reviewed in (Reid and Nicchitta, 2015)). However, our results back up previous findings that reported the localization of mRNAs other than those coding for secretory/membrane proteins to the ER (Diehn et al., 2000; Jagannathan et al., 2014; de Jong et al., 2006; Kraut-Cohen et al., 2013). Some mRNAs have been demonstrated to localize to ER even independent of translation (Kraut-Cohen et al., 2013; Syed et al., 2018). Kraut-Cohen et al. (2013) suggest that mRNAs regardless of their coding capacity, have some inherent propensity to interact with ER. In support of this view, *OXA1* mRNA, which codes for mitochondrial inner membrane insertase (Herrmann et al., 1997) mislocalizes to ER when the

mitochondrial targeting information is removed (Gadir et al., 2011). Reid and Nicchitta (2015) propose the ER as the primary site of protein synthesis for both membrane/secretory and non-membrane/non-secretory proteins. They support their model by the finding that approximately half of all ribosomes in HEK293 and HeLa cells are ER-bound and, additionally, that a similar fraction of total cellular mRNA localizes to ER (Jagannathan et al., 2014).

We also observed an upregulation of transcripts encoding MRPs (including *MRPL39*, *IMG2* and *MRPL44*) in cells lacking the five ER-associated RBPs. Surprisingly, western blot analysis in contrast revealed reduction on the protein level of GFP fusion proteins of Mrpl39p, Img2p and Mrpl44p. We propose that these MRPs are either not efficiently translated or that they are translated but not properly imported into mitochondria and consequently degraded in the cytoplasm. The loss of nuclear-encoded MRPs results in a vast number of mitochondrial defects. In our case, not only is the Cox2 protein not translated in the *quintuple RBP mutant* strain but we also noticed the absence of transcription for *COX1, COX2* and the mitochondrial *21S* rRNA. This explains the inability of this yeast strain to grow on nonfermentable carbon sources, its mitochondrial genome instability and the aberrant mitochondrial morphology. Our observation is consistent with previous findings that deletion of MRPs leads to gradual loss of the mitochondrial genome (Merz and Westermann, 2009). In our case, this mitochondrial phenotype is caused only by the combined deletion of Mrn1p, Pbp2p, Slf1p, Whi3p and Ngr1p, and not any other combination. Literature search revealed that only Slf1p and Whi3p directly bind mRNAs encoding MRPs (Cai and Futcher, 2013; Kershaw et al., 2015). By analyzing the top 200 mRNA published target mRNAs for Whi3p (sorted based on net IP ratio; see Table S1 (Cai and Futcher, 2013)), we find that Whi3p associates with only one MRP mRNA, *MRPL49*. However, Mrpl49p levels are similar in wildtype and *quintuple RBP mutant* strain. In contrast to Whi3p, Slf1p binds several MRP mRNAs, including *MRPL4, MRPL19, MRPL28, RSM7, MRPL36, MRPL8, MRPL13, IMG1, MRP20, MRPL7, RSM18* and *RSM26* as demonstrated by analyzing the top 200 targets (sorted based on false discovery rate (FDR) taking into account the positive Log fold change (Log FC); see S3 Table (Kershaw et al., 2015)). So far, we have checked the expression levels of only five MRPs and found very low levels of Mrpl39p, Mrpl44p and Img2p in the organelle rich fraction. It is possible that many more MRPs are either absent or present in very low quantity in the organelle rich fraction.

In conclusion, we report that mRNAs encoding proteins with nuclear function localize to ER. We further report that the deletion of five RBPs such as Mrn1p, Whi3p, Slf1p, Pbp2p and Ngr1 leads to the up regulation of mRNAs coding for nuclear-encoded MRPs. Although the

transcripts coding for MRPs are upregulated, we see very low levels of Mrpl39p, Mrpl44p and Img2p in the organelle rich fraction. We therefore suggest that these five RBPs might play role in controlling the expression of nuclear-encoded MRPs.

Acknowledgements

We thank Robert H. Singer for proving plasmids pET296-YcpLac111 CYC1p-MCP-NLS-2xyeGFP and pET259-pUC57 24xMS2V6 and Dirk Schwarzer for providing H3 (ab1791) antibody. This work was funded by the Deutsche Forschungsgemeinschaft (DFG), grant JA696-10/1.

Author contributions

MIS performed experiments for figures 1-7 and supporting figures 1-7. SP performed experiments for figures 4-6 and PB did data analysis for figures 4-6. DR performed experiment for figure 7. MIS, DR and RPJ designed the experiments. MIS and RPJ wrote the manuscript.

References

Adesnik, M., Lande, M., Martin, T., and Sabatini, D.D. (1976). Retention of mRNA on the endoplasmic reticulum membranes after in vivo disassembly of polysomes by an inhibitor of initiation. J. Cell Biol. *71*, 307–313.

Aoki, K., Adachi, S., Homoto, M., Kusano, H., Koike, K., and Natsume, T. (2013). LARP1 specifically recognizes the 3′ terminus of poly(A) mRNA. FEBS Lett. *587*, 2173–2178.

Aronov, S., Gelin-Licht, R., Zipor, G., Haim, L., Safran, E., and Gerst, J.E. (2007). mRNAs Encoding Polarity and Exocytosis Factors Are Cotransported with the Cortical Endoplasmic Reticulum to the Incipient Bud in Saccharomyces cerevisiae. Mol. Cell. Biol. *27*, 3441–3455.

Ast, T., and Schuldiner, M. (2013). All roads lead to Rome (but some may be harder to travel): SRP-independent translocation into the endoplasmic reticulum. Crit. Rev. Biochem. Mol. Biol. *48*, 273–288.

Baker Brachmann, C., Davies, A., Cost, G.J., Caputo, E., Li, J., Hieter, P., and Boeke, J.D. (1998). Designer deletion strains derived fromSaccharomyces cerevisiae S288C: A useful set of strains and plasmids for PCR-mediated gene disruption and other applications. Yeast *14*, 115–132.

Bayfield, M.A., Yang, R., and Maraia, R.J. (2010). Conserved and divergent features of the structure and function of La and La-related proteins (LARPs). Biochim. Biophys. Acta - Gene Regul. Mech. *1799*, 365–378.

Bevis, B.J., and Glick, B.S. (2002). Rapidly maturing variants of the Discosoma red fluorescent protein (DsRed). Nat. Biotechnol. *20*, 83–87.

Blake, C.C.F., and Rice, D.W. (1981). Phosphoglycerate Kinase. Philos. Trans. R. Soc. B Biol. Sci. *293*, 93–104.

Buchan, J.R., Muhlrad, D., and Parker, R. (2008). P bodies promote stress granule assembly in Saccharomyces cerevisiae. J. Cell Biol. *183*, 441–455.

Buu, L.-M., Jang, L.-T., and Lee, F.-J.S. (2004). The yeast RNA-binding protein Rbp1p modifies the stability of mitochondrial porin mRNA. J. Biol. Chem. *279*, 453–462.

Cai, Y., and Futcher, B. (2013). Effects of the yeast RNA-binding protein Whi3 on the half-life and abundance of CLN3 mRNA and other targets. PLoS One *8*, e84630.

Cardelli, J., Long, B., and Pitot, H.C. (1976). Direct association of messenger RNA labeled in the presence of fluoroorotate with membranes of the endoplasmic reticulum in rat liver. J. Cell Biol. *70*, 47–58.

Chang, L.-C., and Lee, F.-J.S. (2012). The RNA helicase Dhh1p cooperates with Rbp1p to promote porin mRNA decay via its non-conserved C-terminal domain. Nucleic Acids Res. *40*, 1331–1344.

Chen, D.-C., Yang, B.-C., and Kuo, T.-T. (1992). One-step transformation of yeast in stationary phase. Curr. Genet. *21*, 83–84.

Claros, M.G. (1995). MitoProt, a Macintosh application for studying mitochondrial proteins. Comput. Appl. Biosci. *11*, 441–447.

Cléry, A., Blatter, M., and Allain, F.H.-T. (2008). RNA recognition motifs: boring? Not quite. Curr. Opin. Struct. Biol. *18*, 290–298.

Colomina, N., Ferrezuelo, F., Wang, H., Aldea, M., and Garí, E. (2008). Whi3, a developmental regulator of budding yeast, binds a large set of mRNAs functionally related to the endoplasmic reticulum. J. Biol. Chem. *283*, 28670–28679.

Condeelis, J., and Singer, R.H. (2005). How and why does β-actin mRNA target? Biol. Cell *97*, 97–110.

Cooper, C.E., Nicholls, P., and Freedman, J.A. (1991). Cytochrome c oxidase: structure, function, and membrane topology of the polypeptide subunits. Biochem. Cell Biol. *69*, 586–607.

Costanzo, M., Baryshnikova, A., Bellay, J., Kim, Y., Spear, E.D., Sevier, C.S., Ding, H., Koh, J.L.Y., Toufighi, K., Mostafavi, S., et al. (2010). The genetic landscape of a cell. Science *327*, 425–431.

Cui, X.A., and Palazzo, A.F. (2014). Localization of mRNAs to the endoplasmic reticulum. Wiley Interdiscip. Rev. RNA *5*, 481–492.

Cui, X.A., Zhang, H., and Palazzo, A.F. (2012). p180 Promotes the Ribosome-Independent Localization of a Subset of mRNA to the Endoplasmic Reticulum. PLoS Biol. *10*, e1001336.

Daniel Cietz, R., and Sugino, A. (1988). New yeast-EscicerLSa coli shuttle vectors constructed with iu vitro mutagenized yeast genes lacking six-base pair restriction sites (Recombinant DNA; Saccharomyces cerevkiue; mitotic stability; cloning sites; unique cuts; new alleles).

Denisenko, O., and Bomsztyk, K. (2002). Yeast hnRNP K-like genes are involved in regulation of the telomeric position effect and telomere length. Mol. Cell. Biol. *22*, 286–297.

Diehn, M., Eisen, M.B., Botstein, D., and Brown, P.O. (2000). Large-scale identification of secreted and membrane-associated gene products using DNA microarrays. Nat. Genet. *25*, 58–62.

Diehn, M., Bhattacharya, R., Botstein, D., and Brown, P.O. (2006). Genome-Scale Identification of Membrane-Associated Human mRNAs. PLoS Genet. *2*, e11.

Dobin, A., Davis, C.A., Schlesinger, F., Drenkow, J., Zaleski, C., Jha, S., Batut, P., Chaisson, M., and Gingeras, T.R. (2013). STAR: ultrafast universal RNA-seq aligner. Bioinformatics *29*, 15–21.

Düring, L., Thorsen, M., Petersen, D.S.N., Køster, B., Jensen, T.H., and Holmberg, S. (2012). MRN1 Implicates Chromatin Remodeling Complexes and Architectural Factors in mRNA Maturation. PLoS One *7*, e44373.

Edwards, T.A., Pyle, S.E., Wharton, R.P., and Aggarwal, A.K. (2001). Structure of Pumilio Reveals Similarity between RNA and Peptide Binding Motifs. Cell *105*, 281–289.

Elstner, M., Andreoli, C., Klopstock, T., Meitinger, T., and Prokisch, H. (2009). Chapter 1 The Mitochondrial Proteome Database. In Methods in Enzymology, pp. 3–20.

Emanuelsson, O., Brunak, S., von Heijne, G., and Nielsen, H. (2007). Locating proteins in the cell using TargetP, SignalP and related tools. Nat. Protoc. *2*, 953–971.

Friedlander, M., and Blobel, G. (1985). Bovine opsin has more than one signal sequence. Nature *318*, 338–343.

Gadir, N., Haim-Vilmovsky, L., Kraut-Cohen, J., and Gerst, J.E. (2011). Localization of mRNAs coding for mitochondrial proteins in the yeast Saccharomyces cerevisiae. RNA *17*, 1551–1565.

Garí, E., Volpe, T., Wang, H., Gallego, C., Futcher, B., and Aldea, M. (2001). Whi3 binds the mRNA of the G1 cyclin CLN3 to modulate cell fate in budding yeast. Genes Dev. *15*, 2803–2808.

Gelin-Licht, R., Paliwal, S., Conlon, P., Levchenko, A., and Gerst, J.E. (2012). Scp160-dependent mRNA trafficking mediates pheromone gradient sensing and chemotropism in yeast. Cell Rep. *1*, 483–494.

Genz, C., Fundakowski, J., Hermesh, O., Schmid, M., and Jansen, R.-P. (2013). Association of the yeast RNA-binding protein She2p with the tubular endoplasmic reticulum depends on membrane curvature. J. Biol. Chem. *288*, 32384–32393.

Gietz, R.D., and Schiestl, R.H. (2007). High-efficiency yeast transformation using the LiAc/SS carrier DNA/PEG method. Nat. Protoc. *2*, 31–34.

Gilmore, R., Blobel, G., and Walter, P. (1982). Protein translocation across the endoplasmic reticulum. I. Detection in the microsomal membrane of a receptor for the signal recognition particle. J. Cell Biol. *95*, 463–469.

Glisovic, T., Bachorik, J.L., Yong, J., and Dreyfuss, G. (2008). RNA-binding proteins and post-transcriptional gene regulation. FEBS Lett. *582*, 1977–1986.

Görlich, D., and Rapoport, T.A. (1993). Protein translocation into proteoliposomes reconstituted from purified components of the endoplasmic reticulum membrane. Cell *75*, 615–630.

Haim, L., Zipor, G., Aronov, S., and Gerst, J.E. (2007). A genomic integration method to visualize localization of endogenous mRNAs in living yeast. Nat. Methods *4*.

Harrington, B.J., and Hageage, G.J. (1991). Calcofluor white: Tips for improving its use. Clin. Microbiol. Newsl. *13*, 3–5.

von Heijne, G. (1983). Patterns of amino acids near signal-sequence cleavage sites. Eur. J. Biochem. *133*, 17–21.

Herrmann, J.M., Neupert, W., and Stuart, R.A. (1997). Insertion into the mitochondrial inner membrane of a polytopic protein, the nuclear-encoded Oxa1p. EMBO J. *16*, 2217–2226.

Hitzeman, R.A., Clarke, L., and Carbon, J. (1980). Isolation and characterization of the yeast 3-phosphoglycerokinase gene (PGK) by an immunological screening technique. J. Biol. Chem. *255*, 12073–12080.

Hogan, D.J., Riordan, D.P., Gerber, A.P., Herschlag, D., and Brown, P.O. (2008). Diverse RNA-Binding Proteins Interact with Functionally Related Sets of RNAs, Suggesting an Extensive Regulatory System. PLoS Biol. *6*, e255.

Huch, S., Gommlich, J., Muppavarapu, M., Beckham, C., and Nissan, T. (2016). Membrane-association of mRNA decapping factors is independent of stress in budding yeast. Sci. Rep. *6*, 25477.

Jagannathan, S., Reid, D.W., Cox, A.H., and Nicchitta, C. V. (2014). De novo translation initiation on membrane-bound ribosomes as a mechanism for localization of cytosolic protein mRNAs to the endoplasmic reticulum. RNA *20*, 1489–1498.

Jambhekar, A., and DeRisi, J.L. (2007). Cis-acting determinants of asymmetric, cytoplasmic RNA transport. RNA *13*, 625–642.

Jang, L.-T., Buu, L.-M., and Lee, F.-J.S. (2006). Determinants of Rbp1p localization in specific cytoplasmic mRNA-processing foci, P-bodies. J. Biol. Chem. *281*, 29379–29390.

Janke, C., Magiera, M.M., Rathfelder, N., Taxis, C., Reber, S., Maekawa, H., Moreno-Borchart, A., Doenges, G., Schwob, E., Schiebel, E., et al. (2004). A versatile toolbox for PCR-based tagging of yeast genes: new fluorescent proteins, more markers and promoter substitution cassettes. Yeast *21*, 947–962.

Johnstone, O., and Lasko, P. (2001). Translational Regulation and RNA Localization in *Drosophila* Oocytes and Embryos. Annu. Rev. Genet. *35*, 365–406.

de Jong, M., van Breukelen, B., Wittink, F.R., Menke, F.L.H., Weisbeek, P.J., and Ackerveken, G. Van den (2006). Membrane-associated transcripts in Arabidopsis; their isolation and characterization by DNA microarray analysis and bioinformatics. Plant J. *46*, 708–721.

Kershaw, C.J., Costello, J.L., Castelli, L.M., Talavera, D., Rowe, W., Sims, P.F.G., Ashe, M.P., Hubbard, S.J., Pavitt, G.D., and Grant, C.M. (2015). The Yeast La Related Protein Slf1p Is a Key Activator of Translation during the Oxidative Stress Response. PLoS Genet. *11*, e1004903.

Ketela, T., Green, R., and Bussey, H. (1999). Saccharomyces cerevisiae mid2p is a potential cell wall stress sensor and upstream activator of the PKC1-MPK1 cell integrity pathway. J. Bacteriol. *181*, 3330–3340.

King, M. Lou, Messitt, T.J., and Mowry, K.L. (2005). Putting RNAs in the right place at the right time: RNA localization in the frog oocyte. Biol. Cell *97*, 19–33.

Knop, M., Siegers, K., Pereira, G., Zachariae, W., Winsor, B., Nasmyth, K., and Schiebel, E. (1999). Epitope tagging of yeast genes using a PCR-based strategy: more tags and improved practical routines. Yeast *15*, 963–972.

Kraut-Cohen, J., Afanasieva, E., Haim-Vilmovsky, L., Slobodin, B., Yosef, I., Bibi, E., and Gerst, J.E. (2013). Translation- and SRP-independent mRNA targeting to the endoplasmic reticulum in the yeast

Saccharomyces cerevisiae. Mol. Biol. Cell *24*, 3069–3084.

Lande, M.A., Adesnik, M., Sumida, M., Tashiro, Y., and Sabatini, D.D. (1975). Direct association of messenger RNA with microsomal membranes in human diploid fibroblasts. J. Cell Biol. *65*, 513–528.

Liao, Y., Smyth, G.K., and Shi, W. (2014). featureCounts: an efficient general purpose program for assigning sequence reads to genomic features. Bioinformatics *30*, 923–930.

Linder, P., and Jankowsky, E. (2011). From unwinding to clamping — the DEAD box RNA helicase family. Nat. Rev. Mol. Cell Biol. *12*, 505–516.

Livak, K.J., and Schmittgen, T.D. (2001). Analysis of Relative Gene Expression Data Using Real-Time Quantitative PCR and the 2−ΔΔCT Method. Methods *25*, 402–408.

Love, M.I., Huber, W., and Anders, S. (2014). Moderated estimation of fold change and dispersion for RNA-seq data with DESeq2. Genome Biol. *15*, 550.

Loya, A., Pnueli, L., Yosefzon, Y., Wexler, Y., Ziv-Ukelson, M., and Arava, Y. (2008). The 3'-UTR mediates the cellular localization of an mRNA encoding a short plasma membrane protein. RNA *14*, 1352–1365.

Martin, M. (2011). Cutadapt removes adapter sequences from high-throughput sequencing reads. EMBnet.Journal *17*, 10.

Mechler, B., and Vassalli, P. (1975). Membrane-bound ribosomes of myeloma cells. III. The role of the messenger RNA and the nascent polypeptide chain in the binding of ribosomes to membranes. J. Cell Biol. *67*, 25–37.

Merz, S., and Westermann, B. (2009). Genome-wide deletion mutant analysis reveals genes required for respiratory growth, mitochondrial genome maintenance and mitochondrial protein synthesis in Saccharomyces cerevisiae. Genome Biol. *10*, R95.

Milcarek, C., and Penman, S. (1974). Membrane-bound polyribosomes in HeLa cells: Association of polyadenylic acid with membranes. J. Mol. Biol. *89*, 327–338.

Mize, N.K., Andrews, D.W., and Lingappa, V.R. (1986). A stop transfer sequence recognizes receptors for nascent chain translocation across the endoplasmic reticulum membrane. Cell *47*, 711–719.

Nogae, I., and Johnston, M. (1990). Isolation and characterization of the ZWF1 gene of Saccharomyces cerevisiae, encoding glucose-6-phosphate dehydrogenase. Gene *96*, 161–169.

Palazzo, A.F., Springer, M., Shibata, Y., Lee, C.-S., Dias, A.P., and Rapoport, T.A. (2007). The signal sequence coding region promotes nuclear export of mRNA. PLoS Biol. *5*, e322.

Paquin, N., and Chartrand, P. (2008). Local regulation of mRNA translation: new insights from the bud. Trends Cell Biol. *18*, 105–111.

Pool, M.R. (2005). Signal recognition particles in chloroplasts, bacteria, yeast and mammals (Review). Mol. Membr. Biol. *22*, 1–2.

Prilusky, J., and Bibi, E. (2009). Studying membrane proteins through the eyes of the genetic code revealed a strong uracil bias in their coding mRNAs. Proc. Natl. Acad. Sci. U. S. A. *106*, 6662–6666.

Reid, D.W., and Nicchitta, C. V. (2012). Primary Role for Endoplasmic Reticulum-bound Ribosomes in Cellular Translation Identified by Ribosome Profiling. J. Biol. Chem. *287*, 5518–5527.

Reid, D.W., and Nicchitta, C. V. (2015). Diversity and selectivity in mRNA translation on the endoplasmic reticulum. Nat. Rev. Mol. Cell Biol. *16*, 221–231.

Roncero, C., and Duran, A. (1985). Effect of Calcofluor White and Congo Red on Fungal Cell Wall Morphogenesis: In Vivo Activation of Chitin Polymerization.

Rothstein, R.J., and Sherman, F. (1980). Genes affecting the expression of cytochrome c in yeast: genetic mapping and genetic interactions. Genetics *94*, 871–889.

Rothsteinl, R.J., and Sherman, F. GENES AFFECTING THE EXPRESSION OF CYTOCHROME c

IN YEAST: GENETIC MAPPING AND GENETIC INTERACTIONS.

Schmid, M., Jaedicke, A., Du, T.-G., and Jansen, R.-P. (2006). Coordination of Endoplasmic Reticulum and mRNA Localization to the Yeast Bud. Curr. Biol. *16*, 1538–1543.

Schwarz, D.S., and Blower, M.D. (2016). The endoplasmic reticulum: structure, function and response to cellular signaling. Cell. Mol. Life Sci. *73*, 79–94.

Segref, A., Sharma, K., Doye, V., Hellwig, A., Huber, J., Lührmann, R., and Hurt, E. (1997). Mex67p, a novel factor for nuclear mRNA export, binds to both poly(A)+ RNA and nuclear pores. EMBO J. *16*, 3256–3271.

Serrano, R., Kielland-Brandt, M.C., and Fink, G.R. (1986). Yeast plasma membrane ATPase is essential for growth and has homology with (Na+ + K+), K+- and Ca2+-ATPases. Nature *319*, 689–693.

Sikorski, R.S., and Hieter, P. (1989). A System of Shuttle Vectors and Yeast Host Strains Designed for Efficient Manipulation of DNA in Saccharomyces ceratisiae.

Sobel, S.G., and Wolin, S.L. (1999). Two yeast La motif-containing proteins are RNA-binding proteins that associate with polyribosomes. Mol. Biol. Cell *10*, 3849–3862.

Stillman, D.J. (2010). Nhp6: a small but powerful effector of chromatin structure in Saccharomyces cerevisiae. Biochim. Biophys. Acta *1799*, 175–180.

Stirling, C.J., Rothblatt, J., Hosobuchi, M., Deshaies, R., and Schekman, R. (1992). Protein Translocation Mutants Defective in the Insertion of Integral Membrane Proteins into the Endoplasmic Reticulum.

Syed, M.I., Moorthy, B.T., Jenner, A., Fetka, I., and Jansen, R.-P. (2018). Signal sequence-independent targeting of MID2 mRNA to the endoplasmic reticulum by the yeast RNA-binding protein Khd1p. FEBS Lett. *592*.

Tkach, J.M., Yimit, A., Lee, A.Y., Riffle, M., Costanzo, M., Jaschob, D., Hendry, J.A., Ou, J., Moffat, J., Boone, C., et al. (2012). Dissecting DNA damage response pathways by analysing protein localization and abundance changes during DNA replication stress. Nat. Cell Biol. *14*, 966–976.

Tutucci, E., Vera, M., Biswas, J., Garcia, J., Parker, R., and Singer, R.H. (2017). An improved MS2 system for accurate reporting of the mRNA life cycle. Nat. Methods *15*, 81–89.

Valverde, R., Edwards, L., and Regan, L. (2008). Structure and function of KH domains. FEBS J. *275*, 2712–2726.

Vögtle, F.-N., Wortelkamp, S., Zahedi, R.P., Becker, D., Leidhold, C., Gevaert, K., Kellermann, J., Voos, W., Sickmann, A., Pfanner, N., et al. (2009). Global Analysis of the Mitochondrial N-Proteome Identifies a Processing Peptidase Critical for Protein Stability. Cell *139*, 428–439.

Wach, A., Brachat, A., Pöhlmann, R., and Philippsen, P. (1994). New heterologous modules for classical or PCR-based gene disruptions inSaccharomyces cerevisiae. Yeast *10*, 1793–1808.

Walter, P., and Blobel, G. (1980). Purification of a membrane-associated protein complex required for protein translocation across the endoplasmic reticulum. Proc. Natl. Acad. Sci. U. S. A. *77*, 7112–7116.

Walter, P., and Blobel, G. (1981a). Translocation of proteins across the endoplasmic reticulum III. Signal recognition protein (SRP) causes signal sequence-dependent and site-specific arrest of chain elongation that is released by microsomal membranes. J. Cell Biol. *91*, 557–561.

Walter, P., and Blobel, G. (1981b). Translocation of proteins across the endoplasmic reticulum. II. Signal recognition protein (SRP) mediates the selective binding to microsomal membranes of in-vitro-assembled polysomes synthesizing secretory protein. J. Cell Biol. *91*, 551–556.

Walter, P., and Blobel, G. (1982). Signal recognition particle contains a 7S RNA essential for protein translocation across the endoplasmic reticulum. Nature *299*, 691–698.

Wang, H., Garí, E., Vergés, E., Gallego, C., and Aldea, M. (2004). Recruitment of Cdc28 by Whi3 restricts nuclear accumulation of the G1 cyclin-Cdk complex to late G1. EMBO J. *23*, 180–190.

Weill, U., Yofe, I., Sass, E., Stynen, B., Davidi, D., Natarajan, J., Ben-Menachem, R., Avihou, Z., Goldman, O., Harpaz, N., et al. (2018). Genome-wide SWAp-Tag yeast libraries for proteome exploration. Nat. Methods *15*, 617–622.

Wu, C.-H., Lee, S.-C., and Wang, C.-W. (2011). Viral protein targeting to the cortical endoplasmic reticulum is required for cell–cell spreading in plants. J. Cell Biol. *193*, 521–535.

Yang, R., Gaidamakov, S.A., Xie, J., Lee, J., Martino, L., Kozlov, G., Crawford, A.K., Russo, A.N., Conte, M.R., Gehring, K., et al. (2011). La-related protein 4 binds poly(A), interacts with the poly(A)-binding protein MLLE domain via a variant PAM2w motif, and can promote mRNA stability. Mol. Cell. Biol. *31*, 542–556.

Yofe, I., Weill, U., Meurer, M., Chuartzman, S., Zalckvar, E., Goldman, O., Ben-Dor, S., Schütze, C., Wiedemann, N., Knop, M., et al. (2016). One library to make them all: streamlining the creation of yeast libraries via a SWAp-Tag strategy. Nat. Methods *13*, 371–378.

Yu, W., Farrell, R.A., Stillman, D.J., and Winge, D.R. (1996). Identification of SLF1 as a new copper homeostasis gene involved in copper sulfide mineralization in Saccharomyces cerevisiae. Mol. Cell. Biol. *16*, 2464–2472.

Supporting material

Supporting Figures (Page 33-40)

Supporting Tables for RNA seq analysis (Attached as Excel sheets)

Supporting Tables for Materials and methods (Page 41-54)

Supporting References (Page 55)

Supporting Figures

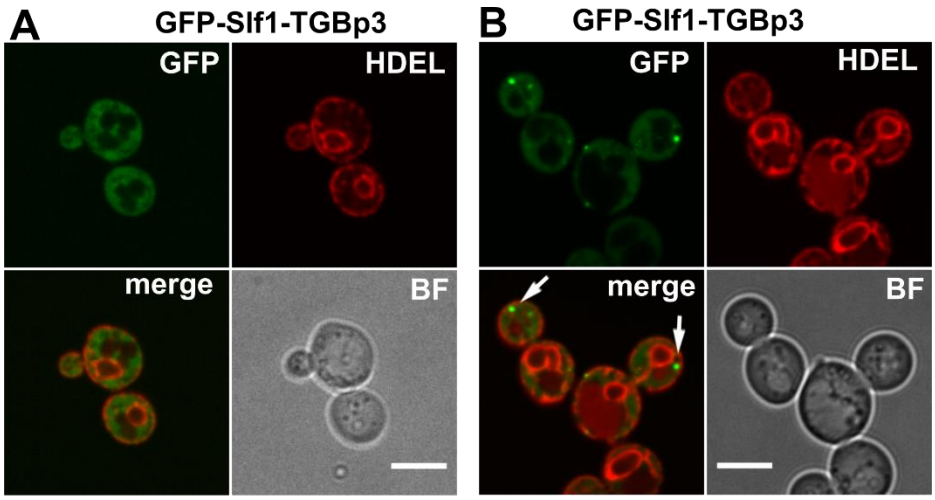

Supporting figure S1. Representative images of Slf1p-TGBP3 fusion protein. HDEL-DsRed was used to label ER. (A) Slf1p-TGBp3 fusion does not form foci. (B) Foci (white arrows) formed by Slf1p-TGBp3 fusion that do not colocalize with the ER marker.

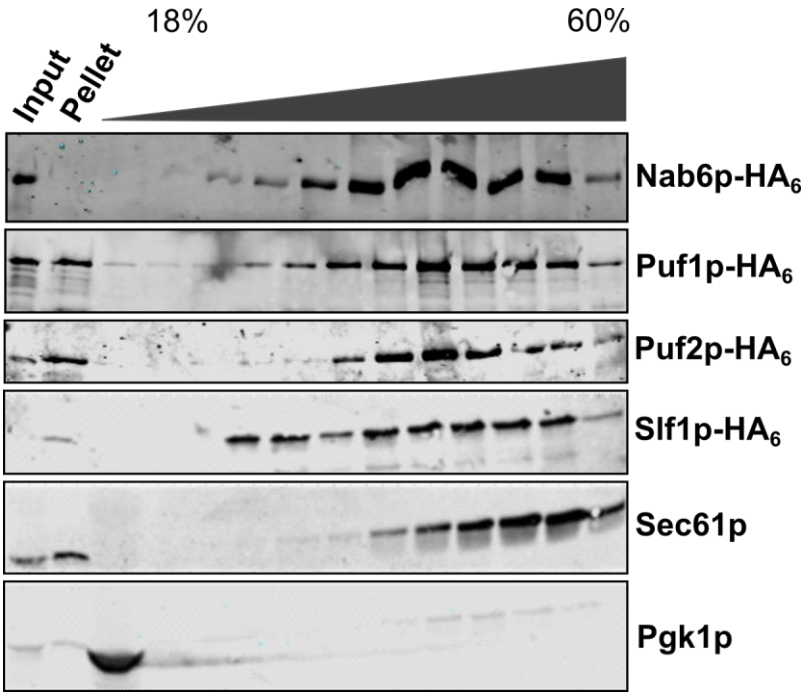

Supporting figure S2. Distribution of HA-tagged RBPs in 18-60% sucrose gradient centrifugation (see materials and methods). After centrifugation, 11 or 12 fractions were collected and precipitated with TCA. Aliquots of these fractions along with whole cell lysates (input) and pellets were analysed by western blot against HA, Sec61p, and Pgk1p. A large fraction of the shown RBPs co-migrate with the microsomal marker Sec61p. Pgk1p is used as a cytosolic marker.

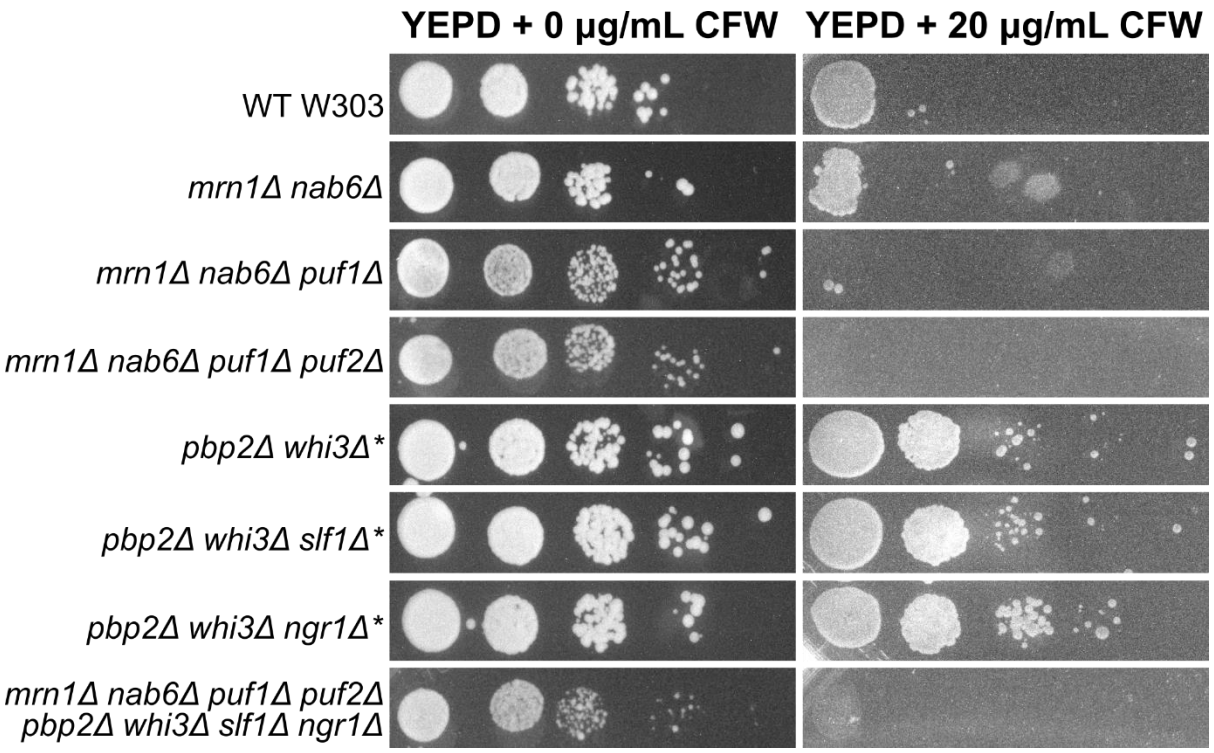

Supporting figure S3. Calcofluor White (CWF) assay to test for cell wall defects. Wildtype and different RBP deletions were serially diluted and spotted on YEPD plates with or without CFW. The asterisk (*) represents a yeast strain with decreased sensitivity against CFW, indicating cell wall defects.

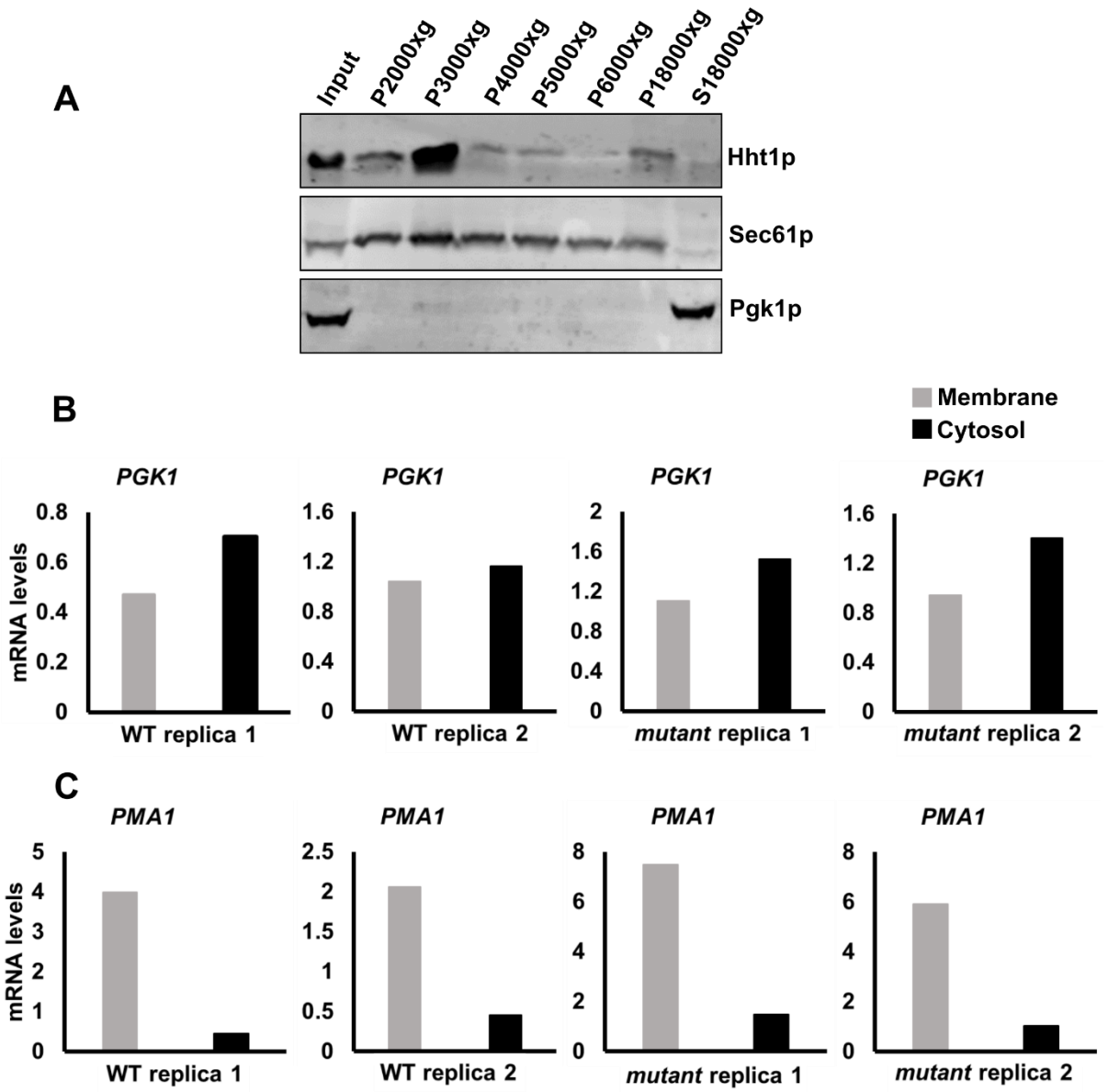

Supporting figure S4. Verification of the quick cell fractionation protocol. (A) Yeast cells were grown to mid-log phase, treated for 15 minutes with 100 µg- mL^{-1} cycloheximide, harvested, and lysed in low salt lysis buffer (see material and methods). The lysate generated was then set to successive centrifugation steps to remove nuclear contamination. Hht1p, Sec61p and Pgk1p were used as markers for nucleus, ER, and cytosol, respectively. (B) and (C) RNA distribution in membrane and cytosolic fractions of wildtype (WT) and *quintuple RBP mutant* (*mutant*) strain. Yeast lysates generated in low salt lysis buffer were centrifuged at 3000 g to deplete the nuclear contamination. The lysates at this stage were considered as nuclei-free whole cell lysates (WCLs) and used as input for further fractionation. Inputs were further fractionated at 18000 g to separate the membrane fractions (pellets) from the cytosolic fractions (supernatants). *PMA1* and *PGK1* levels in these fractions were determined by RT-qPCR. The C_t values of *PMA1* and *PGK1* in the membrane and cytosolic fractions were normalized against the C_t values in the corresponding input.

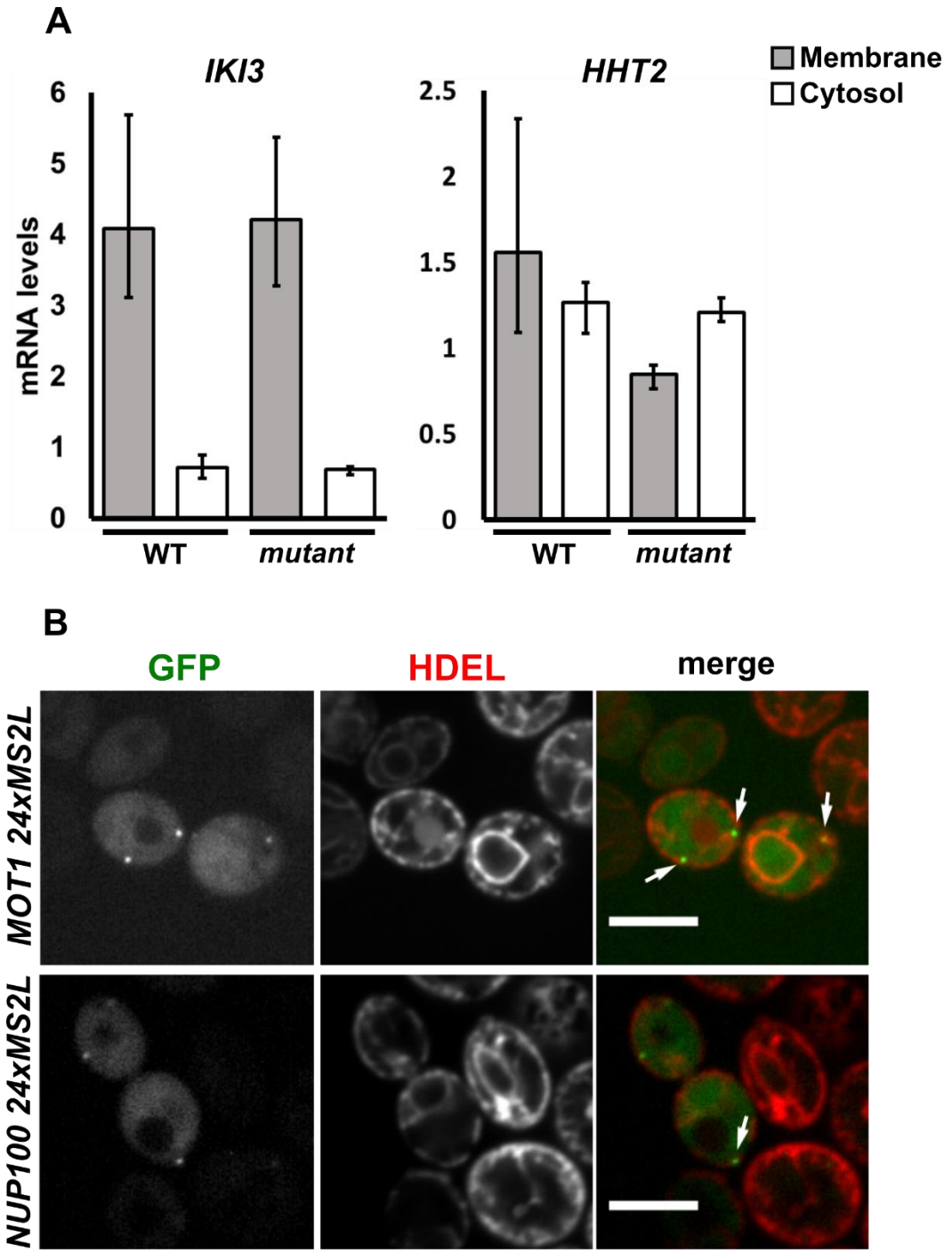

Figure 5. ER localization of mRNAs encoding proteins with nuclear-related function. (A) qPCR analysis for *IKI3* and *HHT2* in membrane and cytosolic fractions of wildtype (WT) and *quintuple RBP mutant* (*mutant*) strain. After fractionation, RNA was extracted. Prior to RT-qPCR, 10 ng of spike RNA was added to each sample. C_t values obtained were normalized against the spike RNA. (B) Representative images of MSL-tagged *MOT1* and *NUP100* mRNAs colocalizing with ER. MSL-tagged mRNAs were visualized by an MCP-2xGFP fusion protein. ER was stained with HDEL-DSRed. mRNA particles that localize at or very close to ER are indicated with white arrows. Scale bar: 5 μm.

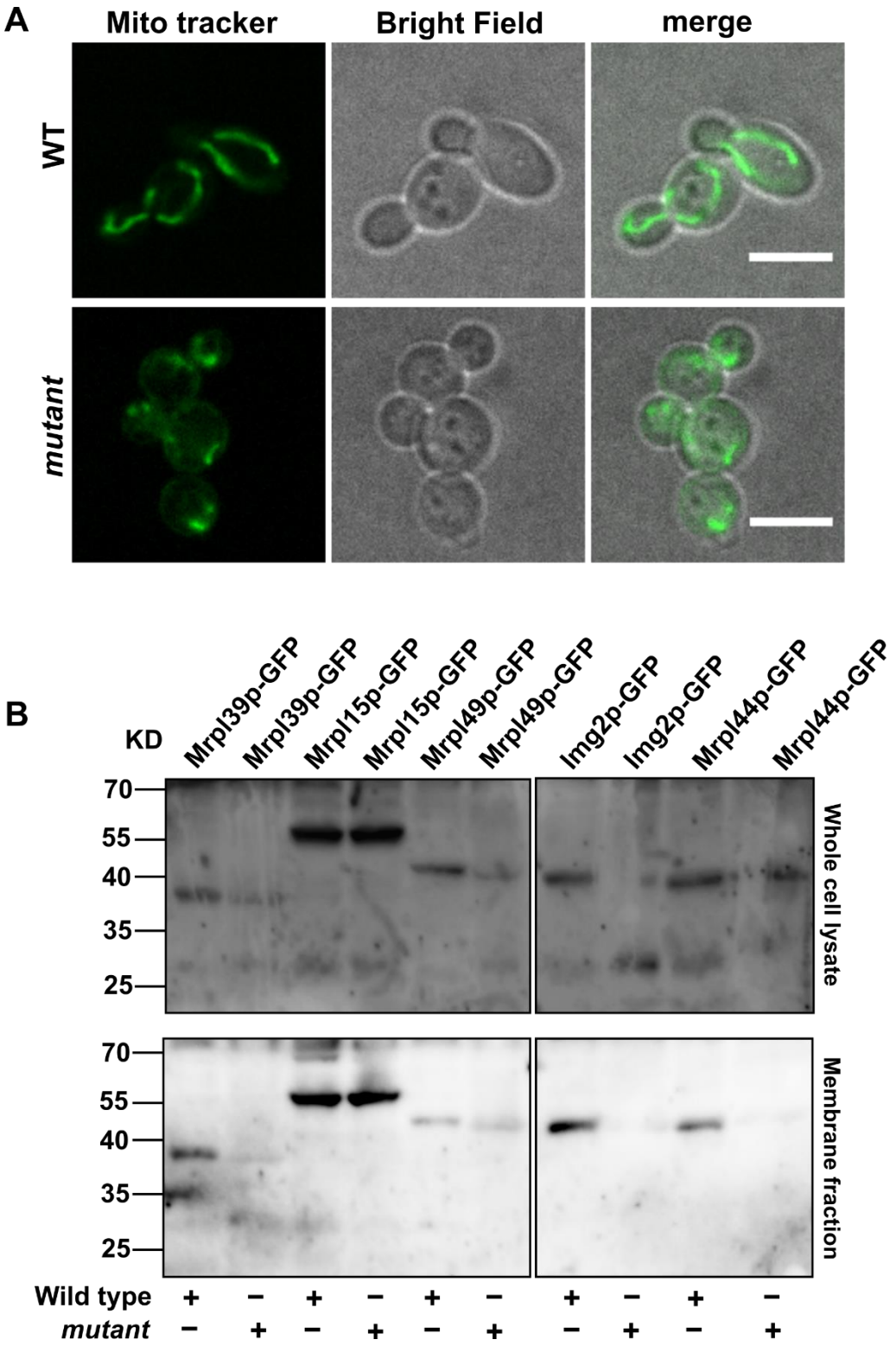

Figure 6. The deletion of five RBPs, such as Mrn1p, Whi3p, Pbp2p, Slf1p and Ngr1p results in aberrant mitochondrial morphology and loss of MRPs in organelle-containing membrane fraction. (A) MitoTracker Green FM with the excitation wavelength in the green fluorescent protein (GFP) range was used to stain the mitochondria in both wildtype (WT) and *quintuple RBP mutant* (*mutant*) strain (for details, see material and methods). The *quintuple RBP mutant* strain forms aggregated mitochondrial structures instead of the extended tubular network as is seen in wildtype strain. Scale bar: 5 μm. (B) Western blot analysis of several MRPs. Whole cell lysates (WCLs) and membrane fractions

from wildtype (WT) and *quintuple RBP mutant* (*mutant*) were set to western blot analysis with MRP-GFP fusions. As compared to wildtype, very faint bands for Mrpl39p, Img2p and Mrpl44p can be seen in the membrane fraction of *quintuple RBP mutant* strain.

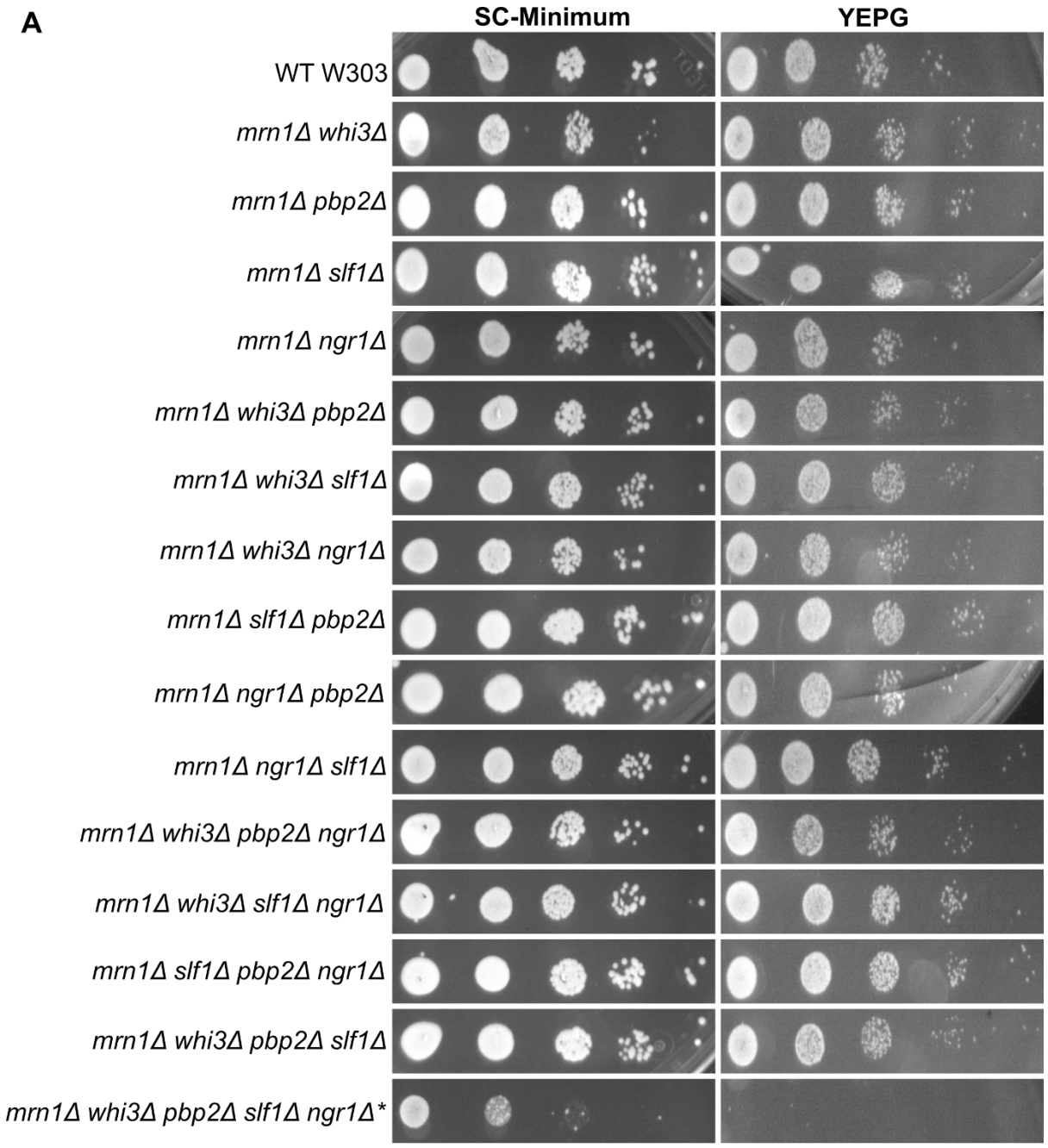
A
SC-Minimum
YEPG
WT W303
mrn1Δ whi3Δ
mrn1Δ pbp2Δ
mrn1Δ slf1Δ
mrn1Δ ngr1Δ
mrn1Δ whi3Δ pbp2Δ
mrn1Δ whi3Δ slf1Δ
mrn1Δ whi3Δ ngr1Δ
mrn1Δ slf1Δ pbp2Δ
mrn1Δ ngr1Δ pbp2Δ
mrn1Δ ngr1Δ slf1Δ
mrn1Δ whi3Δ pbp2Δ ngr1Δ
mrn1Δ whi3Δ slf1Δ ngr1Δ
mrn1Δ slf1Δ pbp2Δ ngr1Δ
mrn1Δ whi3Δ pbp2Δ slf1Δ
mrn1Δ whi3Δ pbp2Δ slf1Δ ngr1Δ*
B
DNA Ladder
WT
mutant
1000 bp
750 bp
500 bp
250 bp
COX2 genomic PCR

Supporting figure S7. Only the quintuple gene deletion causes respiratory-incompetent mitochondria. (A) Spot assay for different deletion strains on synthetic complete (SC-) minimal medium supplemented with dextrose or yeast extract peptone medium supplemented with glycerol (YEPG). The asterisk (*) represents yeast strain with respiratory defect. (B) Nucleic acids from an organelle-enriched fraction from wildtype and *quintuple RBP mutant* strains were used as template for PCR against *COX2*. The primers used bind within the coding region of *COX2*. Mitochondrial DNA from wildtype shows the estimated (610 bp) PCR product for *COX2*. On the other hand, a slightly larger PCR product for *COX2* is obtained from mitochondrial DNA of *quintuple RBP mutant* strain indicating an insertion.

Supporting Tables for Materials and methods

Supporting table S6: List of yeast deletion strains created in this study

Name	Essential genotype	Yeast strain used	DNA template used	Primers used for deletion	Primers used for detection
RJY5041	*MATa mrn1Δ::KANMX6*	RJY358	pRJ1347	RJO5102/RJO5103	RJO5107/RJO2026 RJO5107/RJO5110
RJY5107	*MATa nab6Δ::SpHIS5*	RJY358	pRJ1485	RJO5509-RJO5514	RJO5512/RJO5514
RJY5042	*MATa puf1Δ::hphNT1*	RJY358	pRJ1212	RJO5515-RJO5518 /RJO5523/RJO5524	RJO5517/RJO2026 RJO5517/RJO5518
RJY5043	*MATa puf2Δ::natNT2*	RJY358	pRJ1213	RJO5519-RJO5522 /RJO5523/RJO5524	RJO5521/RJO2026 RJO5521/RJO5522
RJY5086	*MATa pbp2Δ::HIS3MX6*	RJY358	pRJ146	RJO5549/RJO5550	RJO5557/RJO5565 RJO5557/RJO1265
RJY5047	*MATa whi3Δ::LEU2*	RJY358	pRJ297	RJO5555/RJO5556	RJO5563/RJO5565 RJO5563/RJO2711
RJY5087	*MATa slf1Δ::URA3*	RJY358	pRJ827	RJO5551/RJO5552	RJO5559/RJO5565 RJO5559/RJO4685
RJY5088	*MATa ngr1Δ::TRP1*	RJY358	pRJ147	RJO5553/RJO5554	RJO5561/RJO5565 RJO5561/RJO5562
RJY5044	*MATa nab6Δ, mrn1Δ::KANMX6*	RJY5107	Genomic DNA from RJY5041	RJO5107/RJO4472	RJO5107/RJO2026 RJO5107/RJO5110
RJY5045	*MATa nab6Δ, mrn1Δ::KANMX6, puf1Δ::hphNT1*	RJY5044	Genomic DNA from RJY5042	RJO5517/RJO5518	RJO5517/RJO2026 RJO5517/RJO5518
RJY5046	*MATa nab6Δ, mrn1Δ::KANMX6, puf1Δ::hphNT1, puf2Δ::natNT2*	RJY5045	Genomic DNA from RJY5043	RJO5521/RJO5522	RJO5521/RJO2026 RJO5521/RJO5522
RJY5089	*MATa pbp2Δ::HIS3MX6, whi3Δ::LEU2*	RJY5086	Genomic DNA from RJY5047	RJO5563/RJO5564	RJO5563/RJO5565 RJO5563/RJO2711
RJY5091	*MATa pbp2Δ::HIS3MX6, whi3Δ::LEU2, slf1Δ::URA3*	RJY5089	Genomic DNA from RJY5087	RJO5559/RJO5560	RJO5559/RJO5565 RJO5559/RJO4685
RJY5092	*MATa pbp2Δ::HIS3MX6, whi3Δ::LEU2, ngr1Δ::TRP1*	RJY5089	Genomic DNA from RJY5088	RJO5561/RJO5562	RJO5561/RJO5565 RJO5561/RJO5562
RJY5093	*MATa pbp2Δ::HIS3MX6, whi3Δ::LEU2, slf1Δ::URA3, ngr1Δ::TRP1*	RJY5091	Genomic DNA from RJY5088	RJO5561/RJO5562	RJO5561/RJO5565 RJO5561/RJO5562

RJY5278	*MATa pbp2Δ::HIS3MX6, whi3Δ::LEU2, slf1Δ::URA3, ngr1Δ::TRP1, mrn1Δ::KANMX6*	RJY5093	Genomic DNA from RJY5041	RJO5107/RJO4472	RJO5107/RJO2026 RJO5107/RJO5110
RJY	*MATa nab6Δ, mrn1Δ::KANMX6, puf1Δ::hphNT1, puf2Δ::natNT2, pbp2Δ::HIS3MX6, whi3Δ::LEU2, slf1Δ::URA3, ngr1Δ::TRP1*	RJY5046 was used for further successive deletions	Genomic DNA from RJY5093	The same primer sets for all further deletions were used as mentioned before	The same primer sets were used as mentioned before
RJY5299	*MATa whi3Δ::LEU2, mrn1Δ::KANMX6*	RJY5047	Genomic DNA from RJY5041	RJO5107/RJO4472	RJO5107/RJO2026 RJO5107/RJO5110
RJY5300	*MATa pbp2Δ::HIS3MX6, mrn1Δ::KANMX6*	RJY5086	Genomic DNA from RJY5041	RJO5107/RJO4472	RJO5107/RJO2026 RJO5107/RJO5110
RJY5301	*MATa slf1Δ::URA3, mrn1Δ::KANMX6*	RJY5087	Genomic DNA from RJY5041	RJO5107/RJO4472	RJO5107/RJO2026 RJO5107/RJO5110
RJY5302	*MATa ngr1Δ::TRP1, mrn1Δ::KANMX6*	RJY5088	Genomic DNA from RJY5041	RJO5107/RJO4472	RJO5107/RJO2026 RJO5107/RJO5110
RJY5303	*MATa pbp2Δ::HIS3MX6, mrn1Δ::KANMX6, whi3Δ::LEU2*	RJY5300	Genomic DNA from RJY5278	RJO5563/RJO5564	RJO5563/RJO5565 RJO5563/RJO2711
RJY5304	*MATa slf1Δ::URA3, mrn1Δ::KANMX6, whi3Δ::LEU2*	RJY5301	Genomic DNA from RJY5278	RJO5563/RJO5564	RJO5563/RJO5565 RJO5563/RJO2711
RJY5305	*MATa ngr1Δ::TRP1, mrn1Δ::KANMX6, whi3Δ::LEU2*	RJY5302	Genomic DNA from RJY5278	RJO5563/RJO5564	RJO5563/RJO5565 RJO5563/RJO2711
RJY5306	*MATa slf1Δ::URA3, mrn1Δ::KANMX6, pbp2Δ::HIS3MX6*	RJY5301	Genomic DNA from RJY5278	RJO5557/RJO5558	RJO5557/RJO5565 RJO5557/RJO1265
RJY5307	*MATa ngr1Δ::TRP1, mrn1Δ::KANMX6, pbp2Δ::HIS3MX6*	RJY5302	Genomic DNA from RJY5278	RJO5557/RJO5558	RJO5557/RJO5565 RJO5557/RJO1265
RJY5308	*MATa ngr1Δ::TRP1, mrn1Δ::KANMX6, slf1Δ::URA3*	RJY5302	Genomic DNA from RJY5278	RJO5559/RJO5560	RJO5559/RJO5565 RJO5559/RJO4685

RJY5309	*MATa pbp2Δ::HIS3MX6*, *mrn1Δ::KANMX6*, *whi3Δ::LEU2*, *ngr1Δ::TRP1*	RJY5303	Genomic DNA from RJY5278	RJO5561/RJO5562	RJO5561/RJO5565 RJO5561/RJO5562
RJY5310	*MATa slf1Δ::URA3*, *mrn1Δ::KANMX6*, *whi3Δ::LEU2*, *ngr1Δ::TRP1*	RJY5304	Genomic DNA from RJY5278	RJO5561/RJO5562	RJO5561/RJO5565 RJO5561/RJO5562
RJY5311	*MATa slf1Δ::URA3*, *mrn1Δ::KANMX6*, *pbp2Δ::HIS3MX6*, *ngr1Δ::TRP1*	RJY5306	Genomic DNA from RJY5278	RJO5557/RJO5558	RJO5557/RJO5565 RJO5557/RJO1265
RJY5312	*MATa pbp2Δ::HIS3MX6*, *mrn1Δ::KANMX6*, *whi3Δ::LEU2*, *slf1Δ::URA3*	RJY5303	Genomic DNA from RJY5278	RJO5559/RJO5560	RJO5559/RJO5565 RJO5559/RJO4685

All strains are derived from W303 with the genotype *MATa ade2-1 trp1- 1 can1-100 leu2-3,112 his3-11,15 ura3* (Rothstein and Sherman, 1980).

Supporting table S7: List of yeast strains tagged in this study

Name	Essential genotype	Yeast strain used	DNA template used	Primers used for tagging	Primers used for detection
RJY5048	*MATa NGR1-HA6::K.l.TRP1*	RJY358	pRJ277	RJO2299/RJO2300	RJO5561/RJO5562
RJY4290	*MATα MRN1-HA6::K.l.SpHIS5*	RJY359	pRJ1216	RJO4415/RJO4416	RJO4471/RJO4472
RJY5049	*MATa NAB6-HA6::K.l.TRP1*	RJY358	pRJ277	RJO5050/RJO5051	RJO5512/RJO5514
RJY4377	*MATa PUF1-HA6::K.l. SpHIS5*	RJY2049	pRJ1216	RJO4411/RJO4412	RJO4469/RJO4470
RJY4378	*MATa PUF2-HA6::K.l. SpHIS5*	RJY2049	pRJ1216	RJO4413/RJO4414	RJO872/RJO873
RJY2949	*MATa mex67::HIS3MX6* (pUN100-LEU2-mex67-5) *SLF1-HA6::K.l.TRP1*	RJY612	pRJ277	RJO2456/RJO2457	RJO2576/RJO2577
RJY5277	*MATa TOM70-GFP::K.l.hphNT1*	RJY358	pRJ1226	RJO6396/RJO6397	RJO6398/RJO6399
RJY5279	*MATa pbp2Δ::HIS3MX6, whi3Δ::LEU2, slf1Δ::URA3, ngr1Δ::TRP1, mrn1Δ::KANMX6 TOM70-GFP::K.l.hphNT1*	RJY5278	pRJ1226	RJO6396/RJO6397	RJO6398/RJO6399
RJY5281	*MATa MRPL39-GFP::K.l.hphNT1*	RJY358	pRJ1226	RJO6400/RJO6401	RJO6421/RJO6422
RJY5290	*MATa pbp2Δ::HIS3MX6, whi3Δ::LEU2, slf1Δ::URA3, ngr1Δ::TRP1, mrn1Δ::KANMX6 MRPL39-GFP::K.l.hphNT1*	RJY5278	pRJ1226	RJO6400/RJO6401	RJO6421/RJO6422
RJY5286	*MATa MRPL15-GFP::K.l.hphNT1*	RJY358	pRJ1226	RJO6614/RJO6615	RJO6616/RJO6617
RJY5295	*MATa pbp2Δ::HIS3MX6, whi3Δ::LEU2, slf1Δ::URA3, ngr1Δ::TRP1, mrn1Δ::KANMX6 MRPL15-GFP::K.l.hphNT1*	RJY5278	pRJ1226	RJO6614/RJO6615	RJO6616/RJO6617
RJY5287	*MATa MRPL49-GFP::K.l.hphNT1*	RJY358	pRJ1226	RJO6618/RJO6619	RJO6620/RJO6621

RJY5296	*MATa pbp2Δ::HIS3MX6, whi3Δ::LEU2, slf1Δ::URA3, ngr1Δ::TRP1, mrn1Δ::KANMX6 MRPL49-GFP::K.l.hphNT1*	RJY5278	pRJ1226	RJO6618/RJO6619	RJO6620/RJO6621
RJY5405	*MATa IMG2-GFP::K.l.hphNT1*	RJY358	pRJ1226	RJO6672/RJO6673	RJO6733/RJO6673
RJY5406	*MATa pbp2Δ::HIS3MX6, whi3Δ::LEU2, slf1Δ::URA3, ngr1Δ::TRP1, mrn1Δ::KANMX6 IMG2-GFP::K.l.hphNT1*	RJY5278	pRJ1226	RJO6672/RJO6673	RJO6733/RJO6673
RJY5407	*MATa MRPL44-GFP::K.l.hphNT1*	RJY358	pRJ1226	RJO6666/RJO6667	RJO6731/RJO6667
RJY5408	*MATa pbp2Δ::HIS3MX6, whi3Δ::LEU2, slf1Δ::URA3, ngr1Δ::TRP1, mrn1Δ::KANMX6 MRPL44-GFP::K.l.hphNT1*	RJY5278	pRJ1226	RJO6666/RJO6667	RJO6731/RJO6667
RJY5409	*MATa MOT1-24xMS2L* pET296-YcpLac22 CYC1p-MCP-NLS-2xyeGFP pRS415-HDEL-DsRED	RJY358	pRJ2118	RJO6223/RJO6224	RJO6225/RJO6226
RJY5410	*MATa NUP100-24xMS2L* pET296-YcpLac22 CYC1p-MCP-NLS-2xyeGFP pRS415-HDEL-DsRED	RJY358	pRJ2118	RJO6227/RJO6228	RJO6229/RJO6230
RJY5411	*MATα PBP2-HA3::K.l.SpHIS5*	RJY359	pRJ276	RJO4799/RJO4800	RJO1264/RJO4800

RJY2049 is from BY4741 background (*MATa his3*Δ*1 leu2*Δ*0 met15*Δ*0 ura3*Δ*0*) (Baker Brachmann et al., 1998). RJY358 and RJY359 are from W303 background with the genotype *ade2-1 trp1- 1 can1-100 leu2-3,112 his3-11,15 ura3* (Rothstein and Sherman, 1980). RJY358 is *MATa* and RJY359 as *MATα*. RJY612 is from RS453 background (Segref et al., 1997).

Supporting table S8: Additional yeast strains used in this study

Name	Essential genotype	Source
RJY5400	*MATa* p416-ADH1-GFP-MRN1-TGB3(25-52), pRS415-HDEL-DsRED	This study
RJY5401	*MATa* p416-ADH1-GFP-PBP2-TGB3(25-52), pRS415-HDEL-DsRED	This study
RJY5402	*MATa* p416-ADH1-GFP-SLF1-TGB3(25-52), pRS415-HDEL-DsRED	This study
RJY5403	*MATa* p416-ADH1-GFP-WHI3-TGB3(25-52), pRS415-HDEL-DsRED	This study
RJY5404	*MATa* p416-ADH1-GFP-NGR1-TGB3(25-52), pRS415-HDEL-DsRED	This study
RJY5063	*MATa* p416-ADH1-GFP-PUF1-TGB3(25-52), pRS415-HDEL-DsRED	This study

All strains are derived from W303 with the genotype *MATa ade2-1 trp1- 1 can1-100 leu2-3,112 his3-11,15 ura3* (Rothstein and Sherman, 1980).

Supporting table S9: List of plasmids constructed in this study

Reference Name	Short description	DNA template used	Primers used	Restriction enzymes used	Vector backbone used
pRJ2189	pRS416-ADH1-GFP-MRN1-TGB3(25-52)	Genomic DNA from RJY358	RJO4772/RJO4773	SmaI/HindIII	pRJ1846
pRJ2192	pRS416-ADH1-GFP-WHI3-TGB3(25-52)	Genomic DNA from RJY358	RJO4823/RJO4824	SmaI/HindIII	pRJ1846
pRJ2193	pRS416-ADH1-GFP-PUF1-TGB3(25-52)	Genomic DNA from RJY358	RJO4905/RJO4906	BamHI/EcoRI	pRJ1846
pRJ2190	pRS416-ADH1-GFP-PBP2-TGB3(25-52)	Genomic DNA from RJY358	RJO4680/RJO4681	SmaI/EcoRI	pRJ1846
pRJ2191	pRS416-ADH1-GFP-SLF1-TGB3(25-52)	Genomic DNA from RJY358	RJO4684/RJO4685	SmaI/HindIII	pRJ1846
pRJ2194	pRS416-ADH1-GFP-NGR1-TGB3(25-52)	Genomic DNA from RJY358	RJO4981/RJO4982	SmaI/HindIII	pRJ1846
pRJ2196	pET296-YcpLac22 CYC1p-MCP-NLS-2xyeGFP	pRJ2121	N/A	HindIII/SpeI	pRJ138

Note: N/A = Not applicable

Supporting table S10: Additional plasmids used in this study

Reference Name	Short description	Source
pRJ1846	p416-ADH1-GFP-TGB3(25-52)	(Wu et al., 2011)
pRJ1870	pRS415-HDEL-DsRED	(Bevis and Glick, 2002)
pRJ1877	p416-ADH1-GFP-ZWF1-TGB3(25-52)	(Syed et al., 2018)
pRJ2136	p416-ADH1-GFP-RIE1-TGB3(25-52)	(Syed et al., 2018)
pRJ2121	pET296-YcpLac111 CYC1p-MCP-NLS-2xyeGFP	(Tutucci et al., 2017)
pRJ2118	pET259-pUC57 24xMS2V6	(Tutucci et al., 2017)
pRJ1347	pFA6a-KanMx6	(Wach et al., 1994)
pRJ1485	ploxP-HIS5-MS2L	(Haim et al., 2007)
pRJ1212	pFA6-hphNT1	(Janke et al., 2004)
pRJ1213	pFA6-natNT2	(Janke et al., 2004)
pRJ146	pRS303 (HIS3)	(Sikorski and Hieter, 1989)
pRJ297	pRS315 (LEU2)	(Sikorski and Hieter, 1989)
pRJ827	pRS306 (URA3)	(Sikorski and Hieter, 1989)
pRJ147	pRS304 (TRP1)	(Sikorski and Hieter, 1989)
pRJ2133	pcDNA3.1-PRKASE	(Syed et al., 2018)
pRJ1216	PYM15	(Janke et al., 2004)
pRJ277	PYM3	(Knop et al., 1999)
pRJ1226	PYM25	(Janke et al., 2004)
pRJ138	YcpLac22	(Daniel Cietz and Sugino, 1988)

Supporting table S11: Oligonucleotides used in this study

RJO	Name	Sequence	Purpose
4132	PGK1-RT_F	GAACGGTCCACCAGGTGTT	qRTPCR
4133	PGK1-RT_R	GACGGTGTTACCAGCAGCAG	qRTPCR
5267	PMA1_qPCR1_F	AGAGCTGCTGGTCCATTCTG	qRTPCR
5268	PMA1_qPCR1_R	AGTTTTCAGACCACCAACCGA	qRTPCR
6145	MOT1_1	AGGGTCCACGGAGCTTATTT	qRTPCR
6146	MOT1_2	GCGACCCAAAAGTGGAACTA	qRTPCR
6149	NUP100_1	GGGATCTTGTCACCTTTGGA	qRTPCR
6150	NUP100_2	ATTAATGCCTTCGCCCTTTT	qRTPCR
6151	HTA2_1	TGGCTGGTAATGCTGCTAGA	qRTPCR
6152	HTA2_2	GTTTGGCAAAACACCACCTT	qRTPCR
6147	IKI3_1	TGGTGCTTCCAGACGTACAG	qRTPCR
6148	IKI3_2	GCGTCTGGTTTTGTTTGGTT	qRTPCR
6155	HHT2_1	AGCCAGGTACTGTTGCCTTG	qRTPCR
6156	HHT2_2	TTGAGCGATTTCTCTGACCA	qRTPCR
6768	MRPL39-RT-F2	ACAGCGGCAAGTGGATACTC	qRTPCR
6769	MRPL39-RT-R2	TGGCTTTCTTTCTGCCACTT	qRTPCR
6772	MRPL44-RT-F2	CGCAGATTCAATCGGAAATTA	qRTPCR
6773	MRPL44-RT-R2	ACGGTCGAAATGATTGGCTA	qRTPCR
6776	MRP13-RT-F2	GGGAACCATTACAACCGAGA	qRTPCR
6777	MRP13-RT-R2	ATAGCGCGCTTTCTTATGGA	qRTPCR
6674	COX1-q-F	CTACAGATACAGCATTTCCAAGA	qRTPCR
6675	COX1-q-R	GTGCCTGAATAGATGATAATGGT	qRTPCR
6435	COX2_RT_F	AAAGTTGATGCTACTCCTGGTAGA	qRTPCR
6436	COX2_RT_R	CATGACCTGTCCCACACAAC	qRTPCR
6419	21srRNA_F:	AGCGAAATTCCTTGGCCTAT	qRTPCR
6420	21srRNA_R:	TGCATAGGGTCTTTCCGTCT	qRTPCR
4772	MRN1_SmaI_F:	TTTcccgggGTGGTTTCTTATAACAATAATAATAACAA TAAC	Tgbp3 cloning
4773	MRN1_HindIII_R:	TTTaagcttACGTGATTGGTGGGGGACGTTAC	Tgbp3 cloning
4823	WHI3-Clonetech-F	AAAGGATCCCCCGGGCAAAGTTCAGTTTATTTTGACC	Tgbp3 cloning
4824	WHI3-Clonetech-R	CAGATGCTGAAGCTTGTTTTTTATATGACCAACATTAG	Tgbp3 cloning
4905	PUF1_SLIC_FOR	ATGGATGAACTATACAAAGGATCCCCCGGGGATAAAA GTAAGCAGATGAA	Tgbp3 cloning
4906	PUF1_SLIC_REV	GGGCAGATGCTGAAGCTTGATATCgaattcGTTTGCAGAG TGTAAAGTCA	Tgbp3 cloning
4680	PBP2_SmaI_F	TTTcccgggTCCACAGAGACTACAAAACC	Tgbp3 cloning

4681	PBP2_EcoRI_R	TTTgaattcGAGGGGCGACCTTCTTTTAC	Tgbp3 cloning
4684	SLF1_SmaI_F	TTTcccgggTCATCGCAAAACCTCAATGA	Tgbp3 cloning
4685	SLF1_HindIII_R	TTTaagcttATCATTTATTTGTAAGTTTT	Tgbp3 cloning And detection
4981	NGR1_TGB3_F	cactccaccggcggcatggacgagctgtacaagGGATCCCCCGGGATGTC TAACGTTGCTAACG	Tgbp3 cloning
4982	NGR1_TGB3_R	TATTTCACATGGTGGGGGCAGATGCTGAAGCTTGATATC gaattcATGTAGAAGAGAAGGATG	Tgbp3 cloning
4718	GFP_C_F	GATCCCAACGAAAAGAGAGACCACATG	Sequencing
4719	TGB3_N_R	GAGGTGGTGTGGTAGCAGTTGC	Sequencing
5102	MRN1_KO_F:	GTATTTTTTTTTTTCTTCACCATCACATACTACTTCAAT TGCATTAAAACcgtacgctgcaggtcgac	Gene knockout
5103	MRN1_KO_R:	CAGACGGACACTAAACATCTACGTACATACATATACA TATATACATAATGTatcgatgaattcgagctcg	Gene knockout
5107	MRN1-DET_F:	TCCAACTTCAATTCTCAAGGACACTC	Gene knockout And detection
5110	MRN1_CDC_DET_R:	ACCGTTGCTGTTGTGAATCATTTCG	Detection
2026	oMS15_KAN_B_primer_r	CTGCAGCGAGGAGCCGTAAT	Detection
5511	NAB6-del1-LOXP-HIS-R	gttatattaagggttgtcgacctgcagcgATTGGAATCCTCAAAAAAA AC	Gene knockout
5512	NAB6-del1-LOXP-HIS-F	GCCCAAACACTCCCAACCTTTC	Gene knockout And detection
5513	NAB6-del2-LOXP-HIS-F	cgaagttattaggtgatatcaacccggTATAGCTGTGCTGAGCCTG	Gene knockout
5514	NAB6-del2-LOXP-HIS-R	AGAGTCTGTGTAGTGCCTGCTTG	Gene knockout And detection
5509	HIS3-removal-LOXP-R	CCGGGTTGATATCACCTAATAACTTCG	Gene knockout
5510	HIS3-removal-LOXP-F	CGCTGCAGGTCGACAACCCTTAATATAAC	Gene knockout
5515	PUF1-Del1-Hygro-R	gtcgacctgcagcgtacgCTTAAGAAGGAATAAATAGACGTT CACGC	Gene knockout
5516	PUF1-Del2-Hygro-F	cgagctcgaattcatcgatCGTCCCCATGTTTTCTTTTATTTCCG	Gene knockout

5517	PUF1-Del1-Hygro-F	GCTTCCAGTTGTGTGGTGTATCTTCG	Gene knockout And detection
5518	PUF1-Del2-Hygro-R	TTTGGGCTTCCCTGCTAGTTGG	Gene knockout And detection
5523	pFA6a-Gen-Del-F	CGTACGCTGCAGGTCGAC	Gene knockout
5524	pFA6a-Gen-Del-R	ATCGATGAATTCGAGCTCG	Gene knockout
5519	PUF2-Del1-NAT2-R	gtcgacctgcagcgtacgCAGAATTCAGAAAACAGTAGC	Gene knockout
5520	PUF2-Del2-NAT2-F	cgagctcgaattcatcgatCTAATGATTTTAATCATTCTGTTC	Gene knockout
5521	PUF2-Del1-NAT2-F	CCTCCAAGCAAACGGTAAATCGTG	Gene knockout And detection
5522	PUF2-Del2-NAT2-R	GAAACCGCTGAAAGTGACGATGATG	Gene knockout And detection
5549	PBP2-KO-F	CGTCCAGCGCGGCATTAAATAATCTTTCTGTAATA CTCTTTAGCTCAATTagattgtactgagagtgcac	Gene knockout
5550	PBP2-KO-R	TAGTTTCTGTATTTTTATTTTCTATGTGTTTTTATTG ACTAGCAGTATATctgtgcggtatttcacaccg	Gene knockout
5557	PBP2-Det-F	ACACCGTCATCATAGTCGTCACC	Gene knockout And detection
5558	PBP2-Det-R	GGCCAAATCACACAAGTCTCTTCC	Gene knockout And detection
5565	Del-Common-Det-R	GTGCACTCTCAGTACAATCT	Detection
1265	pbp2-ko-select-ass	GTCTTCTCTCCGAAGAGCC	Detection
5555	WHI3-KO-F	GCAGCCTTTATCGATCAATATTTCAGAGGGAAAAA CCTGTATCTCTTAGCAGATTGTACTGAGAGTGCAC	Gene knockout
5556	WHI3-KO-R	CATATAATGTGATACATGCAAGGAAATCAGGTTTT TGCGGAACCATTTTTCTGTGCGGTATTTCACACCG	Gene knockout
5563	WHI3-Det-F	TCGCACTGATTCTATCGCCATCC	Gene knockout

			And detection
5564	WHI3-Det-R	TGTCTAACGGACAACTATCGCAGAAG	Gene knockout And detection
2711	Whi3_ORF_rev1	ACTGGAACGATGACTGGGAG	Detection
5551	SLF1-KO-F	CCAAAAATATAACCAAGATAAAGAAAATCAATCA TAAAGTGAATTCAAAAagattgtactgagagtgcac	Gene knockout
5552	SLF1-KO-R	CATGTTAACTATATACATAATAAAAAAAAAAAAA AAAATATTGTCTAAAActgtgcggtatttcacaccg	Gene knockout
5559	SLF1-Det-F	CTTGTGGTTGATGGTAATTGCGGAC	Gene knockout And detection
5560	SLF1-Det-R	AGAGTTTGAGGCTACCGACCAC	Gene knockout And detection
5553	NGR1-KO-F	AGCTTTTTCATATCCTTCGCCATCGATTTTTGCCTG AAAAATTTACACAAagattgtactgagagtgcac	Gene knockout
5554	NGR1-KO-R	CAGATAAAACTGCGGACAAGATTAAAATTTTCTTT TTTTGTCTTTTGTAActgtgcggtatttcacaccg	Gene knockout
5561	NGR1-Det-F	CGCTTCTTATACTGCAACGATGTTGAC	Gene knockout And detection
5562	NGR1-Det-R	GTCTTCTCTGTAGTCGGGCTGATC	Gene knockout And detection
4472	Mrn1_det_R	CAGATCGCAGTGGCTAATTCTT	Gene knockout And detection
5568	Spike-q1-F	CACACTCATCAGCGACACGA	qRTPCR
5569	Spike-q1-R	CCAAAGCGGTGACTTTCTGC	qRTPCR
2299	ngr1-knop-f	GCATCCTAATAGGAACAATGTTCCGCCAATTCATC CTTCTCTTCTACATcgtacgctgcaggtcgac	Tagging
2300	ngr1-knop-r	GCAGATAAAACTGCGGACAAGATTAAAATTTTCTT TTTTTGTCTTTTGTAATCAatcgatgaattcgagctcg	Tagging
4415	Mrn1_ct_F	AACTTTGGCAAGGATAGATGTGGTAACGTCCCCCA CCAATCACGTcgtacgctgcaggtcgac	Tagging
4416	Mrn1_ct_R	ACTAAACATCTACGTACATACATATACATATATAC	Tagging

		ATAATGTTTAatcgatgaattcgagctcg	
4471	Mrn1_det_F	CTTGCCTGAGAAGAACTGTTG	Detection
5050	NAB6_Knop_F:	CAGCCAATATTTTGGGCGCCTCTGCGGAAGACAAC ACGCATCCTGACGAGcgtacgctgcaggtcgac	Tagging
5051	NAB6_Knop_R:	AATAGTCCGATGGATATGCATTATACTTCAGGCTC AGCACAGCTATACTAatcgatgaattcgagctcg	Tagging
4411	Puf1_ct_F	GACGATAACACCGTTTTTGAAACTCTGACTTTACA CTCTGCAAACcgtacgctgcaggtcgac	Tagging
4412	Puf1_ct_R	GGTCTCCCAATGATGACGGAAATAAAAGAAAACA TGGGGACGTCAatcgatgaattccagctcg	Tagging
4469	Puf1_det_F	TTATCGTTGCCACAACTGAGC	Detection
4470	Puf1_det_R	CATAGGCGGGTAACCTCAGT	Detection
4413	Puf2_ct_F	AATAATAATGATACAAGTTTGTACCGCTACAGGTC ATACGGATATcgtacgctgcaggtcgac	Tagging
4414	Puf2_ct_R	AAAAAAAAAAGTTTAATAGAACAGAATGATTAAA ATCATTAGCTAatcgatgaattcgagctcg	Tagging
872	puf2-select-ss	CCTCTAAGCCGCTCAGTG	Detection
873	puf2-select-ass	GAGCCTAAAGCCTGTTG	Detection
2456	Slf1-Knop-S3	GACCAAGGTGAAATTAGCAGGCAGTTTGAACAAA ACTTACAAATAAATGATCGTACGCTGCAGGTCGAC	Tagging
2457	Slf1-Knop-S2	GTTAACTATATACATAATAAAAAAAAAAAAAAAA ATATTGTCTAAAATTAATCGATGAATTCGAGCTCG	Tagging
2576	Sro99_select_1	GGGCTATCCAAACTTCTT	Detection
2577	Sro99_select_2	GTCCAATTGGCACTGAGG	Detection
4799	pbp2-knoptag-f	GAAATTGATAGATCAAATGCTGAACGTAAAAGAA GGTCGcgtacgctgcaggtcgac	Tagging
4800	pbp2-knoptag-r	GTAGTTTCTGTATTTTTATTTTCTATGTGTTTTTATT GACTAGatcgatgaattcgagctcg	Tagging and detection
1264	pbp2-ko-select-ss	CCCCGATATGGTACTTACACG	Detection
2660	Whi3_Knop_1	GTAAATATGCTTTCCAGTTACAATTCTAATGTTGGT CATATAAAAAACcgtacgctgcaggtcgac	Tagging
2661	Whi3_Knop_2	TATAATGTGATACATGCAAGGAAATCAGGTTTTTG CGGAACCATTTTTatcgatgaattcgagctcg	Tagging and detection
868	whi3-select-ss	GAGCAGTAAGGGAGGTATC	Detection
6396	TOM70-Knop-F:	CTAAAAAGATTCAAGAAACTTTAGCTAAATTACGC GAACAGGGTTTAATGcgtacgctgcaggtcgac	Tagging
6397	TOM70-Knop-R:	CTTAGTTTTTGTCTTCTCCTAAAAGTTTTTAAGTTTA TGTTTACTGTTTAatcgatgaattcgagctcg	Tagging
6398	TOM70-det-F:	ACTAGACCCAAGAAGTGAGCAAGC	Detection
6399	TOM70-det-R:	GTCTCCTCGTTGCCGTTTGTTATG	Detection
6400	MRPL39-Knop-F:	AAAGGAAAGTGGCAGAAAGAAAGCCATTGGATTTC TTGCGTACAGCCAAGcgtacgctgcaggtcgac	Tagging

6401	MRPL39-Knop-R:	GTATTCGATGGGCTTACATGCCGGGGCTCGTGCTTA TTCATATTTCTTCAatcgatgaattcgagctcg	Tagging
6421	MRPL39-det-F:	TTGTCTACAGCGGCAAGTGG	Detection
6422	MRPL39-det-R:	TGCGTAACGTCTGCGTATTCG	Detection
6614	MRPL15-GFP-F	TAGCATCTGCAAAGGCAAAAATATCCGACAAGGAA AATAAAGCATTTCTGcgtacgctgcaggtcgac	Tagging
6615	MRPL15-GFP-R	TTTATACATTTTTGGCCAGTGAACCATCAACTATATT TTTTGTATCTTCAatcgatgaattcgagctcg	Tagging
6616	MRPL15-det-F	CGGGCAACTTTCTTTGCAGTTCAG	Detection
6617	MRPL15-det-R	TGGCGAACAGGCAGACTC	Detection
6618	MRPL49-GFP-F	AGAGTAAAGGTGATTTGACAATCTTAAGAATATCAG AACTGAGTATGAACcgtacgctgcaggtcgac	Tagging
6619	MRPL49-GFP-R	ATTTACATGATTTTATACGTATGCGTATATGTACATA TCCCTAAAATTCAatcgatgaattcgagctcg	Tagging
6620	MRPL49-det-F	CGTCCATATTTGGTGACCGAGG	Detection
6621	MRPL49-det-R	GGGCATTTGGAGGTGGAGTTG	Detection
6672	IMG2-Knop-F	TGCAGTAGAGGCTGTCAAAAGGGTATTAACCAAGAA ATTTcgtacgctgcaggtcgac	Tagging
6673	IMG2-Knop-R	ATATATACATGACAATTATTTTTTTATACATTAGCGA TACCTAatcgatgaattcgagctcg	Tagging and detection
6733	IMG2-Det-F	AGAAGCAGGACCGGAAATCTACC	Detection
6666	MRPL44-Knop-F	CTCGAAACAGCTGGATCTCAAACATATGTTGGAAAT GCATcgtacgctgcaggtcgac	Tagging
6667	MRPL44-Knop-R	GTGCATGCCTACAATGAGATTTGTAGATGCCTTTATT TTCTCAatcgatgaattcgagctcg	Tagging and detection
6731	MRPL44-Det-F	TGCCATTCCACCAACGCAAC	Detection
6223	MOT1-NewMS2-F:	AATACGAGGAGGAGTATAATTTAGACACCTTCATCA AAACTTTACGATAAccgctctagaactagtggat	Tagging
6224	MOT1-NewMS2-R:	ATAAAACAAAAATGACCTTGTATACGCGTCATTCCA ATGCAAGAATTTGTgatatcacctaataacttcgtatag	Tagging
6225	MOT1-Det-F:	ATGATCTACAGGCAATGGACAGAGC	Detection
6226	MOT1-Det-R:	TTGCTAACGAGCGATGCGAG	Detection
6227	NUP100-NewMS2-F:	CCGTAACAGGCACCTATAGTTACACCATAGATCACC CAGTTTTAACTTAAccgctctagaactagtggat	Tagging
6228	NUP100-NewMS2-R:	ATCTAGACTACTTAGACGATACAAGGATTCTCTACA AAAATTATTCCGGTgatatcacctaataacttcgtatag	Tagging
6229	NUP100-det-F:	GGATCTTGTCACCTTTGGACCAA	Detection
6230	NUP100-det-R:	ATCTGGCGATGCCACCAACCTTC	Detection
6437	COX2_det_F	ATTCAGCAACACCAAATCAAGAAGG	Detection
6438	COX2_det_R	GCATGACCTGTCCCACACAAC	Detection

Supporting table S12: Antibodies used in this study

Name	Host species	Type	Serum (Yes/No)	Concentration	Company
HA.11 16B12	Mouse	Primary	No	1:2000	Covance
Sec61	Rabbit	Primary	Yes	1:7500	N/A
Pgk1 (459250)	Mouse	Primary	No	1:2000	Invitrogen
H3 (ab1791)	Rabbit	Primary	No	1:2000	Abcam
Tom70	Rabbit	Primary	Yes	1:2000	N/A
Cox4	Rabbit	Primary	Yes	1:2000	N/A
Cox2	Rabbit	Primary	Yes	1:1000	N/A
GFP	Rabbit	Primary	No	1:2000	Invitrogen
IRDye 680	Goat (Anti-Mouse)	Secondary	No	1:10000	LI-COR
IRDye 800CW	Goat (Anti-Mouse)	Secondary	No	1:10000	LI-COR
IRDye 680	Goat (Anti-Rabbit)	Secondary	No	1:10000	LI-COR
IRDye 800CW	Goat (Anti-Rabbit)	Secondary	No	1:10000	LI-COR
HRP	Donkey (Anti-Rabbit)	Secondary	No	1:10000	Amersham ECL

Note: N/A = Not applicable

Supporting References

Baker Brachmann, C., Davies, A., Cost, G.J., Caputo, E., Li, J., Hieter, P., and Boeke, J.D. (1998). Designer deletion strains derived fromSaccharomyces cerevisiae S288C: A useful set of strains and plasmids for PCR-mediated gene disruption and other applications. Yeast *14*, 115–132.

Bevis, B.J., and Glick, B.S. (2002). Rapidly maturing variants of the Discosoma red fluorescent protein (DsRed). Nat. Biotechnol. *20*, 83–87.

Daniel Cietz, R., and Sugino, A. (1988). New yeast-EscicerLSa coli shuttle vectors constructed with iu vitro mutagenized yeast genes lacking six-base pair restriction sites (Recombinant DNA; Saccharomyces cerevkiue; mitotic stability; cloning sites; unique cuts; new alleles).

Haim, L., Zipor, G., Aronov, S., and Gerst, J.E. (2007). A genomic integration method to visualize localization of endogenous mRNAs in living yeast. Nat. Methods *4*.

Janke, C., Magiera, M.M., Rathfelder, N., Taxis, C., Reber, S., Maekawa, H., Moreno-Borchart, A., Doenges, G., Schwob, E., Schiebel, E., et al. (2004). A versatile toolbox for PCR-based tagging of yeast genes: new fluorescent proteins, more markers and promoter substitution cassettes. Yeast *21*, 947–962.

Knop, M., Siegers, K., Pereira, G., Zachariae, W., Winsor, B., Nasmyth, K., and Schiebel, E. (1999). Epitope tagging of yeast genes using a PCR-based strategy: more tags and improved practical routines. Yeast *15*, 963–972.

Rothstein, R.J., and Sherman, F. (1980). Genes affecting the expression of cytochrome c in yeast: genetic mapping and genetic interactions. Genetics *94*, 871–889.

Segref, A., Sharma, K., Doye, V., Hellwig, A., Huber, J., Lührmann, R., and Hurt, E. (1997). Mex67p, a novel factor for nuclear mRNA export, binds to both poly(A)+ RNA and nuclear pores. EMBO J. *16*, 3256–3271.

Sikorski, R.S., and Hieter, P. (1989). A System of Shuttle Vectors and Yeast Host Strains Designed for Efficient Manipulation of DNA in Saccharomyces ceratisiae.

Syed, M.I., Moorthy, B.T., Jenner, A., Fetka, I., and Jansen, R.-P. (2018). Signal sequence-independent targeting of MID2 mRNA to the endoplasmic reticulum by the yeast RNA-binding protein Khd1p. FEBS Lett. *592*.

Tutucci, E., Vera, M., Biswas, J., Garcia, J., Parker, R., and Singer, R.H. (2017). An improved MS2 system for accurate reporting of the mRNA life cycle. Nat. Methods *15*, 81–89.

Wach, A., Brachat, A., Pöhlmann, R., and Philippsen, P. (1994). New heterologous modules for classical or PCR-based gene disruptions inSaccharomyces cerevisiae. Yeast *10*, 1793–1808.

Wu, C.-H., Lee, S.-C., and Wang, C.-W. (2011). Viral protein targeting to the cortical endoplasmic reticulum is required for cell–cell spreading in plants. J. Cell Biol. *193*, 521–535.

FEBS Letters

FEBS PRESS science publishing by scientists

Signal sequence-independent targeting of *MID2* mRNA to the endoplasmic reticulum by the yeast RNA-binding protein Khd1p

Muhammad Ibrahim Syed[#], Balaji T. Moorthy[#,†], Andreas Jenner, Ingrid Fetka and Ralf-Peter Jansen

Interfaculty Institute of Biochemistry (IFIB), Eberhard Karls Universität Tübingen, Germany

Correspondence
R.-P. Jansen, Interfaculty Institute of Biochemistry, Universität Tübingen, Tübingen 72076, Germany
Fax: +49 7071 295605
Tel: +49 7071 29724543
E-mail ralf.jansen@uni-tuebingen.de

[†]**Present address**
Department of Molecular and Cellular Pharmacology, Miller School of Medicine, University of Miami, FL, USA

[#]These authors contributed equally.

(Received 15 February 2018, revised 26 April 2018, accepted 4 May 2018, available online 28 May 2018)

doi:10.1002/1873-3468.13098

Edited by Lukas Alfons Huber

Localization of mRNAs depends on specific RNA-binding proteins (RBPs) and critically contributes not only to cell polarization but also to basal cell function. The yeast RBP Khd1p binds to several hundred mRNAs, the majority of which encodes secreted or membrane proteins. We demonstrate that a subfraction of Khd1p associates with artificial liposomes and endoplasmic reticulum (ER), and that Khd1p endomembrane association is partially dependent on its binding to RNA. ER targeting of at least two mRNAs, *MID2* and *SLG1/WSC1*, requires *KHD1* but is independent of their translation. Together, our results suggest interdependence of Khd1p and mRNA for their targeting to the ER and presents additional evidence for signal sequence-independent, RBP-mediated mRNA targeting.

Keywords: endoplasmic reticulum; Khd1p; mRNA localization; *Saccharomyces cerevisiae*; SRP-independent targeting

Localization of messenger RNA is essential for establishing cell polarity and spatial control of gene expression [1,2]. In *Saccharomyces cerevisiae*, more than 30 mRNAs are known to be selectively transported to the bud [3–5]. Localization of these transcripts or their localized translation depends on multiple *trans*-acting factors including the myosin motor protein Myo4p, and the RNA-binding proteins (RBPs) She2p, She3p, Khd1p, Loc1p, and Puf6p [6–9]. Khd1p contains three RNA-binding domains of the heterologous nuclear ribonucleoprotein K (hnRNP K)-like homology (KH) type [7,10,11]. During *ASH1* mRNA localization to the yeast bud, Khd1p colocalizes with *ASH1* to the bud tip [7] and acts as a translation repressor [12]. It binds to the *ASH1* transcript and to the C-terminal domain of the translation initiation factor eIF4G1. Binding to the latter presumably disrupts the interaction of eIF4G1 with the cap-binding protein eIF4E, which leads to inhibition of translation initiation [12].

Previous studies revealed that Khd1p binds to several hundred mRNAs besides *ASH1* [10,13]. Its function on these mRNAs is largely unknown and might differ from translational regulation. While Khd1p negatively regulates Ash1 protein expression, its binding to *MTL1* mRNA positively influences expression of the membrane sensor Mtl1p by stabilizing the transcript [10,14]. A large

Abbreviations
ER, endoplasmic reticulum; GST, glutathion-*S*-transferase; KH, K (hnRNP K)-like homology (KH); mSMPs, mRNAs encoding secreted or membrane proteins; qRT-PCR, quantitative RT-PCR; RBP, RNA-binding proteins; SC, synthetic complete; SRP, signal recognition particle; TMD, transmembrane domain; WCE, whole-cell extract.

fraction of Khd1p-interacting mRNAs encode proteins of the plasma membrane, endoplasmic reticulum (ER), and cell wall [13]. Translation of these mRNAs generally occurs at the ER and requires cotranslational recognition of a signal peptide in the encoded protein by the signal recognition particle (SRP). SRP blocks translation and transfers the nascent peptide-ribosome-mRNA complex to the translocon in the ER membrane, where translation resumes [15,16]. Recently, alternative pathways for directing transcripts to the ER have been described that involve the targeting of transcripts to the ER by RBPs before translation [17–19]. Examples of such ER-targeting RBPs have been identified in mammals [20] and yeast [21,22]. Among these RBPs are integral membrane proteins like the mammalian p180, or RBPs that apparently only transiently interact with endomembranes like the yeast She2p.

Here, we report that the RBP Khd1p is involved in the targeting of mRNAs to the yeast ER and demonstrate that Khd1p cofractionates with cellular membranes and protein-free liposomes. Our findings suggest a hitherto unknown role of Khd1p in mediating translation-independent targeting of *MID2* and *SLG1*/*WSC1* mRNAs to the ER, thereby expanding the group of RBPs that facilitate SRP-independent targeting to this organelle.

Materials and methods

All yeast strains and plasmids as well from this study, as well as their construction strategies are listed in the Supporting Information.

Quick subcellular fractionation

Cells from RJY5252 and RJY5253 corresponding to 100 OD_{600} units were harvested, washed twice with ice-cold water and one time with potassium phosphate buffer (100 mM potassium phosphate pH 7.5, 1.2 M sucrose). Glass bead lysis (four pulses of 90 s with 1-min breaks on ice) was done in 500 μL low-salt lysis buffer 1 [20 mM HEPES/KOH pH 7.5, 140 mM potassium acetate, 1 mM magnesium acetate, 1 mM DTT, 250 mM sucrose, 1× EDTA-free Protease Inhibitor Cocktail (Roche, Basel, Switzerland)]. Cell debris was removed by spinning twice at 800 ***g*** for 5 min. The resulting whole-cell extract (WCE) was diluted to 0.1 $\mu g \cdot \mu L^{-1}$ and 200 μL fractionated at 6000 ***g*** (P6) for 5 min, 18 000 ***g*** (P18) for 30 min and supernatant (S18). Pellets P6 and P18 were resuspended in 200 μL low-salt lysis buffer 1 and 15 μL were used for SDS/PAGE followed by western blotting.

Fractionation for RNA analysis was conducted as described in Frey *et al.* [23] with modifications. Yeast cells were grown to mid-log phase and approximately 100 OD_{600} units were lysed in 1 mL low-salt lysis buffer 2 (20 mM HEPES pH 7.6, 100 mM potassium acetate, 5 mM magnesium acetate, 1 mM EDTA, 2 mM DTT) with 0.5 mM PMSF and 1 $U \cdot \mu L^{-1}$ RNasin as inhibitors. RNasin was left out in the case of RNase treatment experiments. Cell debris was pelleted at 1200 ***g*** for 2 min and the supernatant (WCE) fractionated by consecutive centrifugation steps at 6000 (pellet P6), 18 000 (pellet P18), and 200 000 ***g*** (pellet P200) for 20 min each step at 4 °C. After each centrifugation step, pellets were rinsed twice with ice-cold low-salt lysis buffer 2 and resuspended in 100–150 μL low-salt lysis buffer 2. To follow RNA distribution, pellets P6 and P18 (representing the membrane fractions) were pooled and resuspended in 1.5 mL of ice-cold low-salt lysis buffer 2. Pellet P200 and the supernatant S200 were pooled (cytosolic fraction). About 50 μL from the WCE, membrane, and cytosolic fractions were used for RNA extraction. For RNase treatment, 120 μL WCE was supplemented with 1 mM $CaCl_2$ and 5 μL micrococcal nuclease (2 000 000 gel units$\cdot mL^{-1}$), incubated at room temperature for 20 min, and quenched with 2 mM EDTA. Samples were then centrifuged at 18 000 ***g*** for 30 min to separate the membrane fraction (pellet) from cytosolic fraction (supernatant).

Immunoprecipitation

Approximately 500 OD_{600} units of yeast were lysed with glass beads in 1 mL breakage buffer (10 mM Tris-HCl pH 7.5, 150 mM NaCl, 2 mM EDTA pH 8, 0.1% Triton X-100, 1× protease inhibitor cocktail (Roche), and Ribolock RNase inhibitor 0.5 $U \cdot \mu L^{-1}$). Cell debris was removed at 3000 ***g*** for 5 min. Protein concentration was determined and lysates corresponding to 118 μg were used for immunoprecipitation with GFP-Trap®_M (Chromotek, Planegg-Martinsried, Germany). Lysates were precleared with 20 μL magnetic agarose beads (Chromotek). Anti-GFP magnetic beads were blocked with *Escherichia coli* tRNA and heparin in blocking buffer (10 mM Tris-HCl pH 7.5, 150 mM NaCl, 2 mM EDTA pH 8, 0.1% Triton X-100, 0.1 $mg \cdot mL^{-1}$ *E. coli* tRNA, 0.4 $mg \cdot mL^{-1}$ heparin) for 2 h at 4 °C. GFP fusion proteins were immunoprecipitated overnight at 4 °C with 25 μL GFP-Trap®_M. Beads were then washed five times with wash buffer (10 mM Tris-HCl pH 7.5, 150 mM NaCl, 2 mM EDTA pH.8, 0.1% Triton X-100) and then resuspended in 75 μL ultrapure water. A quantity of 50 μL was used for SDS/PAGE followed by western blotting. RNA was extracted from the remaining bead suspension, resuspended in 20 μL RNase-free water, and used for RT-PCR.

RT-PCR and qRT-PCR

A quantity of 50 μL of RNA samples was subjected to RQ1 DNase (Promega, Mannheim, Germany) treatment and reverse transcription using a High-Capacity cDNA Reverse Transcription Kit (Applied Biosystems). To each sample, 10 ng spike RNA (*in vitro* transcribed *Arabidopsis*

phosphoribulokinase RNA) was added before DNAse treatment. Quantitative RT-PCR (qRT-PCR) was performed in 10 μL reaction mixtures containing 2.5 μL of 1 : 20 or 1 : 100 dilutions of the individual cDNA samples. Gene specific primers were designed using PRIMER3 software (http://primer3.ut.ee/) and tested for mispriming or formation of primer dimers by melting curve analysis of the individual amplification products. All reactions were run in duplicates or triplicates. Quantifications were performed by the comparative Ct method [24]. For RNA analysis via quick subcellular fractionation, relative mRNA levels were derived by normalization using input values. In case of immunoprecipitation, normalization was against the spike RNA. For RT-PCR, 1 μL of cDNA was set to PCR with Taq DNA polymerase (Genaxxon Bioscience, Ulm, Germany) using oligos against *OST3* and *PMA1*.

Flotation assay with protein-free liposomes

Flotation experiments with artificial liposomes were performed as described [22]. Liposomes were generated from a soybean phospholipid extract (Sigma, Taufkirchen, Germany) that contains as main phospholipids 55% phosphatidylcholine and 25% phosphatidylethanolamine. Lipids were completely dissolved to a final total lipid concentration of 10 $mg \cdot mL^{-1}$ in degassed liposome buffer [20 mM Hepes (pH 7.4) and 100 mM NaCl], and the emulsion was passed 21 times through an 80 or 200 nm polycarbonate filter membrane mounted in a mini extruder (Avanti Polar Lipids, Alabaster, AL, USA) to create unilamellar liposomes. Liposomes were used immediately for flotation assays or stored at 4 °C for a maximum of 1 week. A quantity of 50 μL of liposomes was mixed with 50 pmol Khd1p, Khd1p$^{(GDDGmt)}$, or glutathion-*S*-transferase (GST), in 190 μL of binding buffer (50 mM Hepes/KOH, 150 mM potassium acetate, 1 mM magnesium acetate, 1 mM EDTA, and 1 mM DTT) and incubated for 15 min on ice. A quantity of 40 μL of the sample was kept as an input control. A quantity of 200 μL was mixed with 3 mL of binding buffer containing 70% sucrose and added to the bottom of a SW40 polycarbonate tube. The sample was then covered with three cushions of 3 mL of binding buffer containing 50%, 40%, and 0% sucrose. After centrifugation to equilibrium (70 000 ***g*** for 4 h at 4 °C), the liposome-containing interface between the 40% and 0% sucrose cushions was harvested, precipitated by TCA, and dissolved in 45 μL of SDS sample buffer.

In vivo imaging and single-molecule fluorescence *in situ* hybridization (smFISH)

For the imaging of fusion proteins, a single yeast colony from a plate grown at 30 °C was resuspended in 1 mL of synthetic complete (SC) medium with 2% glucose. Cells were collected by a short spin and resuspended in 100 μL of SC medium. Cells were spread on thin agarose pads containing SC medium plus 2% glucose and observed using a ZEISS Cell Observer Z1 fluorescence microscope or ZEISS AxioExaminer equipped with a CSU unit (Visitron Systems, Puchheim, Germany). Imaging of *MS2L*-tagged *MID2* and *SLG1* mRNAs was done as previously described [25]. Image processing was performed with AXIOVISION software version 4.8 (Zeiss, Oberkochen, Germany) or FIJI. Single-molecule fluorescence *in situ* hybridization (smFISH) for *MID2* and *ACT1* RNA was performed as described [26] using CAL Fluor Red 610-labeled 20mer antisense DNA oligonucleotides (Biosearch Technologies, Petaluna, CA, USA).

Results

Association of Khd1p with endomembranes

We have previously shown that a subfraction of the yeast RBP She2p cofractionates with the ER and that it can bind to protein-free artificial liposomes, indicating an association of She2p with endomembranes [22,27]. Since Khd1p binds mRNAs encoding secreted or membrane proteins (mSMPs) [10,13,17] that are translated at the cytoplasmic face of the ER, we hypothesized that this RBP has similar features. We first assessed Khd1p subcellular fractionation using sucrose gradients. Myc-tagged Khd1p was found in fractions at the top of the gradient (Fig. 1A; fractions 9–11) where it cofractionated with the cytosolic marker Pgk1p. An additional subpopulation of Khd1p cofractionated with an ER membrane marker protein Sec61p (fractions 1–4) and with She2p, indicating that a fraction of Khd1p might be endomembrane-associated.

Protein-liposome cofloatation experiments, in which recombinant proteins were mixed with artificial liposomes and subjected to ultracentrifugation in sucrose density gradients, have previously shown that She2p can also bind to protein-free liposomes [22]. When performing similar floatation assays with GST-tagged Khd1p, we observed cofloatation of liposomes with Khd1p (67% of input) but not with GST (Fig. 1B). This is similar to that previously observed for She2p (coflotation of > 70% of input) [22]. In addition, whereas She2p-binding increases with liposomes curvature and decreases with liposome size [22], no preference was seen for Khd1p, indicating that it interacts with membranes in a different manner (Fig. 1B).

Imaging revealed that, as previously reported [28], the major fraction of GFP-tagged Khd1p is cytosolic under steady-state conditions (Fig. 2A). Our observation that it also cosegregates with the ER and that the protein binds to liposomes is not necessarily contradictory to this finding, since it is possible that only a subpopulation of Khd1p is membrane-associated under

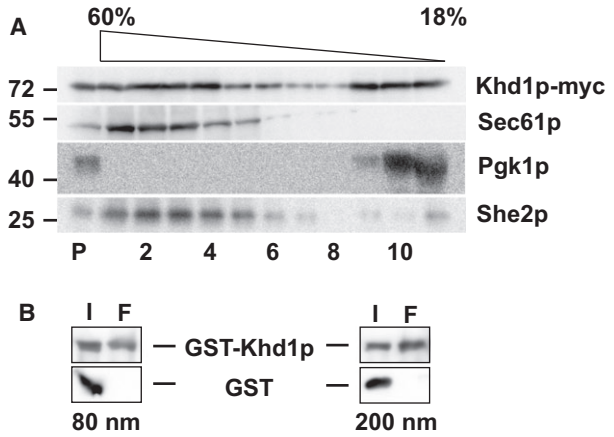

Fig. 1. Khd1p comigrates with yeast microsomes *in vivo* and *in vitro*. (A) WCE from (*KHD1-9xmyc*) was separated on a linear sucrose gradient and fractions were collected and treated as described in Methods. Aliquots of 12 fractions (P as pellet fraction, 11 as top fraction) were analyzed by western blotting against myc epitope, Sec61p, Pgk1p, and She2p. A large fraction of Khd1p-myc comigrates with the ER marker protein Sec61p and RBP She2p (fractions 1–4). (B) Recombinant Khd1p (GST-Khd1p) was incubated with artificial liposomes of 80 nm or 200 nm diameter and centrifuged at 70 000 ***g*** for 4 h. Input (I) and float (F) fractions were analyzed by western blotting against GST. Khd1p was detected in the float fraction with both 80 nm and 200 nm liposomes.

these conditions. In order to confirm our observation that a subpopulation of Khd1p might be membrane-associated, we used an assay that allows the detection of temporary or weak association of proteins with the ER [22,29]. This assay is based on the observation that expression of a C-terminal peptide from the small protein TGBp3 of *Bamboo mosaic potexovirus* in yeast results in targeting of the peptide to and stable integration of it into the ER if it is fused to an integral or peripheral membrane protein [29]. We have previously used this assay to demonstrate membrane-binding potential of She2p *in vivo* [22]. A fusion protein of TGBp3, GFP, and Sec61p colocalizes with ER marked by Rtn1-mCherry (Fig. S1). In contrast to the Sec61p fusion proteins, TGBp3-GFP-Khd1p forms spots that colocalize with the ER (Fig. 2B, arrows). Colocalization with ER structures, in the form of foci, have also been reported for other TGBp3 fusions [29]. In order to test if the colocalization of TGBp3-GFP-Khd1p with the ER is specific, we used two cytosolic control proteins, glucose-6-phosphate dehydrogenase (Zwf1p) [30] and Ygr250c/Rie1p, an RBP that localizes to stress granules upon stress [31]. In contrast to Khd1p, neither of these fusion proteins colocalized with the ER (Fig. 2C,D).

Membrane association of Khd1p depends on RNA binding

Endoplasmic reticulum association of Khd1p could be indirect and mediated by binding to mRNAs actively translated on ER-bound ribosomes. To test this, we treated cell lysates with RNase before fractionation into membrane and cytosolic fractions. Successful treatment was controlled by detection of two mRNAs encoding abundant membrane proteins (*OST3* and *PMA1*, Fig. S2). RNase but not mock treatment resulted in a clear reduction of a GFP-Khd1p in the membrane fraction (Fig. 3A,B), whereas the distribution of two control proteins (cytosolic Pgk1p and the ER marker Sec61p) remained unaffected. Since RNase treatment might also affect ER-associated ribosomes we next generated Khd1p mutants with defective RNA-binding domains.

KH domains are characterized by their^{GxxG} motif [11] and replacement of the two middle residues of the motif to aspartic acids (D) has been demonstrated to render the domain nonfunctional [32]. We generated a Khd1p mutant where the two amino acid residues flanked by the glycines were exchanged against aspartic acid. This was done for KH domains one and two and the mutant named Khd1p$^{(GDDGmt)}$. A fusion protein of GFP with wild-type Khd1p coimmunoprecipitated three mRNAs that were described as Khd1p targets (*MID2*, *SCW11*, *SLG1*, [10,13]), although with different efficiencies (Fig. 3C). Coprecipitation of these mRNAs with GFP- Khd1p$^{(GDDGmt)}$ was severely reduced. Both fusion proteins could be immunoprecipitated at comparable levels (Fig. S3).

After verifying that GFP-Khd1p$^{(GDDGmt)}$ is an RNA-binding mutant, we performed cell fractionation and separated cytosol (S18) from heavy (P6) and lighter (P18) membrane fractions (Fig. 3D). Quantification of Khd1p distribution in these fractions show that GFP-Khd1p$^{(GDDGmt)}$ is increased in the cytosolic fraction although its distribution does not mimic a cytosolic control protein, Pgk1p (Fig. 3E). This suggests that RNA binding is involved in but not essential for Khd1p association with membranes *in vivo*. This is corroborated by liposome flotation using GST-tagged Khd1p$^{(GDDGmt)}$, which shows that even in the absence of RNA binding, the mutant protein cofloats with liposomes at a slightly lower efficiency (50.9% of input) than the wild-type protein (67%; Figs 3F and 1B).

Association of *MID2* and *SLG1*/*WSC1* mRNAs with membranes depends on Khd1p

In parallel to the previous studies which showed an mRNA dependence for Khd1p to associate with the ER, we investigated if Khd1p-target mRNAs require

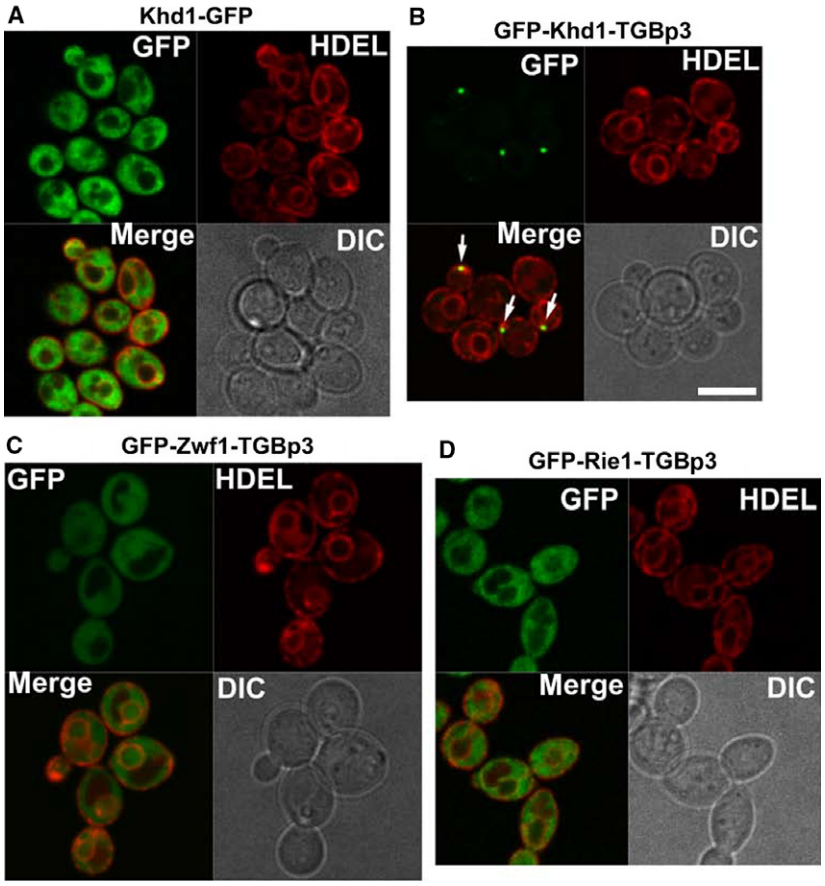

Fig. 2. Khd1p can recruit the viral peptide TGBp3 to the ER. Representative images of cells coexpressing GFP-TGBp3 fusion proteins and HDEL-DsRed (a luminal-ER marker) are shown. Wild-type Khd1-GFP (A) show a diffuse cytoplasmic staining, whereas the fusion protein Khd1p-GFP-TGBp3 (B) forms spots that colocalize with the ER (white arrows). GFP-TGBp3 fusions of two control proteins, Zwf1p (C) and Rie1p (D) do not colocalize with the ER. Scale bar: 5 μm.

the RBP for their binding to the ER. Such a requirement is corroborated by findings that roughly 50% of all transcripts bound by Khd1p encode cell wall or plasma membrane proteins [10,13], which are usually translated at the cytoplasmic face of the ER. We therefore investigated if six select Khd1p bound mRNAs (*DSE2, EGT2, KRE1, SCW11*, *MID2,* and *SLG1*/*WSC1*) copurify with ER-containing membrane fractions [23] and if this is affected by loss of Khd1p. As controls, we included two cytoplasmic mRNAs (*GPH1* and *ZWF1*) reported to be bound by Khd1p [10] as well as a third unrelated mRNA *ACT1*. Using differential centrifugation, membrane fractions were separated from the cytoplasmic fraction (see Methods), from which RNA was extracted and analyzed by qRT-PCR. *ACT1, GPH1,* and *ZWF1* were enriched in the cytoplasmic fraction, independent of the presence of Khd1p (Fig. 4A). In contrast, the other six mRNAs cofractionated with membranes. Membrane/cytoplasmic (m/c) ratios ranged from 3.5 for *SLG1*/*WSC1* to 26.9 for *EGT2* (Fig. 4A). Upon deletion of *KHD1*, two mRNAs, *MID2* and *SLG1*/*WSC1,* shifted from the membrane to the cytoplasmic fraction (m/c ratios changed from 8.7 to 0.1, or 3.5 to 0.2, respectively), whereas the m/c ratios of the other four tested mRNAs did not decrease (Fig. 4A). This suggests that membrane association of only a subset of the mRNAs interacting with Khd1p depends on the presence of the protein.

In order to test if membrane association of the mRNAs is related to translation and/or its signal sequence, we generated a *MID2* mRNA lacking its start codon (*MID2(-AUG)*). Since the next in-frame AUG is 180 nucleotides downstream, translation of the mutant *MID2(-AUG)* mRNA would result in a shortened Mid2p without its signal sequence (Fig. 4B). Both *MID2* and *MID2(-AUG)* were expressed from a plasmid in cells lacking the endogenous copy of

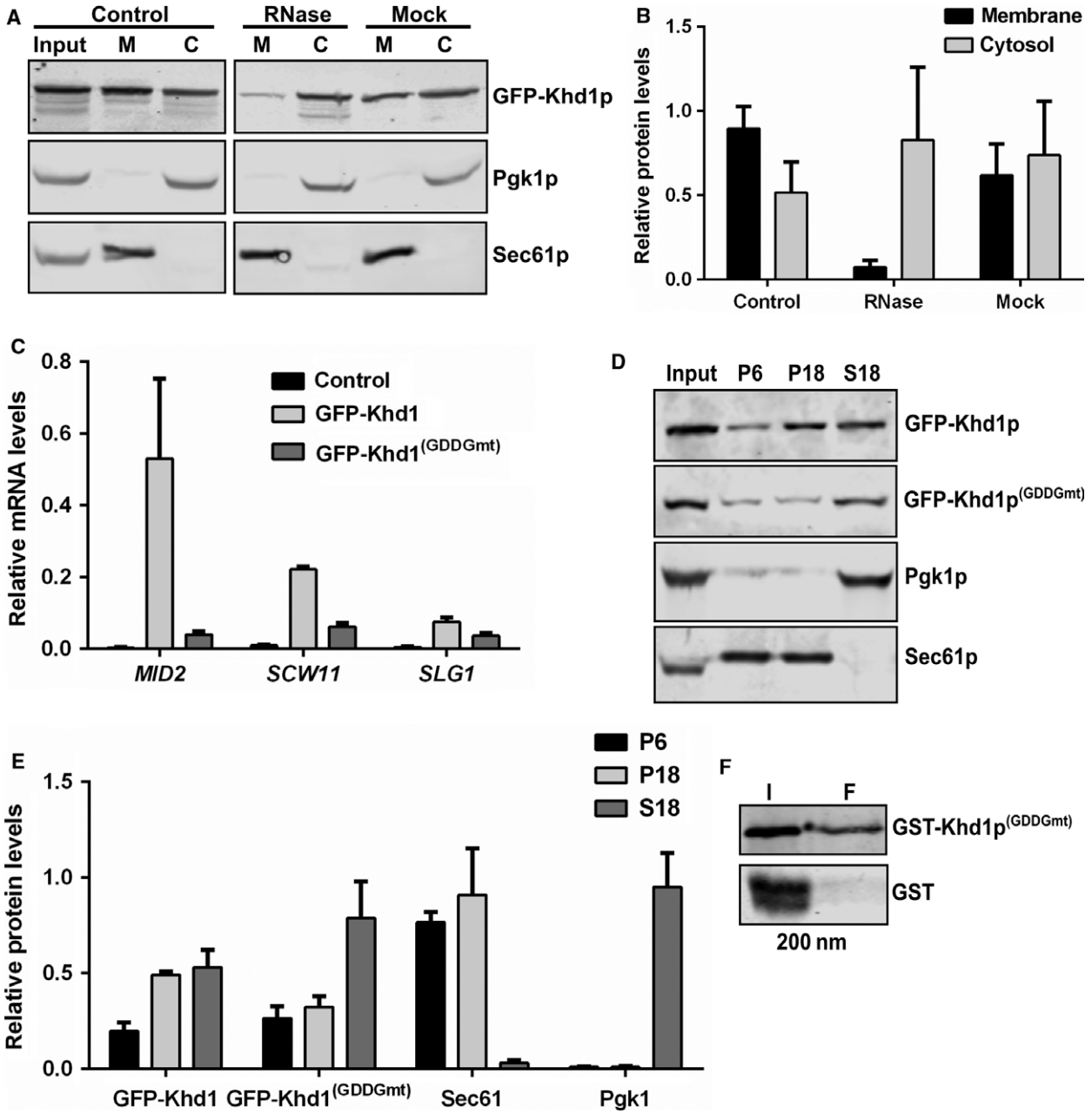

Fig. 3. RNA-binding of Khd1p is required for membrane association. (A) Loss of GFP-Khd1p from the membrane fraction upon treatment with RNase. C, cytosol; M, membrane. (B) Quantification of Khd1p distribution among membrane and cytosolic fractions in three biological replicates. Normalization was done against the input signal. Data are presented as mean ± SEM. (C) RNA-binding was assessed by immunoprecipitation of GFP-Khd1p and mutant GFP-Khd1p$^{(GDDGmt)}$ followed by qRT-PCR. Coprecipitation of *MID2*, *SCW11*, and *SLG1* mRNAs is lost with GFP-Khd1p$^{(GDDGmt)}$. Normalization was performed against spike RNA (see Materials and methods), $n = 3$. (D) Subcellular fractionation shows partial loss of GFP-Khd1p$^{(GDDGmt)}$ from the membrane fraction compared to GFP-Khd1p. P6 and P18 represent membrane fractions, whereas S18 the cytosolic fraction. (E) Quantification of western blots (three biological replicates) normalized against input signal. (F) Flotation assay with GST and recombinant mutant Khd1p (GST-Khd1p$^{(GDDGmt)}$), using 200 nm liposomes. Input (I) and float (F) fractions were analyzed by western blotting against GST.

MID2. In contrast to wild-type *MID2*, expression of *MID2(-AUG)* cannot rescue the Calcofluor white sensitive phenotype of *mid2*Δ yeast [33], indicating that the mutant is nonfunctional (Fig. S4). *MID2* and *MID2(-AUG)* mRNAs were both enriched in the membrane fraction (Fig. 4C), supporting the idea that

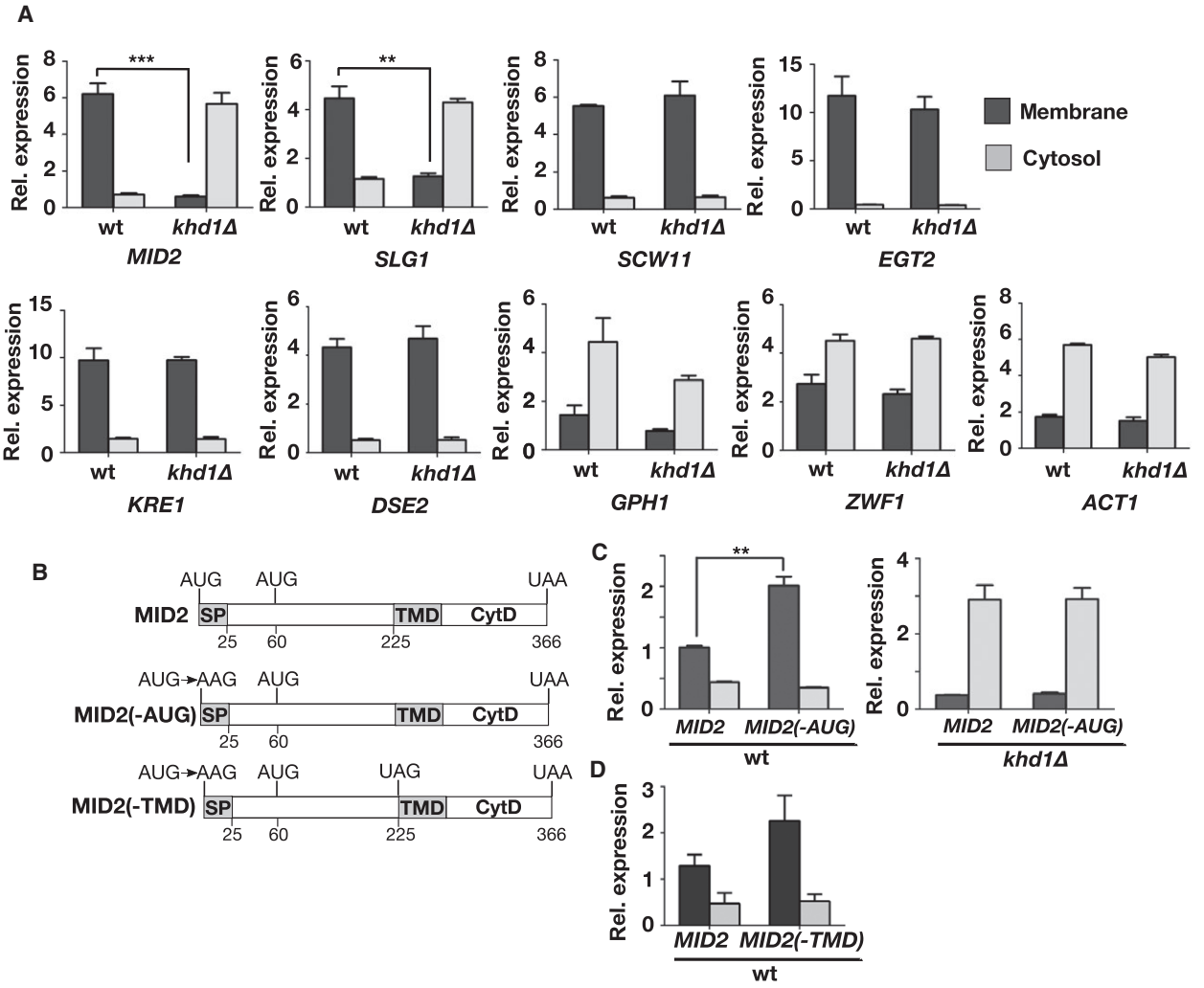

Fig. 4. Khd1p-dependent enrichment of *MID2* and *SLG1/WSC1* mRNAs at the ER. (A) Wild-type and *khd1Δ* lysates were subjected to subcellular fractionation. RNA was isolated from the membrane and cytoplasmic fractions and subjected to qRT-PCR to analyze the distribution of Khd1p target mRNAs: *MID2*, *SLG1*, *SCW11*, *EGT2*, *KRE1*, *DSE2*, *GPH1*, and *ZWF1*. *ACT1* mRNA was used as a control. Relative mRNA level in each fraction were calculated by comparing to input. Data are presented as mean ± SEM (error bars), $n = 3$. *** depicts $P < 0.001$, ** indicates $P < 0.01$. (B) Schematics of *MID2* mutant mRNAs lacking its canonical start codon or TMD. (C) Translation-independent targeting of *MID2* mRNA to membranes. Distribution of wild-type *MID2* and *MID2(-ATG)* in wild-type and *khd1*Δ cells. Data are presented as mean ± SEM (error bars), $n = 3$. (D) Association of *MID2* mRNA with membranes is independent of the TMD of Mid2p. Distribution of wild-type *MID2* (RJY4500) and *MID2(-TMD)* between the membrane and cytosolic fractions were analyzed. Data are presented as mean ± SEM (error bars), $n = 3$.

MID2 membrane association occurs independent of its signal sequence. The m/c ratio of *MID2(-AUG)* mRNA was even higher than that of wild-type *MID2*, indicating that translation might have an adverse effect on the mRNA's copurification with membranes. Deletion of *KHD1* led to redistribution of both mRNAs to the cytoplasm (Fig. 4C). Although *MID(-AUG)* lacks a signal sequence, translation initiation at a downstream AUG codon could code for a protein that has a transmembrane domain (TMD) that could also be recognized by the SRP [34]. Therefore, a stop codon was introduced before the TMD in *MID2(-AUG)* and named *MID2(-TMD)* (Fig. 4B). *MID2(-TMD)* mRNA cofractionated with membranes (Fig. 4D), making SRP-dependent targeting unlikely. This observation underscores the requirement of Khd1p to target *MID2* mRNA to membranes, most likely the ER.

To gain additional evidence for a function of Khd1p in membrane-targeting of *MID2* and *SLG1/WSC1,* we performed colocalization experiments with MS2 loop (MS2L-) tagged *MID2* and *SLG1/WSC1* mRNAs and the cortical-ER marker Rtn1p-mCherry. We grouped

MS2L-tagged mRNPs into three classes (Fig. 5A): not colocalizing (separation of ER and MS2L signal by more than 0.5 μm), peripheral (separation by less than 0.5 μm but no overlap of signals), and colocalizing (overlap of signals). Upon loss of Khd1p, we observed a significant reduction of *MID2* and *SLG1*/*WSC1* mRNPs that colocalized with ER, supporting our fractionation data (Fig. 5B,C). Since recent observations of MS2L-tagged RNAs in yeast indicate that MS2L-tagging results in destabilization of the RNA, accumulation and likely targeting of MS2L-containing fragments to P-bodies [35,36], we used smFISH against untagged *MID2* mRNA to support our live-imaging data. As control mRNA, *ACT1* that encodes yeast actin was used. We again grouped smFISH signals into three classes based on colocalization with an ER marker (Hmg1p-EGFP). In contrast to *MID2*, where less than 5 mRNA signals per cell were detectable (Fig. 5D), *ACT1* was expectedly more prominent (Fig. S5). However, *MID2* mRNAs were detected with a higher frequency to colocalize with the ER although such colocalization was also observed with *ACT1* (Fig. 5E). Loss of *KHD1* resulted in a shift of *MID2* as well as *MID2(-AUG)* signals from ER colocalization to the cytoplasm (Fig. 5E,F) although the change is not as prominent as with the MS2-tagged mRNA. We conclude that Khd1p is partially responsible for colocalization of *MID2* with the ER.

Discussion

Targeting of mRNAs to the cytoplasmic face of the ER can be achieved by different pathways. In the canonical model, mRNAs arrive at the ER as part of nascent chain complexes with ribosomes and the nascent peptide containing a signal recognized by the SRP. In contrast to this cotranslational targeting, alternative pathways involve binding of mRNAs by integral membrane or membrane-associated mRBPs at the ER [17–19]. Examples of such proteins are the ER-membrane protein p180 in mammals [20], or the RBP She2p in budding yeast which shares properties with peripheral membrane proteins [5,22,27]. Here, we report that the yeast RBP Khd1p can also associate with membranes and is involved in translation- and signal sequence-independent targeting of *MID2* and possibly other mRNAs to the yeast ER.

Khd1p has different functions for various target mRNAs. For example, it can act as a translational inhibitor of *ASH1* and *FLO11* mRNAs [7,12,37], or as an mRNA stabilizer in the case of *MTL1* [10,14]. Khd1p interacts with roughly 50% of bud-localized mRNAs [5,10], of which the majority encodes membrane or secreted proteins [3]. In addition, Khd1p binds to many nonlocalized mRNAs encoding proteins of the cell wall or plasma membrane [10,13], suggesting a function in controlling the fate or even localization of these mRNAs.

Taken together, our fractionation, imaging, and *in vitro* binding experiments support the view that Khd1p can in principle associate with intracellular membranes. These findings might reflect that only a subpopulation of Khd1p binds to the ER or that Khd1p binding to the ER is transient and therefore hard to detect. Importantly, cofractionation of Khd1p with membranes depends in large part on RNA association since an RNA-binding mutant showed severely reduced cofractionation. This suggests that association of Khd1p with the ER is indirect and possibly mediated by binding to mRNAs that are translated on ER-bound ribosomes. However, Khd1p-binding to protein-free liposomes suggests that even in the absence of RNA, Khd1p has the propensity to interact with lipids. This has also been observed for another RBP, She2p [22]. An important difference in liposome-binding between the two proteins is the preference of She2p for high-curvature membranes as found in ER tubules. This specific feature might allow She2p to link localized mRNAs to tubular ER that moves into the bud, providing a mechanism for ER-dependent bud localization of certain yeast mRNAs [5,38]. In contrast, Khd1p interacts with many non-bud-localized mSMPs [10,17]. Since these mRNAs are likely translated at the perinuclear ER with a rather flat morphology [39], no specific preference for curved membranes would be required for Khd1p.

Although Khd1p's own association with the ER requires binding to RNA, at least two of its mRNA targets, *MID2* and *SLG1*/*WSC1,* depend on *KHD1* for efficient ER targeting. The requirement of Khd1 for their targeting is also reflected by their genetic interaction since *KHD1* as well as *MID2* and *SLG1*/*WSC1* are involved in the cell wall integrity pathway [40]. Other described Khd1p targets like *EGT2*, *SCW11*, *DSE2*, or *KRE1* associate with ER even in the absence of Khd1p, suggesting that either their ER binding might be mediated by the ribosome nascent chain complex interacting with the translocon or that other RBP might compensate for the loss of Khd1p. In case of *EGT2*, one such candidate could be the ER-associated RBP Whi3p since it also binds to *EGT2* mRNA [41]. For *MID2,* targeting is largely, but not totally, independent of the translation of its signal sequence or its TMD which might serve as a targeting signal. Signal sequence independence for RNA targeting to the ER has been observed for several mRNAs in yeast

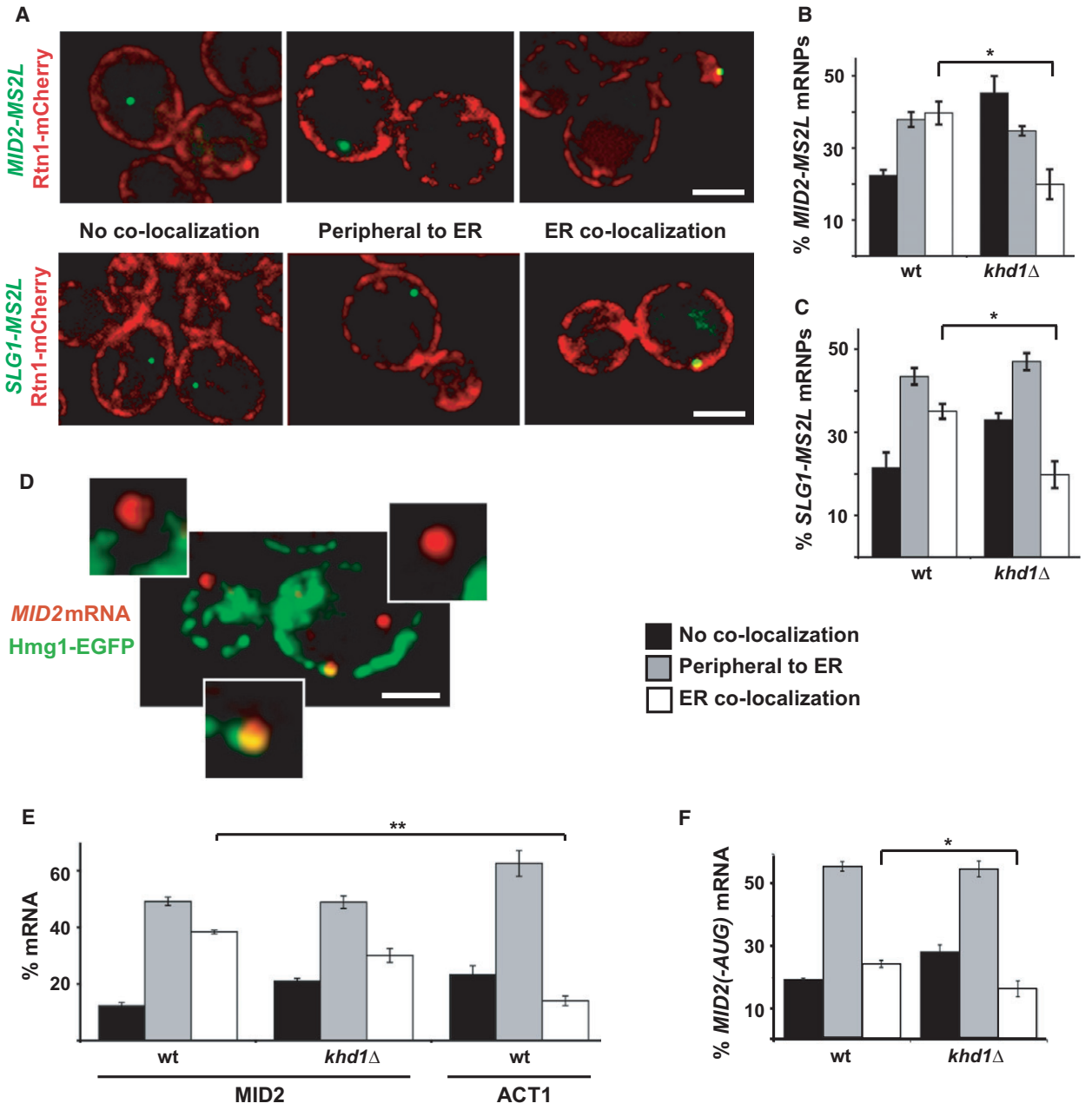

Fig. 5. ER-association of *MID2* mRNA and *SLG1* mRNA is promoted by Khd1p. (A) Representative images of cells expressing *MS2L*-tagged *MID2* or *SLG1* mRNAs (green) and Rtn1p-mCherry as cortical-ER marker (red). Images show both tagged mRNAs localized in the cytosol, close to the cortical ER (distance < 0.5 μm), and colocalizing with the cortical ER. (B,C) Analysis of ER-association of *MID2-MS2L* (B) or *SLG1-MS2L* (C) mRNAs. Data were derived from counting > 250 mRNPs in three biological replicates. mRNPs were grouped based on whether they colocalized with the cortical ER (white bars), localized close to the cortical ER (gray bars), or localized in the cytosol (black bars) in wild-type and *khd1*Δ cells. Data are shown as mean number of particles ± SEM. *$P < 0.1$. (D) smFISH of *MID2* mRNA (red) and Hmg1p-EGFP signals (ER marker, green). Insets show magnifications of *MID2* mRNA signals at the ER periphery (upper left), cytosol (upper right), or colocalizing with the ER (bottom insert). (E) smFISH analysis of ER-association of *MID2* and *ACT1* in wild-type cells and *MID2* in *khd1*Δ cells. (F) smFISH analysis of ER-association of *MID2(-AUG)* mRNAs in wild-type and *khd1*Δ cells. smFISH data were derived from counting > 1000 mRNPs in three biological replicates and grouped based on their localization relative to the ER marker. Data are shown as mean values ± SEM. *$P < 0.1$, **$P < 0.01$. All scale bars: 2 μm.

and other cell types [20,21,38,42]. Localization of these mRNAs to the ER requires RBPs that are ER-associated [5,21] or integral membrane proteins [20]. For some RNAs like *PMP1* and *PMP2* [42,43], signals in the 3′-UTR have been identified that can recruit the SRP prior to translation of the signal sequence [42]. Thus, targeting of mRNAs to the ER might also be mediated by independent, yet redundant mechanisms.

Altogether, our data suggest that the RBP Khd1p weakly or transiently associates with the ER and that this may assist *MID2* and potentially other mRNAs (e.g., *SLG1*/*WSC1*) in reaching the cytoplasmic face of the ER. Our data also support an alternative model of translation-independent mRNA targeting to the ER [17–19,42] and provide further evidence that this targeting can occur via RBP.

Acknowledgements

We are grateful to S. Jellbauer and G. de Andrade for help with the *KHD1-6xHA* expression construct and U. Thiess for help with creating yeast strains with multiple deletions. We thank M. Schuldiner for providing the HDEL-DsRed expression plasmid, P. Chartrand for plasmid pGEX-5X-3-KHD1, and C.W. Wang for the TGBp3-GFP expression plasmid. We thank M. Cheng and B. Singer-Krüger for helpful discussions regarding this project. This work was funded by the Deutsche Forschungsgemeinschaft (DFG), grant JA696-10/1.

Authors' contribution

MIS performed experiments for Figs 2,3, and Figs S1–S3. BTM performed experiments for Figs 1, 4, and S4. AJ and IF performed experiments for Fig. 5 and S5. MIS, BTM, and RPJ designed the experiments. MIS, BTM, and RPJ wrote the manuscript.

References

1 Czaplinski K (2014) Understanding mRNA trafficking: are we there yet? *Semin Cell Dev Biol*, **32**, 63–70.
2 Martin KC and Ephrussi A (2009) mRNA localization: gene expression in the spatial dimension. *Cell* **136**, 719–730.
3 Shepard KA, Gerber AP, Jambhekar A, Takizawa PA, Brown PO, Herschlag D, DeRisi JL and Vale RD (2003) Widespread cytoplasmic mRNA transport in yeast: identification of 22 bud-localized transcripts using DNA microarray analysis. *Proc Natl Acad Sci* **100**, 11429–11434.
4 Oeffinger M, Wei KE, Rogers R, DeGrasse JA, Chait BT, Aitchison JD and Rout MP (2007) Comprehensive analysis of diverse ribonucleoprotein complexes. *Nat Methods* **4**, 951–956.
5 Aronov S, Gelin-Licht R, Zipor G, Haim L, Safran E and Gerst JE (2007) mRNAs encoding polarity and exocytosis factors are cotransported with the cortical endoplasmic reticulum to the incipient bud in *Saccharomyces cerevisiae*. *Mol Cell Biol* **27**, 3441–3455.
6 Böhl F, Kruse C, Frank A, Ferring D and Jansen RP (2000) She2p, a novel RNA-binding protein tethers ASH1 mRNA to the Myo4p myosin motor via She3p. *EMBO J* **19**, 5514–5524.
7 Irie K, Tadauchi T, Takizawa PA, Vale RD, Matsumoto K and Herskowitz I (2002) The Khd1 protein, which has three KH RNA-binding motifs, is required for proper localization of ASH1 mRNA in yeast. *EMBO J* **21**, 1158–1167.
8 Long RM, Gu W, Meng X, Gonsalvez G, Singer RH and Chartrand P (2001) An exclusively nuclear RNA-binding protein affects asymmetric localization of ASH1 mRNA and Ash1p in yeast. *J Cell Biol* **153**, 307–318.
9 Gu W, Deng Y, Zenklusen D and Singer RH (2004) A new yeast PUF family protein, Puf6p, represses ASH1 mRNA translation and is required for its localization. *Genes Dev* **18**, 1452–1465.
10 Hasegawa Y, Irie K and Gerber AP (2008) Distinct roles for Khd1p in the localization and expression of bud-localized mRNAs in yeast. *RNA* **14**, 2333–2347.
11 Valverde R, Edwards L and Regan L (2008) Structure and function of KH domains. *FEBS J* **275**, 2712–2726.
12 Paquin N, Ménade M, Poirier G, Donato D, Drouet E and Chartrand P (2007) Local activation of yeast ASH1 mRNA translation through phosphorylation of Khd1p by the casein kinase Yck1p. *Mol Cell* **26**, 795–809.
13 Hogan DJ, Riordan DP, Gerber AP, Herschlag D and Brown PO (2008) Diverse RNA-binding proteins interact with functionally related sets of RNAs, suggesting an extensive regulatory system. *PLoS Biol* **6**, e255.
14 Mauchi N, Ohtake Y and Irie K (2010) Stability control of MTL1 mRNA by the RNA-binding protein Khd1p in yeast. *Cell Struct Funct* **35**, 95–105.
15 Shao S and Hegde RS (2011) Membrane protein insertion at the endoplasmic reticulum. *Annu Rev Cell Dev Biol* **27**, 25–56.
16 Rapoport TA (2007) Protein translocation across the eukaryotic endoplasmic reticulum and bacterial plasma membranes. *Nature* **450**, 663–669.
17 Kraut-Cohen J and Gerst JE (2010) Addressing mRNAs to the ER: cis sequences act up!. *Trends Biochem Sci* **35**, 459–469.
18 Hermesh O and Jansen R-P (2013) Take the (RN)A-train: localization of mRNA to the endoplasmic reticulum. *Biochim Biophys Acta* **1833**, 2519–2525.

19 Cui XA and Palazzo AF (2014) Localization of mRNAs to the endoplasmic reticulum. *Wiley Interdiscip Rev RNA* **5**, 481–492.
20 Cui XA, Zhang H and Palazzo AF (2012) p180 promotes the ribosome-independent localization of a subset of mRNA to the endoplasmic reticulum. *PLoS Biol* **10**, e1001336.
21 Kraut-Cohen J, Afanasieva E, Haim-Vilmovsky L, Slobodin B, Yosef I, Bibi E and Gerst JE (2013) Translation- and SRP-independent mRNA targeting to the endoplasmic reticulum in the yeast *Saccharomyces cerevisiae*. *Mol Biol Cell* **24**, 3069–3084.
22 Genz C, Fundakowski J, Hermesh O, Schmid M and Jansen RP (2013) Association of the yeast RNA-binding protein She2p with the tubular endoplasmic reticulum depends on membrane curvature. *J Biolo Chem* **288**, 32384–32393.
23 Frey S, Pool M and Seedorf M (2001) Scp160p, an RNA-binding, polysome-associated protein, localizes to the endoplasmic reticulum of *Saccharomyces cerevisiae* in a microtubule-dependent manner. *J Biol Chem* **276**, 15905–15912.
24 Livak KJ and Schmittgen TD (2001) Analysis of relative gene expression data using real-time quantitative PCR and the $2-\Delta\Delta CT$ method. *Methods* **25**, 402–408.
25 Hermesh O, Genz C, Yofe I, Sinzel M, Rapaport D, Schuldiner M and Jansen RP (2014) Yeast phospholipid biosynthesis is linked to mRNA localization. *J Cell Sci* **127**, 3373–3381.
26 Raj A, van den Bogaard P, Rifkin SA, van Oudenaarden A and Tyagi S (2008) Imaging individual mRNA molecules using multiple singly labeled probes. *Nat Methods* **5**, 877–879.
27 Schmid M, Jaedicke A, Du T-G and Jansen R-P (2006) Coordination of endoplasmic reticulum and mRNA localization to the yeast bud. *Curr Biol* **16**, 1538–1543.
28 Huh W-K, Falvo JV, Gerke LC, Carroll AS, Howson RW, Weissman JS and O'Shea EK (2003) Global analysis of protein localization in budding yeast. *Nature* **425**, 686–691.
29 Wu CH, Lee SC and Wang CW (2011) Viral protein targeting to the cortical endoplasmic reticulum is required for cell-cell spreading in plants. *J Cell Biol* **193**, 521–535.
30 Nogae I and Johnston M (1990) Isolation and characterization of the ZWF1 gene of *Saccharomyces cerevisiae*, encoding glucose-6-phosphate dehydrogenase. *Gene* **96**, 161–169.
31 Buchan JR, Muhlrad D and Parker R (2008) P bodies promote stress granule assembly in *Saccharomyces cerevisiae*. *J Cell Biol* **183**, 441–455.
32 Hollingworth D, Candel AM, Nicastro G, Martin SR, Briata P, Gherzi R and Ramos A (2012) KH domains with impaired nucleic acid binding as a tool for functional analysis. *Nucleic Acids Res* **40**, 6873–6886.
33 Ketela T, Green R and Bussey H (1999) *Saccharomyces cerevisiae* mid2p is a potential cell wall stress sensor and upstream activator of the PKC1-MPK1 cell integrity pathway. *J Bacteriol* **181**, 3330–3340.
34 Straede A and Heinisch JJ (2007) Functional analyses of the extra- and intracellular domains of the yeast cell wall integrity sensors Mid2 and Wsc1. *FEBS Lett* **581**, 4495–4500.
35 Garcia JF and Parker R (2015) MS2 coat proteins bound to yeast mRNAs block 5″ to 3″ degradation and trap mRNA decay products: implications for the localization of mRNAs by MS2-MCP system. *RNA* **21**, 1393–1395.
36 Haimovich G, Zabezhinsky D, Haas B, Slobodin B, Purushothaman P, Fan L, Levin JZ, Nusbaum C and Gerst JE (2016) Use of the MS2 aptamer and coat protein for RNA localization in yeast: a response to "MS2 coat proteins bound to yeast mRNAs block 5′ to 3′ degradation and trap mRNA decay products: implications for the localization of mRNAs by MS2-MCP system". *RNA* **22**, 660–666.
37 Wolf JJ, Dowell RD, Mahony S, Rabani M, Gifford DK and Fink GR (2010) Feed-forward regulation of a cell fate determinant by an RNA-binding protein generates asymmetry in yeast. *Genetics* **185**, 513–522.
38 Fundakowski J, Hermesh O and Jansen R-P (2012) Localization of a subset of yeast mRNAs depends on inheritance of endoplasmic reticulum. *Traffic* **13**, 1642–1652.
39 West M, Zurek N, Hoenger A and Voeltz GK (2011) A 3D analysis of yeast ER structure reveals how ER domains are organized by membrane curvature. *J Cell Biol* **193**, 333–346.
40 Ito W, Li X, Irie K, Mizuno T and Irie K (2011) RNA-binding protein Khd1 and Ccr4 deadenylase play overlapping roles in the cell wall integrity pathway in *Saccharomyces cerevisiae*. *Eukaryot Cell* **10**, 1340–1347.
41 Colomina N, Ferrezuelo F, Wang H, Aldea M and Garí E (2008) Whi3, a developmental regulator of budding yeast, binds a large set of mRNAs functionally related to the endoplasmic reticulum. *J Biol Chem* **283**, 28670–28679.
42 Chartron JW, Hunt KCL and Frydman J (2016) Cotranslational signal-independent SRP preloading during membrane targeting. *Nature* **536**, 224–228.
43 Loya A, Pnueli L, Yosefzon Y, Wexler Y, Ziv-Ukelson M and Arava Y (2008) The 3′-UTR mediates the cellular localization of an mRNA encoding a short plasma membrane protein. *RNA* **14**, 1352–1365.

Supporting information

Additional Supporting Information may be found online in the Supporting Information section at the end of the article:

Fig. S1. Cells of strain RJY4959 that coexpress Rtn1p-mCherry and a protein fusion of GFP-Sec61 and TGBp3(aa25-52) were analyzed by confocal microscopy.

Fig. S2. RNase treatment of wild-type lysate followed by fractionation at 18 000 ***g*** to separate the membrane rich fraction from cytosol.

Fig. S3. Immunoprecipitation of GFP-Khd1p and GFP-Khd1p$^{(GDDGmt)}$.

Fig. S4. Calcofluor white assay. Cells were grown to mid-log phase and cultures diluted to 15 000 cells·mL^{-1}.

Fig. S5. Images show exemplary cells after smFISH against endogenous *ACT1* mRNA (red) in strain RJY2321 expressing HMG1-GFP as an ER marker (green).

Table S1. Yeast strains used in this study.

Table S2. Plasmids used in this study.

Table S3. Oligonucleotides used in this study.

Appendix S1. Supporting Methods.

Supporting Information Syed et al., 2018

SUPPORTING METHODS

Yeast strains and growth conditions

All yeast strains from this study are listed in supporting table S1 and were derived from either *W303* or *BY4741* background. Gene deletion or chromosomal gene tagging was carried out by standard PCR-based transformation methods [1]. A rapid one-step yeast transformation protocol was used to introduce plasmids [2] Strain RJY4544 carrying GFP-tagged *MID2* was purchased from Invitrogen. Cells were grown at 30°C to mid log phase in standard rich medium containing 2% glucose (YPD) or synthetic medium containing glucose (synthetic complete; SC) lacking the appropriate amino acid or nucleobase).

Plasmids

All plasmids used in this study are listed in supporting table S2. The oligonucleotides that were used for cloning, gene tagging, and gene disruption are listed in supporting table S3. For all constructs, cloning was verified via sequencing of the inserts. Glutathione-S transferase (GST) was expressed from plasmid pET-23a and purified according the manufacturer's instructions (GE Healthcare). pGEX-5X-3-KHD1 (a gift from P. Chartrand) was used to generate recombinant Khd1p as described [3]. To create pGEX-5X-3-KHD1^{GDDGmt}, KHD1^{GDDGmt} was PCR amplified from pRJ2132 with oligos RJO6503 and RJO6504, digested with EcoRI/XhoI and cloned in pRJ1745.

The GFP-TGBp3(aa25-52) (pRJ1846) construct expressing GFP fused to a TGBp3 peptide from the plant *potexvirus* was a gift from C.W. Wang [4]. Primer pairs RJO4417 and RJO4418, RJO4455 and RJO4456, or RJO4760 and RJO4826 were used to amplify the coding regions of *KHD1*, *ZWF1,* and *RIE1,* respectively. The PCR products were cloned between GFP and the C-terminal peptide of TGBp3 (amino acids 25-52) to create the corresponding fusion proteins. To create GFP-Khd1p without the TGBp3 peptide (RJP2137), *KHD1* ORF was PCR amplified with primers RJO4417 and RJO5675 and cloned in pRJ1846.

pRJ1887 containing *MID2* was created as follows. The *MID2* gene with its promoter region and 3'UTR was amplified from yeast genomic DNA using primer pair RJO4587 and RJO4588. *BamH*I and *EcoR*I sites were introduced with these oligos and the restriction sites were used to insert the PCR product into a pRS313 vector by the SLIC method [5]. pRJ1903 carrying *MID2(-AUG*) was generated as follows: the start codon of *MID2* was mutated to create a *Hind*III restriction site using primer pair RJO4605 and RJO4606. Two PCR products were generated from this template, using primer pairs RJO4587 and RJO4606, or RJO4605 and RJO4588. The PCR products were digested with *Hind*III, *BamH*I, and *EcoR*I,

and cloned into pRS313 that was digested with *BamHI* and *EcoR*I. pRJ1931 was generated by introducing a stop codon before the transmembrane domain of *MID2* in the *MID2(-AUG)* construct by using primer pairs RJO4916 and RJO4917.

pRJ2131 was created as follows: first XhoI and NotI restriction sites were introduced into plasmid pRJ2135 using oligos RJO5729 and RJO5730. Then two additional fragments, one for yEGFP (from pRJ1135 using RJO5731 and RJO5732) and the other for KHD1 with its 3'UTR from yeast genomic DNA (using oligos RJO5733 and RJO5734), were PCR-amplified. The vector and the yeGFP PCR product were digested with XhoI and NotI, and the KHD1+3`UTR PCR product was digested with NotI. The two digested PCR products and the digested vector were ligated in a single reaction to create pRJ2131. For pRJ2132 (GFP-KHD1$^{(GDDGmt)}$), four fragments were PCR-amplified using template pRJ2131 with oligos RJO4933 and RJO6167; RJO6168 and RJO6169; RJO6170 and RJO6171; and RJO6172 and RJO4604. All these fragments were combined together via overlap-extension PCR and the resulting product was digested with XhoI and EcoRI, and cloned in pRJ2131 to create pRJ2132. This resulted in the mutation of threonine at position 62, lysine at 63 and 174, alanine at 175, phenylalanine at 210, and proline at 211 into aspartic acids.

For spike RNA (external RNA) production, pRJ2133 was created by PCR-amplifying a 454bp fragment with RJO5566 and RJO5567 from *Arabidopsis thaliana* cDNA (amplifying a gene region from AtPRKase) and cloning into pcDNA3.1.

Subcellular fractionation by sucrose density gradient centrifugation

Fractionation via sucrose density centrifugation was performed with lysates from strain RJY2662 (Khd1-9xmyc::*K.l.TRP*) as described [6]. In brief, cell lysate corresponding to 66 OD_{600} units was applied onto a linear 18%-60% sucrose gradient in 20mM HEPES pH 6.8, 140mM potassium acetate, and 1mM magnesium acetate. After centrifugation for 2.5 h at 38,000 x *g*, 11 fractions and the pellet were collected, proteins precipitated with trichloroacetic acid (TCA), and prepared for Western blot analysis.

Western blotting

Immunoblotting was done with anti-Myc 1:200 (mouse, c-myc 9E10 (Roche)), anti-GFP 1:1,000 (mouse, from Covance), anti-Pgk1 1:1,000 (mouse, Invitrogen) and anti-Sec61 1:7,500 (rabbit). For density gradient, Western blot was developed via chemiluminescence using ECL (GE Healthcare). Other Western blots were visualised by LICOR Odyssey system using fluorescently labelled secondary antibodies.

Calcofluor white test

Calcofluor white sensitivity tests were done as described[9]. Briefly, mid-log phase cells were diluted to OD_{600}=0.3 and three subsequent 10-fold dilutions were prepared. 5µl of each dilution was spotted onto YEPD plates with or without 20µg/ml Calcofluor white. Plates were incubated at 30°C for 3 days.

Supporting Table S1: Yeast strains used in this study

Name	Essential genotype	Origin
RJY358	*MAT**a** ade2-1 trp1-1 can1-100 leu2-3,112 his3-11,15 ura3*	[10]
RJY359	*MAT**α** ade2-1 trp1-1 can1-100 leu2-3,112 his3-11,15 ura3*	[10]
RJY2321	*MAT**a** HMG1-GFP::URA3*	[6]
RJY2368	*MAT**a** khd1Δ::HIS3MX6*	This study
RJY2662	*MAT**a** KHD1-9XMYC::K.l.TRP*	This study
RJY3266	*MAT**a** she2Δ::natNT2*	This study
RJY4379	*MAT**α*** p416-ADH1-GFP-KHD1-TGBp3	This study
RJY4393	*MAT**α*** p416-ADH1-GFP- KHD1-TGBp3 pRS415-HDEL-DsRED	This study
RJY4394	*MAT**α*** p416-ADH1-GFP-ZWF1-TGBp3 pRS415-HDEL-DsRED	This study
RJY5255	*MAT**a*** p416-ADH1-GFP-RIE1-TGBp3 pRS415-HDEL-DsRED	This study
RJY5254	*MAT**a*** p416-ADH1-GFP-KHD1 (without TGBp3) pRS415-HDEL-DsRED	This study
RJY4495	*MAT**a** mid2Δ::KanMX6*	This study
RJY5252	*MAT**a** khd1Δ::KanMX6* YCplac33-yEGFP-KHD1 pRS415-HDEL-DsRED	This study
RJY4500	*MAT**a*** pRS313-MID2 *mid2Δ::KanMX6*	This study
RJY5253	*MAT**a** khd1Δ::KanMX6* YCplac33-yEGFP-KHD1$^{(GDDGmt)}$ pRS415-HDEL-DsRED	This study
RJY4506	*MAT**a*** pRS313-MID2(-ATG) *mid2Δ::KanMX6*	This study
RJY4543	*MAT**a** mid2Δ::KanMX6 khd1Δ::natNT2*	This study
RJY4544	*MAT**a** MID2-GFP::HIS3MX6*	Invitrogen
RJY4545	*MAT**a*** pRS313-MID2 *mid2Δ::KanMX6*, *khd1Δ::natNT2*	This study
RJY4546	*MAT**a*** pRS313-MID2(-ATG) *mid2Δ::KanMX6*, *khd1Δ::natNT2*	This study
RJY4553	*MAT**a** MID2-GFP::HIS3MX6 khd1Δ::natNT2*	This study
RJY4615	*MAT**α** khd1Δ::natNT2*	This study
RJY4622	*MAT**a** she2Δ::HisMX6 khd1Δ::natNT2*	This study
RJY4669	*MAT**a*** pRS313-MID2(-TMD) *mid2Δ::KanMX6*	This study

RJY4795	*MAT**a** SLG1-12xMSL RTN1-mCherry::natNT2* pCP-MS2-GFPx3	This study
RJY4797	*MAT**a** SLG1-12xMSL RTN1-mCherry::natNT2 khd1::hphNT1* pCP-MS2-GFPx3	This study
RJY4799	*MAT**a** MID2-12xMSL RTN1-mCherry::natNT2* pCP-MS2-GFPx3	This study
RJY4800	*MAT**a** MID2-12xMSL RTN1-mCherry::natNT2 khd1::hphNT1* pCP-MS2-GFPx3	This study
RJY4884	*MAT**a** HMG1-GFP::URA3 khd1Δ::hphNT1*	This study
RJY4940	*MAT**a*** pRS313-MID2(-ATG) *mid2Δ::KanMX6* YCplac22-HMG1-GFP	This study
RJY4941	*MAT**a*** pRS313-MID2(-ATG) *mid2Δ::KanMX6 khd1Δ::natNT2* YCplac22-HMG1-GFP	This study
RJY4959	*MAT**a** RTN1-mCherry::natNT2* p416-ADH1-GFP-SEC61-TGBp3	This study

All strains except RJY4544 and RJY4553 are derived from W303, which has the genotype *ade2-1 trp1-1 can1-100 leu2-3,112 his3-11,15 ura3*. Both mating types were used. The strains RJY2321, RJY4544 and RJY4553 are from BY4741 background (*MAT**a** his3Δ1 leu2Δ0 met15Δ0 ura3Δ0*).

Supporting Table S2: Plasmids used in this study

Name	Short description	Source
pRJ1135	pOM40	[11]
pRJ1341	YCplac22-HMG1-GFP	[6]
pRJ1745	pGEX-5X-3-KHD1	[3]
pRJ1846	p416-ADH1-GFP-TGBp3(25-52)	[4]
pRJ1870	pRS415-HDEL-DsRED	[12]
pRJ1871	p416-ADH1-GFP-KHD1-TGBp3	This study
pRJ1877	p416-ADH1-GFP-ZWF1-TGBp3	This study
pRJ1887	pRS313-MID2	This study
pRJ1903	pRS313-MID2(-AUG)	This study
pRJ1931	pRS313-MID2(-TMD)	This study
pRJ1989	p416-ADH1-GFP-SEC61 -TGBp3	This study
pRJ2131	YCplac33-yEGFP-KHD1	This study
pRJ2132	YCplac33-yEGFP-KHD1$^{(GDDGmt)}$	This study
pRJ2133	pcDNA3.1-PRKASE	This study
pRJ2135	YCplac33-KHD1-GFP	This study
pRJ2136	p416-ADH1-GFP-RIE1 -TGBp3	This study
pRJ2138	p416-ADH1-GFP-KHD1 (without TGBp3)	This study
pRJ2171	pGEX-5X-3-KHD1^{GDDGmt}	This study

Supporting Table S3: Oligonucleotides used in this study

RJO	Name	Sequence	Purpose
2933	KHD1_Spe I_F	TTTTTTACTAGTATGTCACAGTTCTTCGAAGCT	Cloning
2856	KHD1_HindIII_R	TTTTTTAAGCTTTATAGTGAATGATCGTTCCAC	Cloning
4417	KHD1_Sma1_F	TACTCCCGGGATGTCACAGTTCTTCGAAGCTGCT ACTCCCG	Tgbp3 cloning
4418	KHD1_EcoR1_R	TGCAGAATTCCGACTGCTCCTCTTTGTTATCA	Tgbp3 cloning
4455	ZWF1_SmaI_F	TACTCCCGGGATGAGTGAAGGCCCCGTCAAATTC G	Tgbp3 cloning
4456	ZWF1_EcoR1_R	TGCAGAATTCATTATCCTTCGTATCTTCTGGCTTA GTC	Tgbp3 cloning
4488	MID2_qpcr_F	ATGGAGCAAAGCTCCCTTTT	qRTPCR
4489	MID2_qpcr_R	GCTCTCCACCGCTATTGGTA	qRTPCR
4609	Mid2_qp_F	CGTCTTCTACGCAAACGTCA	qRTPCR
4610	Mid2_qp_R	GGAGGTTGAAGGTGCAGAAG	qRTPCR
4490	DSE2_qpcr_F	AACTTTGGCGTCATCGTCTT	qRTPCR
4491	DSE2_qpcr_R	GCATGGATGTCGTTGCTCTA	qRTPCR
4492	SLG1_qpcr_F	GGGAACAAGACAGGATGGAA	qRTPCR
4493	SLG1-qpcr_R	AAGAGGGCCCGTGATTAGAT	qRTPCR
4494	EGT2_qpcr_F	CATTCCAAAAAGCAACAGCA	qRTPCR
4495	EGT2_qpcr_R	TGGAACTTGTTGGCAATGAA	qRTPCR
4760	YGR250C_SmaI_F	TTTcccgggAATATTGCAGAAGAACCATCAGATGA AG	Tgb3p cloning
4826	YGR250C_Eco_R	TTTgaattcGTAGTCCATAGAATAATCACCACTAG	Tgb3p cloning
5675	Khd1-TGB-Remov-R	ACATGACTCGAGAAACCCTACGACTGCTCCTCTTT GTTATC	Cloning
4587	MID2_SLIC_F	GGTGCCGGCCGCTCTAGAACTAGTGGATCCTTCA ATGAGTTCCACGACGCAC	Cloning
4588	MID2_SLIC_R	GACGGTATCGATAAGCTTGATATCGAATTCCGTA TATCGCGTGAATGCTCTT	Cloning
4605	MID2triplecl_F	ACTCAAGCTTTCTTTCACAACCAAGAATAG	Cloning
4606	MID2triplecl_R	ACTCAAGCTTACTATGATTTGCGTATTTTATATGT CC	Cloning
4809	KHD1_KO_F	TTATCGGGTAACTTAGAGACAGCATTAGTATATA TACCAGCCATGCGTACGCTGCAGGTCGAC	Gene deletion
3368	KHD1_KO_R	TAGTTTGTTTTGTCTGTGTGGGACGTGCGCACGC ACACGTATATACTAATCGATGAATTCGAGCTCG	Gene deletion
4611	SCW11_qpcr_F	GGCAACACTCAAAGTCAGCA	qRTPCR
4612	SCW11_qpcr_R	GATTCGGTGGACTCCTGAGA	qRTPCR
4615	GPH1_qpcr_f	ATCTGGCCACCCATGAATTA	qRTPCR

4616	GPH1_qpcr_R	GCTAAAGAAGCCGACGTTTG	qRTPCR
4617	ZWF1_qpcr_F	TGGGTGACCATTCCAACTTT	qRTPCR
4618	ZWF1_qpcr_R	GGTAAATTTCCGGTGTTGGA	qRTPCR
4619	KRE1_qpcr_F	TCCATGTGGGTCACTGTTGT	qRTPCR
4620	KRE1_qpcr_R	AGGGAGAAGCGACTGTTACG	qRTPCR
4916	MID2_STPTM_F	GGTCTTTCTAAAAAAAATAGAAACTAGATCGTCA TTGGTTGTGTGGTT	Site-directed mutagenesis
4917	MID2_STPTM_R	AACCACACAACCAATGACGATCTAGTTTCTATTTT TTTTAGAAAGACC	Site-directed mutagenesis
5729	KHD1_XHO_R	AAACTCGAGGGCTGGTATATATACTAATGC	cloning
5730	KHD1_NOT_F	TTTGCGGCCGCTAGTATATACGTGTGCGTGC	Cloning
5731	yEGFP_XHO_F	TTTCTCGAGatgtctaaaggtgaagaattat	Cloning
5732	yEGFP_KHD1_R	CGAAGAACTGTGAgcggccgcataggccactag	Cloning
5733	KHD1_yEGFP_F	ctatgcggccgcTCACAGTTCTTCGAAGCTGC	Cloning
5734	KHD1_NOT_R	AAAGCGGCCGCTTACGACTGCTCCTCTTTGTTATC	Cloning
4933	KHD1_5UTR_F	CGCTCAGCCAAACAACAAACAAGAC	Cloning
4604	Khd1_500bSLIC_R	gataagcttgatatcgaattcGTTCTTGTCGCCGTTGTAT TG	Cloning
6167	GXXG_1_R	TGGTGGAGCCGTCATCGCCAATGATCTTGGCAGC CT	Site-directed mutagenesis
6168	GXXG_1_F	GATCATTGGCGATGACGGCTCCACCATCTCACGC AT	Site-directed mutagenesis
6169	GXXG_2_R	TGGTGGCGCCGTCATCCCCGATAATCGATGAGAT AT	Site-directed mutagenesis
6170	GXXG_2_F	GATTATCGGGGATGACGGCGCCACCATCAAGTCC CT	Site-directed mutagenesis
6171	GXXG_3_R:	TGATGGATCCGTCATCACCCTGGATCTCGATAATT C	Site-directed mutagenesis
6172	GXXG_3_F	GATCCAGGGTGATGACGGATCCATCACCAATGTA CT	Site-directed mutagenesis
5566	Spike_F	GAAATATCGATTAATACGACTCACTATAGGGatgg ctgtctcaactatctac	Cloning
5567	Spike_R	AAACGCTAGCTTTTTTTTTTTTTTTTTTTTTTTTTT TTTtacatgagatcaaagtcattggc	Cloning
5271	OST3_qPCR1_F	TGGTCCTAAGGGCGAGGTTA	RTPCR
5272	OST3_qPCR1_R	CAATACGACAACCAACGCGG	RTPCR
5267	PMA1_qPCR1_F	AGAGCTGCTGGTCCATTCTG	RTPCR
5268	PMA1_qPCR1_R	AGTTTTCAGACCACCAACCGA	RTPCR
6503	KHD1-pGEX-F	TCCCCAGGAATTCGATGTCACAGTTCTTCGAAGC	Cloning
6504	KHD1-pGEX-R	CGGCCGCTCGAGGGCGACTGCTCCTCTTTGTTAT C	Cloning

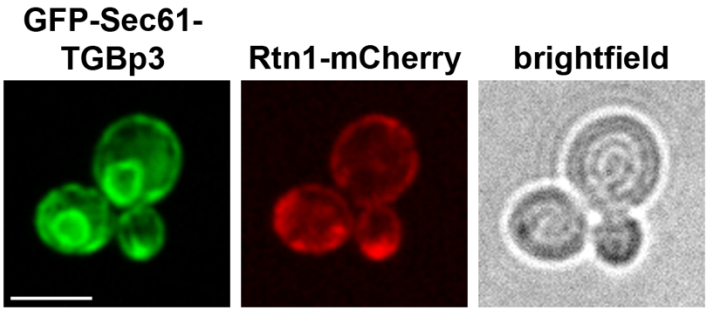

Supporting Figure S1:
Cells of strain RJY4959 that co-express Rtn1p-mCherry and a protein fusion of GFP-Sec61 and TGBp3(aa25-52) were analyzed by confocal microscopy.
GFP-Sec61-TGBp3(aa25-52) shows a typical ER staining unlike TGBp3(aa25-52)-tagged Khd1p, indicating that particle-like staining of is not an artifact caused by the TGBp3 peptide. Scale bar: 5 µm

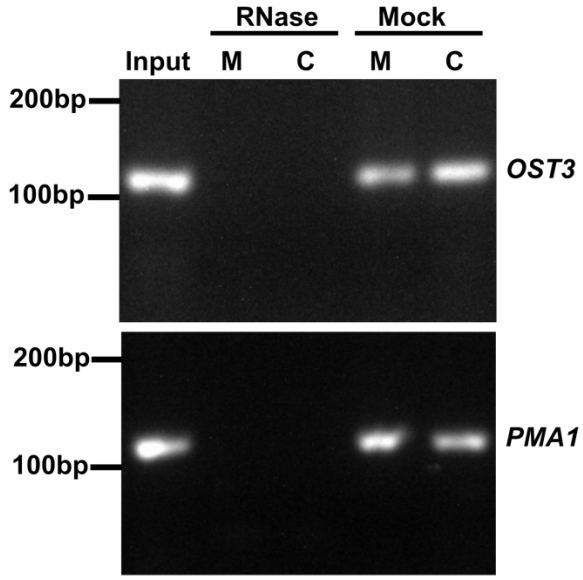

Supporting figure S2: Verification of RNase treatment

RNase treatment of wild-type lysate followed by fractionation at 18000 x g to separate the membrane-rich fraction (M) from cytosol (C). Fractions were treated with RNase or mock and RNAs were extracted and subjected to cDNA synthesis and RT-PCR with primers for two Khd1p-target mRNAs, *OST3* and *PMA1*.

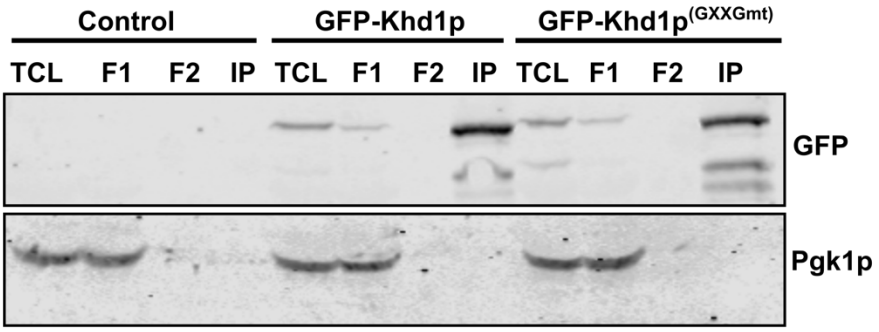

Supporting figure S3: Immunoprecipitation of GFP-Khd1p and GFP-Khd1p$^{(GDDGmt)}$

Western blot showing similar immunoprecipitation of GFP-Khd1p (RJY5252) and GFP-Khd1p$^{(GDDGmt)}$ (RJY5253). TCL= total cell lysate; F1= flow-through 1; F2= flow-through 2 and IP= immunoprecipitate.

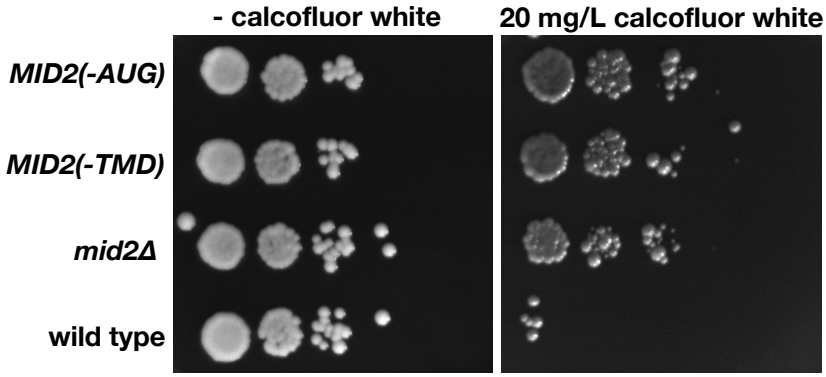

Supporting Figure S4:
Calcofluor white assay. Cells were grown to mid-log phase and cultures diluted to 15000 cells/mL. Four subsequent tenfold dilutions were spotted onto YEPD medium or medium containing 20 mg/L of the cell wall stressor calcofluor white and grown for three days. Wild type (RJY358), *mid2Δ* (RJY4495), *MID2(-AUG)* (RJY4506), *MID2(-TMD)* (RJY4669).

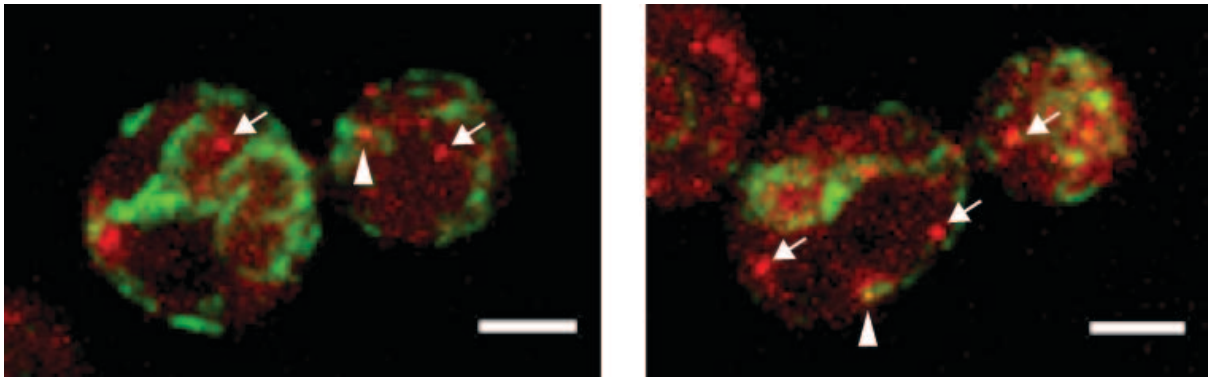

Supporting figure S5: smFISH against *ACT1*

Images show exemplary cells after single molecule fluorescent in situ hybridization (smFISH) against endogenous *ACT1* mRNA (red) in strain RJY2321 expressing HMG1-GFP as ER marker (green). RNA signals co-localizing with ER are marked by arrowheads, non-localizing (cytosolic) ones with arrows. Scale bar: : 2µm.

Supporting References:

1 Janke C, Magiera MM, Rathfelder N, Taxis C, Reber S, Maekawa H, Moreno-Borchart A, Doenges G, Schwob E, Schiebel E & Knop M (2004) A versatile toolbox for PCR-based tagging of yeast genes: new fluorescent proteins, more markers and promoter substitution cassettes. *Yeast* **21**, 947–962.

2 Chen DC, Yang BC & Kuo TT (1992) One-step transformation of yeast in stationary phase. *Current Genetics* **21**, 83–84.

3 Paquin N, Ménade M, Poirier G, Donato D, Drouet E & Chartrand P (2007) Local Activation of Yeast ASH1 mRNA Translation through Phosphorylation of Khd1p by the Casein Kinase Yck1p. *Molecular Cell* **26**, 795–809.

4 Wu CH, Lee SC & Wang CW (2011) Viral protein targeting to the cortical endoplasmic reticulum is required for cell-cell spreading in plants. *The Journal of Cell Biology* **193**, 521–535.

5 Li MZ & Elledge SJ (2007) Harnessing homologous recombination in vitro to generate recombinant DNA via SLIC. *Nature Methods* **4**, 251–256.

6 Schmid M, Jaedicke A, Du T-G & Jansen R-P (2006) Coordination of endoplasmic reticulum and mRNA localization to the yeast bud. *Current Biology* **16**, 1538–1543.

7 Qbadou S (2003) Membrane insertion of the chloroplast outer envelope protein, Toc34: constrains for insertion and topology. *Journal of Cell Science* **116**, 837–846.

8 Genz C, Fundakowski J, Hermesh O, Schmid M & Jansen RP (2013) Association of the Yeast RNA-binding Protein She2p with the Tubular Endoplasmic Reticulum Depends on Membrane Curvature. *Journal of Biological Chemistry* **288**, 32384–32393.

9 Ketela T, Green R & Bussey H (1999) Saccharomyces cerevisiae mid2p is a potential cell wall stress sensor and upstream activator of the PKC1-MPK1 cell integrity pathway. *J. Bacteriol.* **181**, 3330–3340.

10 Rothstein RJ & Sherman F (1980) Genes affecting the expression of cytochrome c in yeast: genetic mapping and genetic interactions. *Genetics* **94**, 871–889.

11 Gauss R, Trautwein M, Sommer T & Spang A (2005) New modules for the repeated internal and N-terminal epitope tagging of genes inSaccharomyces cerevisiae. *Yeast* **22**, 1–12.

12 Bevis BJ & Glick BS (2002) Rapidly maturing variants of the Discosoma red fluorescent protein (DsRed). *Nat. Biotechnol.* **20**, 83–87.

nature structural & molecular biology

Molecular architecture and dynamics of *ASH1* mRNA recognition by its mRNA-transport complex

Franziska Theresia Edelmann[1], Andreas Schlundt[2], Roland Gerhard Heym[1], Andreas Jenner[3], Annika Niedner-Boblenz[4], Muhammad Ibrahim Syed[3], Jean-Christophe Paillart[5], Ralf Stehle[2], Robert Janowski[1], Michael Sattler[1,2], Ralf-Peter Jansen[3] & Dierk Niessing[1,4]

mRNA localization is an essential mechanism of gene regulation and is required for processes such as stem-cell division, embryogenesis and neuronal plasticity. It is not known which features in the *cis*-acting mRNA localization elements (LEs) are specifically recognized by motor-containing transport complexes. To the best of our knowledge, no high-resolution structure is available for any LE in complex with its cognate protein complex. Using X-ray crystallography and complementary techniques, we carried out a detailed assessment of an LE of the *ASH1* mRNA from yeast, its complex with its shuttling RNA-binding protein She2p, and its highly specific, cytoplasmic complex with She3p. Although the RNA alone formed a flexible stem loop, She2p binding induced marked conformational changes. However, only joining by the unstructured She3p resulted in specific RNA recognition. The notable RNA rearrangements and joint action of a globular and an unfolded RNA-binding protein offer unprecedented insights into the step-wise maturation of an mRNA-transport complex.

Motor-dependent localization of mRNAs to subcellular sites has been observed in a wide range of organisms, from yeast to human[1]. Impaired mRNA localization is linked to diverse pathologies, including aneuploidy and neurological disorders[2]. In addition, this mechanism is essential for developmental processes such as the determination of the embryonic body axes of the fruit fly *Drosophila melanogaster*[3]. To achieve intracellular asymmetry of transcripts, mRNAs are recognized by dedicated RNA-binding proteins (RBPs) and incorporated into motor-protein-containing particles[4]. These particles move along the cytoskeleton to distinct cellular sites, where the transcripts are locally translated[5].

A central and largely unresolved issue for understanding mRNA localization is how these transcripts are specifically bound. It is well established that they contain *cis*-acting LEs, which are recognized by motor-associated RBPs[4]. Despite the importance of this interaction, it is not completely understood on a molecular level. A minority of LEs have been identified as consisting of short linear sequence motifs, such as the A2RE element in the *MBP* 3′ UTR[6] or the bipartite *cis*-acting element of the *beta-actin* mRNA[7,8]. The vast majority of LEs form more complex structures with stem loops, containing bulges, mismatches and sometimes even G-quadruplexes[9,10]. Among them, only a few *cis*-acting elements have been characterized structurally. Two examples are the *fs(1)K10* mRNA from *Drosophila* that forms a stem loop with an A' conformation[11] and the spliced *oskar* localization element (SOLE) in the *Drosophila oskar* mRNA[12]. In both cases, the exact protein complex recognizing its RNA target remains unknown.

The situation is further complicated by the observation that different LEs being recognized by the same transport complex usually fail to share recognizable secondary structure or sequence similarities. For instance, during mitosis of the budding yeast *Saccharomyces cerevisiae*, *ASH1* mRNA localizes to the tip of the daughter cell through the action of four functionally redundant LEs[13–15]. A direct comparison of their predicted secondary structures and sequence features showed little similarities. It has been suggested that the latter either consist of a single-stranded CGA-base triplet and a single cytosine on the opposing strand of the stem[16] or contain a single-stranded CG dinucleotide in a stem loop[17]. However, these motifs were only observed in a subset of the *ASH1* LEs and showed different orientations[9,18]. Thus, bioinformatics analyses and even high-resolution structures of LEs alone are not well suited to unravel how an LE is specifically recognized for mRNA transport.

The highly specific recognition of the *ASH1* mRNA[15] and its active transport[19–21] can be recapitulated *in vitro*. During mitosis, the *ASH1* mRNA is co-transcriptionally recognized by the RBP She2p[22–26]. Nuclear joining of Loc1p further stabilizes this complex[27]. Following nuclear export, Loc1p is replaced by the cytoplasmic RBP She3p[27], which then results in a synergistic and specific complex of She2p and She3p with any of the four *cis*-acting elements E1, E2A, E2B and E3 of the *ASH1* mRNA[15]. The complex is tethered via She3p to the type V myosin Myo4p[22,23,28] and moves along actin filaments to the tip of the daughter cell, where it is anchored and translationally activated[29–32].

[1]Institute of Structural Biology, Helmholtz Zentrum München – German Research Center for Environmental Health, Neuherberg, Germany. [2]Center for Integrated Protein Science Munich at Biomolecular NMR Spectroscopy, Department Chemie, Technische Universität München, Garching, Germany. [3]Interfaculty Institute of Biochemistry, University of Tübingen, Tübingen, Germany. [4]Biomedical Center of the Ludwig-Maximilians-Universität München, Department of Cell Biology, Planegg-Martinsried, Germany. [5]Architecture et Réactivité de l'ARN, Université de Strasbourg, Centre National de la Recherche Scientifique, Institut de Biologie Moléculaire et Cellulaire, Strasbourg, France. Correspondence should be addressed to D.N. (dierk.niessing@med.uni-muenchen.de).

Received 22 June 2016; accepted 7 December 2016; published online 16 January 2017; doi:10.1038/nsmb.3351

To date, the crystal structures of the tetrameric She2p alone and She2p bound by five residues of She3p have been determined[24,33,34].

Despite this knowledge, it remains unclear how *ASH1* LEs are recognized by the transport machinery and which features are important for specificity. Here we present three X-ray structures of the *ASH1*-E3 LE alone, in complex with its nuclear RBP She2p, and in the cytoplasmic synergistic ternary complex with She2p and She3p. We also carried out *in vitro* and *in vivo* analyses. Together, these results offer unprecedented insights into the assembly path, dynamics and inner architecture of specific LE recognition by a transport machinery.

RESULTS

Defining a minimal E3 RNA element

To design E3-RNA fragments for structural analysis, we first interrogated the secondary structure of the E3 LE by chemical probing of the full-length *ASH1* mRNA with dimethyl sulfate (DMS)[35]. We used this experimentally validated secondary structure of the E3 (51 nucleotides, nt) RNA (**Fig. 1a**) as the basis for mutations.

Although She2p alone was previously shown to bind RNA only transiently with low specificity[24], She3p alone binds completely non-specifically[15]. Only the synergistic binding of She2p and She3p to LEs yields a highly specific and stable RNA recognition for the transport of transcripts[15]. We therefore assessed synergistic RNA recognition by the She2p-She3p complex using an electrophoretic mobility shift assay (EMSA; **Supplementary Fig. 1a**,**b**). Taken together, these findings allowed us to define the minimal E3 (28-nt loop) element that was specifically recognized by the She2p-She3p complex (**Fig. 1b**).

Structural analysis of the *ASH1* E3 element indicates conformational flexibility

Chemical probing suggested that there was flexibility in positions 1,779 and 1,782–1,783 between helices H1 and H2 (**Fig. 1a**). To better understand the structural basis of this flexibility, we performed crystallization trials with the E3 RNA. Given that the E3 (28-nt loop) RNA itself could not be crystallized, we fused the double-stranded stem of E3 (28 nt) to a tetraloop-tetraloop receptor (TL-TLR)[36] (**Fig. 1c**), which provides defined intermolecular RNA interactions for crystallization. This approach yielded crystals of the 42-nt-long RNA fragment (E3, 42-nt TL-TLR), diffracting to 2.65-Å resolution (**Table 1**).

The final structure consisted of an elongated stem loop with both helical regions (H1 and H2) that flanked the flexible bases (**Fig. 1d**). In these helices, the RNA showed continuous coaxial stacking, mostly involving Watson-Crick base pairing. Chemical probing data (**Fig. 1a**) suggested flexibility and likely structural 'breathing' for bases C1779, A1782, A1783 and A1804/C1805 on the opposing strand. Indeed, in the structure, C1779, A1782 and A1783 pointed toward the solvent and showed very little electron density (**Fig. 1d**,**e** and **Supplementary Fig. 2a**).

Given that this heterologous RNA consisted only in part of the E3 element (**Fig. 1a**,**c**), we compared the base pairing of E3 (42-nt TL-TLR) with E3 (28-nt loop) in solution using nuclear magnetic resonance (NMR). We recorded one-dimensional imino proton and two-dimensional imino-NOESY spectra and observed very similar base pairing in E3 (28-nt loop) and in E3 (42-nt TL-TLR) (**Fig. 1f**, **Supplementary Fig. 2b** and **Supplementary Note 1**). In both cases, the lower and upper stems (H1, H2) formed stable base pairs. In contrast, signals for U1780, G1781 and U1784 in the middle, bulged part of the structure exhibited significant line broadening, some of which was beyond detection. This indicates dynamics in the central bulged region of the E3 LE in solution. Although both RNAs showed some differences, the NMR data revealed that a dynamic ensemble of interconverting conformations with varying angles between the H1 and H2 stems exists in solution. A major conformation likely corresponds to the elongated state of the crystal structure (**Fig. 1d**,**e**).

Crystal structure of the nuclear complex consisting of She2p and the *ASH1* E3 element

We used the E3 (28-nt loop) RNA element for co-crystallization trials with its nuclear interaction partner She2p alone or with various She3p peptides. Using an N-terminally truncated and cysteine-to-serine mutated She2p(6-246, C-S) (**Supplementary Fig. 1c**), we obtained crystals that diffracted to 2.41-Å resolution and solved the structure by molecular replacement (**Table 1**). In the complex, two She2p dimers face each other in a head-to-head conformation with a non-crystallographic twofold point symmetry, resulting in an elongated tetramer (**Fig. 2a**). This RNA-bound tetramer showed no major conformational changes compared with its unbound state (r.m.s. deviation of She2p-Cα atoms with PDB 1XLY: 0.70 Å and PDB-ID 4WNL: 0.97 Å). We also observed a short stretch of extra electron density close to She2p, which we determined to be nonphysiological binding by a She3p peptide (**Supplementary Fig. 3a**–**e**).

In the co-structure (**Fig. 2a**), each of the two stem-loop-forming RNA molecules binds to the surface region between the protruding helices of She2p on one of the two sides of the tetramer. Thus, the co-structure enables us to understand why functionally defined features of She2p, such as its tetrameric state and the protruding helices, are essential for RNA binding. Both RNAs on the opposing sides of the tetramer make almost identical contacts with She2p. Although chemical probing and structural analyses of the unbound RNA confirmed a flexible, partially base-paired region in the middle of the stem (positions 1,779 and 1,782–1,783; **Fig. 1a**,**d**–**f**), these residues underwent marked rearrangement upon She2p binding, resulting in a kinked RNA conformation (**Fig. 2a**–**c**, and **Supplementary Figs. 3f** and **4a**).

To confirm that a stably kinked RNA conformation requires She2p binding, we performed small angle X-ray scattering (SAXS) experiments with the free E3 (28-nt loop) RNA. Fitting of an ensemble comprising the elongated (free) and kinked (bound) structure of the RNA with the scattering curve revealed that the elongated RNA conformation was the predominant species of the unbound RNA in solution (**Supplementary Fig. 4b**–**e**). This finding is consistent with the base-pairing that we observed in our NMR data (**Fig. 1f**).

To achieve those conformational changes in the RNA, part of the double-stranded region either changed its base pairing or became unpaired (**Fig. 2c** and **Supplementary Fig. 3f**). For instance, A1783, whose base points toward the solvent in the free RNA, made *cis* Watson-Crick pairs with C1805 on the opposing strand following binding. The resulting kinked RNA conformation was further stabilized by several contacts (**Fig. 2b**) along the positively charged surface region of She2p.

Among the previously described She2p mutants[15,33,37], the point mutations of N36, R52 and R63 each result in a complete loss of function[33,37]. In the tetramer, the four N36 and R63 residues join forces to specifically recognize two cytosines in each of the two almost identical RNAs (**Supplementary Fig. 3g**). On each RNA-binding surface, one set of N36 and R63 jointly contacted the conserved C1779 in the upper part of the stem (**Fig. 2b**,**d**), whereas another N36/R63 pair interacted with the C1813 at the 3′ end (**Fig. 2b**,**e**). R52 made additional RNA backbone contacts with C1779 (**Fig. 2b**,**d**) and C1813 (**Fig. 2b**,**e**). In summary, two sets of N36, R52 and R63 on each side of the symmetric tetramer are key interactors for base-specific binding of two cytosines

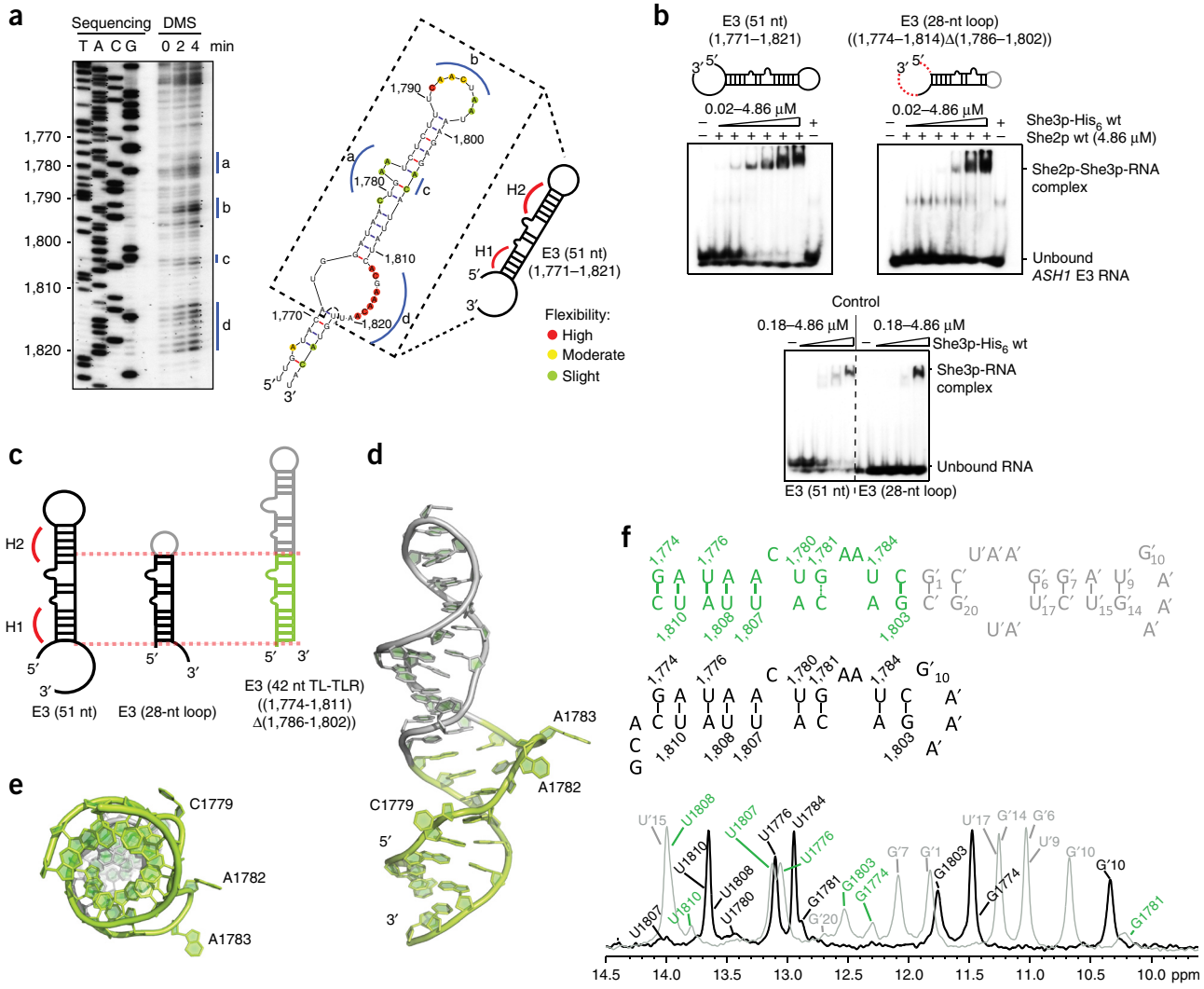

Figure 1 Structure of a minimal *ASH1* E3 localization element. (**a**) Chemical probing of RNA secondary structures with DMS. Left, denaturing TBE-PAGE gel with sequencing reaction next to DMS probing. Right, experimentally validated secondary structure of parts of the *ASH1* E3 element (nt 1,763–1,828). Dashed box indicates the previously defined *ASH1* E3 (51 nt) fragment (nt 1,771–1,821)[15]. Double-stranded RNA helices H1 (nt 1,774–1,778 and 1,807–1,811) and H2 (1,784–1,789 and 1,799–1,804) are highlighted in the scheme. Prediction is based on three independent experiments. (**b**) Representative radioactive EMSA with *ASH1* E3 RNA variants. Red dashed lines indicate base deletions, gray indicates loop base replacements by a GAAA insertion. She2p and She3p were used to identify the minimal E3 RNA fragment. Combining all RNA truncations (**Supplementary Fig. 1**) led to the identification of the minimal E3 element (E3 (28-nt loop)). Final She2p concentrations were 0.02, 0.06, 0.18, 0.54, 1.61 and 4.86 μM. 'Control' shows binding of She3p in the absence of She2p. EMSAs were performed in three independent experiments. (**c**) Secondary structure predictions of different E3 RNA fragments. Green part consists of E3 nucleotides 1,774–1,811, in which positions 1,786–1,802 were replaced by a 17-nt TL-TLR-containing hairpin (gray). (**d**) Crystal structure of the E3 element (green), and the heterologous hairpin (gray) at 2.65-Å resolution. In the stem, bases C1779 and 1,782–1,783 pointed toward the solvent. (**e**) Crystal structure as bottom view of **d**. (**f**) Top, scheme of secondary structures of E3 (42-nt TL-TLR) and E3 (28-nt loop) RNAs based on NMR analyses. Solid lines in the upper scheme represent unambiguous hydrogen bonds indicated by unambiguously assigned imino signals (**Supplementary Fig. 2b**). Dashed line for G1781-C1805 in the 42-mer RNA indicates an assignment of the G imino proton. Bottom, overlay of one-dimensional imino-proton NMR spectra comparing the two RNA fragments.

in each of the asymmetric RNA molecules and act as rulers for their correct distance (37–38 Å between their ribose C1' positions).

In the co-structure, E172 and F176 from the protruding helix of She2p interacted with U1780 (**Fig. 2f**). However, the second set of E172 and F176 amino acids on this side of She2p failed to contact the RNA in the corresponding position (**Fig. 2g**), suggesting that the protruding helix might be less critical for the binary She2p-RNA interaction. In addition, the C terminus of She2p interacts via H238 and K243 with the RNA, or in case of G242 and L244 with one of the two RNAs, explaining its importance for *ASH1* mRNA localization[15].

Minimal C-terminal She3p fragment forming a ternary complex with She2p and RNA

Based on a previous observation that the C terminus of She3p is sufficient for synergistic RNA binding[15], we narrowed down the minimal She3p region to amino acids 331–405 (**Fig. 3a** and **Supplementary Fig. 5a**). However, crystallization trials with this and related fragments in complex with She2p and E3 (28-nt loop) failed. Taking advantage of the fact that She2p and She3p bind to each other with a 1:1 stoichiometry[20], we fused She3p(331–405) to the C terminus of She2p using glycine-serine linkers (GGSGG) of different

Table 1 Data collection and refinement statistics (molecular replacement)

	RNA (5M0H)	RNA-She2p (5M0I)	RNA-She2p-She3p (5M0J)
Data collection			
Space group	$P4_12_12$	$C2$	$C2$
Cell dimensions			
a, *b*, *c* (Å)	64.32, 64.32, 75.19	220.52, 58.34, 146.01	219.03, 58.98, 144.68
α, β, γ (°)	90.0, 90.0, 90.0	90.0, 126.98, 90.0	90.0, 126.91, 90.0
Resolution (Å)	50–2.65 (2.72–2.65)[a]	100–2.41 (2.47–2.41)	100–2.80 (2.87–2.80)
R_{merge} (%)	7.3 (107.2)	6.8 (43.8)	18.9 (98.3)
I/σ (I)	19.93 (2.27)	10.37 (2.13)	10.34 (2.02)
Completeness (%)	99.6 (100.0)	90.1 (91.0)	99.6 (99.6)
Redundancy	7.24 (7.5)	1.9 (1.7)	6.8 (6.8)
Refinement			
Resolution (Å)	45.48–2.65	50.01–2.41	50.01–2.80
Number of reflections	4,920	49,733	35,077
R_{work} / R_{free}	21.1 / 24.0	18.9 / 23.5	19.4 / 24.6
Number of atoms			
Protein	–	7,741	8,218
RNA	894	1,192	1,192
Ion[b,c,d]	5[b]	30[c,d]	4[c]
Ligand[e]	–	44[e]	–
Water	10	333	207
B factors			
Protein	–	83.5	60.1
RNA	91.9	59.2	46.8
Ion[b,c,d]	49.0[b]	64.8[c,d]	59.4[c]
Ligand[e]	–	63.1[e]	–
Water	67.7	50.5	29.7
r.m.s. deviations			
Bond lengths (Å)	0.01	0.02	0.01
Bond angles (°)	1.21	1.88	1.45

For each data set, only one crystal was used.
[a]Values in parentheses are for highest-resolution shell. Specification of ions: [b]sulfate, [c]magnesium, [d]acetate. Identity of ligand: [e]1,2-ethanediol.

lengths (**Supplementary Fig. 5b**). In EMSA, this fusion protein mediated synergistic RNA binding (**Supplementary Fig. 5c**).

Structure of the mature cytoplasmic mRNA-recognition complex

Crystallization trials with the fusion construct She2p(6-246, C-S)-$(GGSGG)_2$-She3p(331-405) and the E3 (28-nt loop) RNA yielded crystals that diffracted to 2.8-Å resolution (**Table 1**). Following RNA binding, the She2p tetramer did not undergo larger changes (r.m.s. deviation of She2p-Cα atoms = 0.68 Å; **Figs. 2a** and **3b**). In addition, electron density was visible for two different regions of each She3p molecule. The first She3p fragment includes residues 338–351 and binds to RNA as well as to She2p. This RNA- and protein-contacting site (R site) (**Fig. 3b**) buried a surface area of 922 $Å^2$ (**Supplementary Fig. 5d–f**). The second She3p fragment spanned residues 361–371 and made exclusively protein contacts with She2p (P site), masking a smaller region of 630 $Å^2$ (**Supplementary Fig. 5d**). This P site interaction is almost identical to a previous crystal structure of She2p bound by a short P site peptide spanning from L364 to K368 (ref. 34).

The R site region of She3p formed a very short alpha helix that was sandwiched between the protruding helix of She2p and the 3′-end of the E3 RNA allowing for numerous protein-protein (**Supplementary Table 1**) and protein-RNA contacts (**Fig. 3c–e**). R341 of She3p has a special role, as it cooperated with K60 of She2p to contact the phosphate backbones of RNA bases U1780 and C1813 in both R sites (**Fig. 3d**,**e**). In addition, the strong quaternary recognition of the conserved cytosines C1779 and C1813 (ref. 18) by She2p (**Fig. 2d**,**e**) was maintained and further stabilized by R341 of She3p (**Fig. 3e**). On the other hand, She3p joining disrupted the third base-specific interaction of She2p between F176 on the protruding helix and U1780 of the RNA (**Fig. 2b**,**f**). As a substitute, She3p Y345 underwent aromatic stacking with She2p F176 (**Fig. 3f**). As a consequence, U1780 pointed toward the solvent (**Fig. 3g**) and was stabilized by R341 (**Fig. 3f**,**g**). The R site binding with She2p was mediated by a total of eight She3p residues (**Supplementary Table 1** and **Supplementary Fig. 5d–f**). In particular, the tight coordination of She3p F344 by She2p residues T53, I56, K57, K60 and Y115 (**Fig. 3h**) demonstrates how well She2p has adapted to specifically interact with the largely unstructured She3p.

Three RNA bases mediate sequence-specific complex formation in solution

To confirm that the nucleotides C1779, U1780 and C1813, which were base-specifically recognized by distinct amino acids of She2p, are also important for LE recognition in solution, we performed EMSA with She2p, She3p and different versions of the E3 (51 nt) RNA. Mutant M1 and M2 (**Fig. 4a** and **Supplementary Fig. 6**) impaired binding, indicating that position 1,780 had to be an uracil. Given that these exchanges potentially changed the capability to form base pairs at least in the unbound state (**Fig. 1a**,**d**,**f**), we introduced a complementary exchange (M3) that resulted in a complete loss of RNA binding (**Fig. 4a**). A closer inspection of base contacts in this region (**Supplementary Fig. 3f**) revealed that mutation of C1805 to G led

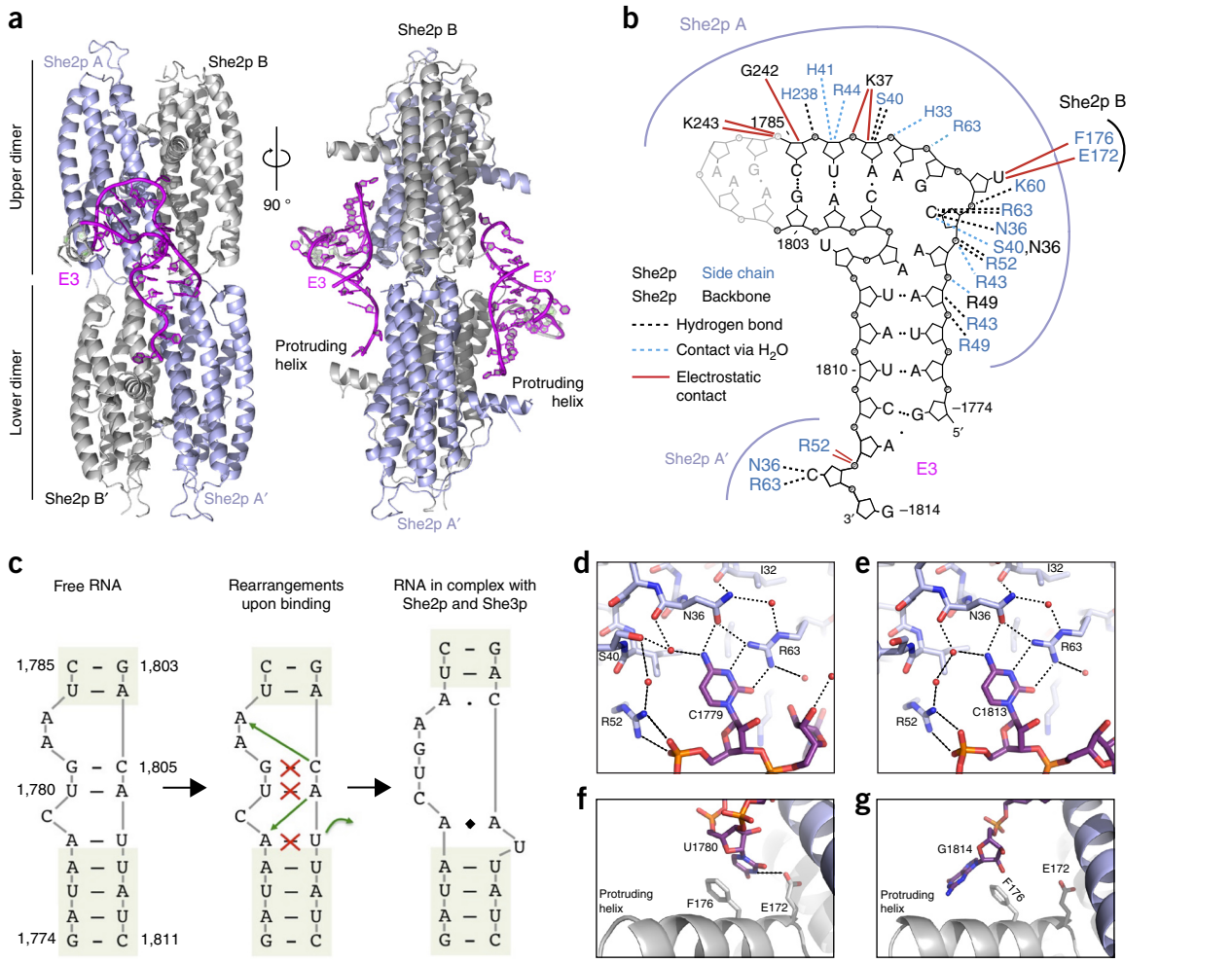

Figure 2 Crystal structure of She2p with RNA. (**a**) Crystal structure of She2p(6-246, C-S) with the *ASH1* E3 (28-nt loop) RNA at 2.41-Å resolution in front view and rotated 90 ° around the vertical axis. She2p forms a tetramer with two dimers in a head-to-head conformation. The two subunits of each dimer are shown in light blue (A, A') and gray (B, B'). She2p binds asymmetrically to two RNA molecules (E3, E3′ in pink) with an L-like shape. The heterologous tetranucleotide-loop is shown in gray. (**b**) Schematic drawing of protein contacts with one of the RNAs. Each of the two RNA chains contacts three She2p subunits. (**c**) Cartoon showing that the central region of the stem in the *ASH1* E3 LE undergoes large conformational rearrangements following complex formation. The She2p-bound conformation (right) is stabilized by protein contacts. Nucleotides marked in gray maintain their base-pairing upon binding. Diamond indicates that A1778 interacts via its base with the ribose of A1806. (**d**–**g**) Close-up images of **a**. (**d**) She2p binding of the conserved C1779 is tightly coordinated by N36 and R63 of the upper dimer. N36 is fixed in its orientation via I32 interaction and hydrogen bonding of S40. Coordination of the second conserved cytosine in position 1813, again by N36, R52 and R63 is depicted in **e**. For better comparison with **d**, image in **e** is rotated. (**f**) Outwards pointing uracil 1780, which binds to E172 and base stacks with F176 of the protruding helix of She2p. (**g**) G1814 at the 3′-end of the RNA, where the proximate F176 and E172 of the lower dimer fail to interact with *ASH1* mRNA.

to repulsive forces with A1783. Mutation A1806U resulted in weaker base stacking between A1777 and A1778. Thus, the sequence in this position is important for RNA binding.

Mutation of either the specifically recognized C1779 or C1813 (**Fig. 3c**) resulted in a complete loss of RNA binding (mutants M4, M5, M6 and M7; **Fig. 4b**,**c**). The requirement of specific interactions on both dimer sides of the tetramer is consistent with the previously described L130Y mutant that disrupts the dimer-dimer interface and results in a loss of mRNA binding and mRNA localization[24]. In summary, both specifically bound cytosines are essential for LE-RNA recognition in solution, whereas U1780 has a more modest influence on binding.

Mutational analysis of She2p and She3p confirm binding mode in solution

In the crystal structure, the R site region 338–351 of She3p intercalates between the protruding helix of She2p and the E3 RNA (**Fig. 3d**,**e**). We designed a triple mutation in She3p(331–405) that abolished three important interactions (K340A, R341A and Y345A) and observed a loss of RNA binding (**Fig. 4d** and **Supplementary Fig. 7a**,**b**). In addition, the single mutations K340A, R341A, R342A, F344A and Y345A all resulted in an impaired RNA binding with She2p (**Supplementary Fig. 8**).

In She2p, the deletion of the protruding helix abolished synergistic RNA binding and mRNA localization[15]. The crystal structure of the binary complex revealed that E172 and F176 in the protruding helix of She2p made important contacts to U1780 (**Fig. 2f**). EMSA with a She2p(E172A, F176A) double mutant and She3p showed a loss of binding (**Fig. 4e** and **Supplementary Fig. 7c**), confirming that these specific contacts are indeed essential for ternary complex formation.

Specific contacts are essential for mRNA localization *in vivo*

To verify key interactions *in vivo*, we analyzed mRNA localization with mutant versions of *SHE2* or *SHE3*, using an MS2-aptamer tagged

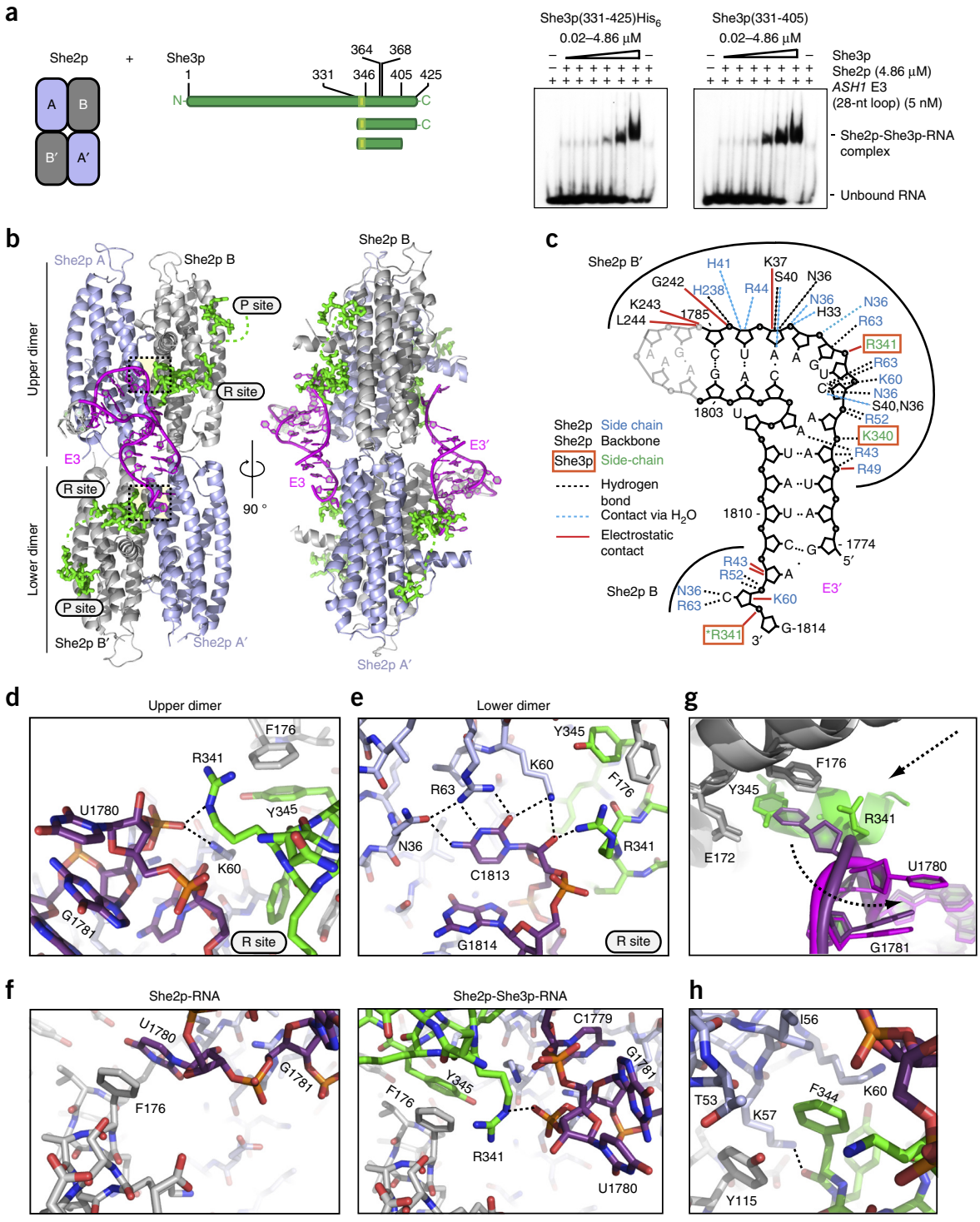

Figure 3 Crystal structure of synergistic ternary complex of She2p, She3p and E3 RNA. (**a**) Schematic drawing (left) of She2p with its four protomers and different She3p fragments. She3p region previously shown to UV-crosslink to *ASH1* E3 (51 nt)[15] is depicted in light green. EMSA (right) with E3 (28-nt loop), She2p and She3p fragments revealed that residues 406–425 of She3p are dispensable for RNA binding. EMSAs were performed as three independent experiments. (**b**) Crystal structure of She2p(6-246, C-S) fused to She3p(331–405) (**Supplementary Fig. 5a–c**) in complex with *ASH1* E3 (28-nt loop) RNA at 2.80-Å resolution in front view and 90° rotated clockwise around the vertical axis. Representation is identical to that shown in **Figure 2;** She3p is depicted in green. Boxed regions in the upper and lower dimer are shown as close-ups in **d** and **e**. (**c**) Schematic drawing of protein-RNA contacts in the ternary complex. Contact R341 marked with an asterisk occurred only in one RNA molecule. (**d–h**) Close-up images of **b**. Close-ups of the upper and lower She2p dimers (boxed regions in **b**) are shown in **d** and **e**, respectively. In both cases, She3p intercalates between F176 of the protruding helix and the RNA. (**f**) The local environment of She2p F176 in the binary and the ternary complex. Following She3p binding, the aromatic stacking of U1780 with F176 of the protruding helix of She2p (left) was displaced by the joining of She3p Y345 (right). As a result, U1780 became solvent exposed. (**g**) Following joining of She3p (R site), U1780 was displaced by Y345 from its interaction with E172 and F176. (**h**) Coordination of the conserved F344 from She3p[15] by I56, K57, K60, T53 and Y115 of She2p via non-bonded contacts with up to 4.6-Å distance. K57 binds to the F344 backbone through a salt bridge.

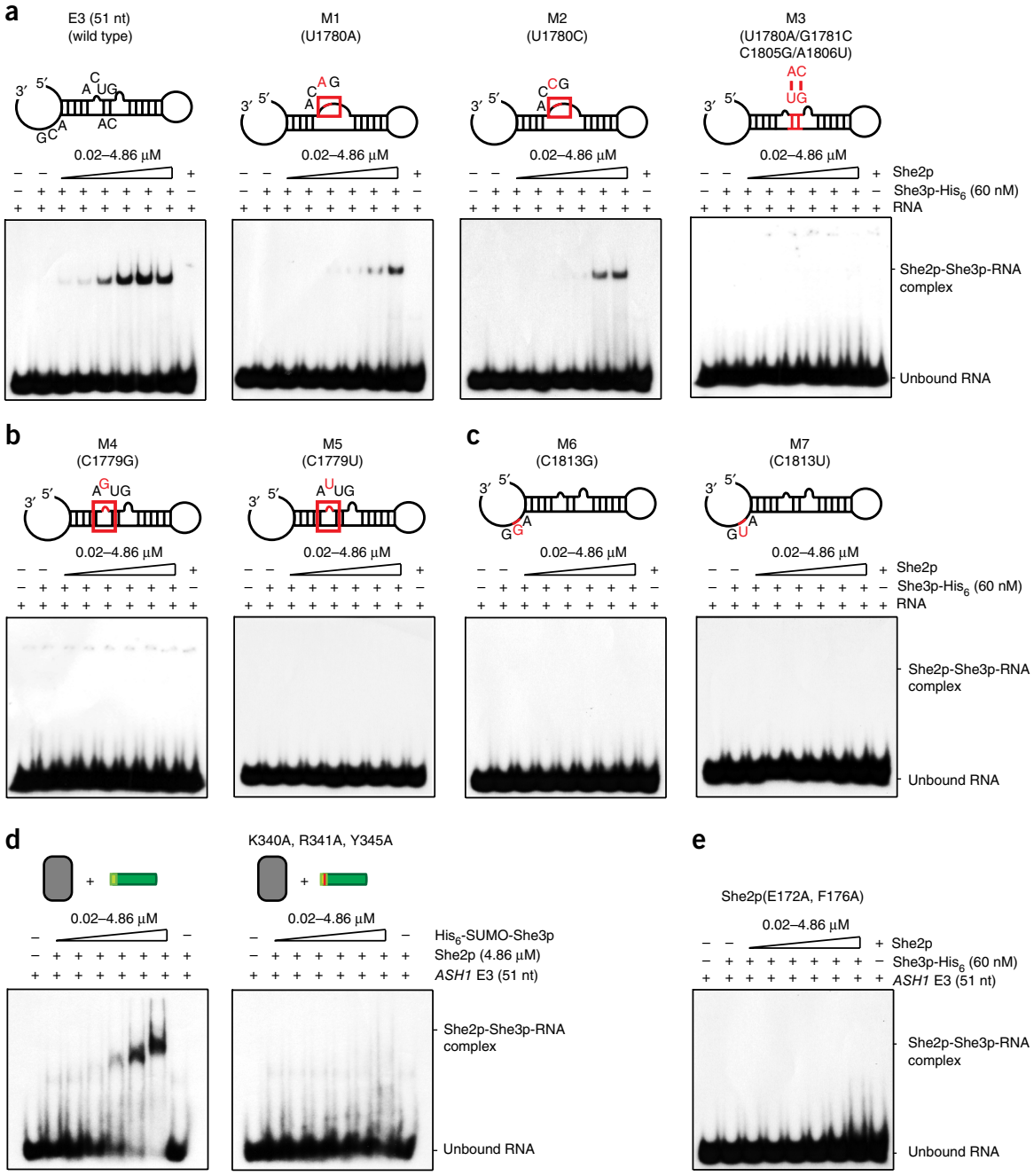

Figure 4 EMSAs with mutated versions of *ASH1* E3 RNA, She2p and She3p. (**a**–**c**) Representative radioactive EMSA with wild-type and mutant versions of *ASH1* E3 (51 nt) RNA assessing the ternary complex formation with She2p and full-length She3p. (**a**) Mutation of U1780 to either A or C diminished RNA binding. EMSA with the quadruple mutant U1780A/G1781C, C1805G/A1806U, which mimics the secondary structure of the E3 (51 nt) RNA in the unbound state, revealed a complete loss of interaction. Mutation of the conserved C1779 (**b**) and C1813 (**c**) either into the purine guanine or the pyrimidine uracil resulted in complete loss of ternary complex formation. (**d**) EMSA with His_6-SUMO-She3p(331–405), She2p and *ASH1* E3 (51 nt) RNA showed binding, whereas ternary complex formation of the triple mutant She3p(331–405; K340A, R341A, Y345A) was markedly decreased. (**e**) EMSA with E3 (51 nt) RNA, full-length She3p and a mutated version of She2p(E172A, F176A) revealed strongly reduced binding. For all EMSAs in this figure, one of three independent experiments is shown.

version of the *ASH1* mRNA[13]. Yeast strains expressing She3p with either mutations in the R site or in the P site essentially abolished mRNA localization (**Fig. 5**, **Table 2** and **Supplementary Fig. 9a**). *In vitro*, mutation of the R site contacts in She2p(E172A, F176A) destroyed synergistic E3-LE binding (**Fig. 4e**). In addition, *in vivo*, this mutant was unable to mediate mRNA localization (**Fig. 5**, **Table 2** and **Supplementary Fig. 9a**). Thus, both the R and the P site are essential for mRNA localization *in vivo*.

DISCUSSION

Specific mRNA localization requires the selective recognition of transcripts by dedicated RBPs. Two problems hamper a detailed

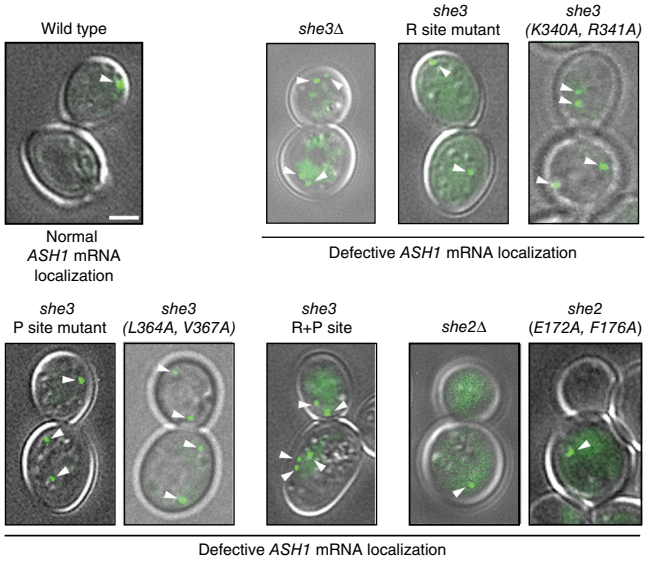

Figure 5 *In vivo* assessment of specific *ASH1* mRNA recognition by She2p and She3p. Using the MS2-GFP reporter system, *ASH1* mRNA localization was assessed. Shown are pictures of the merged differential interference contrast and GFP channels. Cells with exclusive *ASH1*-particle signal at the bud tip were considered to be wild-type localized, and cells with particles only in mother cell or in both cells were considered to be mislocalized. Scale bar represents 2 µm, arrowheads show GFP-containing particles. Corresponding statistical evaluation is listed in **Table 2**.

Table 2 Quantification of *ASH1*-mRNA localization in different yeast strains

Strain	Yeast cells showing normal *ASH1* mRNA localization (%)	Total cell number	Number of experiments (*n*)
Wild type	73.2 ± 7.8	95	3
*she3*Δ	13.4 ± 3.2	89	3
she3 R site mutant (340–346A)	19.7 ± 5.2	95	3
she3 (K340A, R341A)	25.5 ± 7.7	207	6
she3 P site mutant (340–346A)	12.9 ± 3.3	93	3
she3 (L364A, V367A)	18.7 ± 4.7	192	6
she3 R + P site mutant (340–346A, 346–368A)	15.7 ± 3.4	102	3
*she2*Δ	23.0 ± 0.6	104	3
she2 (E172A, F176A)	22.9 ± 6.1	308	9

73% of wild-type cells localized *ASH1* mRNA, whereas in *she2*Δ and *she3*Δ cells or in cells expressing proteins with mutations in the P or R sites only 25% or less localization was observed. Data shown are mean values in percent ± s.d. of budding yeast cells showing bud-tip-only *ASH1* mRNA localization (specified as normal *ASH1* mRNA localization) of *n* independent cell culture replicates. Expression of mutant She2p and She3p proteins was confirmed by western blot (**Supplementary Fig. 9a**). Only the R site mutant *she3* (K340A, R341A, Y345A) failed to show any expression (**Supplementary Fig. 9a**). Thus, no analysis is provided for this mutant. Source data are provided in **Supplementary Data Set 1**.

understanding of these recognition events. First, RBPs rarely recapitulate *in vitro* the highly specific recognition of mRNAs observed *in vivo*[38]. This is most likely a result of specificity-mediating co-factors that have not been identified in most systems. The highly specific binding of the *ASH1* mRNA by the joint action of She2p and She3p constitutes a rare exception. Second, *cis*-acting elements of localizing mRNAs usually show no recognizable conservation on the sequence or secondary structure level, indicating that structural information might be essential. To the best of our knowledge, no high-resolution structure is available for any *cis*-acting LE in complex with its cognate protein complex of the mRNA-transport machinery.

We carried out a comprehensive structural and functional analysis of how an mRNA-transport complex specifically recognizes its stem-loop-containing LE RNA. We observed that the *cis*-acting E3 LE of the *ASH1* mRNA alone adopted an elongated stem loop with a highly dynamic bulge region between helices H1 and H2 (step 1; **Fig. 6**). Following co-transcriptional binding[39], She2p recognized the RNA in its kinked state most likely via conformational selection from a dynamic ensemble of RNA conformations with varying angles of H1 and H2, consistent with NMR and SAXS data. The transition from elongated to kinked state required the RNA to undergo marked conformational changes (step 2; **Fig. 6**). Two LEs interacted on opposing sides of the She2p tetramer, thereby formally establishing that the oligomeric state of the specifically RNA-recognizing She2p is indeed a tetramer. This complex was further stabilized by the nucle(ol)ar RBP Loc1p (step 2; **Fig. 6**)[27]. In the cytoplasm, the motor-bound She3p replaced Loc1p and bound to She2p with two motifs: the P site, which exclusively undergoes protein-protein interactions, and the R site, which contacts both She2p and the RNA (steps 3 and 4; **Fig. 6**). The R sites of She3p intercalated between the two protruding helices of She2p and the kinked E3 LE. This resulted in a stabilization of the complex and additional conformational restraints. Given that She3p-RNA contacts are rather RNA-sequence unspecific, the increase in specificity following She3p binding is mainly achieved by a more precise recognition of the RNA shape.

One of the most notable features of the co-structure is that the She2p tetramer was point symmetric, whereas the RNA was not. As a consequence, each of the two binding surfaces of She2p used two identical sets of amino acids to contact distinct regions of its bound RNA (**Figs. 2a**,**b**, **3b**,**c** and **6**). This dual use approach of residues N36, R43, R52, K60 and R63 explains the marked reduction of binding following their mutation[15,37]. Additional reported contacts between She2p residues 164–179 and a longer *ASH1* E3-RNA fragment[15] can also be explained by our structure. These residues would be perfectly located to interact with a continuation of the 3′ end of the E3 (28-nt loop) RNA, which would be present in longer E3 fragments (**Supplementary Fig. 5g**).

In the co-structure of She2p and RNA only few contacts were observed between the protruding helix and nucleic acids (**Fig. 2b**,**f**). Given that the protruding helix of She2p is important for mRNA localization *in vivo*[15], it is likely to be more critical for the joining of She3p. Indeed, She3p intercalated with its R site between the protruding helix and the RNA, and stabilized their interaction. Similar to the dual binding of She2p residues, the symmetric interaction of She3p at the R site (**Figs. 3b**,**c** and **6**) occurs with two different regions of the RNA that are about 30 Å apart from each other. This provides additional sequence-independent RNA contacts that greatly decrease the spatial freedom of binding and result in strongly improved affinity and specificity.

A comparison of R and P site interactions (**Fig. 3b**) revealed that the R site buries a much bigger surface area (**Supplementary Fig. 5d**) and that the P site does not provide any direct contribution to RNA recognition. Thus, contrary to previous suggestions[34], our findings point to a rather supporting, complex-stabilizing role of the P site. Our *in vivo* analysis revealed that both sites have to work together, as each of them was essential for mRNA localization (**Fig. 5** and **Table 2**).

The two highly coordinated cytosines C1779 and C1813 (**Figs. 2b**–**e** and **3c**,**e**) are essential for mRNA localization[16]. Our structural work revealed that these two bases were the only specifically bound

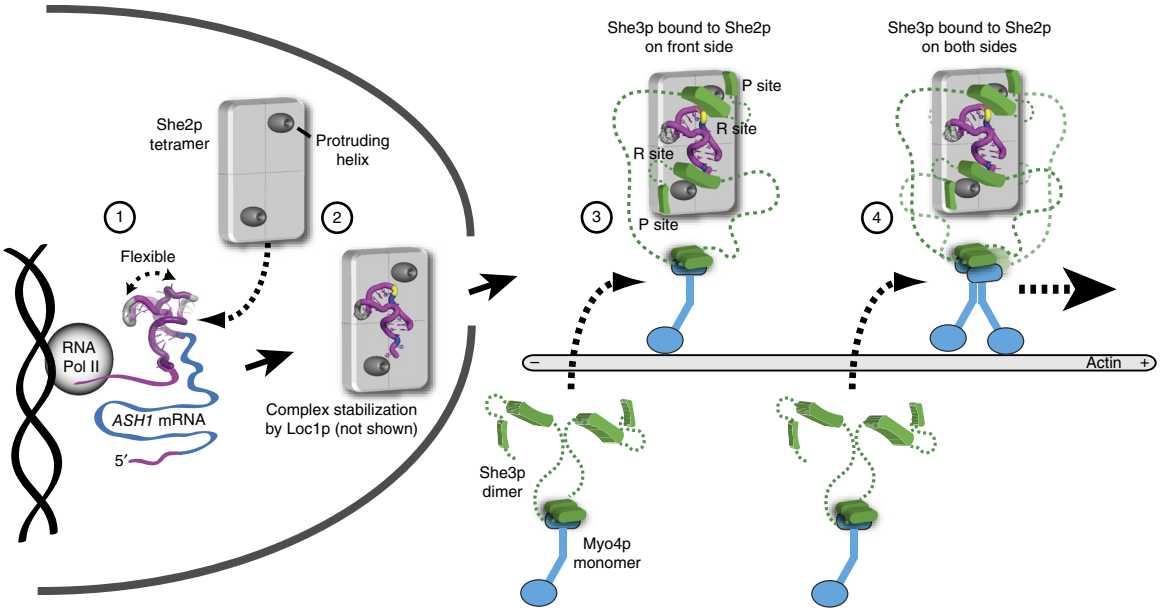

Figure 6 Model of specific *ASH1* mRNA recognition and transport by She2p and She3p. Structure-based model for the step-wise assembly of the synergistic ternary complex. Step 1, the *ASH1* E3 RNA alone forms a stem loop with a dynamic bulge region in its stem that acts as flexible hinge. Step 2, following co-transcriptional binding to She2p, the LE undergoes marked rearrangements in the bulged region of the stem and aligns in an L-like shape along the She2p tetramer. Steps 3 and 4, after nuclear export, She3p joins the She2p-RNA complex on both sides of the She2p tetramer, mainly introducing steric constraints that markedly increase specificity and affinity for the RNA. Given that *ASH1* mRNA contains four zip-code elements and the She complex has two RNA-binding sites, the transcript can either concatenate several SHE complexes into large particles[20] or bind to two different RNA molecules at the same time[20,44].

nucleotides in the nuclear She2p-RNA complex, recognized by the triad of amino acids N36, R52 and R63 in the symmetric tetramer (**Fig. 2b**,**d**,**e**). Following joining of She3p in the cytoplasm, U1780 changed its orientation toward the solvent to make space for the interaction between She3p Y345 and She2p F176 (**Fig. 3d**,**f**,**g**). This conformational change required a uridine in this particular position (**Fig. 4a**). Thus, joining of She3p introduced another sequence requirement in U1780. In addition to the specific recognition of two cytosines and one uridine, mismatches in the stem were essential for allowing major rearrangements during its recognition by She2p and She3p (**Fig. 2c**). In summary, we were able to identify for the first time the features defining a *cis*-acting LE. They consist of a combination of structural and sequence constraints that were impossible to predict. Of note, not only She2p, but also the interacting She3p, recognized the asymmetric RNA in a symmetric way. Thus, the symmetric arrangement of the protein complex is the predominant organization principle of this specific RNA-recognition particle.

Previous studies have shown that the two essential cytosines can also be found in other LEs of the *ASH1* mRNA[16,17]. Even a structural model for LEs was presented[16]. However, this model failed to predict the mismatches and structural flexibility of the RNA, and therefore also the correct spacing of the cytosines (predicted 28 Å instead of 38 Å). Furthermore, uracil in position 1780 of E3 lacked other LEs (**Supplementary Fig. 9b**), indicating an alternative local binding mode in a corresponding position. Thus, additional high-resolution structures will be required to fully comprehend the features unique to all SHE-dependent LEs.

In recent proteome-wide studies, a considerable number of proteins with intrinsically disordered regions (IDRs) were identified as RBPs[40]. This raised the question of how specific these IDR-RBPs bind to RNAs and what their physiologic importance is. The combined *ASH1*-LE RNA recognition by the globular She2p and the unfolded She3p offers a detailed example of how an IDR can be used for specific RNA recognition. Complex joining of the rather unstructured C-terminal part of She3p modulates an existing binding event by the globular She2p to become more specific.

The inability to recapitulate *in vitro* the specific RNA binding of an RBP observed *in vivo* has been often attributed to the potential requirement of additional (globular) RNA-binding domains that jointly recognize RNAs[38]. Our results indicate that this principle can be extended to combinations of globular RBPs and IDR-RBPs. It is tempting to speculate that several of the recently discovered IDR-RBPs[40] act in such combinatorial ways with globular RBPs to achieve higher affinity and specificity in RNA binding.

Another unusual feature is the conformational dynamics of the E3 RNA binding. Such dynamics have been mainly described as being functionally important for non-coding RNAs, including ribosomal RNAs[41], and particularly RNA elements with catalytic activity, such as riboswitches[42] or the spliceosome[43]. In contrast, *cis*-acting RNA elements whose main function is to be specifically recognized are considered to be static in their structure[9]. Our observation that conformational dynamics are also important for the recognition of otherwise passive RNA elements questions this distinction. Given that three out of four *ASH1* LEs reside in the open reading frame, the avoidance of stem-loop rigidity in this area could be a precondition for efficient translation after anchoring at the bud tip. Future work will be needed to determine whether flexibility in LE RNAs is required for functions beyond their sole recognition by the transport machinery.

METHODS

Methods, including statements of data availability and any associated accession codes and references, are available in the online version of the paper.

Note: Any Supplementary Information and Source Data files are available in the online version of the paper.

ACKNOWLEDGMENTS

We thank V. Roman for her support, and M. Seiler and M. Feldbrügge for helpful discussions. We acknowledge the use of the X-ray crystallography platform of the Helmholtz Zentrum München, NMR measurements at the Bavarian NMR center and SAXS measurements at the facility of the SFB1035, Technische Universität München. This work was supported by the Deutsche Forschungsgemeinschaft (SFB1035 to M.S.; SPP1935 to M.S. and D.N.; FOR2333 to R.-P.J. and D.N.; SFB646 to D.N.) and by the Bayerisch-Französisches Hochschulzentrum (BFHZ) to D.N.

AUTHOR CONTRIBUTIONS

F.T.E., A.S., R.G.H., A.J., A.N.-B., M.I.S. and R.S. conducted the experiments. F.T.E., A.S., R.G.H., R.-P.J., J.-C.P. and D.N. designed the experiments. F.T.E., A.S., R.G.H., A.N.-B., R.S., R.J., M.S., R.-P.J. and D.N. analyzed the data. F.T.E. and D.N. wrote the paper.

COMPETING FINANCIAL INTERESTS

The authors declare no competing financial interests.

1. Holt, C.E. & Bullock, S.L. Subcellular mRNA localization in animal cells and why it matters. *Science* **326**, 1212–1216 (2009).
2. Tolino, M., Köhrmann, M. & Kiebler, M.A. RNA-binding proteins involved in RNA localization and their implications in neuronal diseases. *Eur. J. Neurosci.* **35**, 1818–1836 (2012).
3. St Johnston, D. Moving messages: the intracellular localization of mRNAs. *Nat. Rev. Mol. Cell Biol.* **6**, 363–375 (2005).
4. Marchand, V., Gaspar, I. & Ephrussi, A. An intracellular transmission control protocol: assembly and transport of ribonucleoprotein complexes. *Curr. Opin. Cell Biol.* **24**, 202–210 (2012).
5. Buxbaum, A.R., Haimovich, G. & Singer, R.H. In the right place at the right time: visualizing and understanding mRNA localization. *Nat. Rev. Mol. Cell Biol.* **16**, 95–109 (2015).
6. Munro, T.P. *et al.* Mutational analysis of a heterogeneous nuclear ribonucleoprotein A2 response element for RNA trafficking. *J. Biol. Chem.* **274**, 34389–34395 (1999).
7. Chao, J.A. *et al.* ZBP1 recognition of beta-actin zipcode induces RNA looping. *Genes Dev.* **24**, 148–158 (2010).
8. Patel, V.L. *et al.* Spatial arrangement of an RNA zipcode identifies mRNAs under post-transcriptional control. *Genes Dev.* **26**, 43–53 (2012).
9. Jambhekar, A. & Derisi, J.L. Cis-acting determinants of asymmetric, cytoplasmic RNA transport. *RNA* **13**, 625–642 (2007).
10. Pratt, C.A. & Mowry, K.L. Taking a cellular road-trip: mRNA transport and anchoring. *Curr. Opin. Cell Biol.* **25**, 99–106 (2013).
11. Bullock, S.L., Ringel, I., Ish-Horowicz, D. & Lukavsky, P.J. A′-form RNA helices are required for cytoplasmic mRNA transport in *Drosophila*. *Nat. Struct. Mol. Biol.* **17**, 703–709 (2010).
12. Simon, B., Masiewicz, P., Ephrussi, A. & Carlomagno, T. The structure of the SOLE element of oskar mRNA. *RNA* **21**, 1444–1453 (2015).
13. Bertrand, E. *et al.* Localization of *ASH1* mRNA particles in living yeast. *Mol. Cell* **2**, 437–445 (1998).
14. Gonzalez, I., Buonomo, S.B., Nasmyth, K. & von Ahsen, U. *ASH1* mRNA localization in yeast involves multiple secondary structural elements and Ash1 protein translation. *Curr. Biol.* **9**, 337–340 (1999).
15. Müller, M. *et al.* A cytoplasmic complex mediates specific mRNA recognition and localization in yeast. *PLoS Biol.* **9**, e1000611 (2011).
16. Olivier, C. *et al.* Identification of a conserved RNA motif essential for She2p recognition and mRNA localization to the yeast bud. *Mol. Cell. Biol.* **25**, 4752–4766 (2005).
17. Jambhekar, A. *et al.* Unbiased selection of localization elements reveals cis-acting determinants of mRNA bud localization in *Saccharomyces cerevisiae*. *Proc. Natl. Acad. Sci. USA* **102**, 18005–18010 (2005).
18. Niedner, A., Edelmann, F.T. & Niessing, D. Of social molecules: the interactive assembly of ASH1 mRNA-transport complexes in yeast. *RNA Biol.* **11**, 998–1009 (2014).
19. Edelmann, F.T., Niedner, A. & Niessing, D. ASH1 mRNP-core factors form stable complexes in absence of cargo RNA at physiological conditions. *RNA Biol.* **12**, 233–237 (2015).
20. Heym, R.G. *et al. In vitro* reconstitution of an mRNA-transport complex reveals mechanisms of assembly and motor activation. *J. Cell Biol.* **203**, 971–984 (2013).
21. Sladewski, T.E., Bookwalter, C.S., Hong, M.S. & Trybus, K.M. Single-molecule reconstitution of mRNA transport by a class V myosin. *Nat. Struct. Mol. Biol.* **20**, 952–957 (2013).
22. Böhl, F., Kruse, C., Frank, A., Ferring, D. & Jansen, R.P. She2p, a novel RNA-binding protein tethers *ASH1* mRNA to the Myo4p myosin motor via She3p. *EMBO J.* **19**, 5514–5524 (2000).
23. Long, R.M., Gu, W., Lorimer, E., Singer, R.H. & Chartrand, P. She2p is a novel RNA-binding protein that recruits the Myo4p-She3p complex to *ASH1* mRNA. *EMBO J.* **19**, 6592–6601 (2000).
24. Müller, M. *et al.* Formation of She2p tetramers is required for mRNA binding, mRNP assembly, and localization. *RNA* **15**, 2002–2012 (2009).
25. Shahbabian, K., Jeronimo, C., Forget, A., Robert, F. & Chartrand, P. Co-transcriptional recruitment of Puf6 by She2 couples translational repression to mRNA localization. *Nucleic Acids Res.* **42**, 8692–8704 (2014).
26. Shen, Z., Paquin, N., Forget, A. & Chartrand, P. Nuclear shuttling of She2p couples ASH1 mRNA localization to its translational repression by recruiting Loc1p and Puf6p. *Mol. Biol. Cell* **20**, 2265–2275 (2009).
27. Niedner, A., Müller, M., Moorthy, B.T., Jansen, R.P. & Niessing, D. Role of Loc1p in assembly and reorganization of nuclear ASH1 messenger ribonucleoprotein particles in yeast. *Proc. Natl. Acad. Sci. USA* **110**, E5049–E5058 (2013).
28. Takizawa, P.A. & Vale, R.D. The myosin motor, Myo4p, binds *Ash1* mRNA via the adapter protein, She3p. *Proc. Natl. Acad. Sci. USA* **97**, 5273–5278 (2000).
29. Bobola, N., Jansen, R.P., Shin, T.H. & Nasmyth, K. Asymmetric accumulation of Ash1p in postanaphase nuclei depends on a myosin and restricts yeast mating-type switching to mother cells. *Cell* **84**, 699–709 (1996).
30. Chartrand, P., Meng, X.H., Hüttelmaier, S., Donato, D. & Singer, R.H. Asymmetric sorting of ash1p in yeast results from inhibition of translation by localization elements in the mRNA. *Mol. Cell* **10**, 1319–1330 (2002).
31. Long, R.M. *et al.* Mating type switching in yeast controlled by asymmetric localization of *ASH1* mRNA. *Science* **277**, 383–387 (1997).
32. Takizawa, P.A., Sil, A., Swedlow, J.R., Herskowitz, I. & Vale, R.D. Actin-dependent localization of an RNA encoding a cell-fate determinant in yeast. *Nature* **389**, 90–93 (1997).
33. Niessing, D., Hüttelmaier, S., Zenklusen, D., Singer, R.H. & Burley, S.K. She2p is a novel RNA binding protein with a basic helical hairpin motif. *Cell* **119**, 491–502 (2004).
34. Singh, N., Blobel, G. & Shi, H. Hooking She3p onto She2p for myosin-mediated cytoplasmic mRNA transport. *Proc. Natl. Acad. Sci. USA* **112**, 142–147 (2015).
35. Tijerina, P., Mohr, S. & Russell, R. DMS footprinting of structured RNAs and RNA-protein complexes. *Nat. Protoc.* **2**, 2608–2623 (2007).
36. Ferré-D'Amaré, A.R., Zhou, K. & Doudna, J.A. A general module for RNA crystallization. *J. Mol. Biol.* **279**, 621–631 (1998).
37. Gonsalvez, G.B. *et al.* RNA-protein interactions promote asymmetric sorting of the *ASH1* mRNA ribonucleoprotein complex. *RNA* **9**, 1383–1399 (2003).
38. Lunde, B.M., Moore, C. & Varani, G. RNA-binding proteins: modular design for efficient function. *Nat. Rev. Mol. Cell Biol.* **8**, 479–490 (2007).
39. Shen, Z., St-Denis, A. & Chartrand, P. Co-transcriptional recruitment of She2p by RNA pol II elongation factor Spt4-Spt5/DSIF promotes mRNA localization to the yeast bud. *Genes Dev.* **24**, 1914–1926 (2010).
40. Calabretta, S. & Richard, S. Emerging roles of disordered sequences in RNA-binding proteins. *Trends Biochem. Sci.* **40**, 662–672 (2015).
41. McGinnis, J.L. *et al.* In-cell SHAPE reveals that free 30S ribosome subunits are in the inactive state. *Proc. Natl. Acad. Sci. USA* **112**, 2425–2430 (2015).
42. Fürtig, B., Nozinovic, S., Reining, A. & Schwalbe, H. Multiple conformational states of riboswitches fine-tune gene regulation. *Curr. Opin. Struct. Biol.* **30**, 112–124 (2015).
43. Chen, W. & Moore, M.J. The spliceosome: disorder and dynamics defined. *Curr. Opin. Struct. Biol.* **24**, 141–149 (2014).
44. Lange, S. *et al.* Simultaneous transport of different localized mRNA species revealed by live-cell imaging. *Traffic* **9**, 1256–1267 (2008).

ONLINE METHODS

Cloning strategies. A detailed description of cloning strategies (**Supplementary Note 2**) and a complete list of plasmids (**Supplementary Table 2**) and oligonucleotides (**Supplementary Table 3**) have been provided as Supplementary Information.

Protein expression and purification. *SHE2* wild type, *SHE2(6-246, C-S)* and *SHE2_E172A_F176A,* in pGEX-6P-1 were expressed in *Escherichia coli* BL21(DE3) Star cells. Harvested cells (2,449*g*, 10 min, 4 °C) were resuspended in 25 ml GST-A1 buffer (20 mM Hepes/NaOH pH 7.5, 500 mM NaCl, 1 mM EDTA, 2 mM DTT), including cOmplete Protease Inhibitor (Roche Diagnostics) and disrupted by sonification. Cleared lysate (39,191*g*, 30 min, 4 °C), was loaded on a GSTrap FF (5 ml) column (GE Healthcare), pre-equilibrated with GST-A1 buffer. Bound protein was extensively washed with each ≥10 CV GST-A1, GST-A2 (GST-A1 including 1 M NaCl) and Q-A buffer (10 mM Hepes/NaOH pH 7.9, 150 mM NaCl, 1 mM EDTA, 2 mM DTT). GST-tag was removed by protease cleavage on column with 50 µg PreScission protease (GE Healthcare) overnight, 4 °C. The cleaved protein was loaded onto a HiTrap Q FF (5 ml) column (GE Healthcare). After gradient elution (20 CV 0% - 100% Q-B buffer (Q-A including 1 M NaCl)) purest fractions were concentrated and loaded on a Superdex 200 16/60 GL column (GE Healthcare) in the final SEC buffer (20 mM Hepes/NaOH pH 7.8, 200 mM NaCl, 2 mM DTT). Pure proteins were concentrated and the absence of nucleic acids confirmed by detecting an $A_{260\ nm/280\ nm}$ ratio to be ≤ 0.6 (ref. 45).

She3p-His_6 was purified from insect cells as described before[15].

pOPIN-J plasmids for She2p-$(GGSGG)_{1/2}$-She3p fusion proteins (FE#32, #33, #96, #97 and ctrl. #54, see **Supplementary Table 2**) were expressed in *Escherichia coli* BL21 GOLD pRARE at 18 °C after induction with 0.25 mM IPTG. Cells were harvested as described above, additionally 1 mM PMSF, 2% (v/v) glycerol and 0.5% (v/v) Tween 80 were added. Purification was carried out as described for She2p, except for GST-A2, Q-A, Q-B and SEC buffer being without DTT. A Superdex 75 16/60 GL column (GE Healthcare) was used for the final purification step.

His_6-SUMO-SHE3 constructs (FE#89, #94, #98, #99, #108-#110, #113 and #116, see **Supplementary Table 2**) were present in pOPIN-S3C vectors and unless stated otherwise transformed in *E. coli* BL21(DE3)Star. Expression and cell disruption was carried out as for She2p-$(GGSGG)_{1/2}$-She3p fusion proteins in Ni-A1 buffer (20 mM Hepes/NaOH pH 7.8, 500 mM NaCl, 20 mM Imidazole). Protein was loaded on a pre-equilibrated HisTrap FF 5 ml column (GE Healthcare) and washed ≥ 5 CV Ni-A1 buffer, ≥10 CV Ni-A2 buffer (Ni-A1 including 1 M NaCl) and ≥ 5 CV 10% Ni-B (Ni-A1 including 300 mM imidazole). Bound proteins were eluted by gradient elution (20 CV 10% - 100% Ni-B). In case of His_6-SUMO-She3p(331-425)His_6 and His_6-SUMO-She3p(331-405) expression was done in *E. coli* GOLD pRARE cells. Tag-cleavage with 50 µg PreScission protease took place o.n., at 4 °C in Hep-A buffer (10 mM Hepes/NaOH pH 7.9, 150 mM NaCl, 2 mM DTT) and SEC buffer, respectively. She3p(331-425)His_6 was separated from its tag via an additional HiTrap™ Heparin HP (5 ml) (GE Healthcare) purification step using a gradient elution over 30 CV 0% - 100% Hep-B (Hep-A including 300 mM NaCl). To separate She3p(331-405) from its His_6-SUMO tag, another HisTrap purification step was added (gradient elution over 30 CV: 0% SEC buffer - 100% Ni-B). As described before, purest fractions were concentrated and subjected to size exclusion chromatography (Superdex 75 16/60 GL column; GE Healthcare) in SEC buffer without DTT.

RNA preparation. For RNA preparation in general, RNase-free materials, reagents and RNase-free buffers containing DEPC-treated H_2O, were used. RNA sequences are summarized in **Supplementary Table 4**.

Small-scale *in vitro* transcription. All RNAs for EMSA, except for E3 (28-nt loop), were produced by *in vitro* transcription (**Supplementary Table 4**) using the MEGAshortscript T7 Transcription Kit (Ambion). Full length *ASH1* mRNA for chemical probing was *in vitro* transcribed using the MEGAscript T7 transcription kit (Ambion). Sample quality was assessed by native and denaturing TBE-PAGE.

Large-scale *in vitro* transcription. To produce large amounts of E3 (42-nt TL-TLR) and E3 (28-nt loop) RNA for NMR and the latter for SAXS experiments, large scale *in vitro* transcription was used. 4 µM HPLC-purified primer P45 (containing the T7 RNA polymerase promoter region) and 3.3 µM HPLC-purified primer P162 and P96, respectively, (containing the reverse-complement target DNA sequence and T7 RNA polymerase promoter region, **Supplementary Table 3**) supplemented with 33 mM $MgCl_2$ were incubated for 5 min, 60 °C in a total volume of 1.2 ml and cooled to 20 °C. Each 10-ml *in vitro* transcription reaction contained the DNA template mixture, 4 mM of each NTP, 20 mM and 24 mM $MgCl_2$, respectively, 80 mg/ml PEG 8000 and 0.5 mg/ml T7 RNA polymerase in the presence of TRX buffer (40 mM Tris/Cl pH 8.1, 1 mM spermidine, 0.1 ‰ Triton X-100, 5 mM DTT) and was incubated for 3 h, 37 °C. Precipitants were removed by centrifugation and the transcribed RNA ethanol precipitated.

The RNA was solubilized in denaturing loading dye (2 mM Tris/Cl pH 7.5, 20 mM EDTA, 8 M Urea, 0.025% (w/v) bromphenol blue, 0.025% (w/v) xylene cyanol) and separated on 8% denaturing TBE-PAGE gels in an Owl sequencing chamber (Thermo Fisher Scientific) in 1× TBE running buffer for 17 h, const. 300 V. Transcripts were visualized by UV shadowing and excised from the gel. The RNA was extracted by electroelution using the Whatman Elutrap electroelution system (GE Healthcare) at 200 V const. in 1× TBE. Before lyophilization, the RNA was dialyzed against 1 M NaCl, overnight, 4 °C and twice against DEPC H_2O, overnight, 4 °C.

Chemical probing. Experiments were essentially done as previously described[35]. For each reaction 15 µmol *in vitro* transcribed *ASH1* mRNA were refolded by incubating for 2 min at 90 °C and snap cooling on ice for 2 min. Renaturing was performed in buffer with 20 mM Hepes pH 7.9, 200 mM NaCl, 2 mM DTT, and 2 mM $MgCl_2$ for 15 min at 37 °C. After addition of 2 µg of yeast tRNA, samples were incubated 10 min at 21 °C. For chemical probing 0.8 µl DMS (1:20 diluted in ethanol) was incubated at 37 °C for 2 or 4 min and stopped by ethanol precipitation. Modified bases and RNA sequence were detected with AMV reverse transcriptase (New England Biolabs) of γ-^{32}P -labeled primers AN_P26, AN_P27 and AN_P28 (**Supplementary Table 3**). DNA products were separated on an 8% denaturing TBE-PAGE and visualized using X-ray films.

RNA isotope labeling and electrophoretic mobility shift assay. *In vitro* transcribed RNA was 5′ dephosphorylated using FastAP enzyme (Thermo Fisher Scientific) at 37 °C for 30 min in presence of RNase inhibitor. 10 pmol RNA was phosphorylated at the 5′-end with γ-^{32}P ATP by T4 polynucleotide kinase (New England Biolabs) at 37 °C and stopped after 30 min at 75 °C for 10 min. Labeled oligonucleotides were purified by a NucAway Spin column (Ambion). For EMSA, protein complexes with 5 nM γ-^{32}P-labeled RNA were incubated in RNase-free buffer (20 mM Hepes, pH 7.8, 200 mM NaCl, 4% (v/v) glycerol, 2 mM $MgCl_2$, 2 mM DTT, 30 µg/ml yeast tRNA) in a final volume of 20 µl for 30 min at 21 °C. 17 µl of the reaction was loaded on a 4% native TBE-PAGE gel and resolved in 1× TBE running buffer at 70 V for 61 min. After fixing and drying, gels were analyzed with radiograph films. For quantification, EMSAs were scanned with a FujiFilm FLA-3000 system and analyzed using ImageJ version 1.50i.

NMR. For NMR measurements, *in vitro* transcribed E3 (28-nt loop) and (42-nt TL-TLR) RNA samples were prepared by dissolving the lyophilized RNA in 20 mM Hepes, 200 mM NaCl, 2 mM $MgCl_2$, pH 7.8 in DEPC-water with 10% D_2O. The solutions were snap-cooled by boiling at 95 °C for 5 min and transferred to an ice-cold bath for 10 min before use to avoid thermodynamically favored duplex formation.

E3 (28-nt loop) and (42-nt TL-TLR) RNAs were probed for secondary structure-analyzing imino-^{1}H- 1D NMR spectra as described previously[46]. The RNA-NMR data were measured at different temperatures and imino resonances were assigned based on imino-NOESY experiments recorded at 278 K. All experiments were performed using a Bruker AVIII spectrometer at 900 MHz proton Larmor frequency equipped with a triple-resonance-cryogenic probe. Sample concentrations for the 28-mer and 42-mer RNAs were 172 and 200 µM, respectively. Imino-NOESY experiments were recorded with 300 ms mixing time using 2,048 × 220 points and 400–800 scans. Data were acquired and processed with Topspin 3.5 and further analyzed using Sparky (https://www.cgl.ucsf.edu/home/sparky/). Imino protons were assigned manually guided by the base pairing observed in the E3 42-mer crystal structure and suggested by Mfold version 2.3 (ref. 47).

Small angle X-ray scattering. SAXS data with *ASH1* E3 (28-nt loop) RNA from large scale *in vitro* transcriptions were recorded on a Rigaku BIOSAXS1000 instrument (HF007 microfocus generator, Cu-target at 40 kV and 30 mA). Transmissions were measured with a photodiode beamstop, q-calibration was made by a silver-behenate measurement. Measurements were performed with eight 900-s frames, tested for beam damage and averaged as images. Circular averaging and background subtraction was performed with the Rigaku SAXSLab software v 3.0.1r1. ATSAS package v 2.7.0-1 (ref. 48). RNA was measured at 1.5, 7, 11 and 20 mg/ml concentration in 20 mM Hepes, pH 7.8, 200 mM NaCl, 2 mM $MgCl_2$ at 5 °C. Theoretical scattering curves for the RNAs were back-calculated with the program Crysol from the ATSAS package[48] and plots generated with the program Origin.

Circular dichroism (CD) spectroscopy. CD spectra were recorded on a Jasco J-715 spectropolarimeter (JASCO) in the range of 190 nm to 260 nm at 20 °C, using a 1-mm high precision quartz cuvette (Hellma Analytics). Proteins were present at a concentration of 7.5 µM in a 50 mM sodium phosphate buffer pH 7.8 containing 200 mM NaCl and 1.5 mM TCEP. Measurement parameters included a scanning speed of 50 nm/min and five scans (response time: 8 s).

Isothermal titration calorimetry. Recombinant She2p protein and chemically synthesized She3p peptides (JPT Peptide Technologies) were dialyzed in a buffer containing 20 mM Hepes, pH 7.8, 200 mM NaCl and 2 mM TCEP. Using a MicroCal iTC200 machine (Malvern Instruments) either 1 mM She3p(382–405) or 100 µM She3p(342–374)Δ(352-354)[34] in the syringe was titrated in 26 injections a 1.5 µl (first injection 1 µl) to 206 µl of 100 µM or 10 µM wild-type She2p, respectively, using a stirring speed of 750 rpm and 25 °C. Data were corrected against buffer.

RNA preparation for crystallization. Unless stated otherwise, PAGE-purified chemically synthesized RNA (Dharmacon) was deprotected, desalted and lyophilized. The E3 (42-nt TL-TLR) RNA was solubilized in a buffer containing 10 mM sodium cacodylate pH 6.5, 5 mM $MgCl_2$, unfolded for 10 min, 70 °C and refolded via snap cooling on ice. E3 (28-nt loop) RNA for complex crystallization was solubilized in DEPC H_2O after lyophilization. Integrity of the RNA was confirmed using a 10% denaturing TBE-PAGE gel.

Procedures for crystallization, data collection and structure determination. *Crystallization of RNA*. Crystals of the E3 (42 nt TL-TLR) RNA (**Supplementary Table 4**) grew in 50 mM MES, pH 6.0, 5% (w/v) PEG 4000, 5 mM $MgSO_4$ by using the hanging-drop vapor diffusion method with 500 µl reservoir volume in EasyXtal 15-Well plates (Qiagen). Mixing 1 µl well solution and 1 µl RNA (2.94 mg/ml) at 21 °C yielded tetragonal crystals of approximately 125 × 44 × 44 µm size after 3 d. Prior to data collection the crystals were cryo-protected for 30 s in well solution, supplemented with 25% (v/v) PEG400 and flash-frozen in liquid nitrogen.

Native data set was recorded at 100 K at beam line ID 23-2 at the European Synchrotron Radiation Facility (ESRF) at a wavelength of 0.8726 Å. Data were indexed and integrated using XDS and scaled via XSCALE. Structure factor amplitudes were obtained via the Truncate program (CCP4 package)[49]. Phases were obtained by molecular replacement with Phaser using the slightly modified PDB entry 4FNJ (structure of tetra-loop-receptor) as search model. Crystals, diffracting up to 2.65 Å resolution, had space group $P4_12_12$ and one RNA molecule per asymmetric unit (see also **Table 1**). The structure was completed by iterative manual building in COOT and refinement with PHENIX. Images of the crystal structure were prepared with PyMol (Version 1.7; Schrodinger; http://www.pymol.org/). All crystallographic software was used from the SBGRID software bundle[50].

Crystallization of RNA-She2p complex. Crystallization conditions of She2p together with RNA were initially screened at 4 °C and at 20 °C using a Mosquito nanodrop dispenser (TTP Labtech) in 96-well sitting-drop plates and commercial screens. 4 mg/ml She2p(6-246, C-S) were mixed with 0.77 mg/ml E3 (28-nt loop) RNA (**Supplementary Table 4**), in a final buffer containing 20 mM Hepes pH 7.8, 200 mM NaCl and 2 mM $MgCl_2$. The complex was assembled for 10 min at 21 °C and spun down 16,100*g*, 4 °C, 60 min. Thin and plate-shaped crystals were obtained via hanging-drop vapor diffusion by equally mixing 1 µl complex with 1 µl 100 mM Bis Tris propane, pH 6.5, 200 mM NaF, 20% (w/v) PEG 3350, at 4 °C. Native crystals, were soaked with 1 mM HPLC-purified She3p(382-405) peptide (JPT Peptide Technologies). Crystals were cryo-protected by 25% ethylene glycol and flash-frozen in liquid nitrogen.

Data collection at 100 K was performed at a wavelength of 1.0716 Å at beam line ID 23-1 at the ESRF. Data were indexed, integrated and scaled using the XDS program package. Structure factor amplitudes were obtained via the Truncate procedure. Initial electron-density maps were calculated by molecular replacement with the apo-structure of She2p (PDB-ID: 1XLY) as search model using MolRep (CCP4 program suite). RNA and She3p were manually built in COOT. The overall structure at 2.41 Å resolution was refined using RefMac 5.8, including NCS averaging, the maximum-likelihood target function with TLS parameters and PDB_REDO pipeline (version 6.0)[51]. Ramachandran statistics show that 96.03% of all residues are in most favored, 2.14% in generously allowed and 1.82% in disallowed regions. Representation of electron density was prepared with CueMol2 (BKR Laboratory).

Crystallization of ternary RNA-She2p-She3p complex. For complex crystallization of She2p, She3p and the RNA, the E3 (28-nt loop) RNA (**Supplementary Table 4**) was purchased PAGE purified and lyophilized (IBA).

To foster the correct stoichiometric protein-protein ratio in the crystal, She3p was N-terminally fused via a flexible glycine-serine linker to the C terminus of She2p. The complex was assembled using 2.6 mg/ml She2p(6-246, C-S)-$(GGSGG)_2$-She3p(331-405) and a slight stoichiometric excess of RNA over protein (ratio 1.2:2), in a final buffer of 20 mM Hepes, pH 7.8, 200 mM NaCl and 2 mM $MgCl_2$. After centrifugation (16,100*g*, 30 min at 4 °C), 1 µl complex was mixed with 1 µl well solution using the hanging-drop vapor diffusion method in 24-well VDX plates (Hampton Research) with a reservoir volume of 500 µl. Plate-shaped crystals grew at 4 °C in 21% (w/v) PEG3350, 150 mM $NaNO_3$ after two weeks. Crystals were flash-frozen in liquid nitrogen and cryo-protected by 20% (w/v) PEG3350, 200 mM $NaNO_3$, 25% (w/v) ethylene glycol.

Native X-ray diffraction data was collected at 100 K at the X06DA (PXIII) beam line at Swiss Light Source (SLS) at a wavelenth of 0.9175 Å. Processing was done as described for the She2p/RNA complex. Further model building and refinement with the native data set (2.80 Å resolution) was performed with COOT and RefMac5 including NCS averaging. Images of the crystal structure, superimpositions of the complex and apo-structure, as well as electrostatic surface potentials were prepared with PyMol (Version 1.7; Schrodinger; http://www.pymol.org/).

***In vivo* mRNA-localization experiments.** Yeast strains as described in **Supplementary Table 5** were grown in selective media overnight at 30 °C. Expression of the MCP-3xGFP reporter protein was induced for 90 min by placing cells on glass slides with thin-layered agarose containing selective medium. Single images of mitotic cells were taken with an exposure time of 400 ms for GFP and 45 ms for differential interference contrast channels. Adjustment of brightness and contrast and assembly of overlays was done in ImageJ.

Expression of mutant or wild-type proteins was assessed by western blot. Total cell lysates corresponding to 20 µg protein were separated by SDS-Page. She3p-myc expression was probed with an 9E10 mouse monoclonal antibody and an IRDye 680RD Goat anti-Mouse IgG (Li-Cor Biosystems) secondary antibody, whereas general protein levels were probed with an rabbit anti-G6PD antibody (Sigma-Adrich: SAB2100871) and an IRDye 800CW Goat anti-Rabbit IgG (Li-Cor Biosystems) secondary antibody[52]. She2p was detected by a custom-made rat monoclonal anti-She2p antibody (1C3-11)[24]. Pgk1 was detected by a mouse monoclonal antibody (22C5D8, Invitrogen). Secondary antibodies are identical to those for She3-myc or G6PD detection. Detection was performed using an Odyssey-Imaging system (Li-Cor Biosystems).

Statistics. Statistical evaluation and numbers of independent experiments are described in the figure legends. For *in vivo* experiments in **Figure 5**, statistics are listed in **Table 2** and more detailed itemized in the source data file. The chi-square test was used to analyze SAXS data in **Supplementary Figure 4b–e** to describe the discrepancy between the theoretical and experimental curves.

Data availability. Structure files have been deposited in the Protein Data Bank with accession codes 5M0H (RNA), 5M0I (She2p-RNA) and 5M0J (She2p-RNA-She3p). Imino proton chemical shifts have been deposited in the Biological Magnetic Resonance Data Bank (BMRB) and are accessible with identifier

doi:10.1038/nsmb.3351

numbers 26938 and 26939, for E3 (28-nt loop) and E3 (42 nt TL-TLR), respectively. Source data for **Table 2** are provided in **Supplementary Data Set 1**. Other data are available from the corresponding author upon reasonable request.

45. Edelmann, F.T., Niedner, A. & Niessing, D. Production of pure and functional RNA for in vitro reconstitution experiments. *Methods* **65**, 333–341 (2014).
46. Janowski, R. *et al.* Roquin recognizes a non-canonical hexaloop structure in the 3′-UTR of Ox40. *Nat. Commun.* **7**, 11032 (2016).
47. Zuker, M. Mfold web server for nucleic acid folding and hybridization prediction. *Nucleic Acids Res.* **31**, 3406–3415 (2003).
48. Petoukhov, M.V. *et al.* New developments in the ATSAS program package for small-angle scattering data analysis. *J. Appl. Crystallogr.* **45**, 342–350 (2012).
49. Winn, M.D. *et al.* Overview of the CCP4 suite and current developments. *Acta Crystallogr. D Biol. Crystallogr.* **67**, 235–242 (2011).
50. Morin, A. *et al.* Collaboration gets the most out of software. *eLife* **2**, e01456 (2013).
51. Joosten, R.P., Long, F., Murshudov, G.N. & Perrakis, A. The PDB_REDO server for macromolecular structure model optimization. *IUCrJ* **1**, 213–220 (2014).
52. Du, T.G. *et al.* Nuclear transit of the RNA-binding protein She2 is required for translational control of localized ASH1 mRNA. *EMBO Rep.* **9**, 781–787 (2008).

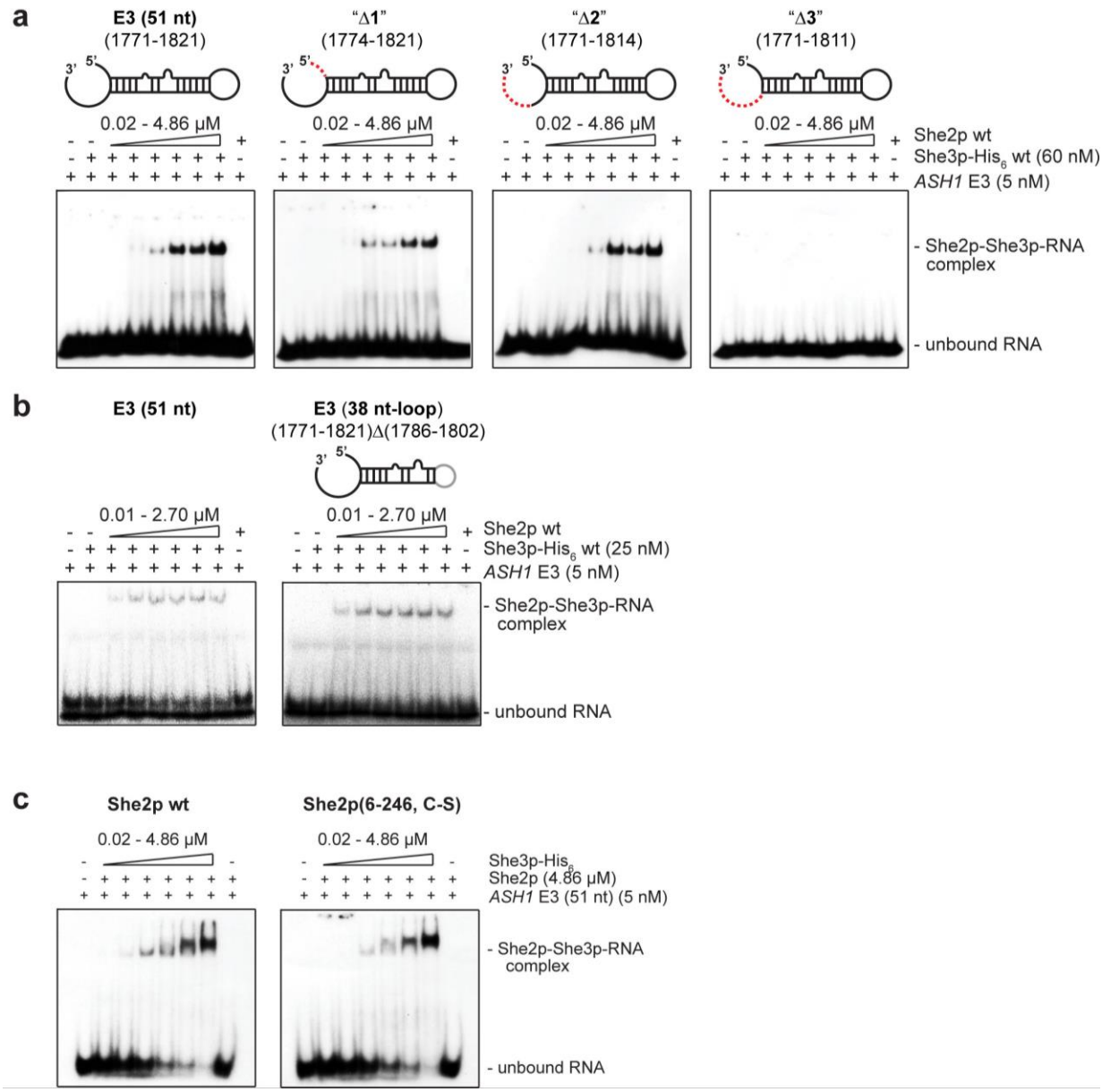

Supplementary Figure 1

Assessment of synergistic RNA recognition by the She2p-She3p complex in electrophoretic mobility shift assays (EMSA).

(**a**) E3-(51 nt) LE was previously shown to mediate full synergistic She2p-She3p binding and is incorporated into motile particles (Heym, R.G. *et al*., *J Cell Biol*. **203**, 971-84 (2013); Müller, M. *et al*., *PLoS Biol*. **9**, e1000611 (2011)). The single-stranded regions at the 5' and 3' ends of E3 (51 nt) relate to a large bulge in the context of full-length *ASH1* mRNA (**Fig. 1a**). Deletion of either the 5' end or part of te 3' regions in the E3-(51 nt) mutants Δ1 and Δ2, respectively, resulted in wild-type binding. In contrast, a complete deletion of the single-stranded bases at the 3' end abolished binding (Δ3). The results indicate that bases 1812-1814 are indispensable. Final She2p concentrations were 0.02 μM, 0.06 μM, 0.18 μM, 0.54 μM, 1.61 μM and 4.86 μM. (**b**) A deletion of the upper part of the stem and of the nona-loop (nt 1786-1802) combined with an insertion of a more compact tetra-loop (38 nt-loop) still allowed for high-affinity binding by She2p and She3p. She2p concentrations were 0.01 μM, 0.03 μM, 0.10 μM, 0.30 μM, 0.90 μM and 2.70 μM. (**c**) Comparative EMSAs of She2p wild type and a cystein-mutated, N-terminally truncated She2p version (She2p(6-246, C-S)). The latter shows wild type-like ternary complex formation with She3p and the E3-(51 nt) RNA. Each EMSA is representative for three independent experiments.

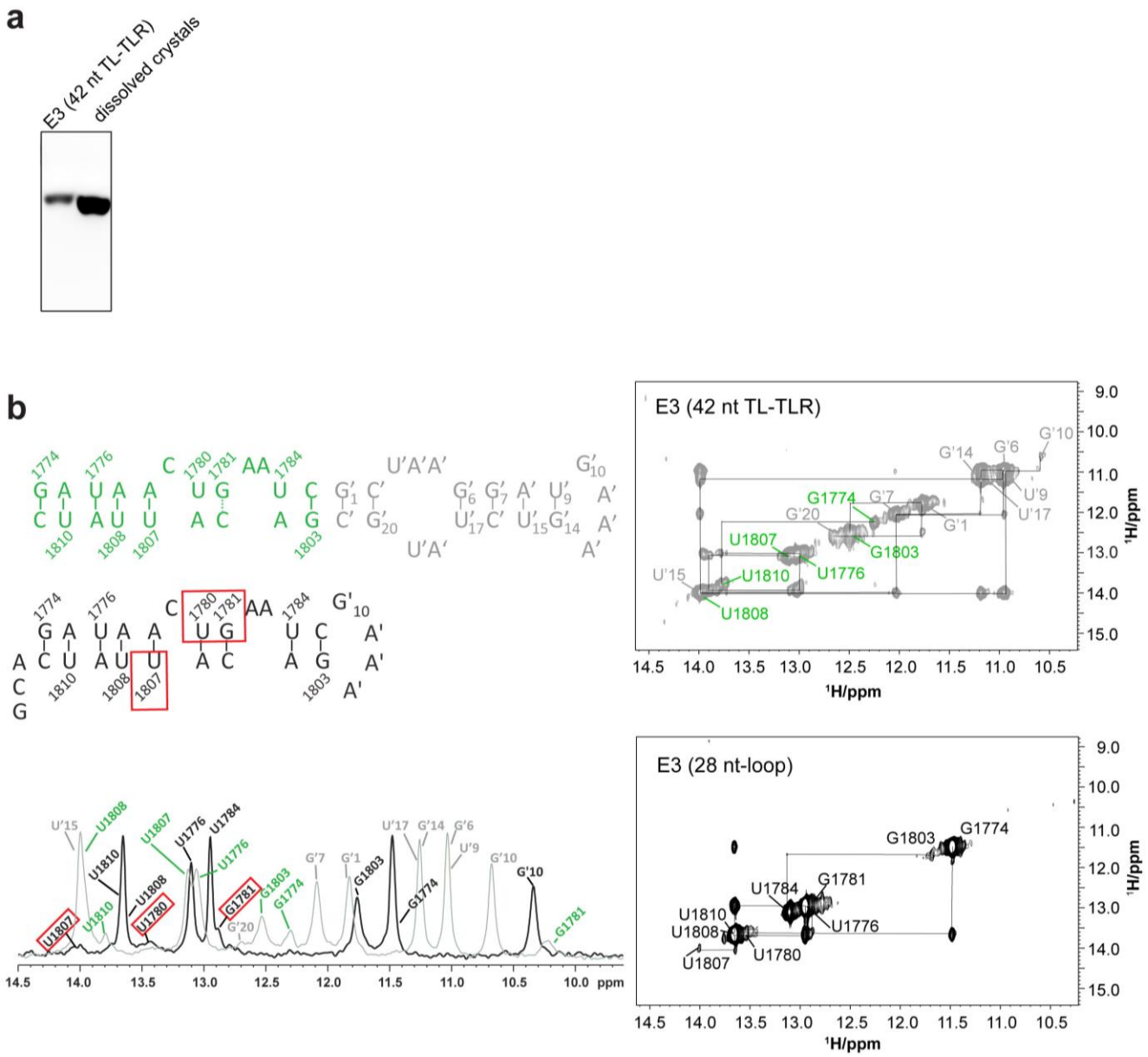

Supplementary Figure 2

NMR analysis of the free RNA in solution.

(**a**) Agarose gel with the denatured RNA sample before crystallization and after extraction from crystals indicates no degradation, suggesting that the lack of electron density in this region is due to structural flexibility. (**b**) 2D-imino NOESY spectra of *ASH1*-E3 (28 nt-loop) and E3-(42 nt TL-TLR) RNAs showing the sequentially assigned observable imino protons. Resonance labels are color-coded as indicated in **Fig. 1f**. Solid lines in the scheme represent unambiguous hydrogen-bonds as obtained from the sequential assignments. The broken line for G1781-C1805 in the 42-mer indicates an assignment of the G1781 imino proton inferred by exclusion, although no cross peak to adjacent nucleotides was observed. Overall the spectra are consistent with the existence of the base pairing observed in the crystal structure (**Fig. 1d,e**) also in solution. However, significant line broadening of imino resonances and undetectable imino signals in the bulged region between H1 and H2 indicate dynamics and flexibility in this part of the RNA. Bases marked with apostrophe indicate heterologous GAAA tetra-loop containing sequences, not belonging to the E3 LE. Bases highlighted with red boxes show peak broadening in the 1D imino spectrum indicating dynamics.

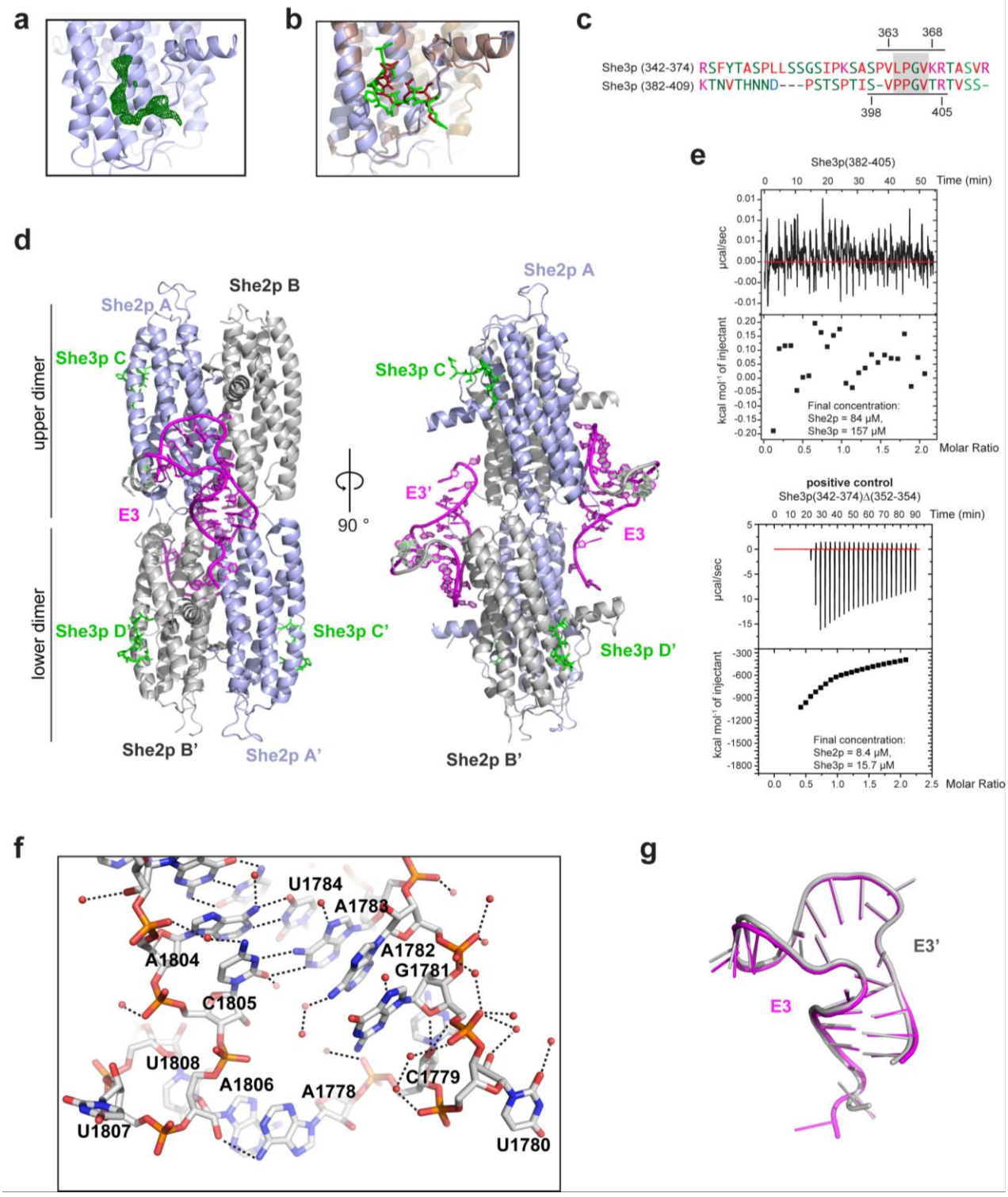

Supplementary Figure 3

Assessment of She2p-RNA structure.

(**a**-**e**) She2p binding of She3p(382-405) is not physiologic. Native crystals of She2p with RNA diffracted best when soaked with a short She3p peptide (residues 382-405). (**a**) In the She2p-RNA co-structure (**Fig. 2a**) additional electron density was observed that could not be assigned to She2p or RNA. The location of this not well-ordered electron density, however, overlaps with a previously

reported interaction site of She3p (364-368) (Singh, N. *et al.*, *Proc Natl Acad Sci U S A*. **112**, 142-7 (2015)). (**b**) The corresponding residues from fragment 382-405 were modeled into electron density (398-405, green) and compared to the previously published peptide 363-368 (red). Interactions were similar but not identical. (**c**) A sequence comparison of the previously described interaction motifs of She3p(364-368) (grey box) and of She3p(382-405) revealed similarities. (**d**) Crystal structure of She2p(6-246, C-S) with the *ASH1*-E3 (28 nt-loop) RNA at 2.41 Å resolution in front view and rotated 90° around the vertical axis. Non-physiologically bound She3p fragments are depicted in green. (**e**) Isothermal titration calorimetry (ITC) experiments with She2p and She3p(382-405) (top) showed no binding even at final She3p concentrations of 157 µM in three independent experiments. Since the positive control (She3p residues 364-368) (Singh, N. *et al.*, *Proc Natl Acad Sci U S A*. **112**, 142-7 (2015)) showed binding to She2p (bottom) in two independent experiments, we conclude that the electron density of She3p(382-405) in the co-structure with She2p and RNA is non-physiologic. (**f**) Close-up of interactions in the kinked region of E3 RNA in the She2p-bound state. Watson-Crick base pairings, hydrogen bonding, base stacking, and water interactions are shown. For better visualization, She2p is hidden. (**g**) Superposition of the two RNA chains E3 (pink) and E3' (grey) observed in the She2p-bound form. The sole difference is visible at the very 3' base (RMSD of all atoms = 0.5 Å).

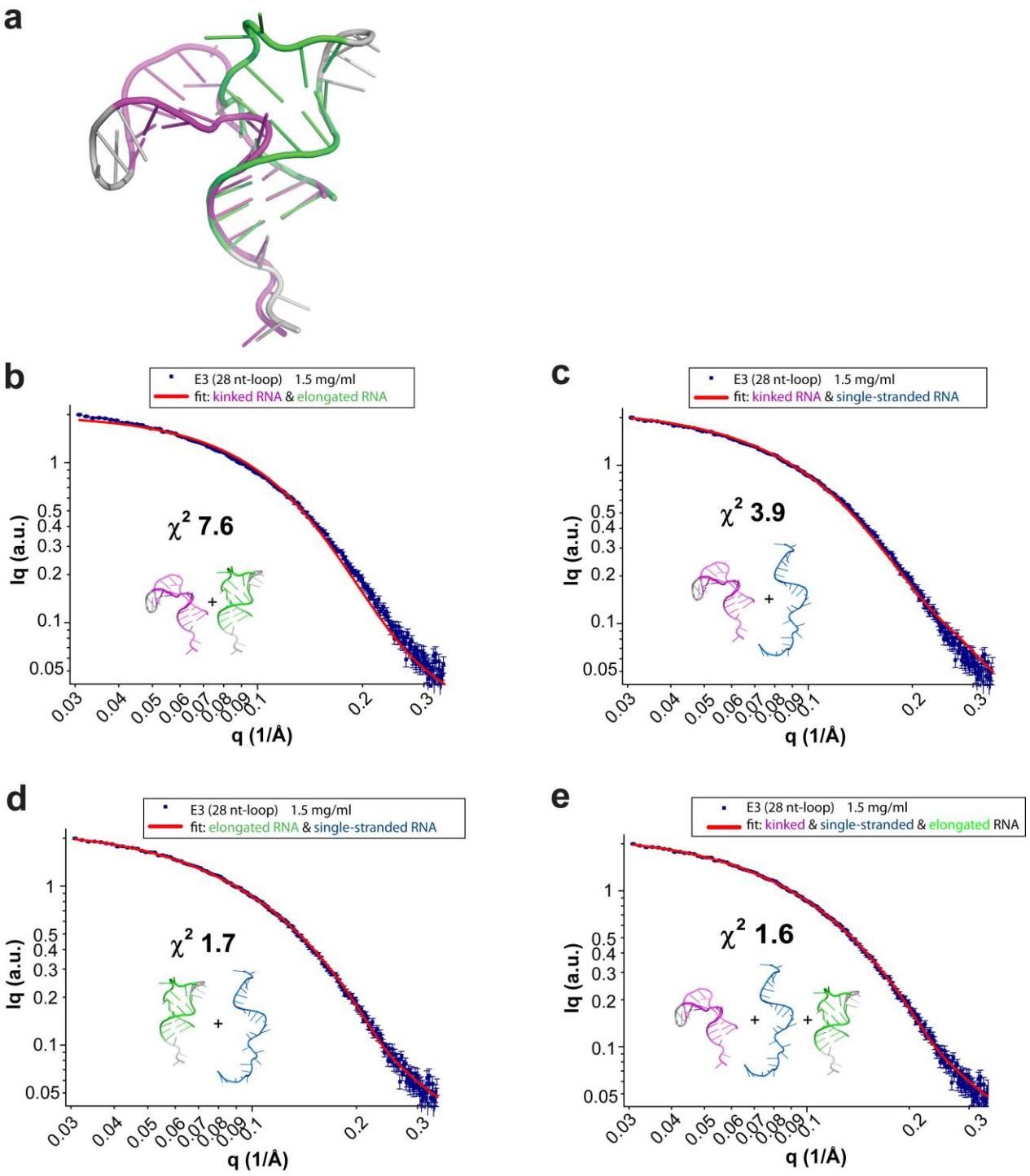

Supplementary Figure 4

Comparison of free RNA with She2p-bound RNA in solution by small angle X-ray scattering.

(a) Overlay of the RNA models from the E3-(42 nt-TL-TLR) RNA crystal structure (green), where the heterologous GAAA-donor acceptor has been replaced *in silico* by a shorter GAAA tetra-loop (grey), and of the E3 (28 nt-loop) RNA from the She2p-She3p bound complex (magenta). Strong rearrangements in the RNA secondary structure pinpoint to a large conformational change upon complex formation (see also Fig. 2c). (b-d) Different RNA models (red) are fitted against the scattering curve of E3-(28 nt-loop) RNA recorded at 1.5 mg/ml concentration in single experiments. (b) The calculated scattering curves for both the bound

(in (c): pink, kinked) and unbound (in c: green, elongated) RNAs, assuming that both conformations could be present (with fitted fractions kinked RNA : elongated RNA = 0.72 : 0.27) does not fit well to the scattering curve especially at low (0.03 $Å^{-1}$) and high (0.3 $Å^{-1}$) q values, which is also reflected by the high χ^2 value of 7.6. (c) When testing a kinked and a melted, single-stranded RNA model (ssRNA) (depicted in blue; ratio kinked RNA : ssRNA = 0.74 : 0.26) the fit becomes better and χ^2 decrases to 3.9. (d) Assuming that an elongated and a single-stranded species (ratio elongated RNA : ssRNA = 0.65 : 0.34) exists in solution, the χ^2 value improves to 1.7. (e) The most accurate fit could be achieved by fitting a combination of the kinked, single-stranded and elongated RNA (ratio kinked : ssRNA : elongated = 0.12 : 0.33 : 0.55). Here χ^2 was 1.6. SAXS data support the observation that the E3-(28 nt-loop) RNA has an elongated conformation in solution. The fact that a single-stranded species is needed to fit the data suggests an ensemble of RNA conformations. Notably, the elongated form represents a major population consistent with the SAXS and NMR data.

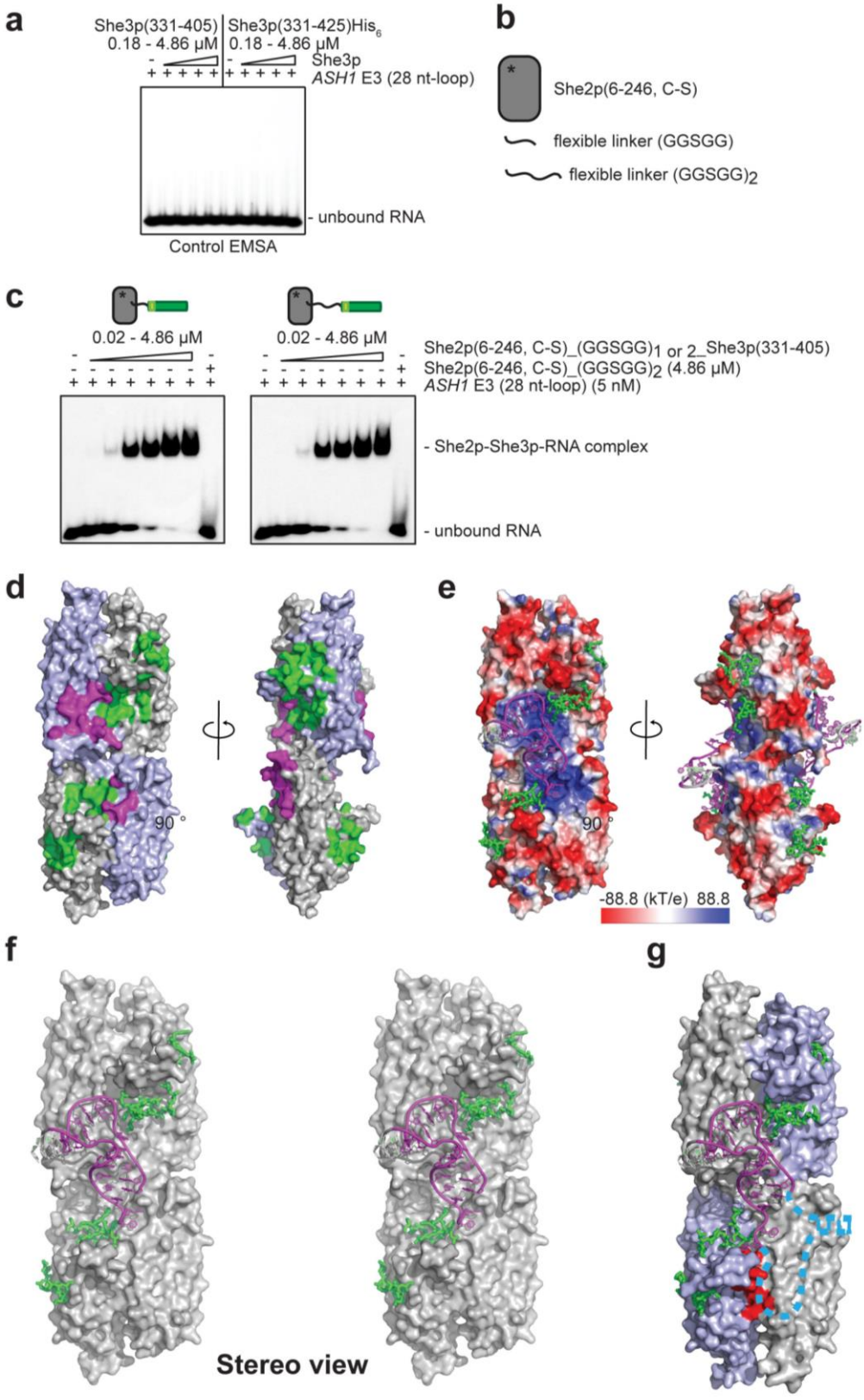

Supplementary Figure 5

Control EMSA and surface representation of the ternary complex.

(**a**) Control EMSA related to **Fig. 3b** showing that none of the used She3p truncation mutants (331-405 or 331-425) is able to bind E3-(28 nt-loop) RNA in the absence of She2p at the given experimental concentrations. (**b**) Schematic drawing of She2p(6-246, C-S) and the N-terminally fused flexible linkers consisting of five (GGSGG) or ten amino acids $(GGSGG)_2$. (**c**) EMSA with She2p-She3p fusion constructs. Since She2p and She3p interact with a 1:1 ratio, they also form synergistic complexes when fused to each other with a glycine-serine linker with different length. The last lane on the right side contains She2p(6-246, C-S) fused to the $(GGSGG)_2$ linker as a control, not showing any band shift. (**d**) She2p alone is depicted in surface representation with its contact sites for She3p (green) and RNA (magenta) in front view and 90 ° rotated around the vertical axis. (**e**) The electrostatic surface potential of She2p shows that E3-(28 nt-loop) RNA (magenta) binds at the positively charged area (blue) in the middle of the She2p tetramer, whereas negatively charged residues (red) surround the binding region. She3p is depicted in green. (**f**) Stereo view of the She2p-She3p complex with *ASH1* E3 (28 nt-loop) RNA. (**g**) Ternary complex as depicted in **Fig. 3b** with She2p in surface representation. Red area marks She2p amino acids 164-179 that were previously shown to UV crosslink with E3 (51 nt) (Müller, M. *et al*., *PLoS Biol*. **9**, e1000611 (2011)). Dashed blue line shows the anticipated projection of the RNA over the crosslinking site. This depicted single-stranded loop region followed by a double-stranded stem (right side) is consistent with the experimentally validated secondary structure shown in **Fig. 1a**. EMSAs in **a** and **c** are representatives for three independent experiments each.

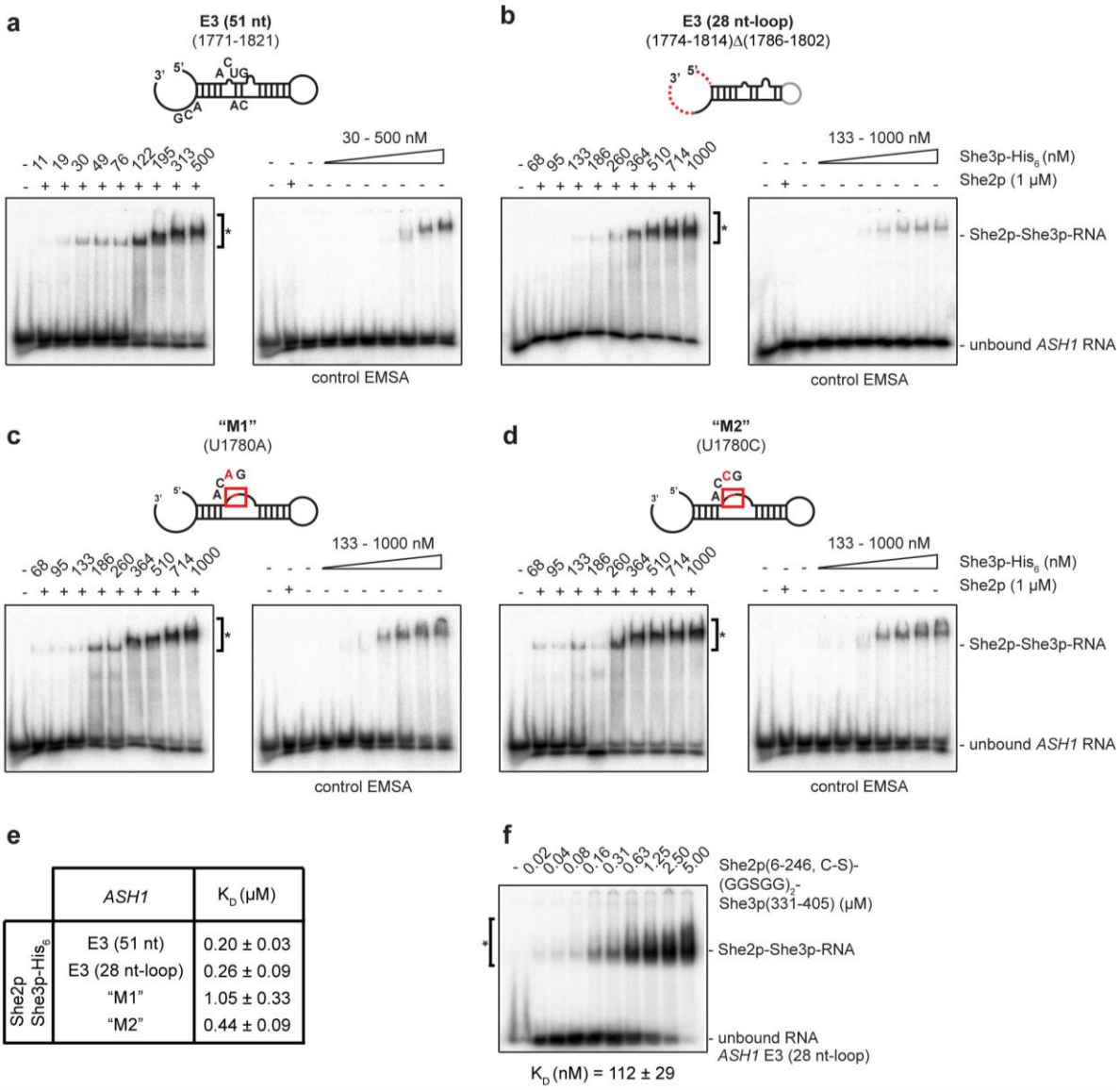

Supplementary Figure 6

Representative EMSAs for apparent K_D determination.

(**a**-**d**) Binding affinities of E3 variants that showed ternary complex formation in **Fig. 4** were quantified in EMSA experiments. Respective control EMSAs show unspecific RNA binding of She3p at high protein concentrations. Nevertheless, when She2p is additionally present, band intensities of the shifted complex increase, thus reflecting the specific ternary complex of She2p-She3p and RNA. In (**a**) radioactively labeled E3-(51 nt) RNA was used. In (**b**) E3 (28 nt-loop) was assessed. (**c**) and (**d**) show EMSAs where RNA mutants "M1" and "M2" were tested. (**e**) Table summarizing apparent mean K_D values ± s.d. for *ASH1* E3-RNA mutants in complex with She2p and She3p. K_Ds were calculated from three independent experiments using the one-site binding equation. While E3 (51 nt) forms the ternary complex with a K_D of 0.20 ± 0.03 μM, the minimal E3-(28 nt-loop) RNA bound She2p and She3p just slightly weaker. Replacing U1780 by the pyrimidine C in mutant "M2" decreased the affinity to a K_D of 0.44 ± 0.09 μM, whereas mutating U1780 to purine A in mutant "M1" had a more severe effect with a K_D of 1.05 ± 0.33 μM. (**f**) Representative EMSA of the crystallized She2p(6-246, C-S)-$(GGSGG)_2$-She3p(331-405) fusion protein with *ASH1* E3-(28 nt-loop) RNA shows high affinity binding. The apparent K_D was 112 ± 29 nM. Square brackets marked by an asterisk delimit the area of the gel, which was used for quantification in **a**-**d** and **f**. All EMSA were performed in three independent experiments.

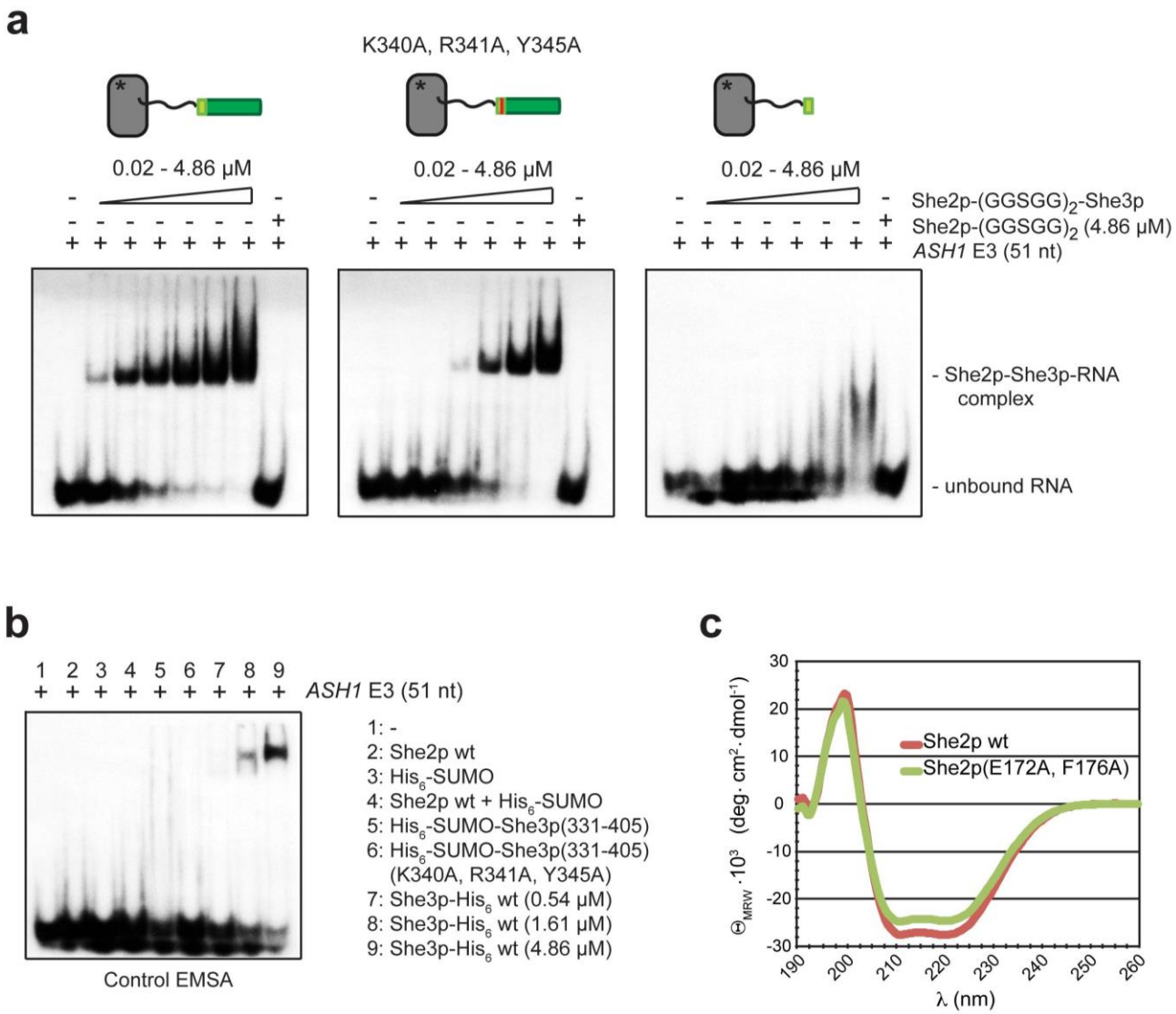

Supplementary Figure 7

Analyses of She2p mutants and fusion constructs with She3p.

(**a**) EMSA testing *ASH1*-E3 (51-nt) RNA-binding by different She2p-She3p fusion constructs. She2p(6-246, C-S) fused to the $(GGSGG)_2$ linker and to She3p(331-405) shows strong ternary complex formation. When in She3p K340, R341 and Y345 are mutated to alanines, band shifts occur only at higher protein concentrations, indicating a reduced RNA-binding affinity. The fusion protein only containing She3p amino acids 331 to 346 is still able to form a weak ternary complex, confirming that this region constitutes an important interaction site. The last lane on the right side contains She2p(6-246, C-S) fused to the ten amino acid glycine-serine linker $(GGSGG)_2$ without She3p as a control, not showing any band shift. (**b**) Control EMSA related to **Fig. 4d**. Unless stated otherwise 4.86 µM protein(s) were tested for *ASH1*-E3 (51-nt) RNA-binding. (**c**) CD spectra of She2p wild type in comparison to the double mutant She2p(E172A, F176A) confirmed the α-helical composition of both protein variants and the secondary structure integrity of the mutant. EMSAs in **a** and **b** are representatives for three independent experiments each. CD spectra in **c** were recorded once.

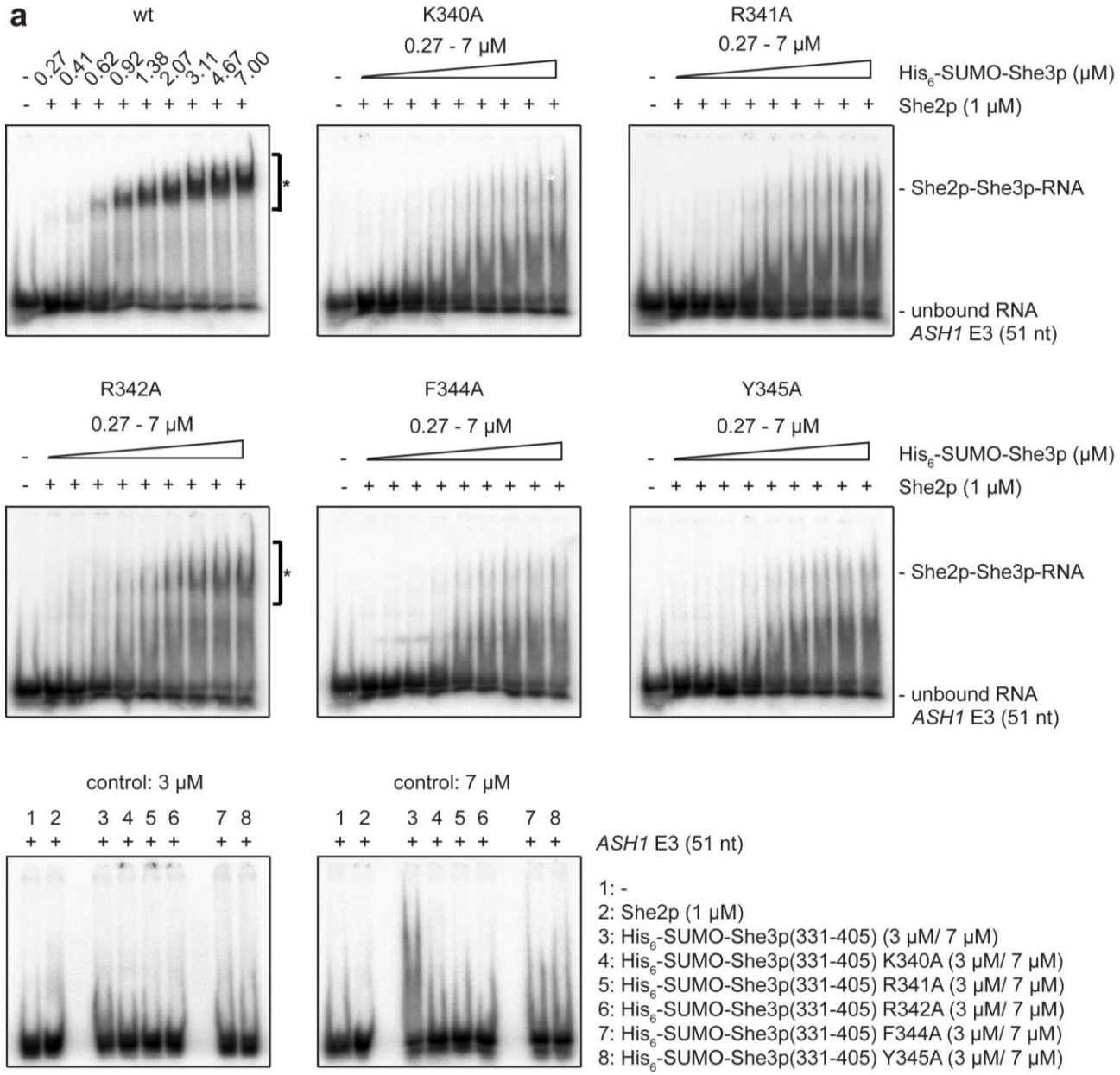

b

	His$_6$-SUMO-She3p(331-405)	K_D (µM)
1 µM She2p wt 5 nM E3 (51 nt)	wt	1.10 ± 0.32
	K340A	n.d.
	R341A	n.d.
	R342A	3.43 ± 1.25
	F344A	n.d.
	Y345A	n.d.

Supplementary Figure 8

Representative EMSAs of She3p mutants for K_D calculations.

(**a**) His_6-SUMO-She3p(331-405) and selected single-amino acid mutants were tested with She2p and *ASH1*-E3 (51 nt) for their ternary complex-formation. Since distinct She2p-She3p-RNA complexes could be detected for wild-type She3p(331-405) and She3p(331-405; R342A) apparent mean K_D values ± s.d. were determined. K_Ds were calculated from three independent experiments using the one-site binding equation. Square brackets marked by an asterisk delimit the area of the gel, which was used for quantification. His_6-SUMO-tagged proteins were used because they yielded higher amounts of protein after purification. (**b**) Table summarizing calculated apparent K_D values for His_6-SUMO-She3p mutants. Binding affinities of She3p(331-405) mutated in positions K340A, R341A, F344A, and Y345A appeared to be worse than for R342A. These were not quantified (not determined, n.d.) due to the lack of distinct band shifts. Of note, only R342 makes intra-molecular contacts. Since R342A shows reduced RNA binding, also this stabilizing interaction seems important for RNA recognition. All EMSA were performed in three independent experiments.

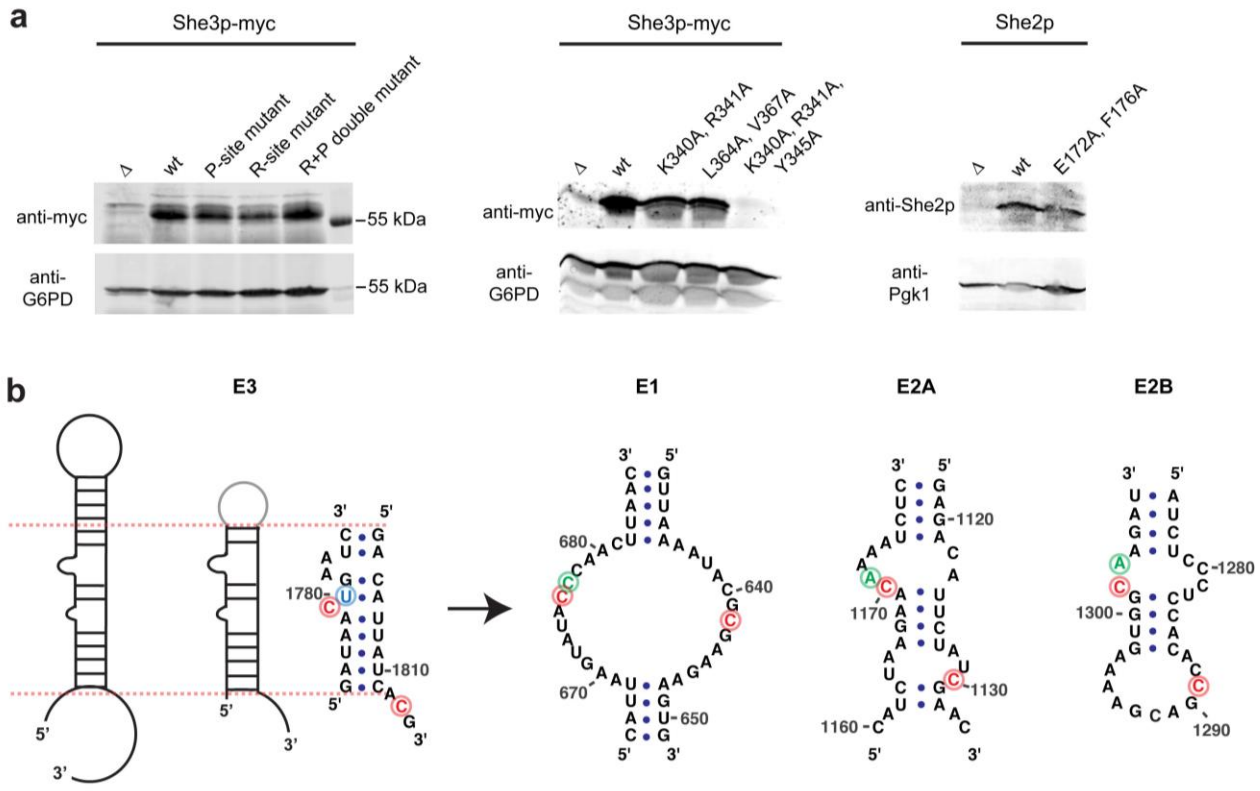

Supplementary Figure 9

Control experiments for *in vivo* studies and comparison of LEs.

(**a**) Western blots with anti-Myc antibody showing the expression levels of wild-type and mutant versions of She3p in corresponding yeast strains. Glucose-6-phosphate dehydrogenase (G6PD) was used as loading control. Only the triple mutant She3p(K340A, R341A, Y345A) showed no expression. Western blots with anti-She2p antibody shows similar expression level of the wild-type strain and a strain expressing the mutant She2p(E172A, F176A). Phosphoglycerate kinase 1 (Pgk1) was used as loading control. Western blots were performed in two independent experiments from different cell extracts. (**b**) Comparison of predicted secondary structures from *ASH1* LEs. Specifically recognized, essential bases in the *ASH1*-E3 LE are highlighted in red (C1779/ C1813), and blue (U1780). Conserved cytosines can also be found in E1, E2A and E2B. Based on secondary-structure predictions at least E2A and E2B are likely to have both cytosines in similar distance on the opposing strand of their stems. However, the base-specific position U1780 in E3 (blue base) is not conserved in the other elements (green bases), indicating that different subclasses of LEs might exist. Since the structural rearrangements observed in E3 upon binding (**Fig. 2c**) are impossible to predict with current bioinformatics tools, experimental approaches are required to understand the exact modes of binding for other LEs.

Supplementary Notes - Edelmann et al.

Supplementary Note 1 – Analysis of the NMR Data

While the *ASH1*-E3 (28 nt-loop) adopts a kinked conformation in complex with She2p (**Fig. 2a**), the crystal structure of *ASH1*-E3 (42 nt TL-TLR) shows an elongated stem-loop conformation (**Fig. 1d**; **Supplementary Fig. 2c**). To assess the conformation of the unbound RNAs we analyzed the base-pairing pattern of both the *ASH1*-E3 (28 nt-loop) and *ASH1*-E3 (42 nt TL-TLR) RNAs using NMR-spectroscopy. Hydrogen bonds across base pairs were determined based on 1D-imino proton spectra of the two RNAs and 2D-imino NOESY experiments to sequentially assign the observable imino protons ("imino walk", **Supplementary Fig. 2b**).

We first aimed at verifying hydrogen-bonding from the crystal structure of the *ASH1*-E3 (42 nt TL-TLR) (**Fig. 1d,e**). Inspection of the solution spectra of *ASH1*-E3 (42 nt TL-TLR) RNA reveals that the base pairing resembles the contacts in the apo-crystal structure (**Fig. 1d**), i.e. Watson-Crick base pairing and characteristic upfield imino proton chemical shifts for G-U pairs[1]. As expected, we found the RNA to be stabilized by the terminal GNRA (GAAA) tetraloop, which is confirmed by the presence of a sharp resonance for the loop-G'10-imino proton (**Fig. 1f**) due to a hydrogen bond to the phosphate backbone[2]. Consequently, the apical part of the stem-loop that mainly consists of the heterologous TL-TLR sequence and that we term helix'2 (H'2; in reference to the corresponding helix 2 of the endogenous E3 RNA) is stably hydrogen-bonded. However, we found significant flexibility indicated by the lack of detectable signals for U1780 and U1784. In line with this, the imino proton signal of the flanking G1781 is significantly line-broadened indicating dynamics. Apart from that, imino protons in the lower H1 stem are completely observable. We thus conclude that the two stems in the *ASH1*-E3 RNA are formed and comparable to the conformation observed in the crystal structure, while the flexibility for U1780 and U1784 indicates conformational flexibility that creates a dynamic hinge between the two stem parts.

For the *ASH1*-E3 (28 nt-loop) RNA we only succeeded in obtaining analyzable NMR data at 278 K indicating a lower thermodynamic stability of this AU-rich RNA. Imino signals indicate that the lower stem region consisting of H1 is formed comparable to the 42-mer RNA. Interestingly, the U1780 and G1781 imino signals in the central hinge region are well detectable for the 28-mer RNA (in contrast to the 42-mer). We expect that the closer proximity to the GNRA tetraloop is responsible for an increased stability of this double base pair in the 28-mer RNA. On the other hand, for *ASH1*-E3 (28 nt-loop) RNA a high degree of flexibility and dynamics is indicated by severe line-broadening of imino resonances U1780, G1781, and U1807 when compared to the other signals in the spectrum.

Altogether, the NMR data for the two RNAs support the presence of a significant population of elongated RNA stem loop, very similar to the crystal structure of the *ASH1*-E3 (42 nt TL-TLR) RNA, with considerable flexibility and base-pair melting along the double-bulge region between H1 and H'2/H2. Notably, we can clearly exclude the presence of a major population of the kinked RNA stem-loop conformation as seen in the She2p complex structure, as for this no detectable imino signals would be expected for U1780, G1781, and U1807. The observed

Nature Structural & Molecular Biology: doi:10.1038/nsmb.3351

flexibility of the base pairs involving these nucleotides indicates conformational flexibility of this hinge region. This suggests that the free RNAs sample a range of conformations with different relative angles for the two stem regions. Thus, formation of the She2p-RNA complex may involve a conformational selection mechanism, where a dynamic conformational ensemble of the free RNA exhibits a minor population of kinked conformations that can be selected by She2 for formation of the complex.

Interestingly, we found limited overlap of analogous RNA resonances when superimposing the two 1D proton spectra of the *ASH1*-E3 (28 nt-loop) and the *ASH1*-E3 (42 nt TL-TLR) RNA species. We speculate that differential conformational dynamics between the two RNA fragments leads to a systematic change in imino chemical shifts. Indeed, the overall lower stability of the *ASH1*-E3 (28 nt-loop) RNA is consistent with upfield-shifted resonances (G1774, U1776, G1803, U1808, and U1810), which can be explained with reduced base stacking compared to the *ASH1*-E3 (42 nt TL-TLR) RNA. As mentioned before, we suggest that the proximity of the GAAA tetraloop in the *ASH1*-E3 (28 nt-loop) is responsible for a higher local stability of basepairs U1780-A1806, G1781-C1805, and U1784-A1804. In the *ASH1*-E3 (42 nt TL-TLR) RNA similar base-pairs could not be determined due to a lack of respective resonances, likely indicating conformational dynamics. In accordance with that, the G1781 imino-proton signal in *ASH1*-E3 (42 nt TL-TLR) RNA is strongly upfield-shifted, suggesting the absence of regular helical base stacking between the double-bulge. Altogether, our NMR data support that the *ASH1*-E3 (28 nt-loop) and *ASH1*-E3 (42 nt TL-TLR) RNAs adopt a dynamic range of conformations, sampling different angles of the RNA helical stems. In summary, this suggests a conformational selection mechanism for complex formation with She2p.

Nature Structural & Molecular Biology: doi:10.1038/nsmb.3351

Supplementary Note 2 – Cloning

Cloning of ASH1 ORF for chemical probing

The *ASH1* ORF was subcloned from the vector pRJ1451 into pRS405 using XhoI and BamH1 restriction sites (using primers AN_P18 and AN_P19). For *in vitro* transcription pRS405*_ASH1* was linearized using BamHI and NaeI restriction enzymes and the fragment was further purified by gel extraction and subsequent ethanol precipitation.

Cloning of constructs for recombinant protein expression

Plasmid FE#95, containing *SHE2_E172A_F176A*, was created using the QuikChange II XL Site-Directed Mutagenesis Kit (Stratagene) with p01 as template and P128/P129 as primers.

All *SHE2-gly-ser-linker-SHE3* constructs (FE#32, #33, #54, #77-#79, #96 and #97) were cloned into the pOPIN-J vector, using the In-Fusion® HD cloning kit (Clontech® Laboratories). For the cloning of FE#32 and FE#33, first plasmid FE#6 containing *SHE3(334-405)*His_6 was created. The *SHE3* fragment was PCR amplified using primers O176/P6 and RHP85 as template and cloned into the pETM-43 vector (EMBL) by using NcoI and EcoRI restriction sites in the respective 5' and 3' primers. Subsequently, constructs FE#32 and FE#33 were cloned via three-point PCR. First PCR products were generated using P48/P49 or P48/P50, respectively, with MM_pGEX6P1_SHE2(6-246, C-S) as template. The second set of PCR products was amplified using primers P51/P54 or P52/P54 and FE#6 as template DNA. The third, overarching PCR was performed using the primer pair P48/P54 and the resulting product then used for In-Fusion® cloning. To generate FE#54, *SHE2(6-246, C-S*) was elongated by a $(GGSGG)_2$ linker, using a primer extension with P48/P73 on MM_pGEX6P1_SHE2(6-246 C-S). FE#77, #78 and #79 served as initial vectors for FE#108-#110. Their InFusion®-inserts were generated by three-point PCR using FE#33 as template and primer pairs P48/P109 & P108/P54, P48/P111 & P110/P54 and P48/P113, P112/P54, respectively. Plasmid FE#96 was again created via primer-extension PCR using the primer pair P48/P136 and template FE#33. *SHE3* mutations in FE#97 were introduced via three-point PCR using primer pairs P48/P137 and P138/P54 on template FE#33.

To create *His6-SUMO-SHE3* constructs (FE#89, #94, #98, #99, #108-#110, #113 and #116), pOPIN-S3C backbone vectors were used for In-Fusion® cloning. For plasmid FE#89, a PCR product with primers P122 and P54 based on FE#33 as template was produced. The control construct FE#94 containing *His6-SUMO* and a small linker sequence, identical to the amino acid rest after PreScission protease cleavage, was produced using primers P126/P127 in 1:1 ratio as In-Fusion® insert. *SHE3* PCR fragments for plasmids FE#98 and FE#99 were amplified using P122/P54 and FE#97 as template or P122/P139 and RH84 as template, respectively. Inserts for FE#108-#110 were generated by PCR with primers P122/P54 on FE#77-79 serving as respective templates. *SHE3* mutations Y345A and F344A were introduced in FE#6 via QuickChange mutagenesis using P156/P157 and P159/P160, respectively, resulting in FE#111 and FE#114. Plasmids FE#111 and FE#114 served as PCR templates to generate In-Fusion® inserts with P122/P54 to produce FE#113 and FE#116.

Nature Structural & Molecular Biology: doi:10.1038/nsmb.3351

Cloning of She2p and She3p constructs for in vivo imaging experiments

Mutated *SHE3* constructs FE#101 and FE#102 were created via three-point PCR using pRJ350 as template, utilizing primer pairs P144/P146, P147/P145 and P144/P148, P149/P145, respectively. To generate FE#117 and FE#118 primer pairs P144/P164, P163/P145 and P144/P166, P165/P145 were used, respectively. The third, overarching PCR was performed using the primer pair P144/P145. Resulting PCR products were cloned in pRJ350 via EcoRI/SalI restriction sites. To create the plasmid FE#103, the same three-point ligation strategy as for FE#101 was used, except for using FE#101 as template for PCR amplification. FE#119 was created using the QuikChange II XL Site-Directed Mutagenesis Kit (Stratagene) with FE#117 as template and P167/P168 as primers. As initial vector for plasmid pRJ1978 (YCplac111-*SHE2_E172A-F176A*), a StuI restriction site was introduced downstream of the stop codon in FE#95, using the QuickChange II XL Site-Directed Mutagenesis Kit and primers P152 and P153. A 523 bp NsiI-StuI fragment containing approximately the posterior half of the *SHE2* ORF was excised and used to replace the corresponding fragment in pRJ33, thereby generating pRJ1978.

Nature Structural & Molecular Biology: doi:10.1038/nsmb.3351

Supplementary Table 1. She2p-She3p R-/P-site protein-protein contacts

She2p residue contacting the She3p R-site	Number of She2p chains with observed interaction	She3p R-site residue contacting She2p	Number of She3p chains with observed interaction
T53	4	K340	1
I56	4	R341	3
K57*	4	S343#	4
K60*	4	F344	4
D111	2	Y345	4
Y115	4	T346	4
T118	2	A347	4
Q119	4	S348#	4
I141	4	L351	2
L142	1		
D145	4		
D146	1		
E172	4		
F176	4		
E183	1		
N193	1		
I194	1		
F195†	1		
She2p residue contacting the She3p P-site	**Number of She2p chains with observed interaction**	**She3p P-site residue contacting She2p**	**Number of She3p chains with observed interaction**
W157	4	L364†,§	4
V173	1	P365§	4
N187	1	G366§	4
G189	1	V367†,§	4
E190	2	K368	3
T191	1	R369	2
D192	1	T370	2
I194	4	A371	2
L196†	2		
Q197†	4		
E198†	4		
I199†	4		
L200	4		
L211	3		
A214	3		
W215§	4		
I218	4		

Mutation of amino acids marked with references showed impaired complex formation and/or mRNA localization:
*: Reference 3. #: Reference 4, double mutant (S343E, S361E). †: Reference 5, double mutant (F195A, L196A), triple mutant (Q197A, E198A, I199A) and double mutant (L364A, V367A). § Reference 6.

Nature Structural & Molecular Biology: doi:10.1038/nsmb.3351

Supplementary Table 2. Plasmids used in this study

Plasmid name	Description	Source	PCR primers	Cloning strategy
p01	pGEX-*SHE2*	Niessing *et* al. 2004		
MM_pGEX6P1_SHE2 (6-246 C-S)	pGEX-6P-1_*SHE2(6-246 C-S)*	Niessing *et* al. 2004		
pRJ33	YCplac111_*SHE2*	Jansen lab		
pRJ350	YCplac22_*SHE3_myc3*	Jansen lab		
pRJ1451	YCplac22_*GAL1-boxB(12x)-ASH1*	Jansen lab		
RHP27	pFastBacDual-*SHE2-SHE3His6*	Müller *et* al. 2011		
RHP85	pGEX-*SHE3(334-425)His6*	Müller *et* al. 2011		
AN_P#5	pRS405_*ASH1*	this study	AN_P18/ AN_P19	Restriction sites: XhoI/BamHI
FE#6	pETM-43_*SHE3(334-405)*	this study	O176/P6	Restriction sites: NcoI/EcoRI
FE#32	pOPIN-J_*SHE2(6-246 C-S)_GGSGG_SHE3(331-405)*	this study	P48/P49, P51/P54	InFusion: 3 point PCR on MM_pGEX6P1_SHE2(6-246 C-S) and FE#6
FE#33	pOPIN-J_*SHE2(6-246 C-S)_(GGSGG)x2_SHE3(331-405)*	this study	P48/P50, P52/P54	InFusion: 3 point PCR on MM_pGEX6P1_SHE2(6-246 C-S) and FE#6
FE#54	pOPIN-J_*SHE2(6-246 C-S)_(GGSGG)x2*	this study	P48/P73	InFusion: Template: MM_pGEX6P1_SHE2(6-246 C-S)
FE#77	pOPIN-J_*SHE2(6-246 C-S)_(GGSGG)x2_SHE3(331-405)_K340A*	this study	P48/P109, P108/P54	InFusion: 3 point PCR on FE#33
FE#78	pOPIN-J_*SHE2(6-246 C-S)_(GGSGG)x2_SHE3(331-405)_R341A*	this study	P48/P111, P110/P54	InFusion: 3 point PCR on FE#33
FE#79	pOPIN-J_*SHE2(6-246 C-S)_(GGSGG)x2_SHE3(331-405)_R342A*	this study	P48/P113, P112/P54	InFusion: 3 point PCR on FE#33
FE#89	pOPIN-S3C_*SHE3(331-405)*	this study	P122/P54	InFusion: Template: FE#33
FE#94	pOPIN-S3C_*His6-SUMO_L*	this study	P126/P127	InFusion: 1:1 primer as insert
FE#95	pGEX-6P-1_*SHE2_E172A_F176A*	this study	P128/P129	QuickChange on p01
FE#96	pOPIN-J_*SHE2(6-246 C-S)_(GGSGG)x2_SHE3(331-346)*	this study	P48/P136	InFusion: Template: FE#33
FE#97	pOPIN-J_*SHE2(6-246 C-S)_(GGSGG)x2_SHE3(331-405)(K340A_R341A_Y345A)*	this study	P48/P137, P138/P54	InFusion: 3 point PCR on FE#33

Nature Structural & Molecular Biology: doi:10.1038/nsmb.3351

FE#98	pOPIN-S3C_*SHE3(331-405)(K340A_R341A_Y345A)*	this study	P122/P54	InFusion: Template: FE#97
FE#99	pOPIN-S3C_*SHE3(331-425)His6*	this study	P122/P139	InFusion: Template: RH84
FE#101	Ycplac22_*SHE3(340-346)A_myc3*	this study	P144/P146, P147/P145	3 point PCR on pRJ350, EcoRI/SalI
FE#102	Ycplac22_*SHE3(364-368)A_myc3*	this study	P144/P148, P149/P145	3 point PCR on pRJ350, EcoRI/SalI
FE#103	Ycplac22_*SHE3(340-346)A(364-368)A_myc3*	this study	P144/P148, P149/P145	3 point PCR on FE#101, EcoRI/SalI
FE#104	pGEX-6P-1_*SHE2_E172A_F176A_StuI*	this study	P152/P153	QuickChange on FE#95
FE#108	pOPIN-S3C_*SHE3(331-405)K340A*	this study	P122/P54	InFusion: Template: FE#77
FE#109	pOPIN-S3C_*SHE3(331-405)R341A*	this study	P122/P54	InFusion: Template: FE#78
FE#110	pOPIN-S3C_*SHE3(331-405)R342A*	this study	P122/P54	InFusion: Template: FE#79
FE#111	pETM-43_*SHE3(334-405)Y345A*	this study	P156/P157	QuickChange on FE#6
FE#113	pOPIN-S3C_*SHE3(331-405)Y345A*	this study	P122/P54	InFusion: Template: FE#111
FE#114	pETM-43_*SHE3(334-405)F344A*	this study	P159/P160	QuickChange on FE#6
FE#116	pOPIN-S3C_*SHE3(331-405)F344A*	this study	P122/P54	InFusion: Template: FE#114
FE#117	Ycplac22_*SHE3(K340A, R341A)_myc3*	this study	P144/P164, P163/P145	3 point PCR on pRJ350, EcoRI/SalI
FE#118	Ycplac22_*SHE3(L364A, V367A)_myc3*	this study	P144/P166, P165/P145	3 point PCR on pRJ350, EcoRI/SalI
FE#119	Ycplac22_*SHE3(K340A, R341A, Y345A)_myc3*	this study	P167/P168	QuickChange on FE#117
pRJ1978	YCplac111_ *SHE2_E172A_F176A*	this study	**-**	Restriction sites: NsiI/StuI

Nature Structural & Molecular Biology: doi:10.1038/nsmb.3351

Supplementary Table 3. DNA oligonucleotides used in this study

Name	Primer sequence (5'→ 3')
	DNA oligonucleotides for molecular cloning
AN_P18	AAAAAACTCGAGTCCTGTCCTATCCTTATTACGTTCA
AN_P19	AAAAAAGGATCCTGCGCAGGAGAAGTTATTAGAATGAT
O176	AAACCATGGGTAATAGCAGTAACAATAAAAG
P6	TTTTGAATTCCTATCTTGTAACACCGGGAGGCACTG
P48	AAGTTCTGTTTCAGGGCCCGGATATCAAAGTCACTCCTGGAACTTCTG
P49	TCCACCACTTCCACCGTTTTTCAATTTACCAAATTTGTCGTGCCA
P50	TCCACCACTTCCACCTCCACCACTTCCACCGTTTTTCAATTTACCAAATTTGTCGTGCCA
P51	GGTGGAAGTGGTGGATCCTCCAATGGTAATAGCAGTAACAATAAAAGAAGAAGTTTC
P52	GGTGGAAGTGGTGGAGGTGGAAGTGGTGGATCCTCCAATGGTAATAGCAGTAACAATAAAAGAAGAAGTTTC
P54	ATGGTCTAGAAAGCTTTATCTTGTAACACCGGGAGGCAC
P73	ATGGTCTAGAAAGCTTTATCCACCACTTCCACCTCCACCACTTCCACCGTTTTTCAATTTACCAAATTTG
P108	GGTAATAGCAGTAACAATGCAAGAAGAAGTTTCTATAC
P109	CGCAGTATAGAAACTTCTTCTTGCATTGTTACTGCTATT
P110	TAATAGCAGTAACAATAAAGCTAGAAGTTTCTATACTGCG
P111	CGCAGTATAGAAACTTCTAGCTTTATTGTTACTGCTATTA
P112	TAGCAGTAACAATAAAAGAGCAAGTTTCTATACTGCGTCG
P113	CGACGCAGTATAGAAACTTGCTCTTTTATTGTTACTGCTA
P122	AAGTTCTGTTTCAGGGCCCGTCCTCCAATGGTAATAGCAG
P126	AAGTTCTGTTTCAGGGCCCGTAAAGCTTTCTAGACCAT
P127	ATGGTCTAGAAAGCTTTACGGGCCCTGAAACAGAACTT
P128	AACCTGCTAGATTTAGCAGTTGTTCAAGCTGCCATTAAATGCGCAGATG
P129	CTGCGCATTTAATGGCAGCTTGAACAACTGCTAAATCTAGCAGGTT
P136	ATGGTCTAGAAAGCTTTAAGTATAGAAACTTCTTCTTTTATTG
P137	TAGCGAAACTTCTTGCTGCATTGTTACTGCTATTACC
P138	TGCAGCAAGAAGTTTCGCTACTGCGTCGCCTTTGCTG
P139	ATGGTCTAGAAAGCTTTAGTGATGGTGATGGTGATGGGATTGGGC
P144	CGACGGCCAGTGAATTC
P145	CCTGCAGGTCGACTCTA
P146	TGCCGCTGCCGCTGCCGCTGCATTGTTACTGCTATTACCATT
P147	CAATGCAGCGGCAGCGGCAGCGGCAGCGTCGCCTTTGCTGTCATCG
P148	GTTCTTGCAGCAGCAGCCGCAACCGGGGATGCAGATTTTG
P149	TTGCGGCTGCTGCTGCAAGAACTGCCTCAGTAAG
P152	TTTGGTAAATTGAAAAACTAAGGCCTCCCGGGTCGACTCGAGCGG
P153	GCGGCCGCTCGAGTCGACCCGGGAGGCCTTAGTTTTTCAATTTACC

Nature Structural & Molecular Biology: doi:10.1038/nsmb.3351

P156	AAAAGAAGAAGTTTCGCTACTGCGTCGCCTT
P157	GCAAAGGCGACGCAGTAGCGAAACTTCTTCTT
P159	CAATAAAAGAAGAAGTGCCTATACTGCGTCGC
P160	GCAAAGGCGACGCAGTATAGGCACTTCTTCTTTTA
P162	GATAATGTCGCATAGACTTTCATCCTTAGCGATTCAGTTATCTATAGTGAGTCGTATTAAATT
P163	GTAATAGCAGTAACAATGCAGCAAGAAGTTTCGCTACT
P164	GCAAAGGCGACGCAGTAGCGAAACTTCTTGCTGCATT
P165	GTTGCGCCTGGTGCTAAAAGAACTGCCTCAGTAAG
P166	TTTAGCACCAGGCGCAACCGGGGATGCAGATT
P167	AGTAACAATGCAGCAAGAAGTTTCGCTACTGCGTCGCC
P168	CAGCAAAGGCGACGCAGTAGCGAAACTTCTTGCTGCAT
	DNA oligonucleotides as templates for *in vitro* transcription
O139	TAATACGACTCACTATAGGGAGATGGATAACTGAATCGAAAGACATTATCACGAAACAAT
O140	ATTGTTTCGTGATAATGTCTTTCGATTCAGTTATCCATCTCCCTATAGTGAGTCGTATTA
O267	AATTTAATACGACTCACTATAGG
O268	ATTGTTTCGTGATAATGTCTCTTATTAGTTGAAAGAGATTCAGTTATCCATCCCTATAGTGAGTCGTATTAAATT
O270	ATTGTTTCGTGATAATGTCTCTTATTAGTTGAAAGAGATTCACTTATCCATCCCTATAGTGAGTCGTATTAAATT
O280	ATTGTTTCGTGATAAACTCTCTTATTAGTTGAAAGAGATTGTGTTATCCATCCCTATAGTGAGTCGTATTAAATT
O281	ATTGTTTCGTGATAATGTCTCTTATTAGTTGAAAGAGATTCAGTTATCCCCTATAGTGAGTCGTATTAAATT
O283	CGTGATAATGTCTCTTATTAGTTGAAAGAGATTCAGTTATCCATCCCTATAGTGAGTCGTATTAAATT
O284	GATAATGTCTCTTATTAGTTGAAAGAGATTCAGTTATCCATCCCTATAGTGAGTCGTATTAAATT
P45	AATTTAATACGACTCACTATAG
P96	CGTGATAATGTCTTTCGATTCAGTTATCTATAGTGAGTCGTATTAAATT
P130	ATTGTTTCGTGATAATGTCTCTTATTAGTTGAAAGAGATTCTGTTATCCATCTATAGTGAGTCGTATTAAATT
P131	ATTGTTTCGTGATAATGTCTCTTATTAGTTGAAAGAGATTCGGTTATCCATCTATAGTGAGTCGTATTAAATT
P132	ATTGTTTCGTGATAATGTCTCTTATTAGTTGAAAGAGATTCAGTTATCCATCTATAGTGAGTCGTATTAAATT
P133	ATTGTTTCCTGATAATGTCTCTTATTAGTTGAAAGAGATTCAGTTATCCATCTATAGTGAGTCGTATTAAATT
P134	ATTGTTTCATGATAATGTCTCTTATTAGTTGAAAGAGATTCAGTTATCCATCTATAGTGAGTCGTATTAAATT
P135	ATTGTTTCGTGATAATGTCTCTTATTAGTTGAAAGAGATTCAATTATCCATCTATAGTGAGTCGTATTAAATT
	DNA Oligonucleotides for chemical probing
AN_P26	TGCGCAGGAGAAGTTATTAG
AN_P27	GGTGAAGAAAACGAAGATGC
AN_P28	AGACAAGGAGAGAAATGTAC

Nature Structural & Molecular Biology: doi:10.1038/nsmb.3351

Supplementary Table 4. RNA sequences used in this study

ASH1 RNA (bases relative to start codon AUG)	Short name (used in text)	Sequence (5'→ 3')	Produced by
E3 (1771-1821)	E3 (51 nt)	$(g)_{1or3}$AUGGAUAACUGAAUCUCUUUCAACUAAUAAGAGACAUUAUCACGAAACAAU	*In vitro* transcription. Template O267/O268; Template P45/P132
E3 (1774-1821)	Δ1	ggGGAUAACUGAAUCUCUUUCAACUAAUAAGAGACAUUAUCACGAAACAAU	*In vitro* transcription. Template O267/O281
E3 (1771-1814)	Δ2	gggAUGGAUAACUGAAUCUCUUUCAACUAAUAAGAGACAUUAUCACG	*In vitro* transcription. Template O267/O283
E3 (1771-1811)	Δ3	gggAUGGAUAACUGAAUCUCUUUCAACUAAUAAGAGACAUUAUC	*In vitro* transcription. Template O267/O284
E3 (1771-1821)Δ(1786-1802)GAAA	E3 (38 nt-loop)	gAUGGAUAACUGAAUCgaaaGACAUUAUCACGAAACAAU	*In vitro* transcription. Template O139/O140
E3 (1774-1814)Δ(1786-1802)GAAA	E3 (28 nt-loop)	GAUAACUGAAUCgaaaGACAUUAUCACG	Chemical synthesis, *in vitro* transcription. Template P45/P96
E3 (1774-1811)Δ(1786-1802)_17nt receptor/TL/TLR stem	E3 (42 nt TL-TLR)	GAUAACUGAAUCgcuaaggaugaaagucuaugcGACAUUAUC	Chemical synthesis, *in vitro* transcription. Template P45/P162
E3 (1771-1821) U1780A	M1	gAUGGAUAAC**A**GAAUCUCUUUCAACUAAUAAGAGACAUUAUCACGAAACAAU	*In vitro* transcription. Template P45/P130
E3 (1771-1821) U1780C	M2	gAUGGAUAAC**C**GAAUCUCUUUCAACUAAUAAGAGACAUUAUCACGAAACAAU	*In vitro* transcription. Template P45/P131
E3 (1771-1821) U1780A, G1781C, C1805G, A1806U	M3	gggAUGGAUAAC**AC**AAUCUCUUUCAACUAAUAAGAGA**GU**UUAUCACGAAACAAU	*In vitro* transcription. Template O267/O280
E3 (1771-1821) C1779G	M4	gggAUGGAUAA**G**UGAAUCUCUUUCAACUAAUAAGAGACAUUAUCACGAAACAAU	*In vitro* transcription. Template O267/O270
E3 (1771-1821) C1779U	M5	gAUGGAUAA**U**UGAAUCUCUUUCAACUAAUAAGAGACAUUAUCACGAAACAAU	*In vitro* transcription. Template P45/P135
E3 (1771-1821) C1813G	M6	gAUGGAUAACUGAAUCUCUUUCAACUAAUAAGAGACAUUAUCA**G**GAAACAAU	*In vitro* transcription. Template P45/P133
E3 (1771-1821) C1813U	M7	gAUGGAUAACUGAAUCUCUUUCAACUAAUAAGAGACAUUAUCA**U**GAAACAAU	*In vitro* transcription: Template P45/P134

Small letters indicate RNA bases not naturally belonging to *ASH1*. Bold letters mark introduced base mutations compared to wild type *ASH1*

Nature Structural & Molecular Biology: doi:10.1038/nsmb.3351

Supplementary Table 5. Yeast strains used in this study

Strain	Genotype
RJY3545	*MAT a ade2-1 trp1-1 can1-100 leu2-3,112 his3-11,15 ura3 ASH1-12xMS2L* pRJ1486 (*pCP_MCP_3xGFP*)
RJY4901	*MAT a ade2-1 trp1-1 can1-100 leu2-3,112 his3-11,15 ura3 she3Δ::hphNT1 ASH1-12xMS2L* pRJ1486 (*pCP_MCP_3xGFP*)
RJY4902	*MAT a ade2-1 trp1-1 can1-100 leu2-3,112 his3-11,15 ura3 she3Δ::hphNT1 ASH1-12xMS2L* pRJ1486 (*pCP_MCP_3xGFP*) FE#101 (Ycplac22*_SHE3(340-346)A_myc3*)
RJY4902-1	*MAT a ade2-1 trp1-1 can1-100 leu2-3,112 his3-11,15 ura3 she3Δ::hphNT1 ASH1-12xMS2L pRJ1486 (pCP_MCP_3xGFP)* FE#118 (Ycplac22*_SHE3(340A 341A)_myc3*)
RJY4902-2	*MAT a ade2-1 trp1-1 can1-100 leu2-3,112 his3-11,15 ura3 she3Δ::hphNT1 ASH1-12xMS2L pRJ1486 (pCP_MCP_3xGFP)* FE#119 (Ycplac22*_SHE3(340A 341A Y345A)_myc3*)
RJY4903	*MAT a ade2-1 trp1-1 can1-100 leu2-3,112 his3-11,15 ura3 she3Δ::hphNT1 ASH1-12xMS2L* pRJ1486 (*pCP_MCP_3xGFP*) FE#102 (Ycplac22*_ SHE3(364-368)A_myc3*)
RJY4904	*MAT a ade2-1 trp1-1 can1-100 leu2-3,112 his3-11,15 ura3 she3Δ::hphNT1 ASH1-12xMS2L* pRJ1486 (*pCP_MCP_3xGFP*) FE#103 (Ycplac22*_ SHE3(340-346)A(364-368)A_myc3*)
RJY4904-1	*MAT a ade2-1 trp1-1 can1-100 leu2-3,112 his3-11,15 ura3 she3Δ::hphNT1 ASH1-12xMS2L pRJ1486 (pCP_MCP_3xGFP)* FE#117 (Ycplac22*_ SHE3(L364A V367A)_myc3*)
RJY4905	*Mat alpha his3Δ1 leu2Δ0 lys2Δ0 ura3Δ0 she2::kanMX4* pRJ1486 (*pCP_MCP_3xGFP*) pRJ1752 (*YCplac33_ASH1-12xMS2L*) pRJ33 (*YCplac111_SHE2*)
RJY4906	*Mat alpha his3Δ1 leu2Δ0 lys2Δ0 ura3Δ0 she2::kanMX4* pRJ1486 (*pCP_MCP_3xGFP*) pRJ1752 (*YCplac33_ASH1-12xMS2L*)
RJY4907	*Mat alpha his3Δ1 leu2Δ0 lys2Δ0 ura3Δ0 she2::kanMX4* pRJ1486 (*pCP_MCP_3xGFP*) pRJ1752 (*YCplac33_ASH1-12xMS2L*) pRJ1978 (*YCplac111_ SHE2_E172A_F176A*)

Nature Structural & Molecular Biology: doi:10.1038/nsmb.3351

References

1. Bahrami, A., Clos, L.J., 2nd, Markley, J.L., Butcher, S.E. & Eghbalnia, H.R. RNA-PAIRS: RNA probabilistic assignment of imino resonance shifts. *J Biomol NMR* **52**, 289-302 (2012).
2. Correll, C.C. & Swinger, K. Common and distinctive features of GNRA tetraloops based on a GUAA tetraloop structure at 1.4 A resolution. *RNA* **9**, 355-63 (2003).
3. Niessing, D., Hüttelmaier, S., Zenklusen, D., Singer, R.H. & Burley, S.K. She2p is a Novel RNA-Binding Protein with a Basic Helical Hairpin Motif. *Cell* **119**, 491-502 (2004).
4. Landers, S.M., Gallas, M.R., Little, J. & Long, R.M. She3p possesses a novel activity required for ASH1 mRNA localization in Saccharomyces cerevisiae. *Eukaryot Cell* **8**, 1072-1083 (2009).
5. Müller, M. et al. A cytoplasmic complex mediates specific mRNA recognition and localization in yeast. *PLoS Biol* **9**, e1000611 (2011).
6. Singh, N., Blobel, G. & Shi, H. Hooking She3p onto She2p for myosin-mediated cytoplasmic mRNA transport. *Proc Natl Acad Sci U S A* **112**, 142-7 (2015).

Nature Structural & Molecular Biology: doi:10.1038/nsmb.3351